THE UNIVERSITY OF CHICAGO

CIRCADIAN RHYTHMS AND GUT MICROBIOTA: IMPLICATIONS OF DIURNAL INTERACTIONS ON HOST METABOLISM AND IMMUNITY

A DISSERTATION SUBMITTED TO
THE FACULTY OF THE DIVISION OF THE BIOLOGICAL SCIENCES
AND THE PRITZKER SCHOOL OF MEDICINE
IN CANDIDACY FOR THE DEGREE OF
DOCTOR OF PHILOSOPHY

COMMITTEE ON MOLECULAR METABOLISM AND NUTRITION

BY
KATYA FRAZIER

CHICAGO, ILLINOIS
DECEMBER 2022

TABLE OF CONTENTS

ACKNOWLEDGMENTS

I must first thank Dr. Eugene Chang for accepting me as your student, for the years of mentorship as my advisor, for your constant support in the scientific endeavors of this project, and for making me the scientist that I am today. I will miss our circuitous discussions about new data, how to frame a manuscript, and how to "put the talking points up front" in everything I write and present. Thank you for fostering such an incredible laboratory team, always encouraging us to ask the big questions, and to not shy away from the unknown "where no man has gone before."

I also owe a huge thank you to my co-mentor, Dr. Vanessa Leone. It has been so inspiring to learn from you, work alongside you in the lab and in our many writing endeavors, and see you succeed in starting your own research lab. Thank you for trusting me to see the Reg3 project to the finish line, and I learned more than I can describe from our endless discussions and collaborations. I will be forever grateful that you took me under your mentorship wing, and I will always look back fondly on our many late nights of mouse work.

I want to thank my thesis committee for their support and contributions over these years, both in and out of our meetings. Dr. Matthew Brady, thank you for being such a supportive and encouraging committee chair, and for always being someone I could turn to for advice on anything related to grad school. Dr. Brian Prendergast, thank you for teaching me everything I know about chronobiology, and for your perceptive comments and interest in the significance of circadian dynamics of the gut microbiome. Dr. Maureen Coleman, thank you for always providing such insightful comments and suggestions to open my mind up to the microbial ecology side of my work, and for bearing through the mammalian physiology focus of my projects.

To the entire Chang Lab, past and present, thank you for such an incredible 5 years working together on so many different projects over the years. This lab has taught me the importance of teamwork to accomplish the huge research goals that we tackle, and I

am thankful for the opportunity to work with so many different people over the years. I particularly want to thank Sumeed Manzoor, Katherine Carroll, and Marissa St. George for their significant and indispensible contributions to the work presented here; Dr. Candace Cham, Dr. Xiaorong Zhu, and Jason Koval for always generously taking the time to answer my unending questions; and Fran Vukovich for keeping the administrative side of the lab afloat. I must also acknowledge Dr. Mrinalini (Meena) Rao for the friendship and mentorship that you have provided. I will always be grateful for your generosity with your time to read almost everything I have written during grad school, and your advice on all things science, career, and life.

To my fellow CMMN students, past and present, thank you for a wonderful community of grad students to always count on for questions, advice, and camaraderie. I also want to thank Dr. Matthew Brady as the CMMN Chair for fostering this graduate program and making it such a wonderful setting to learn from one another.

I must acknowledge the Animal Resource Center and Gnotobiotic Research Animal Facility staff for the amazing support in maintaining our our animal research. I want to particularly acknowledge Melanie Spedale for her constant, diligent work supporting our gnotobiotic and metabolic cage experiments. None of the studies presented here would have been possible without their incredible work.

To my Chicago crew, you all made graduate school and living in Chicago unforgettable and an incredible amount of fun. Between picnics at the point, pub nights, camping trips, weddings, and game nights, I will treasure the memories and friendships forever. I want to acknowledge The Histones, the best a cappella group around; Wednesday nights were always the highlight of my week and our concerts were some of my favorite memories of grad school.

Finally, I want to thank my family for their unending support and love. Mom and Dad, thank you for supporting my love of science my entire life and providing me every opportunity to succeed and learn. I would not be here without you, for which I am forever grateful, and

I love you both so much. Camille, thank you for being such an amazing sister and best friend, I am so proud of the amazing, confident woman you have become, and I love you. To my Funsten in-laws, Melanie, Rob, Jenna, and Cole, thank you for welcoming me into your family and for your love and support. Finally to Matt, I couldn't imagine a better life partner, and I don't know whether I would have made it through grad school without your constant support and love. Saying yes to you was the best decision I ever made, and I love you.

LIST OF FIGURES

LIST OF TABLES

ABBREVIATIONS

Abx antibiotic-treated

Acetyl-CoA Acetyl-coenzyme A

AMP antimicrobial peptide

ASV amplicon sequence variants

AUC area under the curve

BCAA branched-chain amino acid

BMAL1 brain and muscle ARNT-like factor 1

BMI body mass index

BMR basal metabolic rate

BSH bile salt hydrolase

cAMP cyclic adenosine monophosphate

CLOCK circadian locomotor output cycles kaput

CRY cryptochrome

DBP D-box binding protein

DE differentially expressed

DIO diet-induced obesity

EE energy expenditure

eJTK empirical Jonckheere-Terpstra-Kendall CYCLE

FXR farnesoid X receptor

G6Pase glucose-6-phosphatase

GF germ-free

GIP gastric inhibitory polypeptide

GLP-1 glucagon-like peptide 1

GLUT glucose transporter

GTT glucose tolerance test

GWAS genome wide association study

HF high-fat

HDAC histone deacetylase

IEC intestinal epithelial cell

IL interleukin

ITT insulin tolerance test

KEGG Kyoto Encyclopedia of Genes and Genomes

LD light-dark

LKO liver-*Bmal1* knockout

LPS lipopolysaccharide

MyD88 Myeloid differentiation factor 88

NFIL3 repressor nuclear factor interleukin 3

OTU operational taxonomic unit

PCK phosphoenolpyruvate carboxylase

PDK pyruvate dehydrogenase kinase

PER period

PPAR peroxisome proliferator-activated receptor

PTT pyruvate tolerance test

RC regular chow

REG3γ Regenerating islet-derived protein 3 gamma

RER respiratory exchange ratio

ROR Retinoic Acid Receptor-Related Orphan Receptor Alpha

RQ respiratory quotient

rREG3γ recombinant REG3γ

SCFA short-chain fatty acid

SCN suprachiasmatic nucleus

SFB segmented filamentous bacteria

SPF specific pathogen-free

TLR Toll-like receptor

TRF time-restricted feeding

VST variance-stabilizing transformation

WT wild-type

ZT Zeitgeber time

ABSTRACT

Metabolic diseases, including type 2 diabetes and cardiovascular disease, are a worsening epidemic, affecting millions of people worldwide. These disorders are complex and particularly difficult to treat clinically due to their multifactorial nature, which involves both environmental and genetic factors. Metabolic disease onset and progression are impacted by two seemingly disparate systems: the trillions of microbes that make up the gut microbiome and host circadian networks, which govern the host's capacity to adapt to 24-hour environmental rhythms, such as feeding and fasting. Gut microbiota community membership and functional dynamics are shaped by dietary intake, while circadian rhythms are critical for maintaining metabolic homeostasis; disruption of either results in significant physiological dysfunction. Studies have revealed gut microbes exhibit diurnal patterns in abundance and functional outputs, which feeds back onto host circadian networks. Conversely, host circadian disruptions induce changes in the gut microbiome that can feedback onto the host, particularly affecting metabolic regulation. Despite the strong evidence linking these two important systems, fundamental knowledge of the basic mechanisms behind their interactions remains limited.

This thesis describes two studies that explored the complex diurnal interactions between the gut microbiome and mammalian host factors in the context of metabolic disorders. The first study examines the liver circadian clock as an essential transducer of cues from gut microbes that aid in the regulation of diurnal patterns in homeostatic mechanisms associated with fuel utilization, glucose regulation, and lipid metabolism. The second study explores how bidirectional interactions between the host innate immune factor REG3γ and diet-induced gut microbiota are important for maintaining small intestinal, host-microbe interactions and metabolic homeostasis. Together, this thesis fills gaps and provides an essential knowledge base, spanning multiple systems, to interrogate the mechanistic underpinnings of key host-microbe circadian interactions that direct metabolism.

CHAPTER 1

INTRODUCTION

1.1 The Global Epidemic of Metabolic Diseases

Metabolic syndrome is a worldwide epidemic, affecting approximately 25% of adults in the United States and globally [1–3]. Despite increasing awareness of the long-term consequences for these diseases, global incidence continues to rise. Also known as "Syndrome X", metabolic syndrome is defined by the presence of a cluster of symptoms associated with increased risk for development of type 2 diabetes mellitus and cardiovascular disease. These complex diseases place an enormous economic burden on the healthcare system and afflicted individuals. With limited treatment modalities, there is an urgent and unmet need to understand the underlying causes.

As defined by the International Diabetes Federation, persons are medically diagnosed with metabolic syndrome using several clinical markers, including incidence of central obesity with two or more of the following factors: raised fasting plasma glucose, triglycerides, HDL cholesterol, or blood pressure [4]. These symptoms are the result of a complex combination of dysmetabolism, particularly in glucose and lipid metabolic processes, and are driven by a variety of environmental and endogenous factors, including dietary intake, nutritional status, exercise, genetics, epigenetics, endogenous hormone signaling, sleep patterns, circadian rhythms, stress, and the gut microbiome. This wide array of associated and causative factors is one quality that makes metabolic syndrome and other related metabolic diseases extremely challenging to prevent and treat in the clinic. While some inroads have been made to understand certain mechanisms, much remains to be discovered and elucidated.

1.1.1 Driving Factors of Metabolic Syndrome

Metabolic diseases are multi-factorial in nature, including both endogenous and environmental drivers. Genetic programming contributes to much of the documented heritability of metabolic diseases [5], where 47% to 80% of body mass index (BMI), a primary obesity measurement, has been estimated in twin studies [6]. Genome wide association studies (GWAS) have identified hundreds of common sequence variants that are significantly associated with obesity and type 2 diabetes [7, 8]. Epigenetic modifications also play a major role in metabolic dysfunction and may account for the discrepancy of GWAS studies [9]. Histone acetylation patterns define chromatin accessibility and convey proper gene expression of several metabolic pathways, including lipogenesis, insulin hypersensitivity, and gluconeogenesis [10, 11]. RNA methylation also regulates carbohydrate and lipid metabolic gene expression, which can be altered by certain dietary conditions or circadian disruption [12, 13]. Further work must be done in order to fully dissect the role that genetics and epigenetics play in metabolic disease development.

In addition to genetic susceptibility, environmental factors commonly associated with a "Western lifestyle" play a significant role in metabolic disease development. Diets high in simple sugars and saturated fats directly promote an increase in circulating macromolecules, leading to obesity and insulin resistance [14, 15]. While total caloric input is important, the balance of protein vs. non-protein nutrients may be of greater influence on cardiovascular parameters and longevity [16]. A lack of exercise, or reduced caloric output, and a sedentary lifestyle are significant risk factors; increased exercise has been shown to be protective against metabolic diseases [17]. Disturbances in sleep patterns and circadian rhythms are also risk factors, both of which are quite prevalent in modern society and induced by extended exposure to artificial lights, constant access to food, and shift work [18]. Increased exposure to chemical pollutants has been implicated, in that synthetic chemicals can interfere with hormones associated with weight control [19]. Stress also plays a multi-faceted role, impacting

the hypothalamic-pituitary-adrenal axis and cortisol secretion, which can directly interfere with key metabolic signaling hormones, such as leptin, ghrelin, and insulin [20]. Chronic stress can then lead to unhealthy food intake and sedentary behavior, further exacerbating these driving factors.

Inflammation, and the immune system at large, plays a major role in the general development of metabolic disorders [21]. Obesity often presents with chronic, low-grade, systemic inflammation resulting from continuous activation of the immune system, induced by constant exposure to lipopolysaccharide (LPS) derived from gram-negative intestinal bacteria [22]. The presence of LPS in the bloodstream, termed endotoxemia, is significantly increased following exposure to high-fat (HF) diet, and constant intravenous exposure to LPS induces hepatic insulin resistance [23]. The family of Toll-like receptors (TLRs) plays a major role in intestinal barrier function. For example, TLR4 is required for the phagocytosis of LPS across enterocytes, which recruits myeloid differentiation factor 88 (MyD88), activates the nuclear factor kappa B (NF-κB) signaling pathway, and results in secretion of inflammatory cytokines, such as TNF-α and interleukins (i.e., IL-6), by immune cells [24]. TLR4 can also be directly activated via free fatty acids, resulting in increased cytokine expression by macrophages [25]. Conversely, TLR5, which is induced by bacterial flagellin, protects mice from developing diet-induced liver disease by clearing hepatic bacteria, and global loss of TLR5 in mice results in metabolic syndrome and low-grade inflammation [26, 27]. Elevation of inflammatory cytokines in adipocytes can also cause insulin resistance and typically occurs in combination with obesity, while certain individuals with obesity can retain insulin sensitivity and are considered metabolically healthy [28–30]. This association is solidified by evidence that acute weight loss in human subjects via reduced caloric intake induces significant changes in the inflammatory gene expression profile of white adipose tissue [31]. A unique class of adipose tissue macrophages has also been implicated in the link between obesity and insulin sensitivity, exhibiting a pro-inflammatory state that contributes to insulin resistance

[32, 33]. In the obese state, these adipose tissue macrophages adopt a metabolically active phenotype with pro-inflammatory markers that positively correlate with BMI and adiposity and impact the progression of diet-induced obesity in mice [34, 35]. Interestingly, not all cytokines are metabolically pro-inflammatory; IL-22 promotes insulin sensitivity, normalizes lipid metabolism, and reduces inflammation in white adipose tissue of mice [36]. The mechanisms differentiating metabolically healthy and unhealthy individuals are unclear; however, a lack of inflammation in metabolically healthy obese individuals may prevent insulin resistance. Therapeutics aimed at targeting immune-mediated mechanisms may help to treat obesity and metabolic syndrome. However, given the complex role of the immune system in mediating metabolic homeostasis, further work is required to uncover novel mechanisms that may be leveraged to prevent or treat metabolic diseases.

1.1.2 Glucose and Lipid Metabolism in Health and Disease

The development of metabolic syndrome is predominantly driven by glucose and lipid dysregulation, resulting in aberrant circulating levels of sugars, cholesterol, and triglycerides, as well as increased lipid deposition leading in obesity. Circulating hormones play an essential role in the homeostatic maintenance of these metabolic processes. Insulin is a major hormonal metabolic driver during the fed state, which is produced by pancreatic β-cells when glucose and other nutrient levels increase in circulation. Insulin acts by inducing the liver, muscle, and fat to take up circulating glucose, primarily by glucose transporter (GLUT) proteins, which in turn induces glycogenesis, lipogenesis, and other energy storage processes [37]. Insulin also inhibits the expression of the rate-limiting gluconeogenic enzyme phosphoenolpyruvate carboxylase (PCK). When circulating glucose drops, glucagon produced by pancreatic α-cells acts in opposition by activating gluconeogenesis, glycogenolysis, and fatty acid β-oxidation to provide the energy required to maintain physiological homeostasis during periods of fasting. Following chronic excess food consumption, particularly of simple sug-

ars and fats, insulin secretion and signaling can become overstimulated and lead to insulin resistance, insensitivity, and hyperinsulinemia [38]. Insulin also impacts lipid metabolism, promoting lipogenesis and inhibiting lipolysis. However, insulin can impact additional lipid processes that are relevant in metabolic disease. For example, one study provided evidence that insulin contributes to increased uptake of non-esterified fatty acids from circulation in patients with metabolic syndrome [39]. Thus, disruptions to the tightly-controlled secretion and action of insulin can have significant consequences on overall metabolic health.

While the fed state primarily involves energy storage and anabolism, regulation of catabolic processes in the fasted state are vital to provide adequate sources of energy to the body. Gluconeogenesis, glycogenolysis, and fatty acid β-oxidation are the primary processes by which stored energy is broken down to become readily available for essential metabolic processes in tissues throughout the body. Under fasting conditions, hepatic metabolism provides approximately 90% of endogenous glucose production, derived primarily via gluconeogenesis and glycogenolysis [40]. While glycogenolysis involves the breakdown of glycogen into glucose-6-phosphate and glucose, gluconeogenesis can utilize a variety of precursors, including lactate, glycerol, fatty acids, and amino acids, to form pyruvate for *de novo* glucose production. Glycogenolysis occurs solely in the cytosol, whereas gluconeogenesis begins in the mitochondria with the conversion of pyruvate to oxaloacetate and is transported into the cytosol for the remainder of the process, either before or after PCK converts oxaloacetate into phosphoenolpyruvate. Because gluconeogenesis is quite energy-demanding, the ADP/ATP ratio within the cell must be low, which also suppresses glycolysis and several essential Krebs cycle enzymes, in turn promoting gluconeogenesis. In type 2 diabetes, insulin resistance results in aberrant over-activation of gluconeogenesis which directly contributes to hyperglycemia, while glycogenolysis is impaired. One of the most utilized and effective pharmaceutical treatments for type 2 diabetes is metformin, which specifically reduces hepatic gluconeogenesis, further highlighting the importance of this process [41]. Another po-

tential gluconeogenic-based therapeutic target is the recently discovered hormone asprosin, produced by white adipose tissue, which directly induces gluconeogenesis in hepatocytes, elevating circulating insulin and glucose in mice [42]. Mice with diet-induced obesity (DIO) exhibit significantly increased levels of asprosin, and antibody-mediated sequestration of asprosin ameliorates hyperglycemia, hyperinsulinemia, and overall hepatic glucose production. The partitioning of catabolic and anabolic processes that occur in the liver, including gluconeogenesis, is further explored in Chapter 3.

Equally important in maintaining glucose homeostasis is the regulation and metabolism of lipids [43]. As stated above, insulin action can increase expression of lipogenic enzymes, such as fatty acid synthase [37]. The family of nuclear receptors peroxisome proliferator-activated receptors (PPARs) can also enhance insulin action, and is a major point of transcriptional regulation of fatty acid metabolism [44]. PPARγ, predominantly expressed in white adipose tissue, stimulates lipid storage by increasing expression of genes involved in lipid uptake and metabolism. Conversely, PPARα, primarily expressed in liver, muscle, heart, kidney, and brown adipose tissue, upregulates expression of key genes involved in fatty acid catabolism and lipolysis through sensing of long-chain fatty acids. Fatty acid β-oxidation occurs within the mitochondria, by mediating the transport of fatty acids into the mitochondrial matrix via the carnitine shuttle as acyl-CoA. In switching from the fed to the fasted state through activation of fatty acid β-oxidation, PPARα also regulates glucose metabolism by repressing glycolysis and inducing gluconeogenesis [45]. Gluconeogenesis is upregulated via PPARα through several pathways, one being via PPARα's induction of pyruvate dehydrogenase kinase 4 expression (PDK4), which redirects the fate of pyruvate towards gluconeogenesis and away from the Krebs cycle. This is reinforced by evidence that PDK4-mediated induction is blunted in PPARα-null mice [46]. PPARs are also key to glucocorticoid-mediated expression of the rate-limiting gluconeogenesis enzymes PCK and glucose-6-phosphatase (G6Pase) [47]. Mice that globally lack PPARα also exhibit significant reductions in glucose production via

hepatic gluconeogenesis [48].

Similar to the influence of lipid metabolic dynamics on carbohydrate metabolism via PPAR signaling, several other factors regulate these processes. Acetyl-coenzyme A (acetyl-CoA) serves as a central point of regulation for gluconeogenesis as a product of fatty acid β-oxidation [40]. During gluconeogenesis, acetyl-CoA allosterically activates pyruvate carboxylase, which performs the first step of gluconeogenesis converting pyruvate to oxaloacetate. When lipogenesis is upregulated and fatty acid β-oxidation is downregulated during the fed state, mitochondrial acetyl-CoA levels decrease, in turn reducing activation of pyruvate carboxylase and gluconeogenesis. Conversely, during the fed state when fatty acid β-oxidation is upregulated, mitochondrial acetyl-CoA increases, promoting gluconeogenesis. Another regulatory molecule is cyclic adenosine monophosphate (cAMP), which is the mechanism by which glucagon induces gluconeogenesis, binding to the glucagon receptor to increase intracellular cAMP which promotes gluconeogenesis via protein kinase A. cAMP also induces fatty acid β-oxidation by promoting PPARα activity and expression of key fatty acid β-oxidation genes [49]. These regulatory factors ensure that gluconeogenesis and fatty acid β-oxidation are co-regulated in both the fed and fasted states. The temporal specificity of these processes also prevents futile cycling and secures adequate circulating glucose levels throughout the 24-hour day.

The metabolic flexibility of fuel switching in the fed and fasted states between carbohydrates and lipids is another hallmark of the tight regulation of these processes. The capacity for fuel switching can be quantified as the change in respiratory quotient (RQ) over time, which measures the relative utilization of carbohydrates and lipids for fuel, as well as the absolute output capacity of these processes. [50, 51]. Healthy individuals exhibit significant metabolic flexibility, while individuals with metabolic syndrome exhibit little to no flexibility [52]. The glucose and lipid metabolic outputs and processes that define metabolic flexibility are significantly driven by mitochondrial function, thereby implying that impaired mitochon-

drial function would also reduce the capacity for nutrient sensing and metabolic flexibility. Interestingly, subsequent weight loss has been shown to reestablish moderate metabolic flexibility, suggesting that the plasticity of fuel utilization dynamics may be directly tied to metabolic disorders such as obesity. Thus, the molecular signals that induce changes in fuel utilization between periods of feeding and fasting are important to consider in metabolic disease.

Hormones produced by the gastrointestinal tract also contribute to the maintenance of metabolic homeostasis. Compared to intravenous administration, oral glucose administration promotes 2-3 times more insulin secretion, termed the incretin effect [53]. This effect is mediated by incretins, including glucagon-like peptide 1 (GLP-1) derived from proglucagon, and gastric inhibitory polypeptide (GIP), which are produced in the intestinal tract in response to dietary glucose. Recently, GIP has been demonstrated as the dominant incretin in comparison to GLP-1, in part by its dual action on both α-cells and β-cells in the pancreas to directly stimulate insulin secretion, as well as indirectly via glucagon induction [54, 55]. In patients with type 2 diabetes, the incretin effect is almost completely absent, which has been demonstrated as a potential early marker of pancreatic dysfunction and type 2 diabetes onset [56]. In hyperglycemic states, GIP-receptors in the pancreas are down-regulated, which is one mechanism by which the incretin effect is impaired [57]. Ghrelin and leptin are two additional key metabolic regulatory hormones. Ghrelin, termed the "hunger hormone", is produced in the stomach and works to stimulate appetite and program energy balance. Working in concert with the adipose-derived, "satiety hormone" leptin, ghrelin acts on the central nervous system to influence energy balance and control food intake [58]. Circulating ghrelin is inversely correlated with BMI, and over-eating results in increased levels of leptin associated with obesity, often leading to leptin insensitivity. Leptin and ghrelin may serve as clinical predictive markers of obesity or cardiovascular disease risk [59]. Together, these hormones are important regulators of insulin signaling and sensitivity, and are key

considerations when investigating mechanisms of metabolic dysfunction.

1.2 Circadian Rhythms are Central Conductors of Physiology

Circadian rhythms are essential to most life forms, coordinating behaviors to the rising and setting of the sun and compartmentalizing key physiological processes for increased energy balance efficiency [60]. Defined by their self-sustaining and cell-autonomous nature, circadian rhythms are poised to synchronize the myriad of events necessary to adjust physiology to light and dark phases of life [61]. All circadian rhythms exhibit three core qualities: 1) an endogenous free-running rhythm lasting approximately 24 hours, 2) the ability to be entrained by an external stimulus, or Zeitgeber, and 3) exhibition of temperature compensation [62]. Circadian rhythms are present in almost all organisms regularly exposed to light, including both eukaryotes and prokaryotes [63]. One example of this regulation is the crucial transition between fed and fasted metabolic states governed by glucose homeostatic mechanisms, as described above [64]. These patterns also extend to host immune responses, such as the variation in the degree of response to pathogen infection at different times over 24 hours [65].

1.2.1 The Core Circadian Clock

The molecular components of the circadian clock are expressed in nearly all cells, forming an elegant transcriptional-translational feedback loop that controls gene expression patterns [66, 67]. Starting during the subjective day, transcription factors Brain and Muscle ARNT-Like 1 (BMAL1, formerly known as MOP3) and Circadian Locomotor Output Cycles Kaput (CLOCK) heterodimerize to form a complex and activate transcription of many clock-controlled genes by binding to E-box regulatory elements within promoter regions. Some of these genes encode the factors Cryptochrome (CRY) 1/2 and Period (PER) 1-3, which interact with one another, serving as the negative arm of regulation by repressing *Bmal1* and

Clock transcription. The expression of *Crys* and *Pers* are subsequently reduced, releasing the negative feedback arm and allowing the positive arm to resume action. In addition to this primary feedback loop, a secondary loop provides stability to the primary components. BMAL1-CLOCK also activates nuclear receptors Rev-Erbα and Rev-Erbβ, which compete with Retinoic Acid Receptor-Related Orphan Receptors (RORα, RORβ, RORγ) for ROR binding elements. When translated, these two components act in opposition; RORs promote *Bmal1* and *Clock*, while Rev-Erbs inhibit the complex. A third loop provides additional regulation on expression of *Per1/2*, *Ror*α/β, and *Rev-Erbs*, primarily by factors D-box binding protein (DBP) and repressor nuclear factor interleukin 3 (NFIL3). These three interconnected regulatory loops are the basis for the generation of oscillating transcription patterns of clock-controlled genes.

Diurnal patterns of the molecular clock loop can be significantly impacted and reset by various Zeitgebers or external environmental cues. One significant Zeitgeber is light, or the LD patterns that most organisms experience over regular time intervals. Light exposure directly induces expression of *Per1/2* in the core brain clock, located in the suprachiasmatic nuclei (SCN) within the hypothalamus, which can reset the entire clock loop [68]. The level of light intensity can also impact the robustness of phase resetting [69]. Internal Zeitgebers include melatonin, classically known as the sleep promoting hormone, which is produced by the pineal gland during periods of darkness [70]. While the secretion of melatonin is induced by the central circadian clock, it can also impact entrainment or resetting of free-running activity patterns by binding to receptors in the SCN, which also restricts its action by controlling availability of the receptor. Importantly, the commonly used inbred laboratory mouse strain C57BL/6J, which is utilized in all studies presented in this thesis, exhibits profound deficiency of melatonin production, yet these animals still exhibit robust circadian rhythms, such as in locomotor activity [71]. Recent work comparing melatonin-proficient and -deficient mouse strains suggests that while melatonin is not required for the generation

or maintenance of rhythms, it serves a key role in facilitating light-induced phase shifts in response to jet lag or seasonal rhythms. Another important Zeitgeber is food availability, often demonstrated in the laboratory setting with rodent models using food anticipatory activity as a read-out [72]. While mice and rats are nocturnal and consume the majority of their food during their dark, active phase, animals that are only given food in a time-restricted manner during the light hours, typically the resting phase reset their activity to the feeding phase, resulting in inversion of hepatic clock gene expression patterns [73, 74]. This occurs independent of a core brain clock, suggesting the existence of a physiological food-entrainable oscillator that has yet to be anatomically localized. Thus, environmental Zeitgebers are an important consideration when examining the dynamics of the mammalian circadian clock.

1.2.2 The Circadian Clock Regulates Host Metabolism

Although the genes involved in maintaining the circadian network drive many biological pathways, they are especially relevant in metabolism [61, 75, 76]. Clock components, particularly *Bmal1*, exhibit promoter-binding patterns that are enriched for key metabolic genes, which corresponds to rhythmic transcription and translation [77–79]. Transcriptome analysis of several mouse tissues indicate that almost half of all protein-coding genes exhibit 24-hour oscillation in at least one tissue, with the highest percentage of 16% in the liver [80]. Additionally, epigenetic factors exhibit circadian patterns that specifically impact metabolic regulation, in particular histone acetylation [81]. Rhythmic acetylation underlies clock protein interactions [82], particularly in the histone acetyltransferase nature of CLOCK [83, 84]. SIRT1 and histone deacetylase 3 (HDAC3), both histone deacetylases, have been implicated in mechanisms underlying how clock proteins govern insulin sensitivity and lipid synthesis and metabolism [85, 86].

Circadian disruption leads to metabolism and energy network imbalances, resulting in

disorders such as obesity and diabetes [18, 87]. Shift work in humans has been strongly associated with the development of metabolic disorders, including obesity and type 2 diabetes [88, 89]. Experimental shift work can induce significant changes in the circulating metabolome, particularly in diurnal patterns of amino acids, such as tryptophan and alanine [90]. Countless animal models demonstrate that disruption of core circadian clock genes in the form of genetic deletion or mutation (i.e., clock mutant mice) results in widespread negative health outcomes that are primarily metabolic [75]. For example, mice that are globally deficient in the core clock gene *Bmal1* exhibit arrhythmic locomotor activity, disrupted glucose and lipid homeostasis, and insulin resistance [87, 91, 92]. Additional work demonstrates that these animals also exhibit low bone mass and other symptoms of rapid aging [93, 94]. *Clock* mutant mice develop increased body weight and food intake patterns [95]. Deletion of the negative feedback loop elements also results in metabolic dysfunction. Deletion of *Cry1/2*, *Per1/2/3*, or *Rev-Erbα/β* results in hyperinsulinemia, altered lipid metabolism, increased adipose deposition and lipid uptake, as well as altered feeding behavior and activity [96–100].

Many of the endogenous hormones that drive host metabolism exhibit diurnal patterns in secretion and circulation that are lost or dampened under states of metabolic imbalance [101]. For example, circulating ghrelin normally exhibits a circadian oscillation that peaks during the night in healthy human subjects, which is lost in obese subjects [102]. Similarly, obese or overweight subjects exhibit a loss of diurnal circulating GLP-1 compared to lean counterparts [103]. Other studies have shown in rats that exposure to the fatty acid palmitate disrupts the circadian secretion of GLP-1 by intestinal L-cells, potentially in a *Bmal1*-dependent fashion, as diurnal GLP-1 secretion is lost in *Bmal1*-knockout mice [104, 105]. This suggests a parallel to the potential effects of HF diet on GLP-1 production and signaling. These hormonal circadian patterns also extend to glucocorticoids, which themselves exhibit oscillations in circulating levels. Additional circadian regulation is achieved by histone acetylation activ-

ity of the CLOCK/BMAL1 complex, which represses glucocorticoid receptor transcriptional activity acetylation [106]. *Cry1/2* also repress glucocorticoid receptor action and modulate downstream transcription, resulting in defects in gluconeogenesis [107]. These diurnal dynamics and circadian clock gene control of metabolic hormone signaling demonstrate tightly controlled temporal regulation.

1.2.3 The Circadian Clock Regulates Immunity

Circadian dynamics are also evident in host immune responses and function [108]. Infection rates and severity vary over a 24-hour period, in part due to the rhythmic oscillation of several innate and adaptive immune components, including immune cell proliferation and activity, expression of pathogen recognition receptors, and cytokine production [109]. For instance, sepsis severity in mice depends upon and correlates with diurnal expression and functional patterns of TLR9 [110]. Some of these rhythmic immune components are driven by endogenous hormones; diurnal oscillation of circulating glucocorticoids impacts cytokine production, such as the pro-inflammatory cytokine IL-1, as well as immune cell proliferation and trafficking at particular times of day [109]. IL-1 can also feedback to increase glucocorticoid hormone levels in circulation, providing a connection to underlying host metabolic processes. [111]. The cytokine interferon-γ has also been demonstrated to decrease synaptic activity and rhythmic expression of *Per2* in rat SCN cultures [112]. Thus, circadian dynamics of the immune system are bidirectional; immune factors and outcomes are under circadian clock control, and the immune system can also drive major circadian regulators.

Genetic ablation of circadian clock genes in rodent models reveal the wide breadth of the immune system that is under control of circadian networks. Global *Bmal1* mutant mice are more susceptible to infections and exhibit impaired development and circulating levels of B cells [113, 114], while *Clock* mutant mice exhibit reduced expression of pro-inflammatory genes and corresponding reductions in intestinal colonization during *Salmonella* infection

[65]. Altered diurnal expression of cytokines and cytolytic factors in splenic natural killer cells has also been observed in *Per1* mutant mice [115]. Adverse effects on immune function are also present in humans following sleep disruption. Both acute experimental sleep deprivation and chronic sleep loss due to shift work, insomnia, or aging are linked to changes in immune system regulation in humans, including cytokine levels, natural killer cell activity, and T cell function [116]. Likely due to a compromised innate immune system, shift workers exhibit a greater risk for viral infection and inflammatory diseases compared to day workers. Thus, both genetic and environmental circadian disruption induces significant impairments in both innate and adaptive immune function.

1.2.4 Hierarchy of Core and Peripheral Circadian Clocks

Host circadian rhythms are coordinated by a core, master clock located in the SCN of the hypothalamus. The core clock receives light and dark cues from the environment and transmits this information to peripheral tissues to maintain rhythmic processes in physiological outputs. Disruption of the central SCN clock by forebrain-specific *Bmal1* deletion in mice results in arrhythmic locomotor activity and SCN rhythms when exposed to constant darkness, and many peripheral clocks exhibit phase desynchronization [117]. However, despite being desynchronized overall, food anticipation remains intact, and peripheral clocks still maintain their own individual rhythms, albeit with dampened amplitude. Peripheral clocks appear to display local control and receive external signals independent of the SCN, exerting unique oscillation patterns in physiological outcomes [118]. For example, intestinal epithelial cells (IECs) exhibit unique transcription oscillations of core clock genes in comparison to the master clock. This allows for local control of gut functions such as nutrient absorption and intestinal motility to be independent from central clock regulation, a key feature of adaptability of the gut to environmental stimuli. [119–121].

Further demonstrating autonomy of peripheral tissue clocks, time-restricted feeding

(TRF) of mice shows that liver transcription patterns can be entrained independently from the SCN [73, 122] and can restore hepatic transcription rhythms in circadian-disrupted or HF fed mice [123], even while SCN expression remains arrhythmic [117, 124]. Restoration of a single peripheral clock in a globally clock-deficient mouse model has shed further light on the independence and autonomy of certain tissue clocks. For example, when only the peripheral liver clock is functional in mice, circadian clock gene expression and key hepatic metabolic processes continue to exhibit rhythmicity, including glycogen and NAD+ salvage metabolism [125]. Peripheral clocks can also feedback and influence the central clock in the brain, where the adipocyte clock partially governs feeding behavior patterns and intake [126]. Interestingly, apart from tissue specific core circadian clock genes, mice exposed to the glucocorticoid hormone analog dexamethasone at varying times of day exhibit shifts in hepatic *Per* expression, while the phase of the central SCN clock remains intact [127]. Thus, peripheral tissue clocks can uniquely function and respond to external cues independent of the core circadian clock in the brain.

Numerous mouse models employing conditional tissue-specific knockouts of various clock components display metabolic phenotypes that deviate from both their global knockout and wild-type (WT) counterparts [76, 128]. This is especially evident with *Bmal1*; mice lacking *Bmal1* only in specific tissues exhibit a variety of phenotypes completely distinct from the global knockout. For example, the liver-specific *Bmal1* knockout mouse does not display arrhythmic behavior, accelerated aging, or increased adiposity relative to the global knockout counterpart, but instead has a unique glucose tolerance profile with more efficient glucose clearance, as well as reduced mitochondrial respiration [129–131]. Muscle-specific loss of *Bmal1* in mice results in glucose intolerance and fasting hyperglycemia [132], β-cell-specific loss results in a dampened insulin response to available nutrients [133], while adipocyte-specific loss results in larger adipocyte size, reduced energy expenditure, and altered feeding behavior during the rest phase [126]. This phenomenon is also apparent when the clock is

disrupted only in immune cells, where loss of *Bmal1* in either myeloid or lymphoid cells results in reduced infection clearance rates and eliminates rhythmicity in trafficking [134–136]. Interestingly, *Bmal1* deletion only in monocytes induces a significant increase in weight gain under HF feeding as compared to HF-fed WT controls [126]. While tissue-specific transgenic approaches have shown that peripheral circadian clocks exhibit more nuanced effects on host physiology than previously considered, more work is required to delineate how peripheral clocks interact with other systems, as well as with each other.

1.3 The Gut Microbiome is a Major Driver of Host Health

Comprised of trillions of microorganisms that reside in various niches throughout the gastrointestinal tract, the gut microbiome influences the development, maintenance, and deterioration of many host systems and processes. A broad range of hosts, from plants to animals, tolerate and nurture these commensal microbes due to the vast number of functions they perform, at times compensating for functions that are not contained within the host genome. The gut microbiome has been recognized for its importance in regulating several physiological systems, including those involved in immunity, metabolism, and the nervous system. When the microbial community is significantly altered, functional outputs can become disturbed and have been associated with the development of many diseases, such as inflammatory bowel diseases, type 2 diabetes, obesity, atherosclerosis, colon cancer, and non-alcoholic fatty liver disease [137, 138]. Like any other organ in the body, the gut microbiome is a vital, albeit acquired organ that is wholly interconnected with other vital life systems, and its composition and functions are very responsive to environmental and dietary stimuli. Environmental changes, such as diet, can rapidly alter microbial community membership abundance and function that feedback onto the host [139–142]. The use of germ-free (GF) mice raised in complete absence of microbes has revealed many essential mechanisms provided by gut microbes, particularly in the maintenance of metabolic homeostasis [143].

1.3.1 Gut Microbes Regulate Host Metabolism

Gut microbiota are exquisitely sensitive to environmental changes, both dietary and physiological, exhibiting rapid shifts in community membership and functions that can feedback onto host health outcomes [139, 140, 144–146]. Animals or humans given a dietary challenge with differences in macronutrient composition exhibit rapid and significant shifts in community membership of intestinal microbiota, as well as functional genetic programming and outputs [144, 147, 148]. Related to diet, metabolic disease incidence is also associated with changes in gut microbiome dynamics. Humans with obesity exhibit significant differences in gut microbial community profiles in comparison to lean individuals, and leptin-deficient obese mice display a similar phenomenon [149, 150]. This association has also been extended to causation via gut microbiota transfer; mice that receive microbiota derived from obese conventional mice display increased adiposity compared to those that receive microbes from lean donors, despite no differences in food consumption between recipient groups [151]. A similar experimental protocol utilizing indirect calorimetry revealed that mice conventionalized with microbiota from lean donors exhibit increased energy expenditure and oxygen consumption compared to those that received microbes from an obese donor [152]. These observations suggest that diet can functionally alter host physiology via gut microbes, ultimately inducing metabolic disease, yet more work is needed in order to understand why and how gut microbes induce such profound and unique metabolic phenotypes.

Gut microbes perform and aid in several essential metabolic processes for the host, in particular digestion and absorption of specific dietary nutrients, essential vitamin production, and gut hormone stimulation [137, 153]. Studies that utilize GF mice describe a unique metabolic profile compared to conventionally-raised, Specific Pathogen-Free (SPF) mice, including reduced adiposity, improved glucose tolerance, and improved insulin sensitivity [141, 143, 154]. Gut microbes contribute to the programming of host energy balance, including lipid absorption and storage, inducing vast changes in patterns of intestinal gene

expression, and have a major influence on overall metabolic health [142, 151]. GF mice are also resistant to DIO, and microbiota transplantation quickly results in increased adiposity similar to levels observed in SPF counterparts, implying that gut microbes can induce drastic metabolic changes, even when acquired later in life [141, 143, 154, 155]. Conventionalization of GF mice induces changes in intestinal and peripheral tissue transcription patterns of key metabolic genes relating to lipid absorption and transport, such as Apolipoprotein A4 (*Apoa4*), Pancreatic Lipase Related Protein 2 (*Pnliprp2*), and *Pparα*, demonstrating that gut microbes directly influence host metabolic programming [155, 156].

In addition to lipid metabolism and absorption, the gut microbiome also plays a significant role in host glucose regulation. Gut hormones relevant to host metabolism are also susceptible to regulation by microbes, in particular GLP-1. GF mice exhibit significantly higher levels of circulating GLP-1 compared to conventional counterparts, thought to be driven by reduced levels of short-chain fatty acids (SCFAs) which are a primary source of energy for colonocytes [157]. Increased GLP-1 in GF mice also results in slower transit time to allow for greater nutrient absorptive capacity in the absence of gut microbes that can . In the context of obesity, treatment of HF-fed conventional mice with the probiotic VSL#3 improved metabolic outcomes, potentially via GLP-1 induction through increased bacterially-derived SCFA butyrate from the probiotic [158]. In addition to mediation by GLP-1, gut microbes also play a significant role in promoting hepatic gluconeogenesis, although the mechanism behind this phenomenon remains unknown [159]. While microbially-mediated mechanisms driving hepatic gluconeogenesis are unclear, microbially-derived SCFAs and succinate have both been shown to induce intestinal gluconeogenesis, and the SCFA propionate can act as a precursor to gluconeogenesis in the intestine [160, 161]. Inhibition of intestinal gluconeogenesis by G6Pase intestinal-specific deletion directly impacts gut microbial community membership and metabolomic outputs [162], pointing to a bidirectional relationship between gluconeogenesis and the gut microbiome.

1.4 Interactions Between Gut Microbes and Circadian Rhythms

Host–microbe crosstalk in the context of circadian and biological rhythms is well conserved across vertebrates and invertebrates, eukaryotes and prokaryotes [163, 164]. Not only do microbes exhibit oscillations in abundance and functional outputs within multicellular hosts, but circadian disturbances impart changes in microbial community dynamics. Gut microbes and their outputs can act as non-photic cues to the host circadian network. There is also emerging evidence that non-photosynthetic bacteria encode their own internal clocks. Still, much remains to be delineated concerning the mechanisms underlying these conserved diurnal interactions between these two complex systems, which continues to be a question many research groups are currently pursuing.

1.4.1 Cyanobacteria and Bacteria Models

Self-sustaining microbial biological rhythms have been extensively characterized in photosynthetic cyanobacteria [165]. *Synechococcus elongatus* is the primary cyanobacterium model for examining circadian clock molecular mechanisms [166]. Similar to eukaryotic clocks, a circadian loop is responsible for driving essential physiological outputs, including timing of cell division, nitrogen fixation, and metabolism, largely mediated by ATPase activity and regulation of gene transcription and translation [167]. Three clock proteins, *kaiA*, *kaiB*, and *kaiC*, comprise the circadian system within cyanobacteria [168]. KaiC exhibits autokinase, autophosphatase, and ATPase functions that are activated or inhibited by the phosphorylation of specific residues. During the light phase, KaiA stabilizes the autokinase function of KaiC; conversely, KaiB inhibits KaiA action by sequestration, resulting in KaiC autophosphatase activity. This phosphorylation feedback loop self-maintains over approximately 24 hours, and the oscillation can self-sustain *in vitro* in combination with ATP. Unlike most bacteria found in the gut, the photosynthetic nature of cyanobacteria allows for coordination to LD environmental stimuli. Light exposure resets the clock phase via molecular detection of

the cell's photosynthetic status, such as sensing the cellular redox state via input component CikA [169, 170] or intracellular ratios of ATP/ADP [171].

While this model serves an important system by which to study prokaryotic circadian clocks, much remains to be deciphered concerning rhythmicity and clocks in non-photosynthetic, light-sensing bacteria. This is particularly relevant to the gut microbiome, which does not receive direct LD environmental cues. One study recently characterized the free-running, entrainment, and temperature compensation of *ytvA* promoter gene expression rhythms in *Bacillus subtilis*, a gram-positive, non-photosynthetic bacterium found in soil and the gastrointestinal tract of humans [172]. Other non-photosynthetic bacteria have also been investigated similarly, such as the entrainment of *Klebsiella aerogenes* to temperature cycling followed by free-running expression patterns *in vitro* [173], and the circadian swarming and motility patterns of *Enterobacter aerogenes* in response to melatonin entrainment [174]. While these results are intriguing, microbial circadian clocks are still not well understood and require significantly more investigation. They may also aid in our still burgeoning exploration of how the circadian dynamics of a complex microbial community, like the gut microbiome, interacts with a eukaryotic host.

1.4.2 Squid-vibrio Model

The squid-vibrio model of symbiosis involves a specific microbial species that interacts with the host in a rhythmic fashion. Consisting of a relationship between the bobtail squid *Euprymna scolopes* and the gram-negative bacterium *Vibrio fischeri*, the squid swim in shallow oceanic waters to feed at night, at which point *V. fischeri* enter the squid's light organ and luminesce to camouflage the squid [175]. These two organisms exhibit a diel relationship; *V. fischeri* colonize the light organ each evening and a significant portion of the community is expelled in the morning, following a circadian pattern [176]. The host provides specific amino acids as metabolic substrates for the microbes, and its light organ crypts undergo

a structural change wherein the residing microbes metabolically shift to favor anaerobic glycerol respiration. In turn, the microbial luminescence induces diurnal host *cryptochrome* expression which may induce critical changes in host transcriptional metabolic and signaling pathways for the night feeding period. The reduced complexity of this system with a single microbial species has enabled researchers to manipulate specific mechanisms, such as the luminescence activity of *V. fischeri*, and delineate the direct effects of this relationship on host physiology [177].

1.4.3 Mouse Models

Recent studies have revealed elegant associations between host circadian rhythms and gut microbiota in mouse models. Although gut microbes are not exposed to light, diurnal host signals induce oscillations in both abundance and function of gut bacteria in mice [141, 178, 179]. Specific microbial taxa, as well as key microbially-derived products, exhibit diurnal oscillations in relative abundance over a 24-hour period [141, 180, 181]. Despite potential confounders in starting microbiomes across mouse cohorts, differences between animal facilities, and unique study designs to manipulate the circadian system, microbial oscillations persist across studies [182, 183]. In addition to oscillations in taxa, total biomass of gut bacteria also fluctuates over 24-hours, as does approximately 20% of Kyoto Encyclopedia of Genes and Genomes (KEGG) functional pathways [180, 183].

The functional link between gut microbiota and circadian rhythms in mammalian models appears to elicit a substantial impact on both host and microbes. Some host-derived mediators that have been shown to influence the gut microbiome in a circadian context include antimicrobial peptides [65], glucocorticoid hormones [184], and intestinal mucus secretion [181]. Conversely, microbially-derived mediators have been identified as circadian modulators, such as hydrogen sulfide, SCFAs, certain vitamins, and tryptophan derivatives [185]. Some distinct mechanisms have been described to explain the functional metabolic signifi-

cance of how the gut microbiome and circadian rhythms interact to drive host metabolism. One such example is work by Wang *et al.*, who identified a role of the transcription factor NFIL3, an accessory loop of the circadian gene network, in this context. This work showed that in SPF mice, IEC-specific NFIL3 is regulated by gut microbiota signals via the circadian clock mediator Rev-Erbα, and disruption to this signal negatively impacts metabolic outcomes of DIO [186]. This interaction is mediated in part via a MyD88-dependent signaling relay initiated by gut microbes through innate lymphoid cells that ultimately influence the core circadian clock component Rev-erbα and downstream induction or suppression of *Nfil3*, driving host metabolism. Using serial deletion of each signaling component, Wang *et al.*, outlined a precise signaling pathway for the interaction between gut microbes, host circadian rhythms and metabolism. The same research group has also examined the implications of rhythmic interactions between a host-derived intestinal innate immune factor and specific gram-positive bacterial strain [187]. These studies illustrate that host immune cells may be a key link that contributes to diurnal patterns of gut microbes, which can impact host circadian systems and physiology.

The host circadian clock status and integrity, particularly that of peripheral clocks, influence the diurnal dynamics of intestinal microbes. Mice with genetic mutations in *Bmal1* and *Per1/2* exhibit significantly altered microbial community profiles and loss of rhythms in specific microbial taxa [178, 180]. Gut microbes have also been linked as drivers of host molecular rhythms; without gut microbes, GF and microbiome-depleted mice exhibit entirely unique diurnal dynamics in SCN and hepatic transcriptional patterns, particularly in core circadian clock and metabolic pathways [141, 181, 188]. A similar effect has also been observed in IECs of GF or microbiome-depleted mice, in which clock and metabolic gene expression is reduced, and diurnal histone signaling is significantly dampened, via lack of HDAC3 [189, 190]. This begs the question of whether the absence of gut microbes or core clock components, resulting in loss of homeostatic rhythmicity, allows for gain of secondary

oscillations that can exert entrainment effects on the host, which could explain the emergence of unique rhythmic patterns. The reprogramming of these host rhythms may contribute to the development of certain disease states that are known to be associated with disturbed microbiomes and circadian disorganization.

Perturbations to metabolic homeostasis also influence both host circadian rhythms and gut microbiome oscillations. When mice are fed HF diet, not only is circadian clock gene expression significantly modulated in both the SCN and liver, but many of the microbial oscillations in relative abundance observed in lean mice are also disturbed or dampened [141, 179, 191]. Another study showed that mice exposed to HF liquid diet exhibited significant changes in microbial community profile following weekly LD phase reversals, while their chow-fed counterparts maintained a more stable community [192]. Further, HF diet-induced microbiota transferred into RC-fed mice induced significant changes in hepatic *Dbp* and *Per2* expression, increased adiposity, and transcriptional reprogramming via activation of PPARγ [193]. Functional output of microbes is also affected by HF feeding, observed by the overall reduction and absence of diurnal abundance of SCFAs, which are known to heavily influence host metabolism [141]. Other dietary regimens, including ketogenic and high-protein low-carbohydrate diets, have also begun to be investigated in this context and thus far revealed changes in both circadian organization and microbial community dynamics [147, 194–196]. These host-microbe misalignments persist in consistent light entrainment and appear to contribute to the associated negative metabolic consequences, but can be realigned by TRF regimens. Not only does TRF of HF-fed mice during the animal's active phase prevent the negative metabolic effects of the diet, including abnormal fat deposition and glucose tolerance, but it also partially restores the microbial oscillations that are lost due to dietary intervention, particularly several *Lactobacillus* species [179, 197]. Thus, the environmental cues of consolidated feeding may prevent diet-induced metabolic disturbance mediated in part via the maintenance of microbial oscillations.

1.4.4 Human Models

Several findings support the notion that diurnal dynamics of gut microbes are also important in humans. Fecal microbes originating from jet-lagged humans induce obesity and glucose intolerance in GF mice receiving microbial transplantation, while GF mice receiving non-jet-lagged stool remain lean [180]. Another study revealed that time of meal intake in humans corresponded with diurnal dynamics of the oral microbiome, particularly TM7 and Fusobacteria groups [198]. Rhythmic microbiota signatures have also been significantly associated with the risk and development of obesity and type 2 diabetes by reconstruction of 24-hour profiles of timestamped samples from large human cohorts [199]. The entrainment of these systems, both to environmental cues and each other, can vastly influence metabolic health and status, which thus far has been difficult to target clinically. Investigating the specific mechanisms that these two "organs" utilize to regulate metabolism will allow researchers to adapt that information and eventually manipulate these and other systems for medical intervention of metabolic diseases.

1.5 Mediators of Circadian-Microbe Interactions

Although some studies have outlined potential molecular mechanisms of microbial-circadian dynamics, the basic mechanisms that underlie how microbial communities within a multicellular host maintain oscillations remains poorly understood. Thus far, some specific microbially-derived or -associated metabolites have been implicated in these interactions. Both SCFAs and microbial modifications to host-derived bile acids exhibit 24-hr oscillations in response to host and environmental signals, indicating that microbes exhibit diurnal patterns in both abundance and function [141, 180]. Both SCFAs and bile acids are involved in regulating glucose and lipid metabolic homeostasis, demonstrated in part by significant changes in insulin sensitivity in response to direct administration of either specific SCFAs or bile acid species [200–202]. Host-derived antimicrobial peptides (AMPs) are also a group of

microbially-associated factors with strong circadian implications in driving host immunity and metabolism. These mediators are described in detail below.

1.5.1 Short-chain Fatty Acids

Short-chain fatty acids (SCFAs), primarily consisting of butyrate, propionate, and acetate, are a major functional by-product of gut microbes derived from fermentation of specific fibers [203]. SCFA production in the intestine is largely attributed to microbes belonging to the phylum Firmicutes [204, 205]. While SCFAs can be used as an energy source for certain host cells (colonocytes, hepatocytes, adipocytes) [203], this group of microbially-derived metabolites also exhibit the capacity to act as signaling molecules. For example, delivery of SCFAs to GF mice were are sufficient to induce specific chromatin states via modulation of histone acetylation and methylation [206]. Butyrate specifically alters histone acetylation patterns that impart anti-inflammatory properties to some immune cell populations [207], but have also been shown to induce intestinal macrophages that are hyper-responsive to commensal gut bacteria [208]. Additionally, SCFAs stimulate certain G-protein coupled receptors, such as free fatty acid receptors, which influence gut hormone secretion [209, 210]. Although SCFAs influence many aspects of host metabolism, glucose metabolism is directly regulated by SCFAs via hormone signaling, modulation of gut barrier function, and more [211]. Additionally, propionate can be directly taken up and utilized by the liver and intestines to serve as a precursor for gluconeogenesis.

SCFAs are generally associated with improved metabolic outcomes. For example, colonic delivery of propionate to humans for 6 months drastically reduced body weight and adipose tissue in overweight humans [211]. Similar studies have also been performed with rodents in which administration of butyrate, propionate, acetate, or a mixture of all three significantly reduced body weight gain associated with HF diet feeding [209, 212]. However, conflicting evidence has also emerged suggesting that SCFAs may be associated with obesity and other

negative metabolic outcomes. For example, human subjects with obesity exhibit increased levels of SCFAs as compared to lean subjects [213], and an "obese" gut microbial community in leptin-deficient rodents has also been shown to produce increased SCFA levels [151]. Additionally, GF mice are resistant to DIO, yet these animals are almost completely devoid of SCFAs, apart from acetate which can also derive from the host. While mechanisms are still coming forth, it is possible that differential timing of SCFA production and delivery can have specific effects on the host; if the diurnal pattern of delivery is altered or disrupted, perhaps due to circadian disruption, negative metabolic consequences could arise.

In this regard, SCFAs display an additional layer of regulation via their interactions with the host circadian system. Leone *et al.* showed that butyrate and propionate levels in cecal and fecal contents from C57BL/6J WT mice exhibit diurnal oscillations in abundance under regular chow feeding, which are lost under HF diet [141]. This was validated by quantitative measurement of key microbial genes responsible for butyrate production, which displayed significant oscillation in regular chow but not HF dietary conditions. To explore direct effects on hepatic regulation, Leone *et al.* also treated murine, hepatic-derived organoids with individual SCFAs, revealing that both butyrate and acetate can significantly shift the period of expression of major circadian genes. A similar experimental approach validated these findings *in vivo*; treatment of C57BL/6J WT mice with butyrate caused significantly altered ratios of in hepatic *Bmal1* and *Per2* gene expression patterns. This study provided support that microbially-derived SCFAs can directly modulate hepatic circadian gene expression, possibly serving as a mechanism by which gut microbes and peripheral circadian clocks regulate host metabolism.

Further work supports the notion that SCFAs and circadian rhythms are linked. Mice with global *Bmal1* knockout lack rhythmicity in fecal SCFA levels [214]. Treatment of murine intestinal organoids with individual SCFAs (acetate, butyrate, or propionate) directly induce phase delays of circadian clock gene expression, indicated by PER2::LUC expression, while

the SCFA formate did not induce these changes [215]. Tahara *et al.* showed that direct administration of SCFAs induced circadian entrainment in certain tissues in mice [216]. These studies also showed oral administration of mixed SCFAs to antibiotic-treated PER2::LUC mice induced significant phase changes in luciferase bioluminescence in peripheral tissues (kidney, liver, and submandibular gland), but only when administered at specific times of day. When treated with a single SCFA species, few significant phase shifts were observed, suggesting that a combination of mixed SCFAs is required for adequate circadian signaling. Jet-lagged mice given SCFA treatment entrained faster to a new LD cycle, implicating SCFAs in potential resetting of the central clock. Further, these studies revealed that exposure of GF mice to specific SCFAs directly modulates hepatic circadian gene expression. However, application of SCFAs directly to hepatic tissue ex vivo did not induce any changes in PER2 expression, implying that the complexity of an intact *in vivo* system is required for mediating signals involved in SCFA-peripheral circadian regulation.

1.5.2 Bile Acids

Derived from cholesterol, primary bile acids are synthesized in the liver, conjugated with either glycine or taurine residues to form primary bile salts, and delivered to and from the intestinal tract to facilitate dietary fat digestion and absorption [217]. Bile acids and salts are major regulators of metabolic pathways via activation of receptors, notably nuclear receptor farnesoid X receptor (FXR) and membrane receptor TGR5 [218]. Bile acids also play a role in regulating lipid metabolism by inducing expression of PPARα [219]. Of particular interest is the role that gut microbes play in bile acid metabolism and regulation. First, microbes have been shown to regulate hepatic expression of key rate-limiting enzymes involved in bile acid synthesis, including CYP7a1, CYP7b1, and CYP27a1, mediated by signaling in the ileum [220]. Second, although most primary bile acids are reabsorbed back into circulation, some undergo deconjugation of taurine and glycine residues and dehydroxylation by gut microbes,

resulting in secondary bile acids. Deconjugation of primary bile salts occurs primarily by taxa in the phylum Firmicutes via bile salt hydrolase (BSH) activity [221]. When absorbed systemically, secondary bile acids can act as signaling molecules in the host, such as via FXR or TGR5 activation, influencing host glucose and lipid homeostasis [222]. The bidirectional relationship between gut microbes and host-mediated bile acid profiles is particularly complex because they respond to and influence each other, and can be altered by additional cues such as diet [139]. These interactions can activate signaling pathways via the previously mentioned receptors and impact a wide array of host metabolic pathways, including cholesterol, glucose, and lipid homeostasis [217]. Bile acids also can act as AMPs, or stimulate release of other AMPs via FXR [223, 224], suggesting a role in innate immune function. Inflammation, energy expenditure, atherosclerosis, and thermogenesis are also known to be impacted by bile acid signaling [225, 226].

Microbial modifications of host-derived bile acids have also been shown to influence circadian gene expression [227], providing additional evidence of a direct link between gut microbiota and circadian rhythms on host metabolism. On the host side, several key enzymes in bile acid synthesis exhibit diurnal expression patterns following regulation by core circadian clock genes [228, 229]. In mice, both primary and secondary bile acids exhibit significant oscillations in abundance in circulation, with peak levels occurring near the end of the dark phase, whereas unconjugated bile acid levels peak during the light phase [230]. This indicates that altered microbial regulation of bile acid metabolism occurs at different times in the murine circadian cycle. Similar patterns were also observed in liver bile acid levels, implying that gut microbes can influence key metabolic organs in peripheral clocks via shifts in bile acids, and potential perturbations to either bile acid synthesis or gut microbes could significantly impact the host.

Circadian disruption in mice by sleep disruption, TRF, or global knockout of core clock genes significantly alters expression of key genes involved in bile acid regulation

[228, 231, 232]. BSH activity among gut microbiota induces significant changes in host lipid metabolism and circadian rhythm gene expression in both ileum and liver tissue [233]. Increased BSH activity reduces body weight, serum cholesterol, and liver triglycerides, supporting the notion that deconjugated bile acids derived from gut microbes directly influence host metabolic physiology. It has also been shown that GF mice monocolonized with bacteria lacking functional BSH revealed different changes in metabolism as well as both hepatic and intestinal gene expression, including circadian rhythm genes, as compared to strains containing functional BSH [234]. Another study measured circadian gene expression *in vitro* (immortalized Caco-2 cells) and *in vivo* (C57BL/6 mice) settings following treatment with conjugated versus deconjugated bile acids [227]. Unconjugated bile acids uniquely induced significant oscillation in circadian gene expression *in vitro*. Similarly, *in vivo* exposure also altered ileal, colonic, and hepatic gene expression, although the presence of significant oscillation patterns could not be determined because only one timepoint for data collection was performed. This work showed that direct exposure to microbially-altered bile acids shifts peripheral circadian clock gene expression, implying the potential circadian influence of certain bile acids on a complex host *in vivo*, but requires further investigation to validate these findings.

1.5.3 Antimicrobial Peptides

Antimicrobial peptides (AMPs) are molecular components produced by IECs that act as an innate immune defense to prevent aberrant microbial growth and infection by commensals [235]. This is particularly important in the gastrointestinal tract where such a high density of microbes resides and exhibits close contact with the host. Production of AMPs is induced by a few different mechanisms; some are constitutively expressed such as α-defensin, and others are induced by TLR-MyD88 signaling and IL-22 derived from innate lymphoid cells [236]. AMP mechanisms of action vary from physically targeting the bacterial cell wall

to enzymatically inducing immune reactions within the microorganism. The production of AMPs, primarily by enterocytes and Paneth cells [237], can also shift in response to changes in microbial composition [238]. For example, metabolic disruption in mice via HF feeding correlated with significant decreases in key AMPs, including Regenerating islet-derived protein 3 gamma (REG3γ), lysozyme, and angiogenin 4, while inflammatory cytokines were significantly upregulated in the small intestinal epithelium [239]. Conversely, overexpression of the AMP *Reg3*γ can induce significant changes in both small bowel gut microbial community membership and anti-inflammatory macrophage populations [240].

Interestingly, intestinal expression of *Reg3*γ exhibits diurnal patterns that are regulated by the gut microbiome. Absence of these microbial signals, such as in GF or antibiotic-treated mice, results in an overall loss of oscillating *Reg3*γ intestinal expression [187, 190]. Diurnal REG3γ appears to be mediated by the circadian component *Rev-Erb*α and *ROR*α via TLR4/STAT3 and NF-κB signaling that requires the presence of gut microbes. Diurnal *Reg3*γ expression is also responsible for rhythmic patterns of bacterial adherence to the proximal colonic mucosal surface, which associates with rhythmic metabolic gene expression in the intestine [181]. GF mice mono-colonized with mouse-derived gram-positive segmented filamentous bacteria (SFB) exhibited diurnal rhythmicity in bacterial abundance and localization to the mucus layer [181, 187]. SFB mono-colonization also restores oscillatory colonic gene transcriptional patterns resembling SPF mice, which requires *Reg3*γ [181]. A functional host circadian clock is also required for diurnal *Reg3*γ expression and SFB epithelial attachment, perhaps via food intake patterns [187]. These studies demonstrate an intricate circadian cross-talk between specific microbes and the innate immune component *Reg3*γ. Additional host metabolic implications of diurnal interactions between *Reg3*γ and gut microbiota are presented and discussed in Chapter 4.

1.6 Current Challenges and Gaps in Knowledge

Although significant progress has been made to elucidate the mechanistic interactions between circadian rhythms and the microbiome, there remain many gaps in knowledge. Not only is each system incredibly complex alone, but their interactions are essentially a set of positive feedback loops; one system signals to the other, causing the other to respond and signal back to the first one. This is demonstrated by evidence showing that when either system is impaired, the other is subsequently affected. For instance, when key circadian genes are knocked out in mice, shifts in gut microbiota ensue [180]; similarly, GF mice exhibit impaired circadian gene expression patterns in absence of microbial cues [141].

This brings about the question of how the hierarchy of these systems develop and interact with one another. If the ultimate goal is to manipulate one or both of these systems to improve or reset metabolic health, hierarchical drivers and downstream processes must first be thoroughly defined in the proper context and relative to time of day. Where and when does one intervene in such a dynamic and complex circuit? What are the central drivers that can be manipulated with accuracy and precision? In the absence of central drivers, how does the emergence of secondary drivers contribute to reprogramming of the host in the context of disease states associated with the microbiome or circadian disorganization? Similar to obesity, diseases such as aging [241], type 2 diabetes [180], colorectal cancer [242], and inflammatory bowel diseases [243] exhibit unique microbiome and circadian profiles, but therapies that target or attempt to reset these altered profiles will not be possible until the key drivers, either primary, secondary, or tertiary, are identified and characterized. In addition to gastrointestinal and metabolic diseases, neurological disorders are also of interest in this context through connections via the gut-brain axis, the microbiome serving as a major signaling component of the gut and the central circadian clock housed in the brain. For example, hepatic encephalopathy is associated with both severe changes in gut microbiome function [244] and central circadian disorganization [245], so it follows that functional alter-

ations of either or both would influence each other and the host in turn. However, it remains unknown how the circadian-microbiome network influences manifestation of the disease, or how commonly prescribed antibiotic treatments affect these interactions. These questions remain elusive and further progress in the circadian-microbiome research field are hindered by challenges presented by time and space.

To understand temporal relationships between host-microbe events, frequent and accurate time sequence samples must be obtained from specific locations. Reliance on stool for human microbiome sampling is limiting in this regard because subjects are rarely able to provide multiple samples throughout the day and night. Transit time through the colon can vary considerably among individuals and is usually on the order of hours, confounding any attempt to correlate microbiome changes with blood and biological assessments made elsewhere in real time. It is also technically infeasible to sample microbiomes of other intestinal regions that exhibit vastly different community profiles and functions. Finally, the inter-individual variations of the gut microbiome are enormous, making any type of cross-sectional analysis of human populations difficult to power and perform. For host circadian-microbiome studies, strong consideration should be given to longitudinal study designs where time-sequence samples of individual subjects are obtained and where they serve as their own controls. As mentioned above, sequential stool samples from human study subjects are very difficult to obtain. An alternative is to sample from the beginning of the GI tract – specifically the salivary microbiome where time sequence samples can be readily obtained. A recent human study demonstrated a correlation between food intake patterns and diurnal variation in microbiome abundance via repeat-sampling of saliva, validating the relevance of circadian-microbiome murine studies, in which repeat-sampling is much more feasible, in humans [198].

Many of the challenges associated with human studies can be circumvented by using animal models where time-relevant events from host tissues and regional gut microbiomes

are more readily assessed. However, these studies often require large numbers of animals to be sacrificed at specific time points within a 24-48 hour period under highly controlled environmental and feeding conditions. Inbred mice commonly used in most circadian studies are nocturnal, awake and eating during the dark phase and sleeping and inactive during the light phase – species variations from humans that could result in significantly different temporal relationships between microbes and host. On the other hand, time-sequence stool collections can be performed on individually-housed animals, providing opportunity to assess changes in colonic microbiota over time.

Yet another complex layer of these interactions is the sexual dimorphism of both the microbiome and host circadian expression patterns. Microbiome profiles in mice differ significantly by sex, and the effects of gonadectomy of both males and females depend upon dietary content [246]. Sexual dimorphism is also observed in reference to circadian rhythms; gonadectomy of male mice drastically reduces locomotor activity in comparison to females, and testosterone treatment eliminates that difference [247]. In contrast to males, female mice are resistant to DIO and retain normal activity and feeding rhythms, an effect that is lost upon ovariectomization [248]. Mice also exhibit sexual dimorphism in hepatic gene expression of key metabolic genes, while those differences are lost in *Cry1/2* knockout mice [249]. The circadian rhythm-microbiome dynamic also presents sexual dimorphism. Female mice exhibit more significant microbial oscillations in stool than male counterparts; this difference is lost in *Bmal1* global knockout mice [178]. More recently, Weger *et al.* showed that many of the differences in hepatic diurnal gene expression patterns between the sexes in mice are lost in GF conditions [188]. Understanding how sex and sex hormones affect diurnal microbiome patterns may be crucial to elucidating how these systems communicate and develop relationships. Integration of large-scale sequencing and metabolomics studies may inform on how sex hormones and sexual development play such a major role in circadian-microbiome interactions and influence on host metabolism.

Together, the specific mechanisms underlying how local, gut microbial oscillations are sustained and maintained is complex and still poorly understood. What are the dynamics and factors that orchestrate host-microbiome circadian cross-talk? When one system or mediator is eliminated, how does the other system compensate and what are the resulting host metabolic or physiological outcomes? Do mucosal immune cells or factors initiate diurnal patterns of gut microbes, or do microbially-associated metabolites drive host factors? The main objective of this thesis was to shed light on these gaps in knowledge relating to the functional hierarchy of host circadian drivers that are mediated by gut microbiome. We hypothesized that reciprocal interactions between the host and gut microbiota differentially impact their diurnal patterns, resulting in differential host metabolic outcomes and programming.

CHAPTER 2

MATERIALS AND METHODS

2.1 Experimental Models

2.1.1 Mice

All animal protocols and experimental procedures were approved by the University of Chicago Institutional Animal Care and Use Committee (IACUC), and performed in the University of Chicago animal vivarium.

For data presented in Chapter 3, all mice used were on a C57BL/6J background. Specific pathogen-free (SPF) *Bmal1*$^{fl/fl}$ (B6.129S4(Cg)-*Arntl*^{tm1Weit}/J; Strain #007668; The Jackson Laboratory) and Albumin-Cre (AlbCre) (B6.Cg-*Speer6-ps1*$^{Tg(Alb\text{-}cre)21Mgn}$/J; Strain #003574; The Jackson Laboratory) male and female mice were bred in-house as described in Lamia *et al.* [130]. SPF *Bmal1*$^{fl/fl}$-AlbCre mice were re-derived under germ-free conditions and maintained in flexible film isolators (CBC Ltd. Madison, WI, USA) in the UChicago Gnotobiotic Research Animal Facility. SPF *Bmal1*$^{fl/fl}$ mice were crossed with CamiCre mice (a generous gift from Dr. Joseph Takahashi, as described in [117]) to achieve forebrain-specific knockout of Bmal1. All mice were maintained under standard 12:12 LD conditions (lights on beginning at 6am, Zeitgeber Time (ZT) 0) and fed autoclaved *ad libitum* JL Rat and Mouse/Auto 6F 5k67 (LabDiet, St. Louis, MO, USA) for at least 2 weeks prior to and throughout all experiments. Body weight and food consumption were monitored weekly throughout the studies. At 10-14 weeks of age, mice were acclimatized to individual housing for 14 days, after which stool was collected every 6 hours for 48 hours. After 3 weeks, mice were sacrificed via CO2 asphyxiation followed by cervical dislocation over a 24-hour period at six ZT time points: ZT2=8 AM, ZT6=12 PM, ZT10=4 PM, ZT14=8 PM, ZT18=12 AM, and ZT22=4 AM. Immediately prior to sacrifice, basal blood glucose was measured from tail snip blood via Accu-Check Compact Plus Diabetes Monitoring Kit and test strips (Roche

Diagnostics, Indianapolis, IN, USA), or OneTouch Ultra 2 Blood Glucose Monitoring System (OneTouch, LifeScan, Malvern, PA, USA). Blood lactate was measured from tail snip blood via Lactate Plus Meter and test strips (Nova Biomedical, Waltham, MA, USA). Blood was also collected via heparin-coated microvette tubes (Sarstedt, Numbrecht, Germany) for insulin measurement by the Ultra-sensitive Insulin ELISA (ALPCO). Liver, plasma, brain, and intestinal luminal contents were snap frozen in liquid nitrogen and stored at -80C.

For data presented in Chapter 4, specific pathogen-free (SPF) C57BL/6J (Stock#000664; The Jackson Laboratory) male mice, aged 8-10 weeks, were utilized. Male, age-matched SPF *MyD88*$^{+/-}$, *MyD88*$^{-/-}$ (B6.129P2(SJL)-*Myd88*$^{tm1.1Defr}$/J; Stock#009088; The Jackson Laboratory), *Reg3γ*$^{+/-}$ and *Reg3γ*$^{-/-}$ (B6.129-*Reg3g*$^{tm1.1Lvh}$/J; Stock#017480; The Jackson Laboratory), as well as germ-free WT mice on a C57BL/6J background, were purchased and bred in-house. *Reg3γ*$^{+/-}$ and *Reg3γ*$^{-/-}$ mice were cohoused up until the onset of experimental manipulations. GF mice were maintained in plastic flexible film isolators (CBC Ltd. Madison, WI, USA). All mice were held under standard 12:12 LD conditions (lights on beginning at 6am, Zeitgeber (ZT) 0), individually housed and fed *ad libitum*. After two weeks acclimatization, mice were allotted to one of two dietary treatments: regular, low-fat (RC) chow (10% dietary fat, TD.2018S, Envigo, Madison, WI, USA) or high fat (HF) diet (37.4% dietary fat, TD.97222, custom diet, Envigo, Madison, WI, USA) (see supplemental information in Leone *et al.* [141] for detailed dietary components). GF diets were irradiated and tested before and after experiments for sterility. Body weights and food consumption were monitored weekly throughout the study. After 4 weeks, mice were sacrificed via CO2 asphyxiation followed by cervical dislocation over 24 hours at six ZT time points: ZT 2=8 AM, ZT 6=12 PM, ZT 10=4 PM, ZT 14=8 PM, ZT 18=12 AM, and ZT 22=4 AM. Luminal contents and mucosal scrapings were snap frozen in liquid nitrogen and stored at -80C until further analyses.

2.1.2 Preparation of isolated epithelial cells

A modified version of the Weiser method was utilized to isolate epithelium from the villus-crypt axis [250]. Briefly, the distal 11cm of the ileum was isolated from RC or HF-fed male mice at ZT2 or 10. Sections were perfused with ice cold PBS plus 1mM DTT, followed by eversion, tied at one end, and filled to distension with ice cold PBS. Ileal segments were then incubated at 37°C for 15min in 15mL citrate buffer , followed by transfer to a PBS buffer containing 1.5mM EDTA, 0.5mM DTT, and 1mg/mL bovine serum albumen and shaken at 175 RPM at 37°C for 10 min. Intestinal segments were then transferred to fresh PBS buffer solution and incubated nine consecutive times for 10, 6, 5, 5, 9, 10, 15, 25, and 30 min., respectively as previously described [251]. Fractions 1-4 and 5-8 were pooled and considered villi while fraction 9 was considered crypt, containing Paneth cells. Combined fractions were spun for one minute at 13,000G and resuspended in Trizol, followed by RNA extraction and cDNA synthesis for qPCR analysis as described below.

2.1.3 Enteroid culture

Enteroids were grown as previously described [252]. Briefly, the distal 11cm of the SI was removed from male GF or SPF C57BL/6J WT, *MyD88*$^{+/-}$, or *MyD88*$^{-/-}$ mice and opened longitudinally. Tissues were rinsed in ice-cold PBS to remove contents. A glass slide was used to gently remove the villi, and the mucosa was minced into 1- to 2-mm pieces with a scalpel and collected into 10ml of ice-cold PBS. Pieces were agitated and rinsed several times using a serum-coated serological pipette. Intestinal pieces were resuspended in 25ml of ice-cold 2.5 mM EDTA-PBS and rotated at 4°C for 30min. Following incubation, EDTA-PBS was replaced with 10 ml of Advanced DMEM/F12 (ADF) medium (Thermo Scientific). After gently disrupting with a pipette three times, supernatant was discarded and fresh ADF medium was added and repeated three times. Cells were centrifuged at 300 g at 4°C for 5 min, resuspended in 10ml ADF medium, and passed through a 70-μm cell strainer to

remove debris. Cells were centrifuged at 300 g at 4°C for 3 min and resuspended in complete ADF medium containing GlutaMAX (Thermo Scientific), HEPES buffer (Thermo Scientific), penicillin-streptomycin (Thermo Scientific), N2 supplement (Thermo Scientific), B-27 Supplement Minus Vitamin A (Thermo Scientific), murine EGF (50 ng/ml; Thermo Scientific), noggin (100 ng/ml; Peprotech, Rocky Hill, NJ), jagged-1 (1 μM; Anaspec), Y27632 (10 nM; Cayman Scientific, Ann Arbor, MI, USA), and R-spondin-1 (500 ng/ml; Peprotech). The cell pellet was resuspended in a ratio of 1:2 ADF to Matrigel (BD Biosciences, San Jose, CA, USA) and plated onto a pre-warmed, collagen-coated, 24-well-plate. Matrigel beads were allowed to solidify for 1hr at 5% CO2 at 37°C before adding 500 μl ADF culture media.

2.1.4 Bacterial culture

Strains *Enterococcus faecalis* (ATCC #BAA-2128), *Escherichia coli* K12 (ATCC #PTA-7555), *Lactobacillus rhamnosus GG* (ATCC #53103), *Lactobacillus reuteri* (isolated in-house, Accession #NR_075036.1), *Lactobacillus intestinalis* (isolated in-house, Accession #NR_025449.1), *Lactobacillus murinus* (isolated in-house, Accession #NR_112689.1), *Lactobacillus johnsonii* (isolated in-house, Accession #NR_117574.1), *Peptoanaerobacter stomatis* Sizova (ATCC #BAA-2664 CM2), *Peptostreptococcus anaerobius* (ATCC #27337), and *Bacteroides thetaiotamicron* (ATCC #29148) were streaked out from frozen glycerol stocks onto agar-containing plates of either brain heart infusion media (BHI, *E. faecalis*), Luria-Bertani media (LB, *E.coli* K12), BHI-Supplemented media (BHIS, *P. stomatis* Sizova), RCM media (*P. anaerobius*), or de Man, Rogosa and Sharpe media (MRS, *Lactobacillus* strains). Single colonies were inoculated into their respective liquid media and cultivated under aerobic or anaerobic conditions (Coy Laboratory Products, Inc., Grass Lake, MI) at 37°C for 24-48 hours. Genomic DNA of indigenous strain *L. reuteri*, *L. intestinalis*, *L. murinus*, and *L. johnsonii* were isolated from individual colonies. Forward and reverse 16S rRNA gene sequences were obtained using universal PCR primers (16S_universal_F and 16S_universal_R;

Table 2.1), joined, and BLAST results were used to identify most closely related species.

2.1.5 Conventionalization studies

For conventionalization, fresh stool from adult C57BL/6J male mice was collected and immediately resuspended in sterile PBS (100mg stool/1mL PBS) and vortexed, followed by a brief spin to remove debris. Individually housed GF *Bmal1*$^{fl/fl}$ or *Bmal1*$^{fl/fl}$-AlbCre 11- to 13-week-old *ad libitum*-fed male mice were orally gavaged with 150 μL of this suspension. Body weights and food consumption were monitored weekly.

2.1.6 Monoassociation studies

LGG and *L. reuteri* were streaked from frozen glycerol stocks onto MRS agar plates and incubated at 37°C. Single LGG or *L. reuteri* colonies were used to inoculate 5mL of MRS or BHIS broth and grown overnight under static conditions at 37°C either under microaerophilic (5% CO2) or in an anaerobic chamber (Coy Laboratory Products, Inc., Grass Lake, MI). The next day, cells were passaged 1/50 into fresh MRS or BHIS and grown to an O.D. of 0.4-0.6 nm. Cells were pelleted at 10,000 RPM for 20min at 4°C and resuspended in reduced PBS. 8–12-week-old GF C57BL/6J male mice were fed and maintained on RC or HF in flexible film isolators for 4 weeks. After 1 week of diet switch, each mouse received 1.74 x10^8 CFUs via gavage in 100μL. Colonization was confirmed in fecal pellets. Serial dilutions of both gavage solution as well as fecal pellets from monoassociated mice after 4 weeks were plated onto MRS or BHIS agar and incubated at 37°C anaerobically. Mice monoassociated with LGG exhibited an average colonization of 2.85x10^9 $\pm$ 1.79x10^9 CFUs/gram of feces and *L. reuteri* mice were colonized with 2.14x10^8 $\pm$ 2.72x10^7 CFUs/gram of stool.

2.1.7 Antibiotic-treatment studies

For antibiotic treatment, SPF *Bmal1*$^{fl/fl}$ or *Bmal1*$^{fl/fl}$-AlbCre 11- to 13-week-old male mice were administered an antibiotic cocktail consisting of vancomycin (0.5 mg/mL), neomycin (1 mg/mL), and cefoperazone (0.5 mg/mL) prepared in autoclaved water and sterile-filtered. The protocol involved using a combination of daily gavage for 7 days followed by incorporation and *ad libitum* delivery in drinking water for 1 additional week. Body weights were monitored daily.

2.1.8 Primary hepatocyte isolation and culture

Isolation and culture of primary hepatocytes was performed as described in http://mouselivercells.com. 15-week-old SPF and GF *Bmal1*$^{fl/fl}$ and *Bmal1*$^{fl/fl}$-AlbCre male mice were anesthetized (90 mg ketamine/kg body weight, 6 mg xylazine/kg body weight), perfused via portal vein cannulation with Collagenase Type IV (Worthington Biochemical) *in situ*, digested in low-glucose DMEM (Corning), and isolated in high-glucose DMEM (Gibco). Live hepatocytes, determined via Trypan blue exclusion, were seeded at a density of 600,000 hepatocytes in 6-well collagen-coated plates (Thermo Scientific) and cultured in low-glucose DMEM (Corning) for two days with daily media change prior to initiating downstream assays.

2.2 Method Details

2.2.1 Western blot

For Western blots presented in Chapter 3, liver and brain tissue (5-10 mg) were collected at ZT16 and placed in 250-500 μL of ice-cold RIPA lysis buffer (Thermo Scientific RIPA Lysis and Extraction Buffer, cOmplete Mini Protease Inhibitor Cocktail, 100μM PMSF). Protein concentrations were determined via Bicinchoninic Acid (BCA) Protein Assay (Thermo

Scientific) and 30μg of protein was separated on 4-20% Mini-PROTEAN gel (Bio-Rad) and transferred to a PVDF membrane (Millipore). Membranes were blocked with 5% nonfat milk in Tris-buffered saline (TBS) (20 mM Tris pH7.6, 150 mM NaCl) and incubated overnight at 4°C in 5% nonfat milk in TBS-Tween (TBS-T) (20 mM Tris pH7.6, 150 mM NaCl, 0.1% Tween-20) containing primary antibodies: anti-BMAL1 (1:1000; Abcam, #ab93806) or anti-GAPDH (1:100000; Invitrogen, #AM4300). Membranes were washed 6 times for 5 min in TBS-T and incubated for 1 hour at room temperature in TBS-T containing 5% nonfat milk and either anti-mouse or anti-rabbit secondary antibody (1:10,000; Abcam, #7076S and #7074S respectively). Membranes were washed 6 times for 5 min each in TBS-T, developed with SuperSignal West Pico PLUS Chemiluminescent Substrate (Thermo Scientific), and exposed using the Chemi-Doc MP Imaging System (Bio-Rad Laboratories, Hercules, CA, USA). Analysis was performed using ImageJ [253].

For Western blots presented in Chapter 4, 5 mg of tissue from distal ileal mucosal scrapings was lysed in 250 μL of ice-cold protein lysis buffer (Cell Signaling Technology Cell Lysis Buffer, cOmplete Mini Protease Inhibitor Cocktail, Sigma-Aldrich, 100µM PMSF). 20-30μg of protein extract was separated on a 4-20% precast polyacrylamide gel and transferred to a PVDF membrane (Millipore). Membranes were blocked with 5% nonfat milk in Tris-buffered saline (TBS) (20 mM Tris pH7.6, 150 mM NaCl) and incubated overnight at 4°C in 2% nonfat milk in Tris-buffered saline -Tween (TBS-T) (20 mM Tris pH7.6, 150 mM NaCl, 0.1% Tween-20) containing primary antibodies: anti-REG3γ (1:500; Abcam #ab198216), anti-GAPDH (1:1000; Invitrogen #AM4300). Membranes were washed three times for 5 min in TBS-T and incubated for 1hr at room temperature in 2% nonfat milk in TBS-T containing goat anti-rabbit Alexa Fluor 680 (1:100,000 Abcam #ab175773) and Donkey anti-mouse Alexa Fluor 790 secondary antibody (1:100,000 Abcam #ab186699). Membranes were washed three times for 5 min each in TBS-T and imaged using the LI-COR Odyssey (LI-COR Biosciences). Analysis was performed using ImageJ [253].

2.2.2 Quantitative Real-time PCR

Total RNA was isolated by homogenizing tissue using TRIzol (1559018, Ambion, Hampton, NH) and chloroform extraction method, as previously described [141]. RNA purity was validated through UV-Vis spectrophotometry via Nanodrop Lite (Thermo Scientific, Wilmington, DE, USA). 1μg of total RNA was reverse-transcribed to complementary DNA (cDNA) using the Transcriptor First Strand cDNA Synthesis Kit (Roche, Indianapolis, IN, USA) according to manufacturer's instructions. Relative quantification of gene expression was performed using a LightCycler 480 Real-Time PCR System (Roche) or a CFX384 Touch Real-Time PCR Detection System (Bio-Rad). Forward and reverse primers were combined with SYBR Green PCR Supermix (Bio-rad) and nuclease-free water to amplify the following host-specific gene expression: *Reg3*γ, *Lysozyme1*, *Cryptidin4*, *Ang4*, *Tlr1, 2, 3, 4, 9*, *Clock*, *Bmal1*, *Per1-3*, *Cry1-2*, *Muc2*, *Sucrase Isomaltase*, and *Gapdh*. Gene expression data are presented as $2^{-\Delta Ct}$ (housekeeping gene – target gene), where the house-keeping gene is *Gapdh*. Quantification of the following microbial genes in DNA extractions of stool samples were also performed using a CFX384 Touch Real-Time PCR Detection System (Bio-Rad): 16S (universal and Earth Microbiome Project), butyryl-CoA:acetate CoA-transferase (*but*) [254], dissimilatory sulfite reductase (*dsrAB*) [139], and taurine:pyruvate aminotransferase (*tpa*). Oligonucleotide sequences are listed in Table 2.1.

2.2.3 Tissue histology and immunofluorescence

For immunofluorescence, sections were fixed in 4% paraformalydehyde overnight. Fixed tissue sections were processed (Tissue-Tek VIP, Sakura Finetek, Torrance, CA) and embedded in paraffin. Five µm sections were cut and mounted on charged glass slides, and deparaffinized. To visually localize and semi-quantitatively measure REG3γ protein within the ileal epithelium and Paneth cells, immunofluorescence was performed on paraformalydehyde-fixed sections. Following deparaffinization and rehydration, antigen retrieval was performed

by boiling slides in a 10 mM/L sodium citrate bath (pH 6.0). Slides were then blocked with 10% bovine serum albumin (BSA)-PBS for 1hr. Samples were incubated with primary antibody for Lysozyme (1:400, rat monoclonal IgG, Abcam #ab108508) or REG3γ (1:500, rabbit polyclonal IgG, Abcam #ab198216) overnight in 1% BSA-PBS at 4°C in a humidified chamber. Remaining solutions were washed and samples were incubated with respective secondary antibodies in 1% BSA-PBS (1:1000, Alexa Fluor 594; Invitrogen). Slides were imaged following DAPI staining and coverslip placement.

2.2.4 16S DNA extraction, sequencing, and analysis

For data presented in Chapter 3, stool was beadbeaten using 0.1-mm-diameter zirconia/silica beads (BioSpec Products, Bartlesville, OK, USA) as previously described [141]. Supernatants were extracted using equal volumes of Phenol:Chloroform:Isoamylalcohol (25:24:1; Ambion, Austin, TX, USA) and DNA precipitated using an equal volume of 100% isopropanol. DNA concentration was measured using the Quant-iT PicoGreen dsDNA Assay kit (Invitrogen, Grand Island, NY) and diluted to 1-20 ng/μL. The V4-V5 region of the 16S rRNA encoding gene was amplified using standard Earth Microbiome Project protocols. Sequencing was performed at the High-Throughput Genome Analysis Core (HGAC; part of the Institute for Genomics and Systems Biology [IGSB]) at Argonne National Laboratory. Paired-end reads were imported into Quantitative Insights Into Microbial Ecology version 2 (QIIME2) software suite [255] (https://qiime2.org) and demultiplexed using Dada2 [256]. To maximize sampling depth while prioritizing equal retention of samples across groups, 10598 (48-hr fecal collection) or 15578 (co-housing vs separate housing fecal collection) reads were included per sample, determined by the mean subtracted by 1.5 times standard deviation of sample read counts across all samples within experiment. Taxonomy was compiled using the classify-sklearn plugin with Silva database version 132 2020.8 [257, 258]. Raw sequencing reads are deposited at NCBI (Accession #PRJNA815335).

For data presented in Chapter 4, distal ileum luminal contents and mucosal scrapings were collected in screw cap tubes as previously described in DNA lysis buffer [141]. After addition of 0.1-mm-diameter zirconia/silica beads (BioSpec Products, Bartlesville, OK, USA), samples were disrupted using a Mini-Beadbeater-8k Cell Disrupter (BioSpec Products). Supernatants were extracted with an equal volume of Phenol:Chloroform:Isoamylalcohol (25:24:1; Ambion, Austin, TX, USA) and DNA precipitated using an equal volume of 100% ethanol. DNA concentration was then measured via Nanodrop Lite (Thermo Scientific, Wilmington, DE, USA) and subsequently diluted to 25 μg/μl. The V4-V5 region of the 16S rRNA encoding gene was amplified using standard Earth Microbiome Project protocols. Sequencing was performed at the High-Throughput Genome Analysis Core (HGAC; part of the Institute for Genomics and Systems Biology [IGSB]) at Argonne National Laboratory. Forward and reverse reads were joined, trimmed and aligned using EA-utils, then classified using the Quantitative Insights Into Microbial Ecology (QIIME) toolkit [259]. OTUs were picked at 97% sequence identity using open reference OTU picking protocol against the Greengenes database. These representative sequences were aligned using PyNAST, taxonomy was assigned using the RDP Classifier, and rarefaction was performed at a depth of 35,000. The PyNAST-aligned sequences were also used to build a phylogenetic tree with FastTree and Bray Curtis and Canberra distances were used to statistically compare beta-diversity, and visual comparisons were performed via Principal Coordinate Analysis (PCoA) ordination. To evaluate which microbial taxa exhibited rhythmic oscillations, empirical-JTK cycle with asymmetry (eJTK) software was implemented [260]. Spearman and Pearson correlation was performed to determine which microbial taxa were correlated with host *Reg3*γ gene expression. Analysis and Visualization Platform for 'Omics data (anvi'o) [261] was used to create at heatmap for visually assessing 16S rRNA gene changes in taxonomic membership and abundance by diet and ZT. Raw sequencing reads are deposited at NCBI (Accession #SRP187770).

2.2.5 Bacterial gene quantification

16S rRNA gene copy number was determined from intestinal contents and stool as previously described [141, 254, 262]. The 16S rRNA gene was quantified using a standard curve for gene copy number using primer sequences cloned into a PCR4-TOPO plasmid. For Chapter 3, Earth Microbiome Project primers were used (16S_F, 16S_R); for Chapter 4, 16S_universal_F and 16S_universal_R were used (see Table 2.1 for sequences).

2.2.6 Enteroid stimulation with bacterial culture conditioned media

Stimulation of enteroids with bacterial culture media was performed by adding 10% of filter-sterilized conditioned media collected from stationary-phase *Lactobacillus rhamnosus GG* (ATCC 53103), *L. reuteri*, *P. stomatis* (ATCC BAA-2664 CM2), or *P. anaerobius* to complete ADF enteroid culture media. Some conditioned media was size fractionated using Amicon® Ultra-15 Centrifugal Filters to less than 30, 10, or 3kDa (Sigma-Aldrich) and heat-treated at 100°C for 2 hours [263] prior to enteroid stimulation. Conditioned media treatment was compared to blank sterile-filtered media controls. Treated enteroid culture plates were kept at 5% CO_2 at 37°C until collection at 6, 12, and 24 hours post-treatment. RNA collection, cDNA synthesis, and qPCR analysis were performed as described above.

2.2.7 REG3G bactericidal assay

Recombinant REG3γ (rREG3γ) was prepared as previously described [264] and stored at -80°C. *E. faecalis*, *E. coli* K12, LGG, *Peptostreptococcaceae*, *Bacteroides Thetaiotamicron*, and *L. reuteri* were re-inoculated into fresh media and incubated at 37°C to mid-log phase. Cultures were spun, resuspended in standard assay buffer (10mM MES pH6, 25mM NaCl), re-pelleted, and diluted 1:25 in standard assay buffer. rREG3γ (0μM, 5μM, 10μM, 20μM) was added followed by incubation at 37°C for 2 hours. After 2hr, dilution plating (1:10 and 1:100) was performed on agar media plates and incubated at 37°C for 24-48 hours

under aerobic or anaerobic conditions. Colony forming units (CFUs) were determined and the average % remaining bacteria was calculated relative to 0μM CFUs for each respective bacterial strain.

2.2.8 LC-MS/MS for the detection of small molecules in bacteria conditioned media

Samples were thawed on ice and 50 μL was transferred to a microcentrifuge tube for extraction. To each sample, 200 μL cold methanol was added (80% final concentration v/v). Samples were vortexed for 10 s, and then centrifuged at 14,000 x g for 5 min at 4°C to precipitate any protein. 100 μL of the supernatant was dried by vacuum concentration in amber glass autosampler vials and resuspended in 50 μL of 30% Acetonitrile/70% H2O (v/v). For LC-MS analysis, 10 μL of extract was injected by a Vanquish Split Sampler HT autosampler (Thermo Scientific) onto an Acquity CSH C18 column held at 50°C (100 mm x 1 mm x 1.7 μm particle size; Waters) using a Vanquish Binary Pump (60 μL/min flow rate; Thermo Scientific), using a gradient as previously described [265]. Mobile phase A was 0.2% formic acid in water, and mobile phase B was 0.2% formic acid in IcanACN (90:10, v/v) with 5 mM ammonium formate. Mobile phase B was initially held at 0% for 1 min and then increased to 28% over 42 min. Mobile phase B was further increased to 66% over 6 min, then 70% over 1 min, then 80.5% over 5 min, then 85% over 2 min, then to 89.5% over next 5 min, raised to 91% over next 3 min, and finally raised to 100% over 5 min and held at 100% for 10 min. The column was then returned to 0% Mobile Phase over 2 min and re-equilibrated for 8 min before the next injection.

The LC system was coupled to a Q Exactive Orbitrap mass spectrometer through a heated electrospray ionization (HESI II) source (Thermo Scientific). For the first 50 min of analysis RF was set to 60, and for 50-90 min RF was set to 90. The MS was operated with polarity switching; positive mode source settings were as follows: ion capillary temperature

was set to 275°C, vaporization temperature was set to 300°C, sheath gas was set to 30 units, aux gas was set to 6 units, sweep gas was set to 0 units, spray voltage was set to |4.5 kV|. Negative mode source settings were as follows: ion capillary and vaporization temperature were set to 350°C, sheath gas was set to 25, aux gas was set to 15, sweep gas was set to 5, and spray voltage was set to |3.5 kV|. Alternating MS and MS2 spectra (Top2) were acquired for each polarity. For the first 0-50 min of analysis, full scans were acquired with scan range 75-1125 m/z for both positive and negative mode, with 35,000 resolution, 3×10^6 automatic gain control (AGC) target, 50 ms ion accumulation time (max IT), and 17,500 resolution, 1 x 10^5 AGC, 100 ms max IT for MS2. For 50-90 min, full scans were acquired with scan range 200-1600 m/z, with 35,000 resolution, 1 x 10^6 AGC, 100 ms maxIT, and 35,000 resolution, 1 x 10^5 AGC, and 50 ms max IT for MS2. For all MS2, the isolation window was set to 1.0 m/z, stepped normalized collision energy (NCE) to 20, 30, 40, and a 30.0 s dynamic exclusion.

The resulting LC–MS data were processed using Compound Discoverer 3.1 (Thermo Scientific) All peaks between 0 min and 49.5 min retention time, between 75 Da to 1275 Da MS1 precursor mass, and with signal-to-noise (S/N) greater than 1.5 were grouped into distinct chromatographic profiles, and aligned using a 15-ppm mass and 0.3 min retention time tolerance. Features were grouped using 15ppm tolerance, 100% Intensity Tolerance, 3 S/N threshold, and 1 x 100^6 minimum peak intensity. Peaks greater than 0.5 min or fewer than 5 scans per peak were excluded. Compounds were grouped with a 5ppm mass tolerance, 0.2 min retention time tolerance, and preferred ions were [M+H]+1; [M-H]-1. Fill Gaps node was used with 5ppm mass tolerance, 1.5 S/N threshold and 'use real peak detection' set to True. Features that were not 5-fold higher than blanks were excluded from further analysis. Compound annotations were made using mzCloud Search and predicted compositions using default settings in Compound Discoverer 3.1.

Raw LC/MS-MS data was deposited at MassIVE repository

(Accession #MSV000088248).

2.2.9 Tolerance tests

For data presented in Chapter 3, oral glucose (GTT) and intraperitoneal pyruvate (PTT) tolerance tests were performed on 12- to 16-week-old male GF and SPF mice, which were fasted overnight for 14 hours starting at ZT12, and tests were performed starting at ZT2. For insulin tests (ITT), mice were fasted for 5 hours, starting at ZT22 and ITT was performed starting at ZT2. For dark cycle PTT, mice were fasted during the day for 14 hours starting at ZT2 and PTT was performed starting at ZT14. Baseline blood glucose was measured via tail snip using a hand-held glucometer. Mice were administered either an oral bolus of 20% dextrose (Hospira) in sterile water solution (2g/kg body weight), an intraperitoneal (IP) injection of sterile-filtered sodium pyruvate (Sigma-Aldrich) in PBS (2g/kg body weight), or an intraperitoneal injection of 0.1U/mL Humulin R Insulin (Eli Lilly) in PBS (1U/kg body weight). For GTT and PTT, blood glucose was then measured at 15-, 30-, 60-, and 120-minutes post gavage or injection. For ITT, blood glucose was then measured at 15-, 30-, 60-, 90-, and 120-minutes post injection. During GTT, insulin levels were determined at baseline, 30, 60, and 120 minutes in blood collected in heparin-coated microvette tubes (Sarstedt, Numbrecht, Germany) using the Ultra-sensitive Insulin ELISA (ALPCO). Area under the curve (AUC) was calculated and compared between genotypes using GraphPad Prism v9.

For data presented in Chapter 4, male 8–10-week-old SPF mice were individually housed for 3 weeks. Mice were fasted overnight for 12 hours. A 20% glucose in water solution (2 g/kg body weight) was administered by intraperitoneal (IP) injection. Tail vein blood glucose was measured before and after intraperitoneal injection at 0, 15, 30, 60, and 120 minutes using a OneTouch Glucose Meter (ADW Diabetes, Pompano Beach, FL). Area under the curve (AUC) was calculated and compared between genotypes using GraphPad Prism v8.

2.2.10 Primary hepatocyte glucose production assay

Cultured mouse hepatocytes were serum-starved overnight and washed with PBS with $MgCl_2$ and $CaCl_2$ (Sigma-Aldrich). Hepatocytes were exposed to glucose-free DMEM (Sigma-Aldrich) (20 mM sodium lactate, 2 mM sodium pyruvate, 2 mM L-glutamine, 15 mM HEPES) with or without 0.1 mM pCPT-cAMP (Sigma-Aldrich) for 11 hours. Media was collected and glucose concentrations measured via Autokit Glucose enzymatic assay (FUJIFILM Medical Systems Inc, Lexington, MA, USA) and normalized to protein content determined via bicinchoninic acid (BCA) assay.

2.2.11 Glycogen assay

Frozen liver samples were weighed, and glycogen measurement was performed using the Glycogen Assay Kit II (Colorimetric) (Abcam, Cambridge, UK) following the published kit instructions.

2.2.12 Liver RNA extraction, sequencing, and analysis

Total RNA was isolated by homogenizing bulk liver tissue in TRIzol (Ambion, Hampton, NH) followed by chloroform extraction, as previously described [141]. RNA quality and quantity was assessed using the Agilent bio-analyzer and RNA-SEQ libraries were generated using the Illumina Stranded mRNA Prep at the UChicago Genomics Core Facility. Sequencing of mRNA directional, single-end 50 base pair reads was performed on the HiSEQ4000 with Illumina reagents and protocols. Data was demultiplexed using the Illumina bcl2fastq software. All 72 samples were run on 6 lanes, and fastq files were concatenated. Quality control was performed using FastQC v0.11.5 and MultiQC v1.10.1. Sequence alignment was performed by STAR version 2.6.1b by mapping to the mm10 whole genome [266]. Gene transcript counts were determined by Subread:featurecounts v2.0.0.

Differential analysis was performed via DESeq2, both on all timepoints pooled and within

each individual timepoint. Protein coding genes were identified via biomaRt (version 2.40.5) using GRCm39 mouse genes. Two-way analysis for each pair of experimental groups were performed. The Wald statistic, calculated via DESeq2 [267], was used to build a ranked list of genes for each comparison for each timepoint. Fast Gene Set Enrichment Analysis (fGSEA, version 1.10.1) [268] was utilized to identify differentially regulated pathways (with parameter nperm=10000) within multiple annotated gene sets from Molecular Signatures Database (MSigDB, version 7.0). Significantly identified pathways were filtered by adjusted $p < 0.05$, and subsequently binned into categories via custom R script. fGSEA was utilized to calculated normalized enrichment score (NES) and identify leading edge genes. For oscillation analysis, feature counts were normalized by variance-stabilizing transformation (VST) in DESeq2 (version 1.24.0). VST-normalized data was used for principal component analysis (PCA). VST-normalized data was analyzed to identify significantly oscillating transcripts via empirical JTK_CYCLE [260]. Heatmaps were generated from VST-normalized data, ordered by time of peak expression, and normalized by the median value for each transcript within each group over time, and visualized using Orange3 (https://orangedatamining.com) [269]. Metascape was utilized to identify statistically enriched pathways from each list of oscillating transcripts [270] (http://metascape.org), which were then binned into categories via a custom R script.

Network co-occurrence analysis was performed using RNA-seq raw transcript abundance counts. Transcripts with low abundance counts (<50 counts in all samples or genes with 0 counts in more than 2 samples per timepoint) were removed. Spearman correlation values for comparisons between pairs of transcripts were calculated within each genotype. Transcript count values were randomly selected from one of the three samples for a given timepoint (ZT 2, 6, 10, 14, 18, 22), then correlation p and r values between transcripts over time were calculated in R, repeated over 500 permutations ('dplyr', 'rcorr', 'Hmisc'). Correlation matrices for the 500 permutations were averaged to generate a single matrix

of transcript correlation values. The matrix was flattened into a network-importable table format in R ('cormat', 'pmat'): flatCorrMatrix $< -$ function(cormat, pmat) ut $< -$ upper.tri(cormat) data.frame(row = rownames(cormat)[row(cormat)[ut]], column = rownames(cormat)[col(cormat)[ut]], cor =(cormat)[ut], p = pmat[ut]). Correlations were filtered for $p < 0.001$ and spearman $r > 0.95$, and all self-relationships removed. This filtered correlation table was used for network visualization in Cytoscape [271] (https://cytoscape.org), as well as for downstream analyses of node connectivity and centrality. Annotations from KEGG were added (ensemble.org) and utilized to identify transcript nodes in each network with specific functionally related pathways.

Raw sequencing reads are deposited at NCBI GEO (Accession #GSE184303).

2.2.13 Metabolic cage studies

Mice were acclimatized to individual housing for 5 days prior to metabolic monitoring, which was conducted using the Promethion Metabolic System (Promethion High-Definition Multiplexed Respirometry System for Mice; Sable Systems International, Las Vegas, NV, USA). All measurements were recorded at 3 minute intervals across all cages. Food and water intake were recorded by gravimetric measurement. Physical movement was determined by infrared sensor beam breaks. Oxygen consumption, carbon dioxide production, and respiratory quotient were measured by indirect calorimetry. Energy expenditure (kcal/hr) was calculated by the Weir equation [272].

Basal metabolic rate (BMR) was measured on the first day of metabolic cage housing. Following transfer into metabolic cages at ZT3, food was immediately removed. During the 3-hr period between ZT7 to ZT10, the lowest average post-absorptive energy expenditure value over a 5-minute period was identified as BMR [273]. Food was returned at ZT10 and mice were allowed to acclimatize for 2 days, followed by 4 days of resting metabolic rate measurements. At the end of each experiment involving GF mice, validation of GF status

was performed using 16S rRNA gene PCR on DNA extracted from fecal samples collected pre- and post-metabolic caging. Any mice that were identified as positive were excluded from the study.

All data was recorded via IM3 software v21.0.2 and converted to xml via a custom Sable Systems macro. Data was wrangled and cleaned in Python, including identification of each diurnal cycle using environmental lux values. Within each time period, sum was calculated for beam breaks and movement, range was calculated for food and water intake. EC50 [274] was calculated for RQ, VO_2, and energy expenditure in R using nplr v.1-7. ANCOVA (body weight as covariant) was performed for each measurement between two groups using R.

2.2.14 SCFA measurements

SCFAs were extracted from cecal contents as previously described ([275]). Fresh samples were collected, weighed, homogenized in water, and centrifuged at 13,000 x g. Supernatants were acidified and 4-methylvaleric acid (300 mM) was added as internal standard. SCFAs were extracted using diethyl ether, derivatized using MTBS-TFA, and run on an Agilent Single Quad GCMS (5977A Single Quad and 7890B GC).

2.2.15 Bile acid measurements

Extraction solvent (80% methanol spiked with internal standards and stored at -80°C) was added to pre-weighed fecal/cecal samples at a ratio of 100 mg of material/mL of extraction solvent in beadruptor tubes (Fisherbrand; 15-340-154). Samples were homogenized at 4°C on a Bead Mill 24 Homogenizer (Fisher; 15-340-163), set at 1.6 m/s with 6 thirty-second cycles, 5 seconds off per cycle. Samples were then centrifuged at -10°C, 20,000 x g for 15 min and the supernatant was used for subsequent metabolomic analysis.

Samples were incubated at -80°C for at least one hour, or up to overnight. Extraction solvent (4 volumes of 100% methanol spiked with internal standards and stored at -80°C) was

added to the liquid sample (1 volume) in a microcentrifuge tube. Tubes were then centrifuged at -10°C, 20,000 x g for 15 min and supernatant was used for subsequent metabolomic analysis.

Bile acids were analyzed using LCMS. The metabolite extract (75 μL) was added to prelabeled mass spectrometry autosampler vials (Microliter; 09-1200) and dried down completely under a nitrogen stream at 30 L/min (top) 1 L/min (bottom) at 30°C (Biotage SPE Dry 96 Dual; 3579M). Samples were resuspended in 50:50 Water:Methanol (750 μL). Vials were added to a thermomixer C (Eppendorf) to resuspend analytes at 4 oC, 1000 rpm for 15 min with an infinite hold at 4°C. Samples were then transferred to prelabeled microcentrifuge tubes and centrifuged at 4°C, 20,000 x g for 15 min to remove insoluble debris. The supernatant (700 μL) was transferred to a fresh, prelabeled mass spectrometry autosampler vial. Samples were analyzed on a liquid chromatography system (Agilent 1290 infinity II) coupled to a quadrupole time-of-flight (QTOF) mass spectrometer (Agilent 6546), operating in negative mode, equipped with an Agilent Jet Stream Electrospray Ionization source. The sample (5 μL) was injected onto an XBridge© BEH C18 Column (3.5 μm, 2.1 x 100 mm; Waters Corporation, PN) fitted with an XBridge© BEH C18 guard (Waters Corporation, PN) at 45°C. Elution started with 72% A (Water, 0.1% formic acid) and 28% B (Acetone, 0.1% formic acid) with a flow rate of 0.4 mL/min for 1 min and linearly increased to 33% B over 5 min, then linearly increased to 65% B over 14 min. Then the flow rate was increased to 0.6 mL/min and B was increased to 98% over 0.5 min and these conditions were held constant for 3.5 min. Finally, re-equilibration at a flow rate of 0.4 mL/min of 28% B was performed for 3 min. The electrospray ionization conditions were set with the capillary voltage at 3.5 kV, nozzle voltage at 2 kV, and detection window set to 100-1700 m/z with continuous infusion of a reference mass (Agilent ESI TOF Biopolymer Analysis Reference Mix) for mass calibration. A ten-point calibration curve was used for quantitation. Data analysis was performed using MassHunter Profinder Analysis software (version B.10, Agi-

lent Technologies) and confirmed by comparison with authentic standards. Normalized peak areas were calculated by dividing raw peak areas of targeted analytes by averaged raw peak areas of internal standards.

2.3 Quantification and Statistical Analysis

For Chapter 3, data are presented as mean ± SEM, or box-and-whisker plots represented as median ± min/max. Statistical analysis was performed using either GraphPad Prism v9 software or R packages. Two-tailed unpaired Welch's t tests or ANCOVA were performed between two groups, and Brown-Forsythe and Welch ANOVA followed by Dunnett's tests were performed between three or more groups; $p < 0.05$ was considered statistically significant. Metascape was used to identify significantly enriched pathways from oscillation transcriptome profiles by $q - value < 0.05$. Spearman correlation was performed to identify significantly correlated gene expression over time by $p < 0.001$ and $r < 0.95$. fGSEA was used to identify significantly enriched pathways from differential gene expression analysis by $padj < 0.05$ and $nperm = 10000$. 16S rRNA paired-end reads were analyzed via QIIME2 [255]. CircWave V1.4 (http://clocktool.org) or empirical JTK_CYCLE [260] were used to identify significantly oscillating data by $p < 0.05$ (CircWave) or $GammaBH < 0.05$ (p-value calculated from Gamma fit of empirical null distribution, adjusted for Benjamini-Hochberg false-discovery rate, eJTK). Statistical outliers were identified via 2 standard deviations ± mean and removed from the analysis. Metabolic cage statistical outliers were removed based on Sn values [276] using the R package robustbase (https://robustbase.r-forge.r-project.org). A consistency factor of 1.1926 was used to calculate the S_n value for each channel within each cycle, and outliers were defined as ± 3 times the Sn value from the median. Python v3.7.5 and R v3.6.3 were used. Agilent Mass Hunter Qualitative Analysis software was used to analyze SCFA metabolomics.

For Chapter 4, data from *in vivo* and *in vitro* studies are presented as mean±SEM, or

box and whisker plots as median±min/max. Two-tailed paired Welch's tests were performed for statistical analysis between two groups. Analysis of mass spec data comparisons between two groups was performed by students t-test and fold change calculated by $\log_2$ transformed data [277]. One-way Brown-Forsythe and Welch Analysis of Variance (ANOVA) followed by Dunnett's tests or two-way ANOVA followed by Tukey's test were performed between three or more groups. $p < 0.05$ was considered statistically significant. Significant changes in OTU abundances were assessed using ANOVA, as implemented in QIIME (Bonferroni correction for multiple tests; $\alpha = 0.05$) [259]. Multivariate statistical tests run on microbial community structure data include Analysis of Similarity (ANOSIM) and adonis tests, as implemented in QIIME. Relative abundances of individual OTUs over the course of 24 hours were compared against the relative expression of host expression of *Reg3*γ in the ileum of both RC and HF SPF mice using Pearson Linear Regression correlation analysis and Spearman RHO non-parametric correlation analysis. False Discovery Rate (FDR) and Bonferroni were used as multi-test correction factors to correct the p-values to reduce Type I statistical error. Significant circadian oscillation of gene expression or copy number was determined using the software CircWave V1.4; a rhythm was determined as present by $p < 0.05$. Significant microbial OTU abundance oscillations were determined via empirical JTK_Cycle; an OTU was determined rhythmic at $GammaP < 0.05$ [260].

Table 2.1: Oligonucleotides, related to Materials and Methods

Name	Oligonucleotide (5' → 3')
*16S*_F (Ch 3)	GTGYCAGCMGCCGCGGTA
*16S*_R (Ch 3)	GGACTACNVGGGTWTCTAAT
*but*_F	TCAAATCMGGIGACTGGGTWGA
*but*_R	TCGATACCGGACATATGCCAKGAG
*dsrAB*_F	CCAACATGCACGGYTCCA
*dsrAB*_R	CGTCGAACTTGAACTTGAACTTGTAG
*tpa*_F	ACTTCTGTTCGACGGTGGTG
*tpa*_R	GCAAGACCTCTCGCTCCTTC
*Reg3γ*_F	CCACTCACCTGCTGCTACTCAT
*Reg3γ*_R	TGGTGATCCTCTTGTAGCTCTCC
*Lysozyme1*_F	GAGACCGAAGCACCGACTATG
*Lysozyme1*_R	CGGTTTTGACATTGTGTTCGC
*Cryptidin4*_F	TCGTGGGACATTCGTGAAGA
*Cryptidin4*_R	GCGGGCTGCTGTCCAG
*Clock*_F	GGGAGTTTGGCTCCAGAGTTT
*Clock*_R	TGTGTCTTCAGGGGTCCTTAG
*Bmal1*_F	GGGAGTTTGGCTCCAGAGTTT
*Bmal1*_R	TGTGTCTTCAGGGGTCCTTAG
*Per1*_F	TGAAGCAAGACCGGGAGA
*Per1*_R	CACACACGCCGTCACATC
*Per2*_F	TGTGCGATGATGATTCGTGA
*Per2*_R	GGTGAAGGTACGTTTGGTTTGC
*Per3*_F	AAAAGCACCACGGATACTGGC
*Per3*_R	GGGAGGCTGTAGCTTGTCA
*Cry1*_F	CACTGGTTCCGAAAGGGACTC
*Cry1*_R	CTGAAGCAAAAATCGCCACCT
*Cry2*_F	CACTGGTTCCGCAAAGGACTA
*Cry2*_R	CCACGGGTCGAGGATGTAGA
*Rev-erba*_F	ATGCCCATGACAAGTTAGGC
*Rev-erba*_R	GGGCTACCTGATGCATGATT
*RORa*_F	ACGCCCACCTACAACATCTC
*RORa*_R	TGCCCATCCATATAGGTGCT
*Sucrase_Isomaltase*_F	ATGAGCAAAATGTTTGGGTG
*Sucrase_Isomaltase*_R	GGCCATACCTCTCCAATAAG
*Gapdh*_F	GGCAAATTCAACGGCACAGT
*Gapdh*_R	AGATGGTGATGGGCTTCCC
*Ang4*_F	GGTTGTGATTCCTCCAACTCTG
*Ang4*_R	CTGAAGTTTTCTCCATAAGGGCT
*Muc2*_F	GCTGACGAGTGGTTGGTGAATG
*Muc2*_R	GATGAGGTGGCAGACAGGAGA
*16S_universal*_F (Ch 4)	ATGGYTGTCGTCAGCTCGTG
*16S_universal*_R (Ch 4)	GGGTTGCGCTCGTTGC
*Tlr1*_F	TGAGGGTCCTGATAATGTCCTAC
*Tlr1*_R	AGAGGTCCAAATGCTTGAGGC
*Tlr2*_F	GCAAACGCTGTTCTGCTCAG
*Tlr2*_R	AGGCGTCTCCCTCTATTGTATT
*Tlr3*_F	GTGAGATACAACGTAGCTGACTG
*Tlr3*_R	TCCTGCATCCAAGATAGCAAGT
*Tlr4*_F	ATGGCATGGCTTACACCACC
*Tlr4*_R	GAGGCCAATTTTGTCTCCACA
*Tlr9*_F	ATGGTTCTCCGTCGAAGGACT
*Tlr9*_R	GAGGCTTCAGCTCACAGGG

CHAPTER 3

GUT MICROBES AND THE LIVER CIRCADIAN CLOCK PARTITION GLUCOSE AND LIPID METABOLISM

3.1 Preface

The contents of this chapter were modified and adapted from "K. Frazier, S. Manzoor, K. Carroll, O. DeLeon, S. Miyoshi, J. Miyoshi, M. St. George, A. Tan, M. Izumo, J. S. Takahashi, M. C. Rao, V. A. Leone, E. B. Chang, Gut Microbes and the Liver Circadian Clock Partition Glucose and Lipid Metabolism. bioRxiv (2022), p. 2022.05.24.491361" [278]. K. Frazier performed most of and oversaw all of the experiments reported in the paper. K. Frazier and S. Manzoor performed and analyzed the RNA-sequencing and metabolic cage experiments. K. Carroll performed the Western blot experiments, analyzed 16S sequencing data, and assisted with many other experiments. O. DeLeon performed the network co-occurrence analysis. M. St. George performed quantitative PCR. K. Frazier, S. Miyoshi, J. Miyoshi, and V. Leone performed tissue collections. K. Frazier, M. St. George, and A. Tan performed tolerance test experiments. M. Izumo and J. Takahashi provided experimental mouse models. K. Frazier wrote the manuscript. K. Frazier, M. Rao, V. Leone, and E. Chang edited the manuscript. K. Frazier, V. Leone, and E. Chang conceived the project.

3.2 Abstract

Circadian rhythms govern glucose homeostasis, and their dysregulation leads to complex metabolic diseases. Gut microbes also exhibit diurnal rhythms that influence host circadian networks and metabolic processes, yet underlying mechanisms remain elusive. Here, we show hierarchical, bidirectional communication between the liver circadian clock, gut microbes, and glucose homeostasis in mice. The liver clock, but not the forebrain clock, requires gut microbes to drive glucose clearance and gluconeogenesis. Liver clock dysfunctionality expands proportions and abundances of oscillating microbial features by two-fold relative to controls. The liver clock is the primary driver of differential and rhythmic hepatic expression of glucose and fatty acid metabolic pathways. Absent the liver clock, gut microbes provide secondary cues that dampen these rhythms, resulting in reduced utilization of lipids as fuel relative to carbohydrates. Together, the liver clock transduces signals from gut microbes necessary to regulate glucose and lipid metabolism and meet energy demands over 24 hours.

3.3 Introduction

As described in Chapter 1, gut microbes and host circadian rhythms interact significantly and can induce dramatic changes in host metabolism. Shifts in diet can disrupt diurnal oscillations of microbial abundance and metabolite levels [141, 179, 279]. Conversely, mice with global genetic mutations in circadian clock genes exhibit significantly altered microbial community profiles and loss of oscillations in specific taxa [178, 180, 187]. In absence of gut microbial cues, germ-free (GF) WT mice exhibit dampened rhythmicity in the expression of core circadian clock genes in both brain and liver, as well altered transcriptomic patterns in liver, small intestine, and white adipose tissue [141, 188]. While the link between circadian rhythms, gut microbiota, and host metabolism is established, few mechanisms have been proposed to explain how these phenomena occur, how the circadian clock in specific metabolic organs such as the liver are involved, and how this impacts global metabolic regulation.

One metabolic pathway that has been implicated in this interaction is gluconeogenesis, the endogenous production of glucose primarily by the liver, which is critical during periods of prolonged fasting [280]. Along with the significant influence of endogenous hormones [281], both circadian rhythms and gut microbial cues drive gluconeogenesis, and disruption of either leads to aberrant hepatic gluconeogenesis [159, 282]. Mice deficient in hepatic *Bmal1*, which uniquely display increased fasted glucose clearance, altered expression of hepatic gluconeogenesis genes, and reduced functionality of mitochondria [129, 130], have previously revealed a role of the peripheral liver circadian clock in gluconeogenic regulation. Importantly, the liver clock is uniquely autonomous from the central clock in metabolic regulation [283]. Gut microbes have also been demonstrated to mildly impact the liver circadian clock, but impart significant changes in rhythmic hepatic gene expression, dependent on sex [188]. Yet, few mechanistic insights explain how these consequences arise, or how gut microbes may contribute, thus gaining a deeper understanding of how these systems function in the context of metabolic homeostasis is of utmost importance.

Here, we hypothesized that hepatic gluconeogenesis is driven by bidirectional interactions between the hepatic circadian clock and gut microbiota. Using the liver-specific *Bmal1* knock-out mouse raised in both conventional and GF conditions, we demonstrate a hierarchy of signals between the gut microbiome and liver clock that coordinates hepatic gluconeogenesis and fatty acid β-oxidation that are essential to maintain diurnal rhythms in glucose homeostasis. We identify that regardless of microbial status, the liver clock is a primary driver of hepatic transcription, particularly of genes involved in the organization and function of key metabolic pathways. Secondarily, the liver clock transduces timed signals from the gut microbiome to promote coordinated differential, oscillatory, and correlated transcription patterns in glucose and lipid metabolic pathways. When either of these two components (host clock or microbes) are absent or dysfunctional, we observe a significant gain in oscillating hepatic transcripts that are disorganized. The absence of a functional clock also results in expansion of oscillations in specific fecal microbial abundances. Together, we reveal interactions between the liver circadian clock and gut microbes that aid in glucose and lipid homeostasis that govern whole-body metabolism and fuel utilization.

3.4 Results

3.4.1 Gut microbes are essential for liver circadian clock regulation of insulin-independent glucose clearance

To assess the effects of a dysfunctional liver clock and gut microbes on mammalian host metabolism, we utilized male and female mice with liver-specific deletion of *Bmal1* gene expression via Albumin-cre: *Bmal1*$^{fl/fl}$-AlbCre (LKO) versus control, *Bmal1*$^{fl/fl}$ (WT) [284, 285]. We confirmed *Bmal1* deletion in the liver, while expression in the brain remained intact (Figure 3.1A). We maintained both WT and LKO mice in conventional, specific-pathogen free (SPF) or GF conditions.

First, we observed that SPF LKO male mice exhibited significantly increased body weight compared to SPF WT, while oppositely GF LKO mice exhibited a slight, non-significant trend of decreased body weight relative to GF WT (Figure 3.1B, upper panel). This difference in body weight could not be explained by changes in gross liver or fat pad tissue weight (Figure 3.2A,B, upper panels). Daily caloric consumption revealed similar patterns; SPF LKO mice ate slightly but significantly more than WT, while GF mice exhibited no difference between genotypes (Figure 3.1C, upper panel). Interestingly, we did not observe any differences between genotype in female mice for body weight or food intake (Figure 3.1B,C, lower panels; Figure 3.2A,B, lower panels).

We then measured resting blood glucose levels every 4 hours over a 12:12 LD cycle and found that overall levels were not drastically different between groups of male mice by non-repeat measurements (Figure 3.3A, data split by SPF and GF). However, analysis by CircWave revealed only WT mice, regardless of microbial status, exhibited significant oscillation of blood glucose levels, indicating that diurnal circulating blood glucose is driven by the liver clock and not gut microbes. Similar patterns in circulating glucose were observed in male mice repeatedly-measured every 6 hours over 24 hours (Figure 3.4). Conversely, we observed very little difference in diurnal blood glucose values in female mice, and only the GF WT group exhibited a significant oscillation (Figure 3.3B, data split by SPF and GF).

Given previous work by Lamia *et al.* [130], we performed an oral glucose tolerance test (GTT) and observed that male GF mice exhibit more rapid glucose clearance than SPF by area under the curve (AUC) (Figure 3.5A). We also observed a genotype-driven effect in SPF conditions where LKO mice cleared glucose significantly faster than WT. Circulating insulin levels during GTT were not significantly different between WT and LKO mice in either SPF or GF conditions, suggesting that insulin secretion is not impacted by liver clock functionality (Figure 3.5B). GTT of female mice revealed no significant differences in AUC between any group (Figure 3.5C), suggesting that liver-clock-mediated glucose clearance is

in part driven by sex. We then interrogated insulin sensitivity by intraperitoneal insulin tolerance test (ITT) on SPF and GF, WT and LKO male mice and revealed no difference in insulin sensitivity between genotypes in either microbial condition (Figure 3.5D), suggesting that *Bmal1*-driven glucose clearance in male mice is insulin-independent.

Importantly, all SPF and GF animals in our study were *ad libitum* fed autoclaved JL Rat and Mouse/Auto 6F 5k67 (LabDiet, St. Louis, MO, USA) for at least 2 weeks prior to and throughout all experiments. However, our SPF mouse colonies are normally fed a different regular chow diet, Envigo 2018S, while our GF mouse colonies are normally fed LabDiet 5K67. While these two diets are compositionally similar, they do present slight differences, such as crude fiber content (macronutrient breakdown of diets presented in Table A.1). Therefore, we set out to determine if exposure to either regular chow (RC) diet impacted glucose tolerance. We performed a baseline GTT on adult male and female C57BL/6J mice, then provided mice either SPF-RC (Envigo 2018S) or GF-RC (LabDiet 5K67) for 1 month and performed a second GTT (Figure A.1). We observed no difference in glucose tolerance by AUC between any groups within sex, suggesting that exposure to either RC diet does not impact glucose tolerance. Following, we proceeded with the LabDiet 5K67 for all SPF mice to match the diet given to GF mice.

Together, these data suggest the liver circadian clock imparts an insulin-independent effect on glucose clearance in male mice that is dependent on the presence of gut microbes.

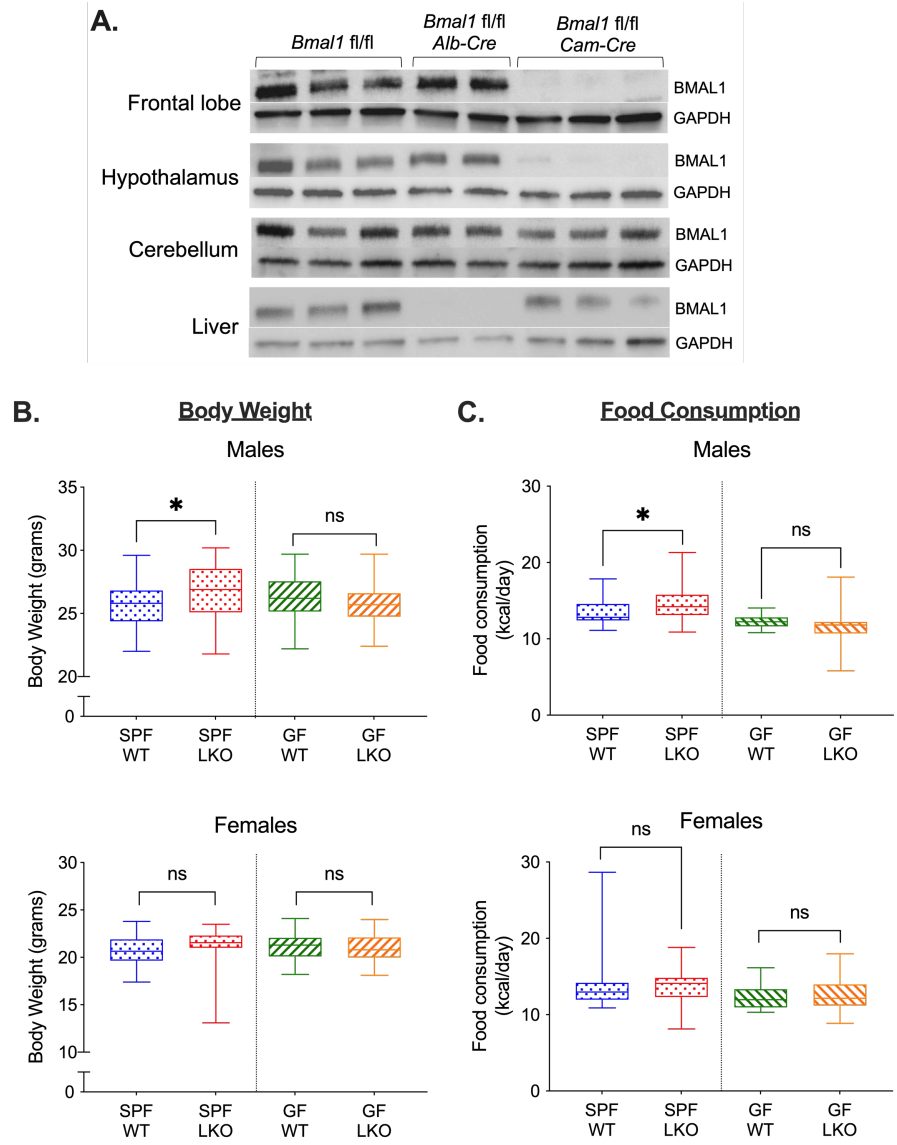

Figure 3.1: **Body weight and food consumption are mediated by liver clock and gut microbes in male mice.** (A) Western blot of BMAL1 and GAPDH (control) in brain (frontal lobe, hypothalamus, cerebellum) and liver protein extracts collected at ZT16 from male $Bmal1^{fl/fl}$ (WT), $Bmal1^{fl/fl}$-Alb-Cre (LKO), and $Bmal1^{fl/fl}$-Cam-Cre (Forebrain-Bmal1-KO). (B) Body weight (grams), and (C) daily food intake (digestible kcals/day) of SPF and GF, WT and LKO male and female mice; (n=18-32/group). Box plots represent median±min/max, $^*p < 0.05$, ns=not significant.

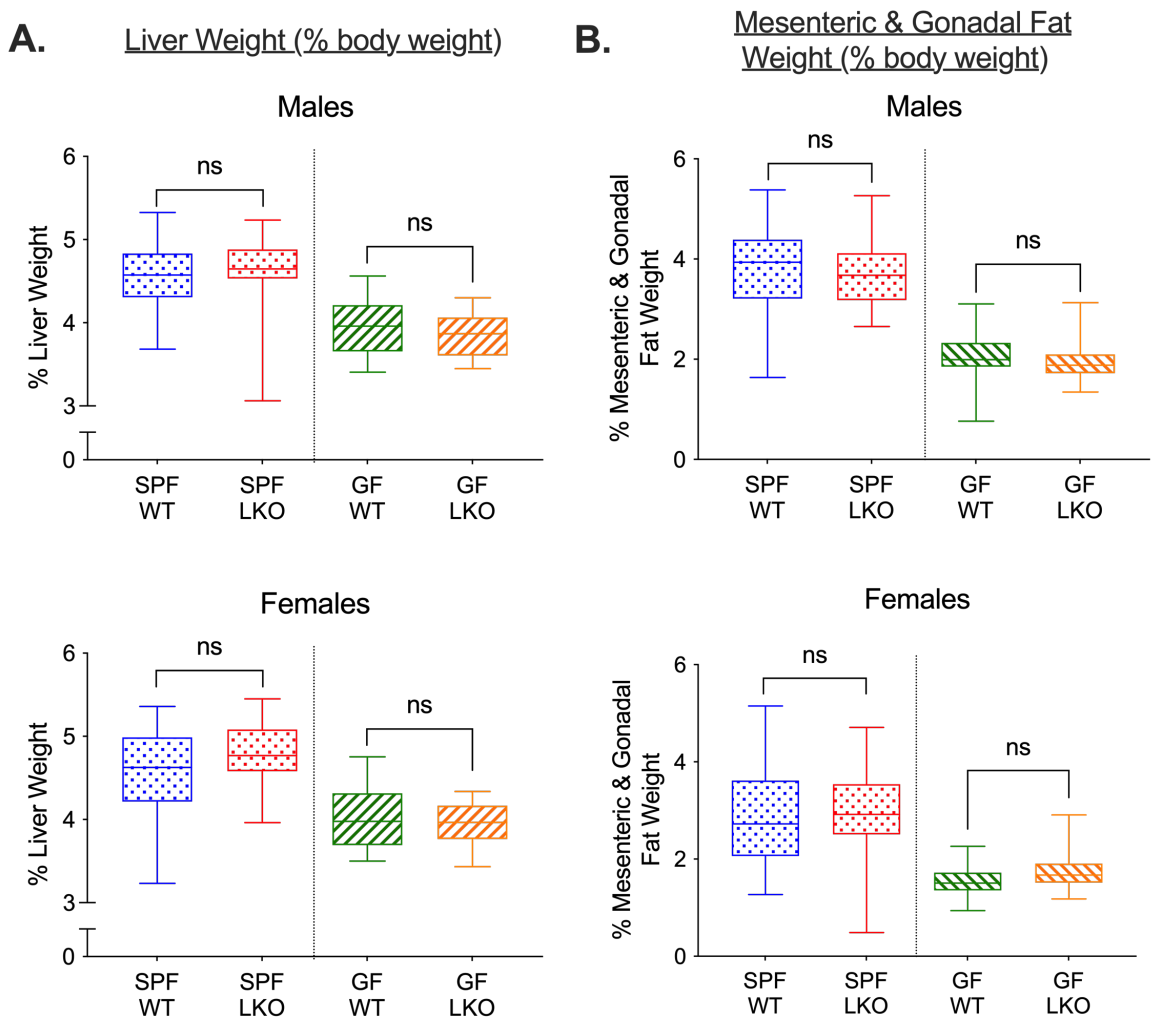

Figure 3.2: **Liver and fat pad weight is not driven by a functional liver clock.** Liver (A), and mesenteric and gonadal fat pad weight and SPF and GF, WT and LKO male and female mice (n=30-34/group). Box plots represent median±min/max, ns=not significant.

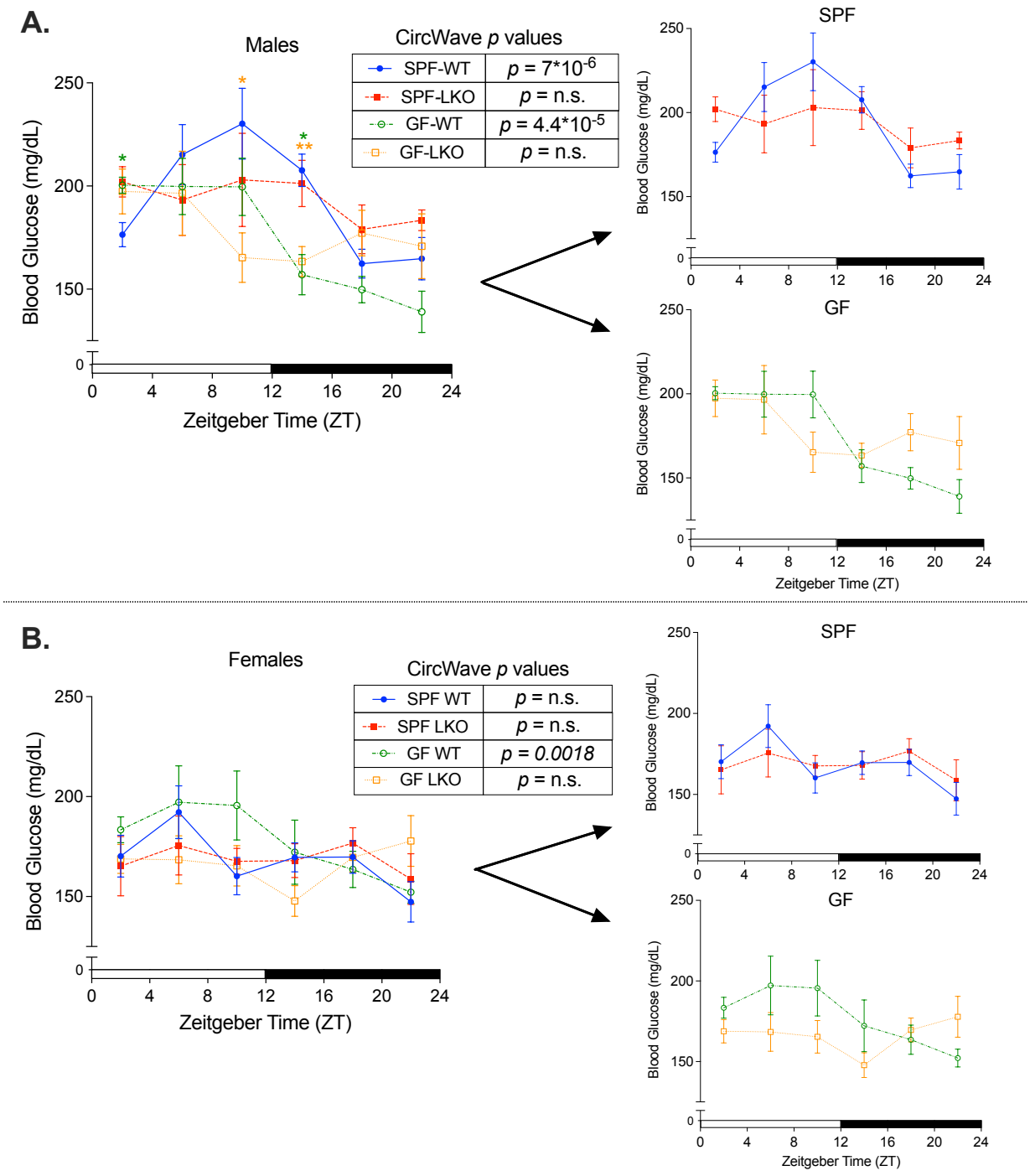

Figure 3.3: **Diurnal blood glucose is driven by liver clock, not gut microbes, in male mice.** Resting blood glucose levels measured via tail snip of SPF and GF, WT and LKO male (A) and female (B) mice every 4 hours over 24 hours (n=4-6/group/timepoint, SPF and GF groups also shown separately). CircWave statistics indicate significantly oscillating ($p < 0.05$) or not oscillating ($p > 0.05$) values. Data points represent mean±SEM, $^{**}p < 0.01$, $^{*}p < 0.05$, colored stars indicate significant difference relative to SPF WT.

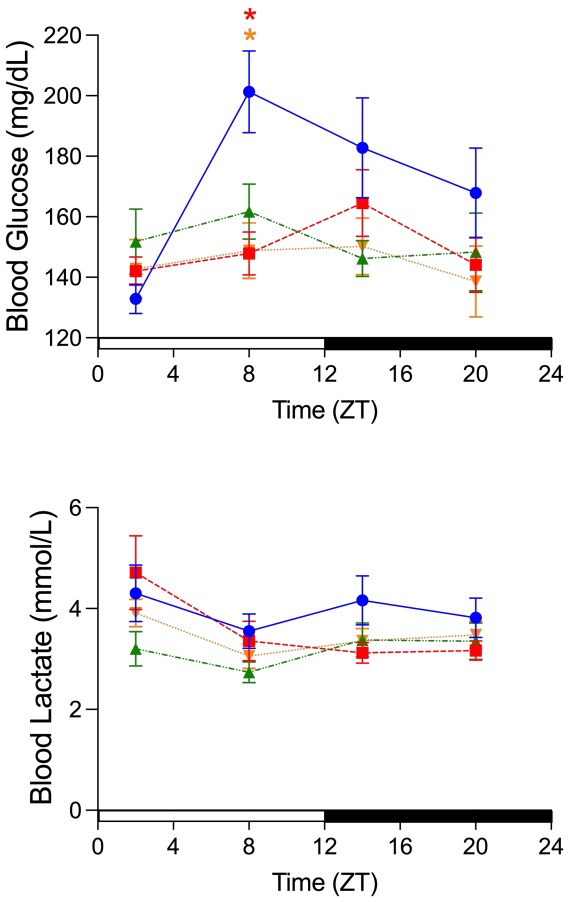

Figure 3.4: **Repeat-measurements of diurnal blood glucose and lactate in male mice.** Resting blood glucose (upper panel) and lactate (lower panel) levels measured via tail snip of SPF and GF, WT and LKO male mice every 6 hours over 24 hours(n=9-11/group/timepoint). Data points represent mean±SEM, $*p < 0.05$, colored stars indicate significant difference relative to SPF WT.

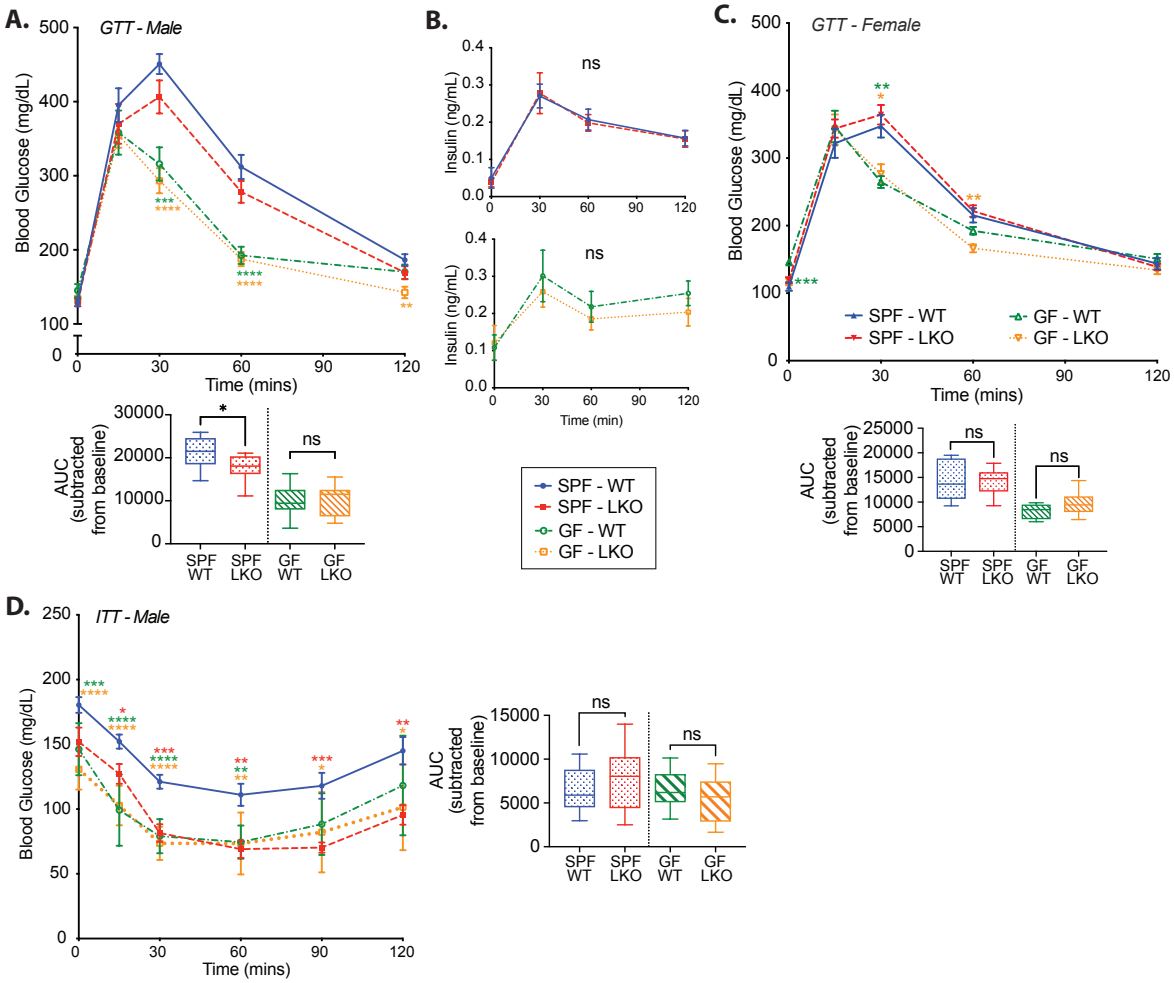

Figure 3.5: **Gut microbes are essential for liver circadian clock-mediated glucose clearance in male mice, independent of insulin tolerance.** (A) Oral Glucose Tolerance Test (GTT) of SPF and GF, WT and LKO male mice (n=10-13/group). (B) Circulating insulin levels during GTT (n=10-13/group). (C) GTT of SPF and GF, WT and LKO female mice (n=8-10/group). (D) Intraperitoneal Insulin Tolerance Test (ITT) in SPF and GF, WT and LKO male mice (n=11-17/group). Data points represent mean±SEM, box plots represent median±min/max. $****p < 0.0001$, $***p < 0.001$, $**p < 0.01$, $*p < 0.05$, ns=not significant; colored stars represent significance relative to SPF WT. Associated graphs represent area under the curve (AUC) normalized to baseline glucose.

3.4.2 Circadian clock and microbiome-driven gluconeogenesis is liver-specific and requires in vivo *signals*

To interrogate the role of the liver clock on gluconeogenesis, we performed an intraperitoneal pyruvate tolerance test (PTT). First, we revealed GF mice exhibit significantly lower gluconeogenesis rates than SPF counterparts regardless of genotype (Figure 3.6A). The phenotypic difference in gluconeogenesis is also present when PTT is performed during the dark cycle starting at ZT14, as opposed to all other tolerance tests presented in this Chapter which were performed during the light cycle starting at ZT2 (Figure 3.7A). Second, we observed LKO mice exhibit reduced gluconeogenesis in SPF conditions, while no differences between genotypes in GF conditions were evident. Interestingly, we observed no differences in resting circulating lactate over 24 hours in male mice from all four conditions, indicating that lactate availability and utilization as a precursor to gluconeogenesis may not contribute to reduced gluconeogenesis in these conditions (Figure 3.4, lower panel). Additionally, we performed PTT of female SPF WT and LKO mice and observed no difference in gluconeogenesis (Figure 3.6B). Following our results that liver-clock-mediated glucose clearance and gluconeogenesis is male-specific, we proceeded with only male mice for the duration of the study.

To determine whether reduced gluconeogenesis is liver-clock-specific, we performed PTT on mice lacking a functional core brain clock by *CamkIIa-cre* forebrain-specific *Bmal1* knockout, while peripheral clocks remain intact [117, 286] (Figure 3.1A). We found no difference in gluconeogenesis rates between WT and forebrain-*Bmal1*-KO mice (Figure 3.7B), indicating that clock-mediated changes in gluconeogenesis are specific to hepatic *Bmal1* and liver clock. We also measured core circadian clock gene expression in mediobasal hypothalamus, or SCN, samples from SPF and GF, WT and LKO male mice and found minimal differences between groups (Figure 3.8). These results corroborate previous evidence that the liver clock, specifically hepatic *Bmal1*, is somewhat autonomous from the core clock located in

the brain [125].

Since both gluconeogenesis and glycogenolysis are co-stimulated during periods of prolonged fasting, we measured glycogen levels in liver samples collected from each group every 4 hours over 24 hours. We observed no difference between SPF groups at any timepoint, and glycogen content was only elevated in GF WT relative to LKO mice at ZT22 (4am) (Figure 3.9A). In all groups, liver glycogen levels exhibited significant and remarkably similar oscillations over a 24-hour period, as evident by CircWave statistics. These data indicate that hepatic glycogenolysis is not a major contributor to either the microbe- or clock-mediated effect on the observed glucose homeostasis phenotype, further supporting that gluconeogenesis is the major contributor.

Finally, we examined glucose production in primary hepatocytes isolated from SPF and GF WT vs LKO *ex vivo* following stimulation with gluconeogenic-inducing substrates in glucose-free media. We revealed no difference in glucose production in media between groups following gluconeogenic stimulation with a cell permeable cAMP analog (cPT-cAMP) (Figure 3.9B). This suggests the cellular machinery to perform gluconeogenesis is not affected by liver clock functionality or prior exposure to gut microbes, and additional *in vivo* signals are necessary for liver clock- and microbe-mediated gluconeogenesis.

Overall, we reveal a microbiota-dependent effect of liver circadian clock-mediated gluconeogenesis that requires real-time in vivo signals.

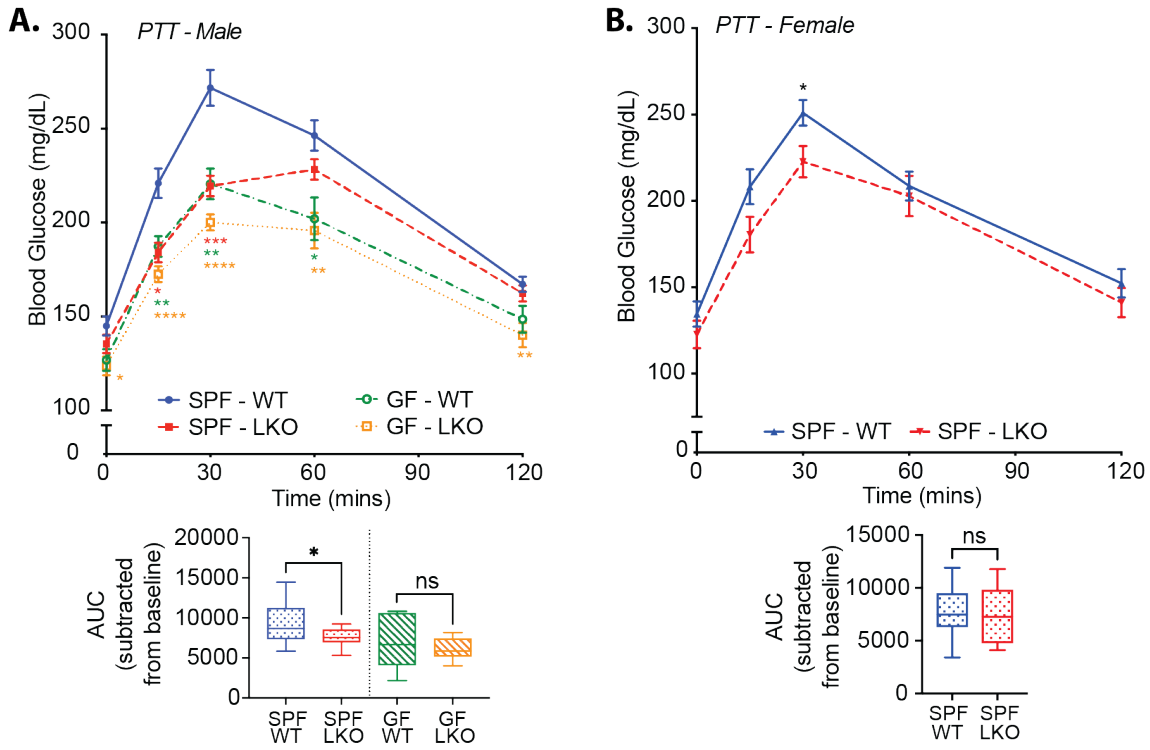

Figure 3.6: **Gut microbes are essential for liver circadian clock-mediated gluconeogenesis in male mice.** (A,B) Intraperitoneal Pyruvate Tolerance Test (PTT) of SPF and GF, WT and LKO male mice (A), and SPF WT and LKO female mice (B) (n=10-15/group). Data points represent mean±SEM, box plots represent median±min/max. $*p < 0.05$, ns=not significant; colored stars represent significance relative to SPF WT. Associated graphs represent area under the curve (AUC) normalized to baseline glucose.

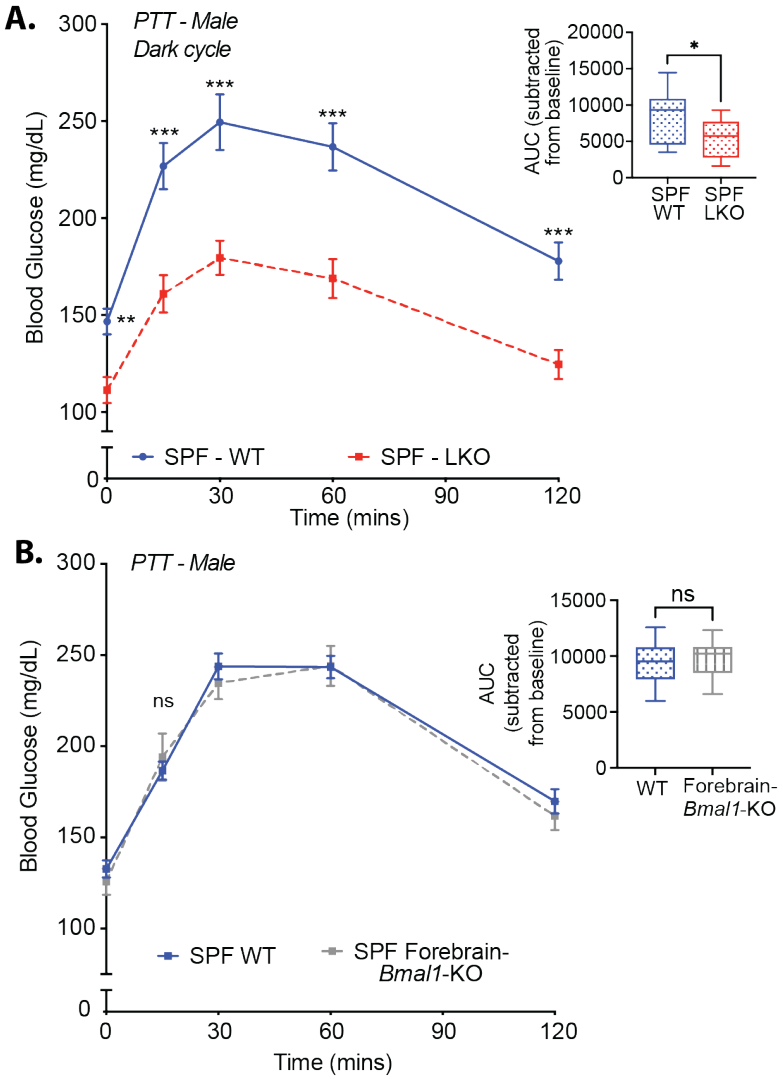

Figure 3.7: **The liver circadian clock mediates gluconeogenesis independent of light and the core brain clock.** (A) Intraperitoneal Pyruvate Tolerance Test (PTT) of SPF WT and LKO male mice at ZT14 during the dark cycle (n=11-14/group). (B) PTT of SPF WT and Forebrain-*Bmal1*-KO male mice (n=12-17/group). Data points represent mean±SEM, box plots represent median±min/max. $***p < 0.001$, $**p < 0.01$, $*p < 0.05$, ns=not significant. Associated graphs represent area under the curve (AUC) normalized to baseline glucose.

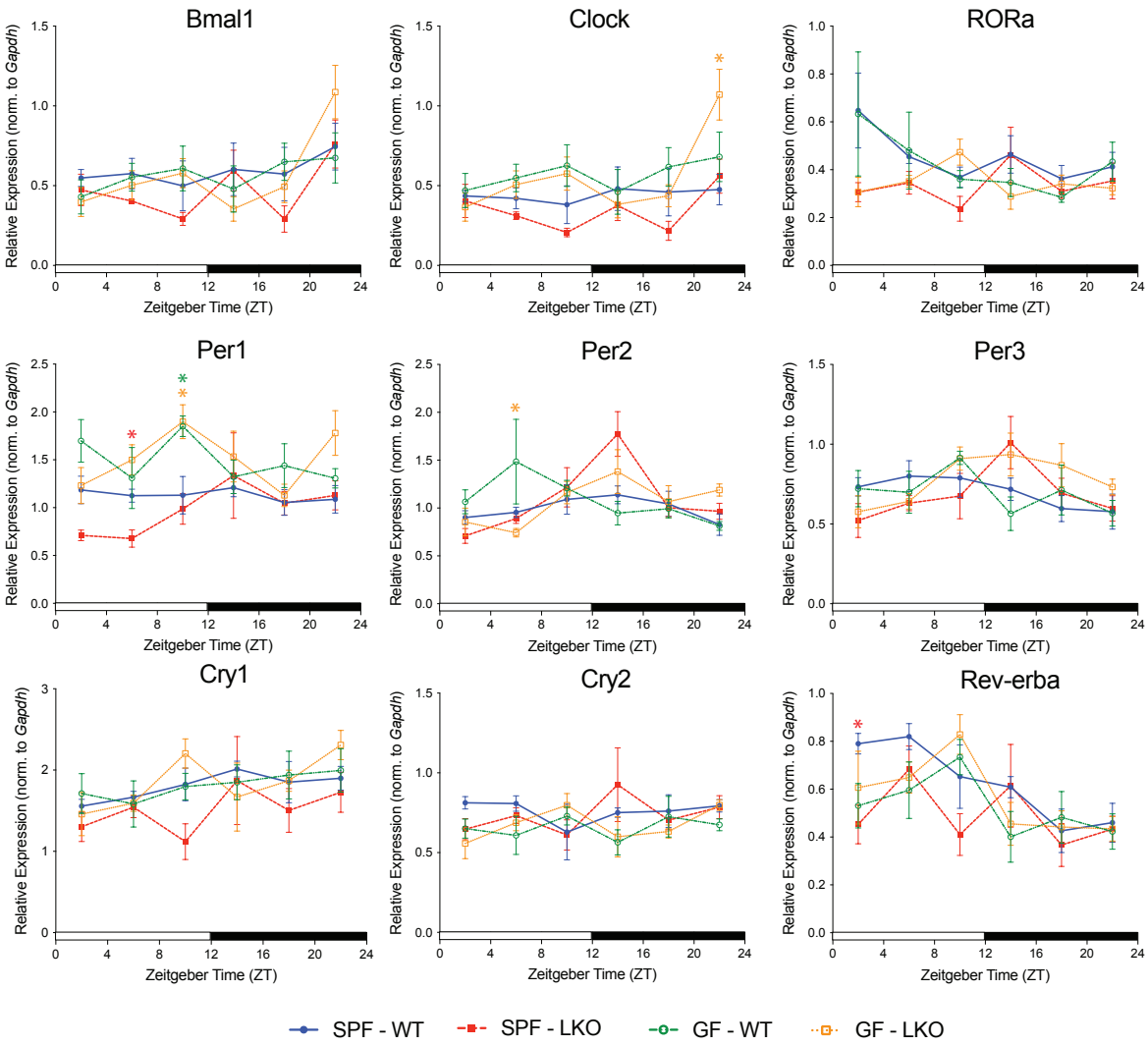

Figure 3.8: **Mediobasal hypothalamus core circadian clock gene expression is not impacted by the liver circadian clock or gut microbes.** Core circadian clock gene expression in mediobasal hypothalamus samples collected from SPF and GF, WT and LKO male mice over 24 hours. Data points represent mean±SEM; $*p < 0.05$, star color indicates group exhibiting significance relative to SPF WT.

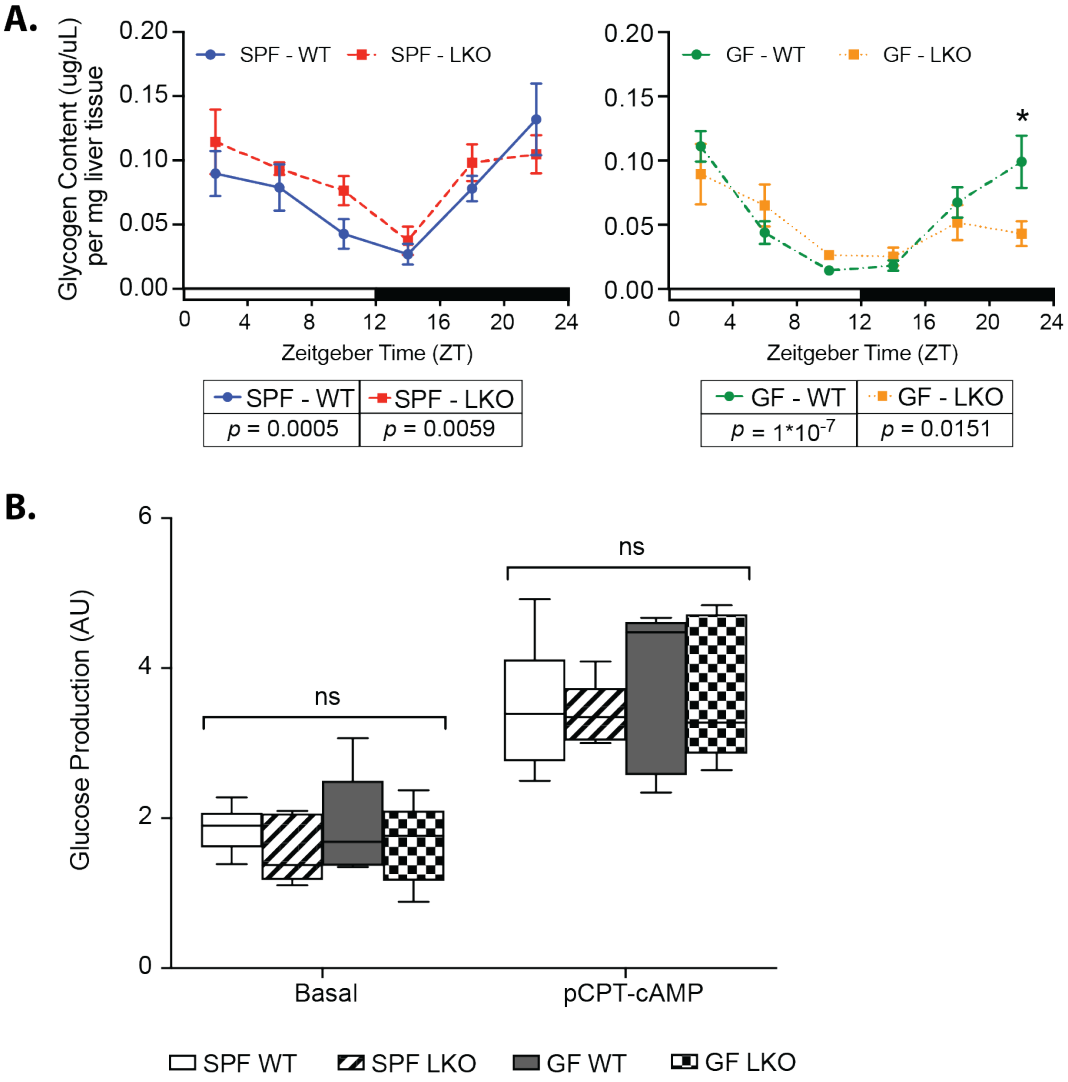

Figure 3.9: **Liver circadian clock and gut microbes do not mediate hepatic glycogen, or hepatic gluconeogenesis *ex vivo*.** (A) Glycogen content in liver tissue from SPF and GF WT vs LKO male mice collected every 4 hours over 24 hours from animals maintained in 12:12 LD (n=5-7/group); CircWave statistics indicate significantly oscillating ($p < 0.05$) or not oscillating ($p > 0.05$) values. (B) Glucose production by primary hepatocytes, isolated from SPF and GF WT vs LKO male mice, following 11 hours of treatment with vehicle control (Basal) vs pCPT-cAMP, normalized to protein content and represented as arbitrary units (AU) (n=5/group). Box plots presented as median±min/max. $*p < 0.05$, ns=not significant.

3.4.3 Gut microbes are necessary, but not sufficient, for liver clock-mediated gluconeogenesis

To investigate the role of gut microbes, we performed PTT in adult SPF WT and LKO mice both before (Pre-Abx) and after (Post-Abx) acute elimination of gut microbes via daily antibiotic treatment (Abx) for 2 weeks (Figure 3.10A). We also confirmed significant bacterial reduction by 16S gene copy number in Post-Abx stool (Figure 3.10B). While PTT of Pre-Abx mice mimicked our SPF results in Figure 3.6A, we observed no differences in gluconeogenesis between genotypes Post-Abx, closely resembling outcomes in GF mice (Figure 3.10C). This supports the hypothesis that gut microbial cues are essential for *in vivo* coordination of gluconeogenesis mediated by the liver clock.

Next, we conventionalized adult GF C57BL/6J WT mice via fecal microbiota transplant from either WT or LKO SPF donor mice and performed PTT. Here, we did not observe significant differences between recipient groups (Figure 3.11A). This suggests gut microbes selected by the presence or absence of a functional liver clock alone were insufficient to transfer the gluconeogenesis phenotype, implying that genotype is the primary driver of gluconeogenesis. We then performed a different microbiota transplant in which we conventionalized GF WT or LKO recipient mice with identical WT donor fecal microbes (Figure 3.11B). We observed significantly reduced gluconeogenesis in LKO mice relative to WT recipients, indicating that restoration of the LKO SPF phenotype requires both gut microbes and genetic absence of a liver clock.

Given that gut microbes directly modulate gluconeogenesis via the liver clock, we sought to determine if loss of *Bmal1* impacts microbiota community membership. Co-housing mice can normalize microbiota differences and mask the impact of genotype, largely due to the coprophagic tendencies of mice. With this in mind, we compared SPF WT and LKO mice in a mixed housing scenario (WT + LKO) with mice separated by genotype at weaning (WT + WT vs. LKO + LKO) (Figure 3.12A). Stool was collected at 12 weeks of age

for Illumina Mi-Seq 16S rRNA gene sequencing. Regardless of housing, we detected no significant differences in overall community membership via Beta-diversity metrics (Figure 3.13) or by relative abundance of amplicon sequence variants (ASVs) belonging to dominant phyla (Figure 3.12B) or less abundant phyla (Figure 3.12C).

Taken together, liver clock functionality does not impact overall gut microbiota community assemblage but serves as the primary driver of gluconeogenesis, while microbes are key secondary drivers. This suggests a concurrent interaction between gut microbes and the liver clock that requires real-time signals from gut microbes to mediate gluconeogenesis.

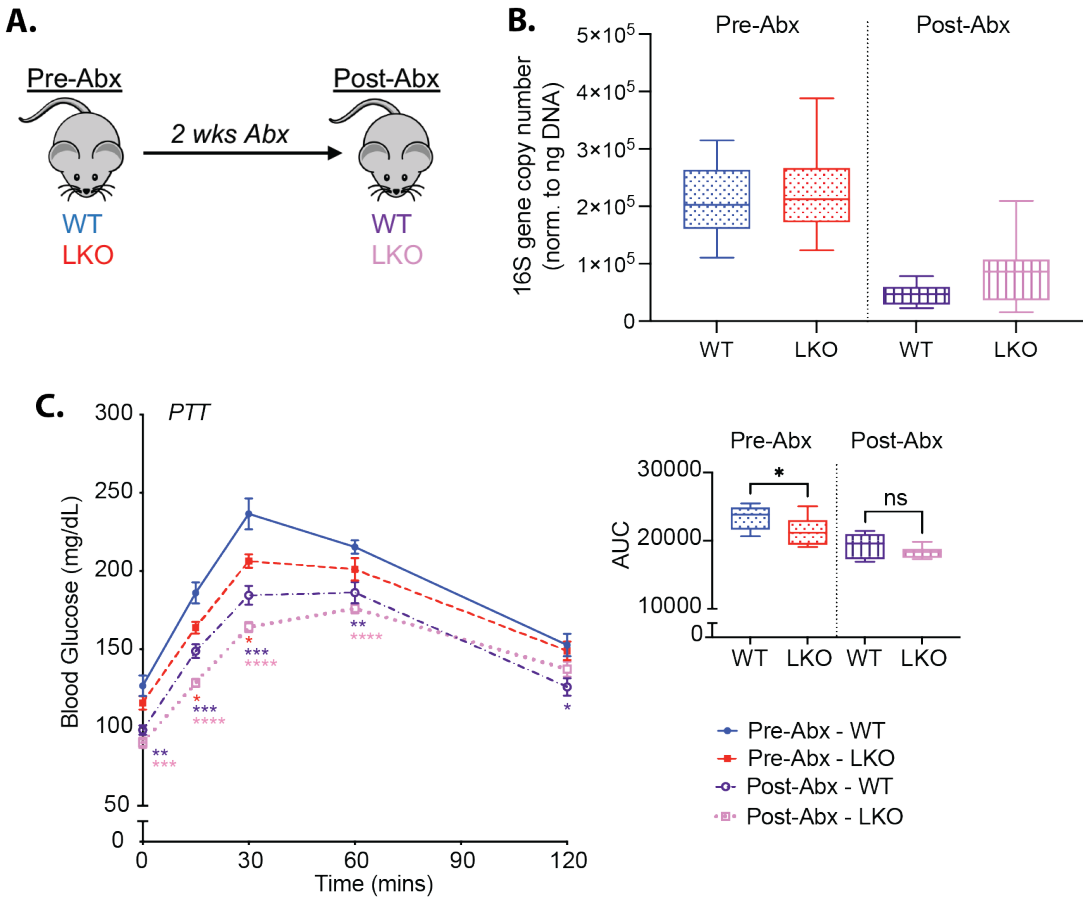

Figure 3.10: **Antibiotic treatment eliminates liver-clock mediated gluconeogenesis.** (A) Experimental scheme; PTT was performed on SPF WT and LKO male mice (Pre-Abx), then mice were given daily antibiotic treatment for 2 weeks (Post-Abx) before performing a second PTT (n=12-13/group). (B) 16S rRNA gene abundance in stool collected from Pre-Abx and Post-Abx mice, measured via quantitative PCR and normalized to DNA concentration. PTT of Pre-Abx and Post-Abx mice; side graph represents AUC. Data points represent mean±SEM, box plots represent median±min/max. $****p < 0.0001$, $***p < 0.001$, $**p < 0.01$, $*p < 0.05$, ns=not significant; colored stars represent significance relative to Pre-Abx WT.

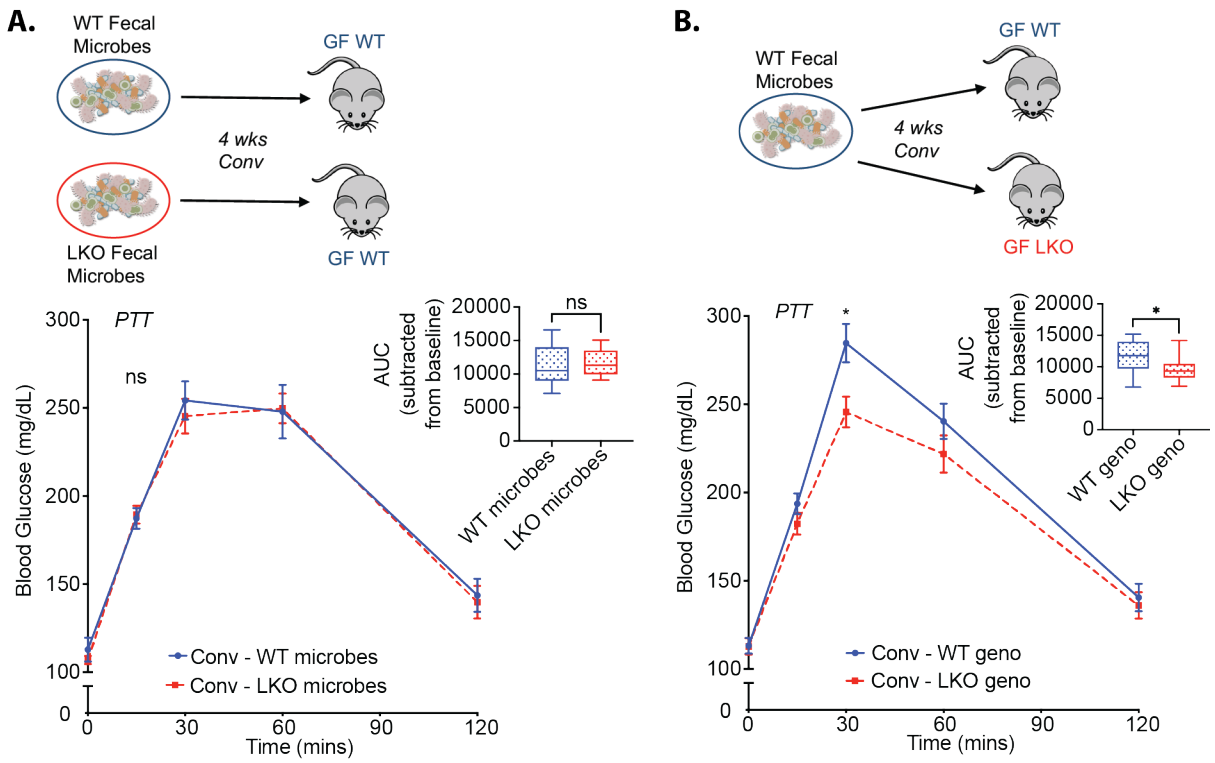

Figure 3.11: **Gut microbes are necessary, but not sufficient, for liver clock-mediated gluconeogenesis.** (A) PTT in GF WT male mice conventionalized with fecal microbes from SPF WT or LKO male mice (n=11-12/group). (B) PTT in GF WT and LKO male mice conventionalized with fecal microbes from SPF WT male mice (n=15-16/group). Inset graphs represent AUC normalized to baseline glucose. Data points represent mean±SEM, box plots represent median±min/max. $*p < 0.05$, ns=not significant.

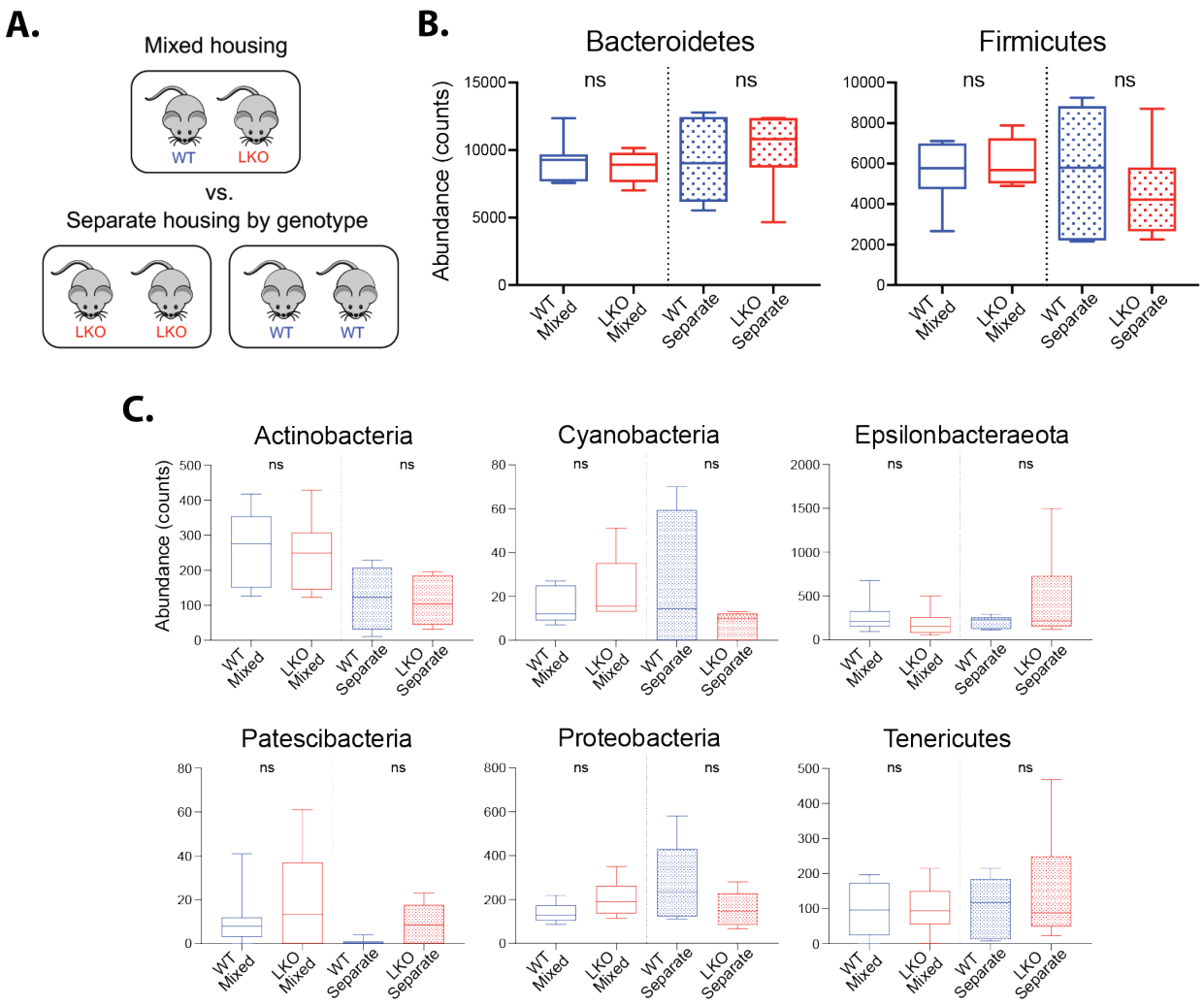

Figure 3.12: **Liver circadian clock status does not impact gut microbial community membership.** (A) Experimental scheme of mixed vs. separate housing at time of weaning. (B,C) 16S rRNA gene sequencing analysis of stool collected from WT vs LKO male mice housed either by mixed genotypes (WT+LKO) or via separate housing of genotypes (WT+WT and LKO+LKO) (n=6-7/group); abundance counts of major (B) and minor (C) phyla. Box plots represent median±min/max; ns=not significant.

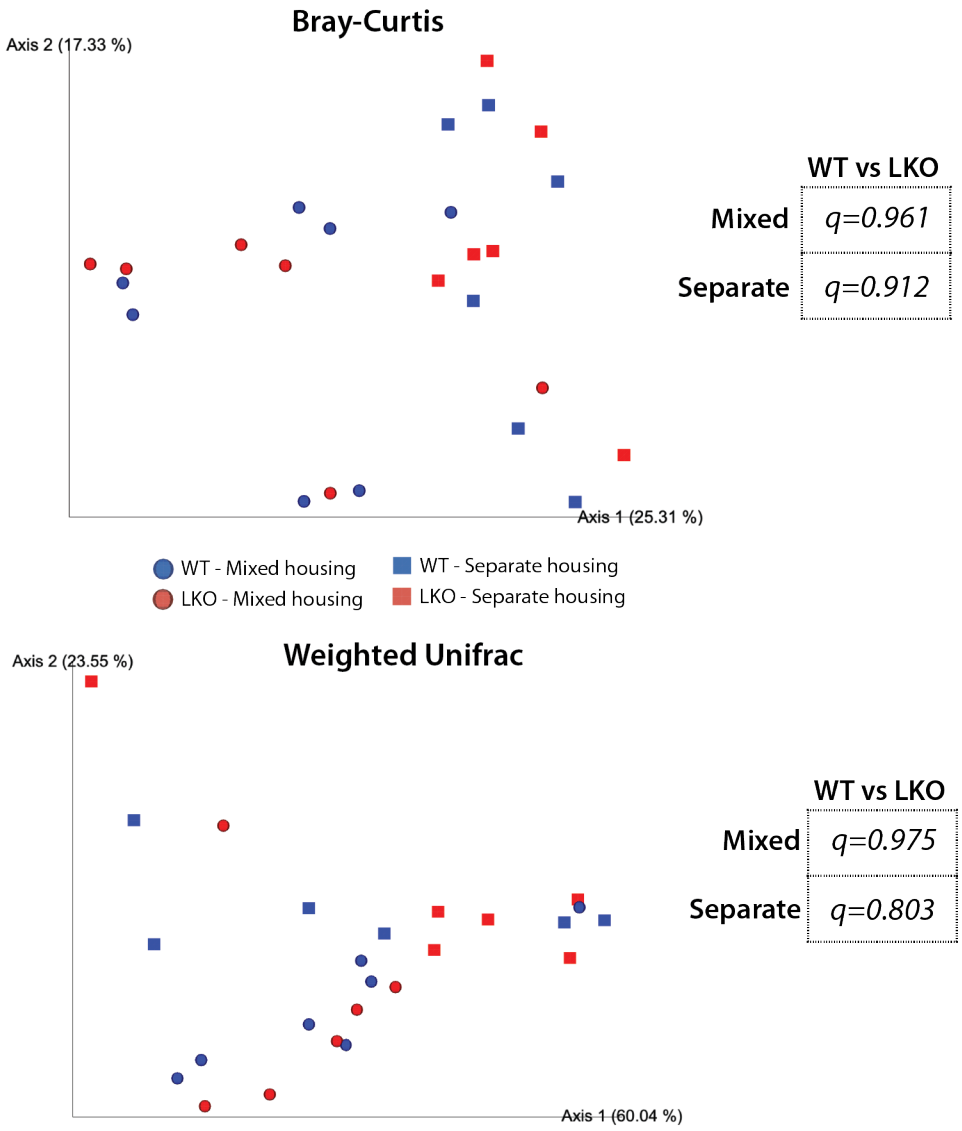

Figure 3.13: **Liver circadian clock status does not impact gut microbial community membership by beta-diversity metrics.** 16S rRNA gene sequencing analysis of stool collected from WT vs LKO male mice housed either by mixed genotypes (WT+LKO) or via separate housing of genotypes (WT+WT and LKO+LKO) (n=6-7/group). Principle Coordinate Analysis of β-diversity Bray-curtis and Weighted Unifrac distance metrics, with associated q-values by PERMANOVA calculated via QIIME2.

3.4.4 The liver clock drives oscillations of specific microbiota community members

Global murine deletion of Bmal1 has been shown to alter diurnal oscillations of fecal microbiota [178]. We inquired whether liver clock functionality impacted diurnal oscillations of fecal microbiota collected from WT and LKO male and female mice every 6 hours over 48-hours (Figure 3.14A). We found that bacterial load was similar between WT and LKO across all timepoints in both sexes (Figures 3.14B, 3.15A). We next employed empirical Jonckheere-Terpstra-Kendall CYCLE (eJTK) to identify significantly oscillating ASVs and discovered that LKO mice exhibit nearly twice the number of oscillating ASVs compared to WT (Figure 3.14C,D). The influx of unique oscillating microbes in LKO was mostly attributed to ASVs identified to class Clostridiales. However, we observed little difference in the number of oscillating Bacteroidales ASVs, suggesting LKO may specifically impact diurnal oscillations of Clostridiales microbes. Conversely, in female mice, we observed an opposite pattern of fewer significantly oscillating ASVs in LKO compared to WT (Figure 3.15B), and no oscillating Clostridiales ASVs in common between groups (Figure 3.15C). Similar to our tolerance test data, this suggests that liver clock-modulation of oscillating fecal microbiota is impacted by sex.

Aside from proportion, the relative abundance of oscillating ASVs was also significantly greater in LKO relative to WT (Figure 3.16A). Upon plotting abundance of total vs oscillating Bacteroidales and Clostridiales ASVs, we identified that overall abundance was not different between WT and LKO, but only Clostridiales exhibited increased abundance of oscillators in LKO (Figure 3.16B). We then examined oscillating Clostridiales at the family level and identified that Lachnospiraceae and Ruminococcaceae accounted for the gain of uniquely oscillating ASVs in LKO (Figure 3.17A). While the total abundance of either family was not different between genotypes, the abundance of oscillating ASVs significantly increased within LKO (Figure 3.17B). Interestingly, among the ASVs annotated to species,

Lactobacillus murinus followed the same pattern of gained oscillation in LKO while total abundance remained constant (Figure 3.17C).

Despite no changes in overall microbiota abundance profiles, the loss of a functional liver clock drives a unique signature of increased diurnal oscillations in specific stool microbiota community members, particularly those belonging to the class Clostridiales.

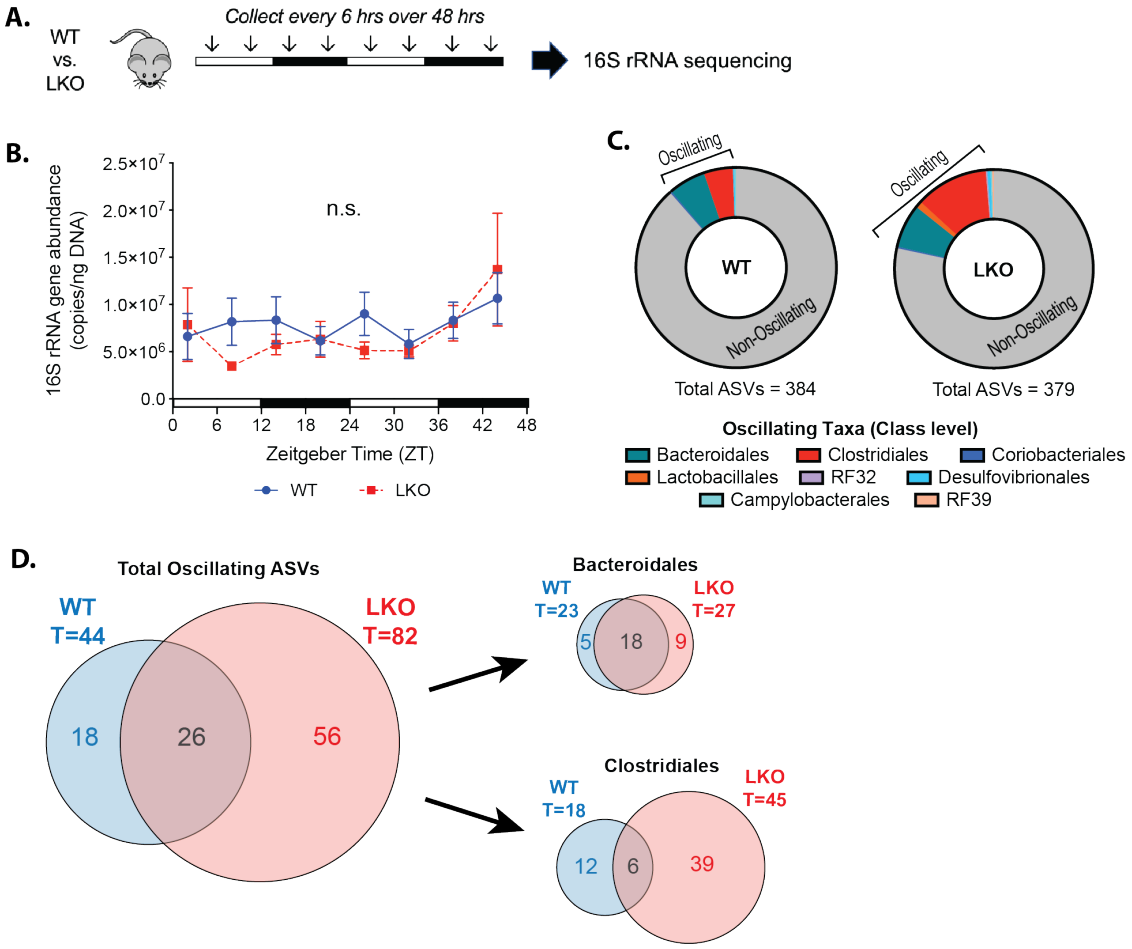

Figure 3.14: **Liver circadian clock drives unique oscillation patterns of Clostridiales in stool from male mice.** 16S rRNA gene sequencing analysis of stool sampled from WT and LKO male mice every 6 hours over two consecutive 24-hr LD cycles (8 samples per animal) via repeat collections from the same mouse (n=7-8/group). (A) Experimental scheme of 48-hr stool collection. (B) 16S rRNA gene abundance measured via qPCR normalized to DNA concentration. (C) Proportion of non-oscillating (grey area) vs significantly oscillating (colored areas) Amplicon Sequence Variants (ASVs) identified via eJTK; oscillating ASVs divided by taxonomic class. (D) Venn diagrams presenting total (T), shared, and unique oscillating ASVs among all taxonomic groups, as well as within specific classes Bacteroidales and Clostridiales. Data represent mean±SEM. ns=not significant.

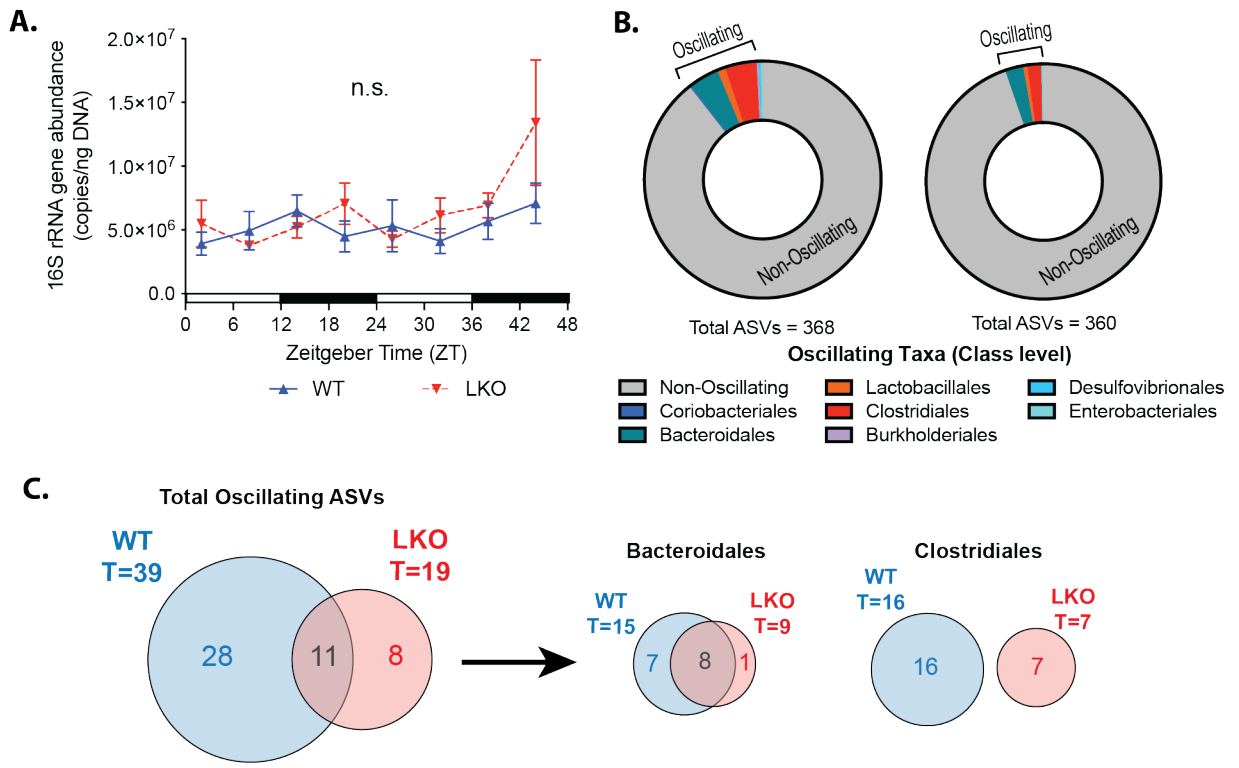

Figure 3.15: **Liver circadian clock disruption reduces oscillating microbial features in stool from female mice.** 16S rRNA gene sequencing analysis of stool sampled from WT and LKO female mice every 6 hours over two consecutive 24-hr LD cycles (8 samples per animal) via repeat collections from the same mouse (n=8/group). (A) 16S rRNA gene abundance measured via qPCR normalized to DNA concentration. (B) Proportion of non-oscillating (grey area) vs significantly oscillating (colored areas) ASVs identified via eJTK; oscillating ASVs divided by taxonomic class. (C) Venn diagrams presenting total, shared, and unique oscillating ASVs among all taxonomic groups, as well as within specific classes Bacteroidales and Clostridiales (none shared between WT and LKO). Data represent mean±SEM. ns=not significant.

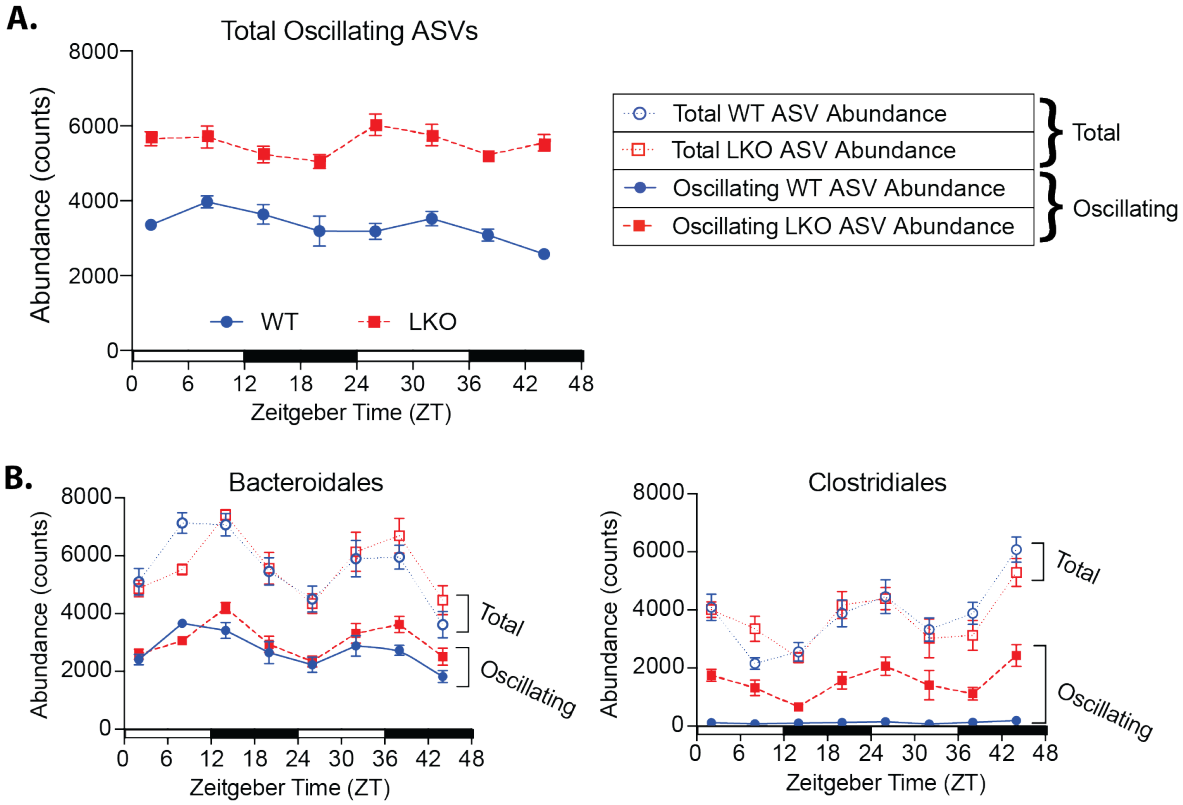

Figure 3.16: **Loss of a functional liver clock results in increased abundance of oscillating Clostridiales.** 16S rRNA gene sequencing analysis of stool sampled from WT and LKO male mice every 6 hours over two consecutive 24-hr LD cycles (8 samples per animal) via repeat collections from the same mouse (n=7-8/group). (A) Abundance counts of all oscillating ASVs. (B) Abundance counts of total vs oscillating ASVs within classes Bacteroidales and Clostridiales. Data represent mean±SEM.

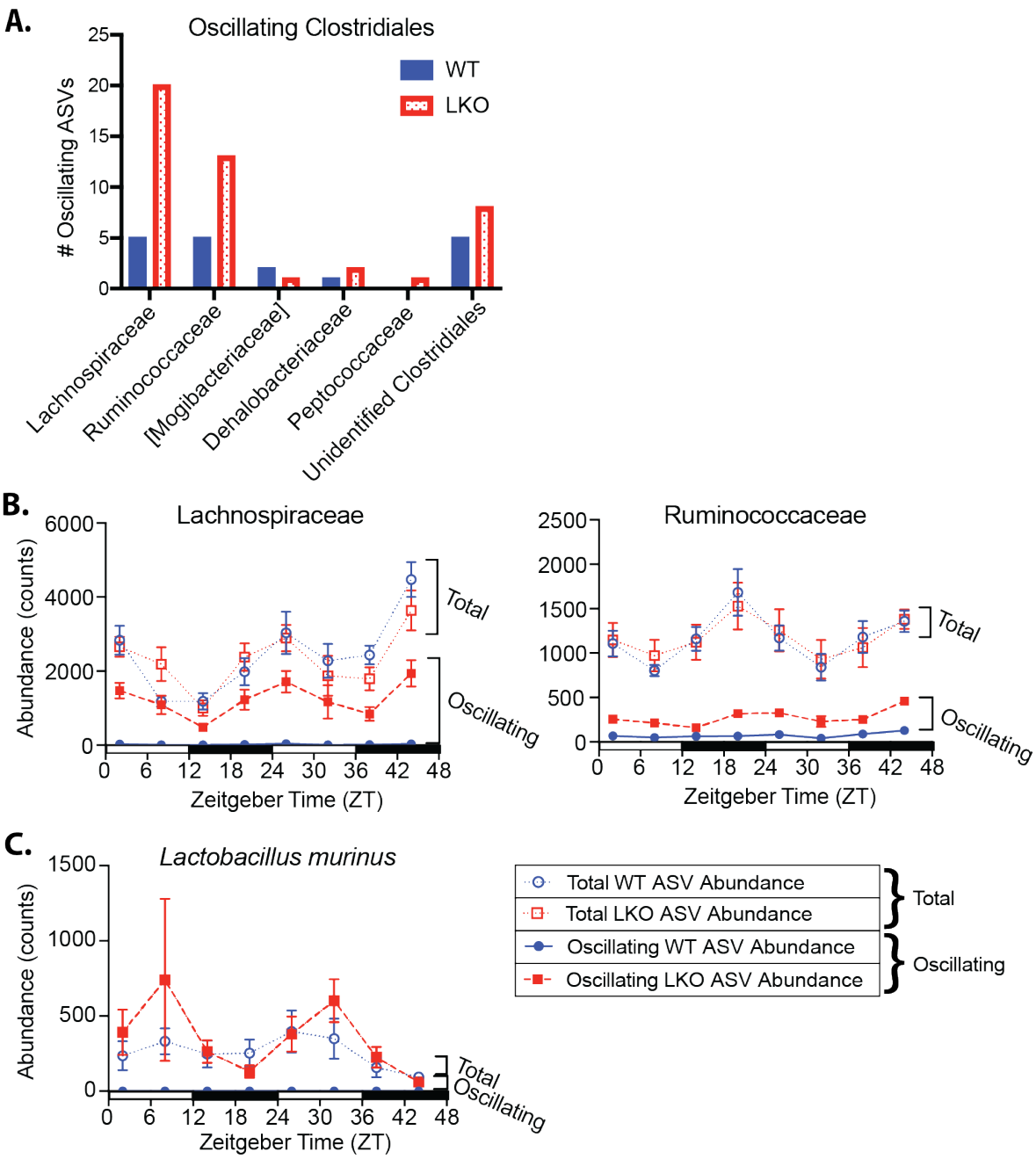

Figure 3.17: **Loss of a functional liver clock results in increased abundance of oscillating Ruminococcaceae and Lachnospiraceae.** 16S rRNA gene sequencing analysis of stool sampled from WT and LKO male mice every 6 hours over two consecutive 24-hr LD cycles (8 samples per animal) via repeat collections from the same mouse (n=7-8/group). (A) Number of oscillating Clostridiales ASVs at the family level in WT and LKO. (B) Abundance counts of total vs oscillating ASVs within families Lachnospiraceae and Ruminococcaceae. (C) Abundance counts of total vs oscillating ASVs within *Lactobacillus murinus*. Data represent mean±SEM.

3.4.5 The liver clock is the main driver of hepatic transcriptomes, secondarily influenced by gut microbes

Given that liver clock and gut microbes regulate gluconeogenesis, we sought to determine if other metabolic pathways were impacted. We performed RNA-sequencing of liver samples collected every 4 hours over 24-hours from SPF and GF, WT and LKO male mice, and the data were analyzed via three approaches (Figure 3.18A). Principle Component Analysis of pooled samples revealed distinct separation by genotype along PC1 and microbial status along PC2 (49% and 12% of variance, respectively) (Figure 3.18B). Similar patterns were observed when samples were divided by timepoint, demonstrating consistency across a 24-hour period (Figure 3.18C). We also examined circadian clock gene expression over time and found very similar genotype-driven patterns in SPF and GF conditions, revealing that presence or absence of gut microbes does not greatly alter expression patterns (Figure 3.19). *Per3* and *Rev-erbα* were exceptions to this trend, in which GF groups exhibited lower expression compared to SPF counterparts of the same genotype. Overall, these data suggest a hierarchy in which liver clock functionality (genotype) is the primary driver of the hepatic transcriptome, while the gut microbiome serves as a secondary driver.

We began with our first approach by performing differential gene expression analysis via DESeq2 and fast Gene Set Enrichment Analysis (fGSEA) to identify molecular pathways impacted by the liver clock and/or gut microbes (Figure 3.18A, Approach 1). Analysis using KEGG revealed nearly all differentially expressed (DE) metabolic pathways were downregulated in LKO compared to WT, regardless of microbial status (Figure 3.20). However, the GF condition exhibited more downregulated metabolic pathways in LKO than SPF conditions. This may suggest that gut microbes stabilize pathway transcriptional regulation; that is, certain Bmal1-driven effects only emerge in absence of microbes. Differential analysis within collection timepoint revealed nearly identical patterns of overall downregulation of metabolic pathways (Figure 3.21). Importantly, we observed downregulation of "Glycoly-

sis_Gluconeogenesis" in SPF LKO compared to WT (Figure 3.20, upper panel), confirming our evidence that gluconeogenesis is impaired in SPF LKO (Figure 3.6A). We also observed downregulation of gluconeogenic pathways, including "Pyruvate_Metabolism", in GF LKO compared to WT (Figure 3.20, lower panel), while our physiological evidence reveals no difference in overall gluconeogenic output between GF WT and LKO (Figure 3.6A). This suggests that although differences in transcription between genotypes are similar in GF and SPF, additional signals contribute to reduced gluconeogenesis in GF conditions regardless of genotype.

Apart from gluconeogenesis, we observed LKO downregulation of several metabolic pathways involved in fatty acid and lipid metabolism, including "Fatty_Acid_Metabolism", "PPAR_Signaling_Pathway", "Peroxisome", and "Biosynthesis_of_Unsaturated_Fatty_Acids" (Figure 3.20). This corroborates previous findings that lipid metabolic gene expression is downregulated in SPF LKO mice compared to WT via RNA methylation [13]. The regulation of gluconeogenesis and fatty acid metabolism are intricately tied; under fasting conditions, fatty acid β-oxidation is activated to provide acetyl-CoA to generate ATP, which sustains the conversion of pyruvate and other gluconeogenic substrates into glucose [287]. Thus, the regulation of these two processes is closely linked and changes in one directly impact the other [288].

Given this differential regulation, we plotted median-normalized expression for all leading-edge transcripts within relevant pathways, confirming significant down-regulation in LKO compared to WT in both SPF and GF (Figure 3.22). We next examined expression of specific transcripts within these pathways, in particular key transcripts involved in fatty acid metabolism (Figure 3.23A; *Aldh3a2*: Aldehyde dehydrogenase 3 family member A2; *Cpt1a*: Carnitine palmitoyltransferase 1A), PPAR signaling (Figure 3.23B; *Ppar*α: Peroxisome proliferator activated receptor alpha; *Fabp1*: Fatty acid binding protein 1), and gluconeogenesis (Figure 3.23C,D; *Fbp1*: Fructose-bisphosphate 1; *Eno1*: Enolase 1; *Pck1/2*:

Phosphoenolpyruvate carboxylase 1/2). Expression was significantly reduced in many of these transcripts in LKO compared to WT regardless of microbiota status (Figure 3.23A-C). However, expression of the key rate-limiting gluconeogenesis enzymes *Pck1* and *Pck2* exhibited more nuanced patterns (Figure 3.23D). *Pck1* revealed significantly reduced expression in SPF LKO compared to WT, while both GF groups exhibited expression levels similar to SPF WT. Conversely, *Pck2* was significantly reduced in SPF LKO compared to WT, and both GF groups were reduced compared to SPF, mirroring our PTT results (Figure 3.6A). Thus, *Pck2* may be key for liver-clock- and microbially-mediated effects on gluconeogenesis, while *Pck1* is only differentially expressed in the presence of microbes.

In summary, the liver clock is the primary driver of transcriptome differential regulation, particularly for key metabolic pathways such as gluconeogenesis that are downregulated following loss of liver clock. However, gut microbes provide additional cues to modulate expression, including LKO-driven expression of the rate-limiting gluconeogenic enzyme *Pck2*.

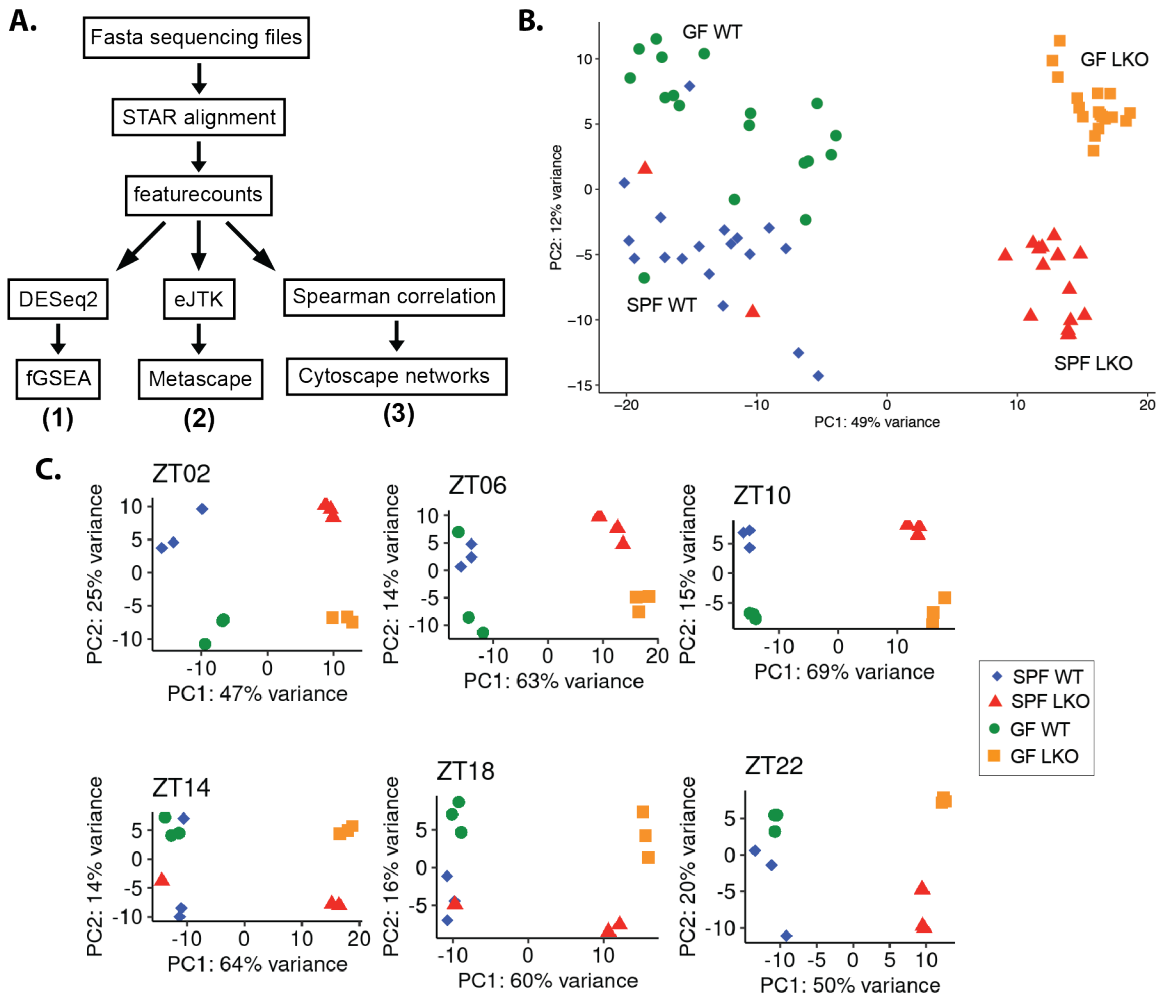

Figure 3.18: **Liver clock is the main driver of hepatic transcriptomes, secondarily influenced by gut microbes.** Diurnal transcriptome analysis of liver samples collected every 4 hours over 24-hours from animals maintained in 12:12 LD (ZT2, 6, 10, 14, 18, 22) from SPF and GF, WT and LKO male mice ($n = 3$/timepoint/group). (A) Data analysis workflow, demonstrating three arms of analysis: 1. differential expression, 2. oscillation, and 3. network co-occurrence. (B) Principal Component Analysis of transcriptome profiles, all samples pooled. (C) Principal Component Analysis of transcriptome profiles, samples divided by collection timepoint.

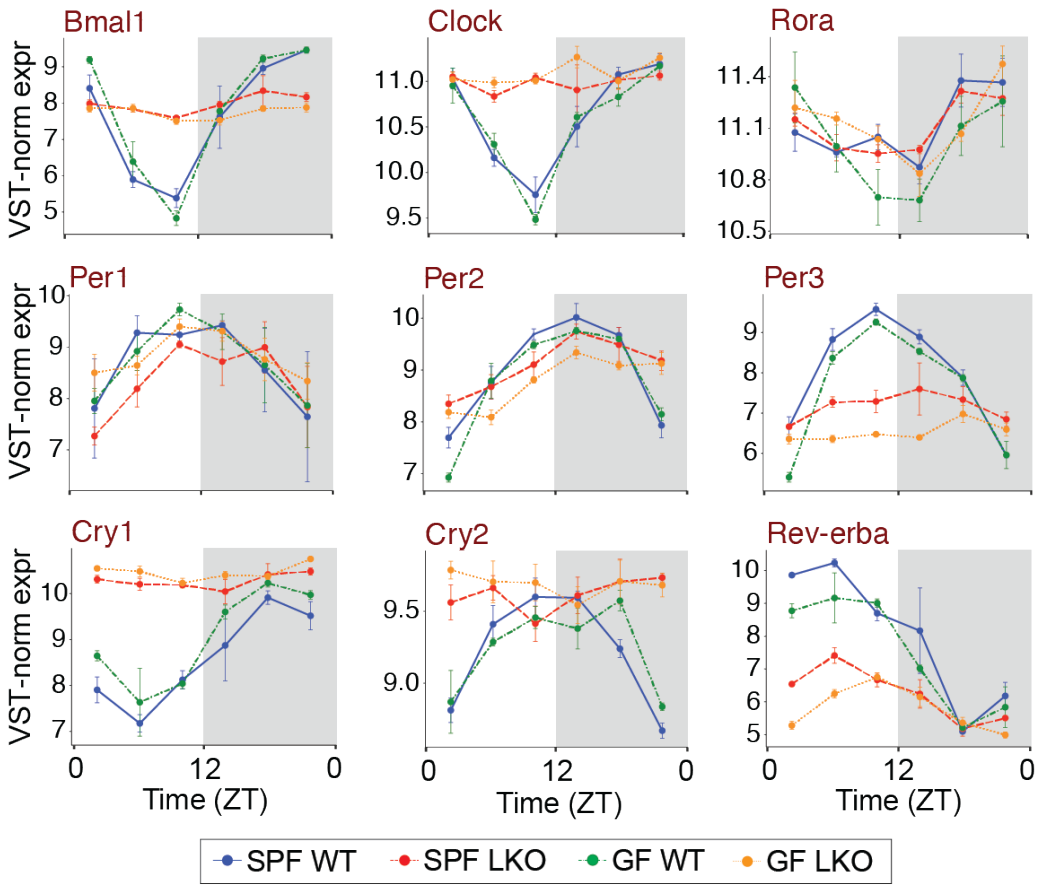

Figure 3.19: **Gut microbes do not greatly impact circadian clock gene expression patterns in the liver.** Diurnal transcriptome analysis of liver samples collected every 4 hours over 24-hours from animals maintained in 12:12 LD (ZT2, 6, 10, 14, 18, 22) from SPF and GF, WT and LKO male mice (n = 3/timepoint/group). Variance-stabilizing transformed (VST)-normalized expression of core circadian clock genes. Data represent mean±SEM.

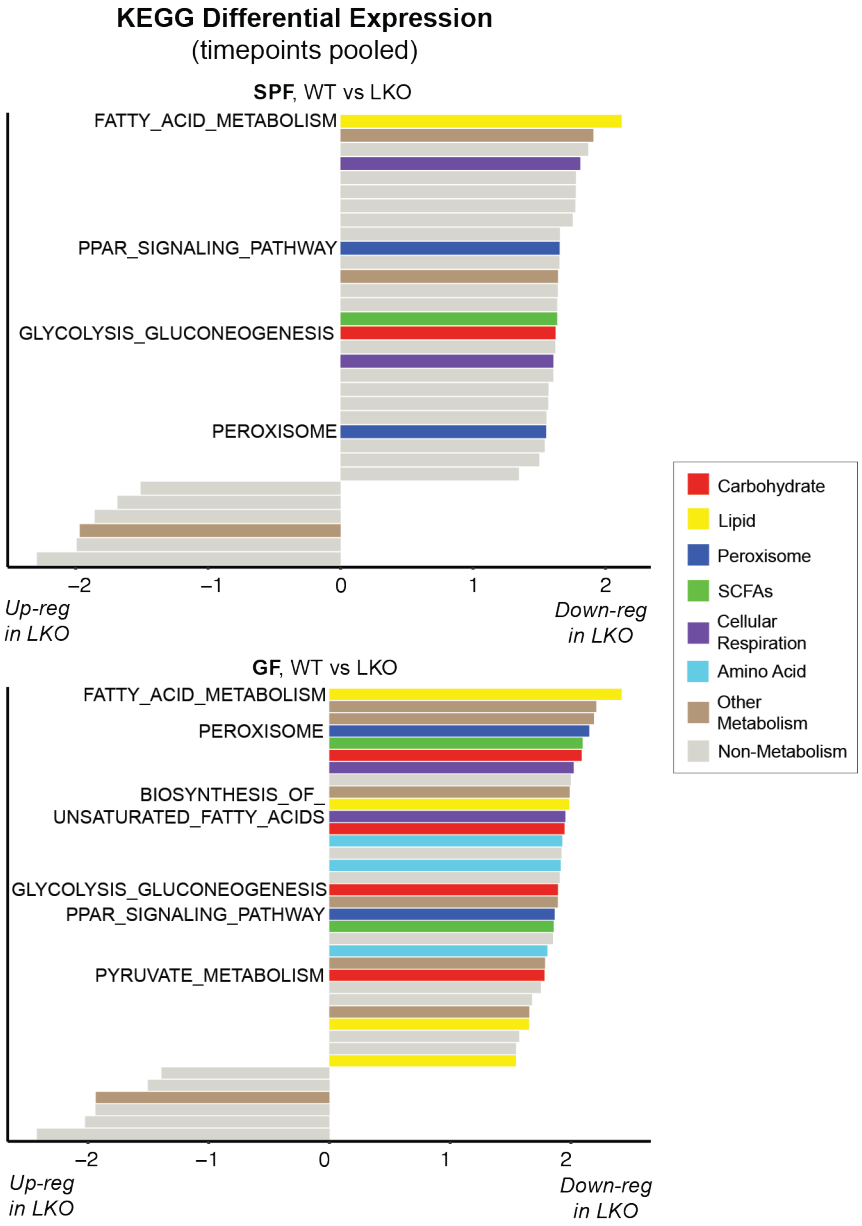

Figure 3.20: **Metabolic pathway gene expression is downregulated in absence of a liver clock across time, regardless of microbial status.** Diurnal transcriptome analysis of liver samples collected every 4 hours over 24-hours from animals maintained in 12:12 LD (ZT2, 6, 10, 14, 18, 22) from SPF and GF, WT and LKO male mice ($n = 3$/timepoint/group). Differentially regulated KEGG pathways between WT and LKO, within SPF and GF, timepoints pooled. Metabolic pathways colored according to legend, non-metabolic pathways colored gray. Bars to the right of plot midline represent pathways downregulated in LKO compared to WT; bars to the left represent pathways upregulated in LKO compared to WT. Listed pathway titles are addressed intext.

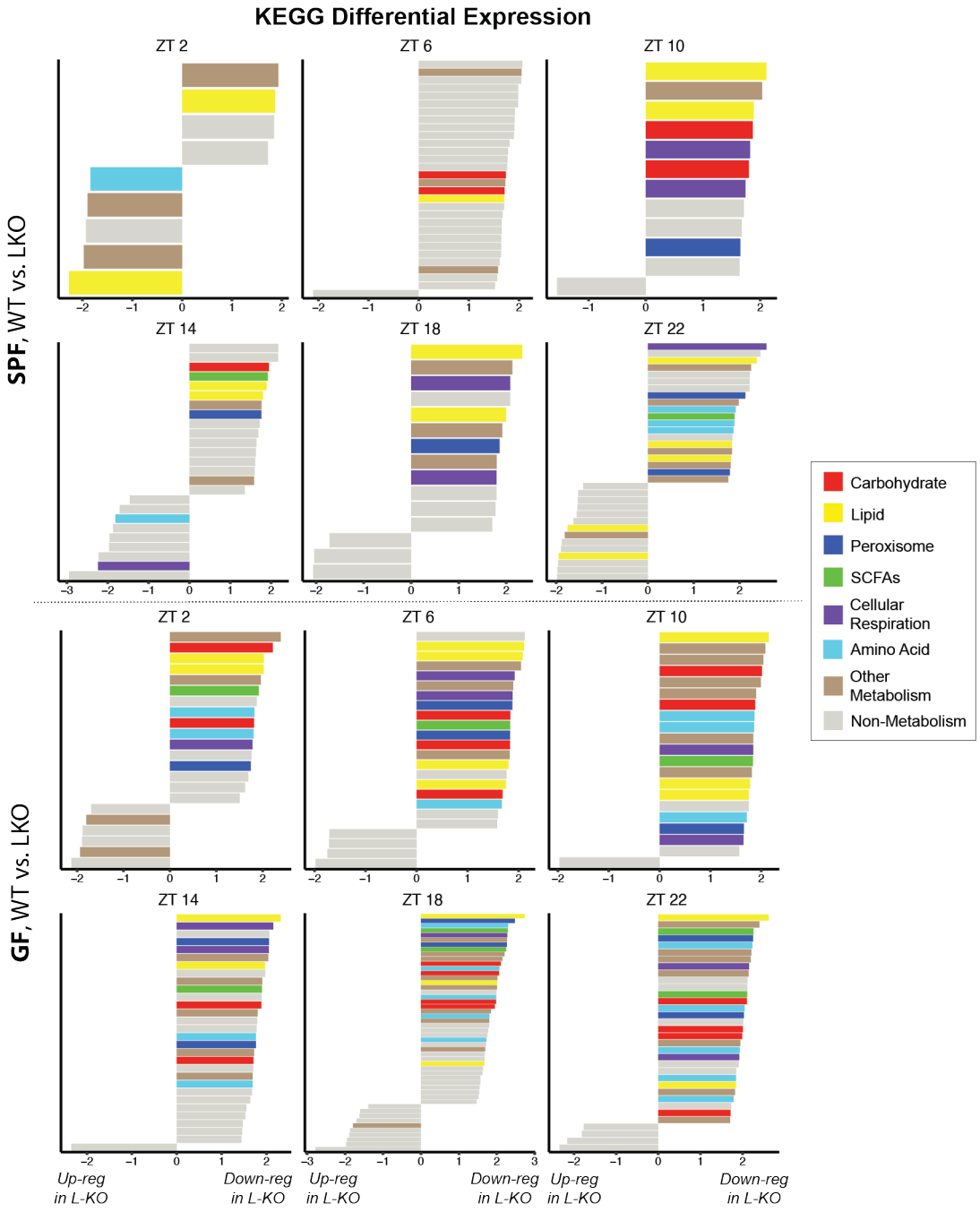

Figure 3.21: **Liver-clock downregulation of metabolic pathways is evident across all timepoints.** Diurnal transcriptome analysis of liver samples collected every 4 hours over 24-hours from animals maintained in 12:12 LD (ZT2, 6, 10, 14, 18, 22) from SPF and GF, WT and LKO male mice (n = 3/timepoint/group). Differentially regulated KEGG pathways between WT and LKO, within SPF and GF, divided by ZT collection timepoint. Metabolic pathways are highlighted according to the legend, and non-metabolic pathways are colored gray.

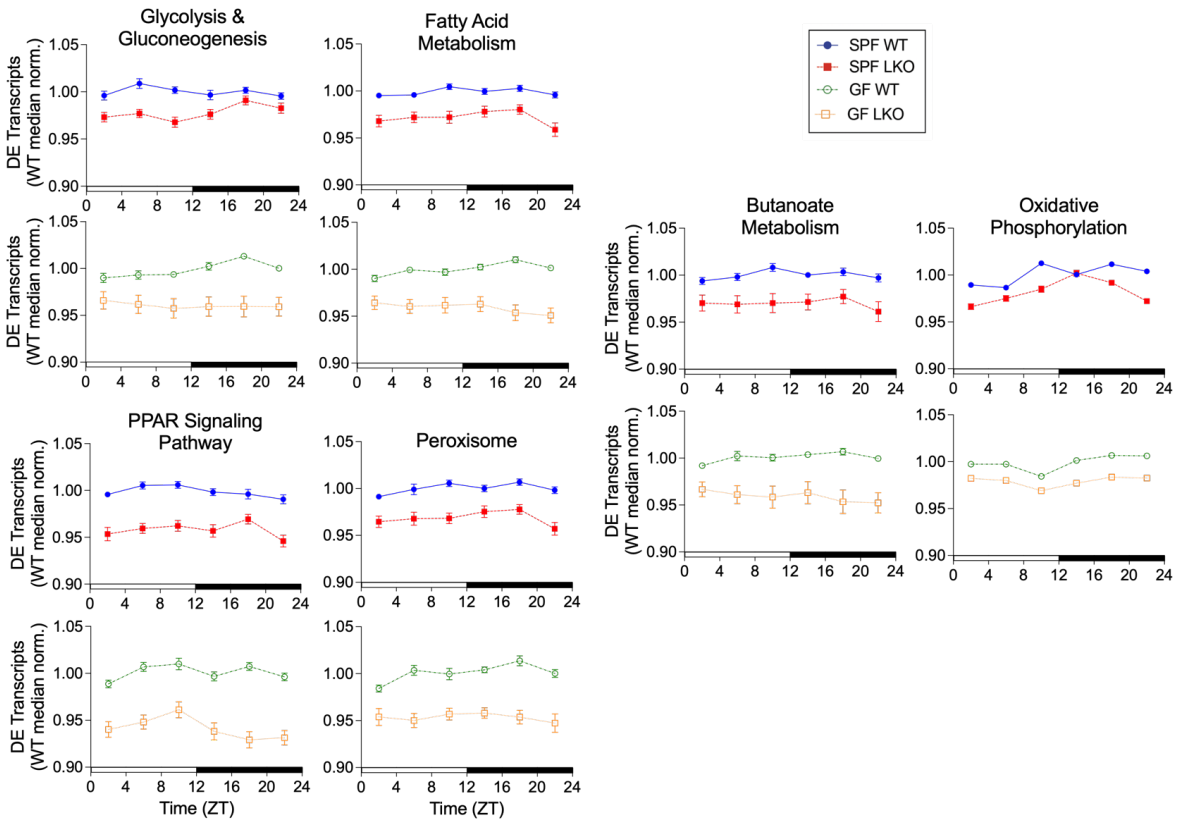

Figure 3.22: **Absence of a liver clock results in downregulation of glucose and lipid metabolic pathways is evident across all timepoints, regardless of microbes.** Diurnal transcriptome analysis of liver samples collected every 4 hours over 24-hours from animals maintained in 12:12 LD (ZT2, 6, 10, 14, 18, 22) from SPF and GF, WT and LKO male mice (n = 3/timepoint/group). WT-median-normalized expression of differentially expressed (DE) genes within identified KEGG pathways. Data represent mean±SEM.

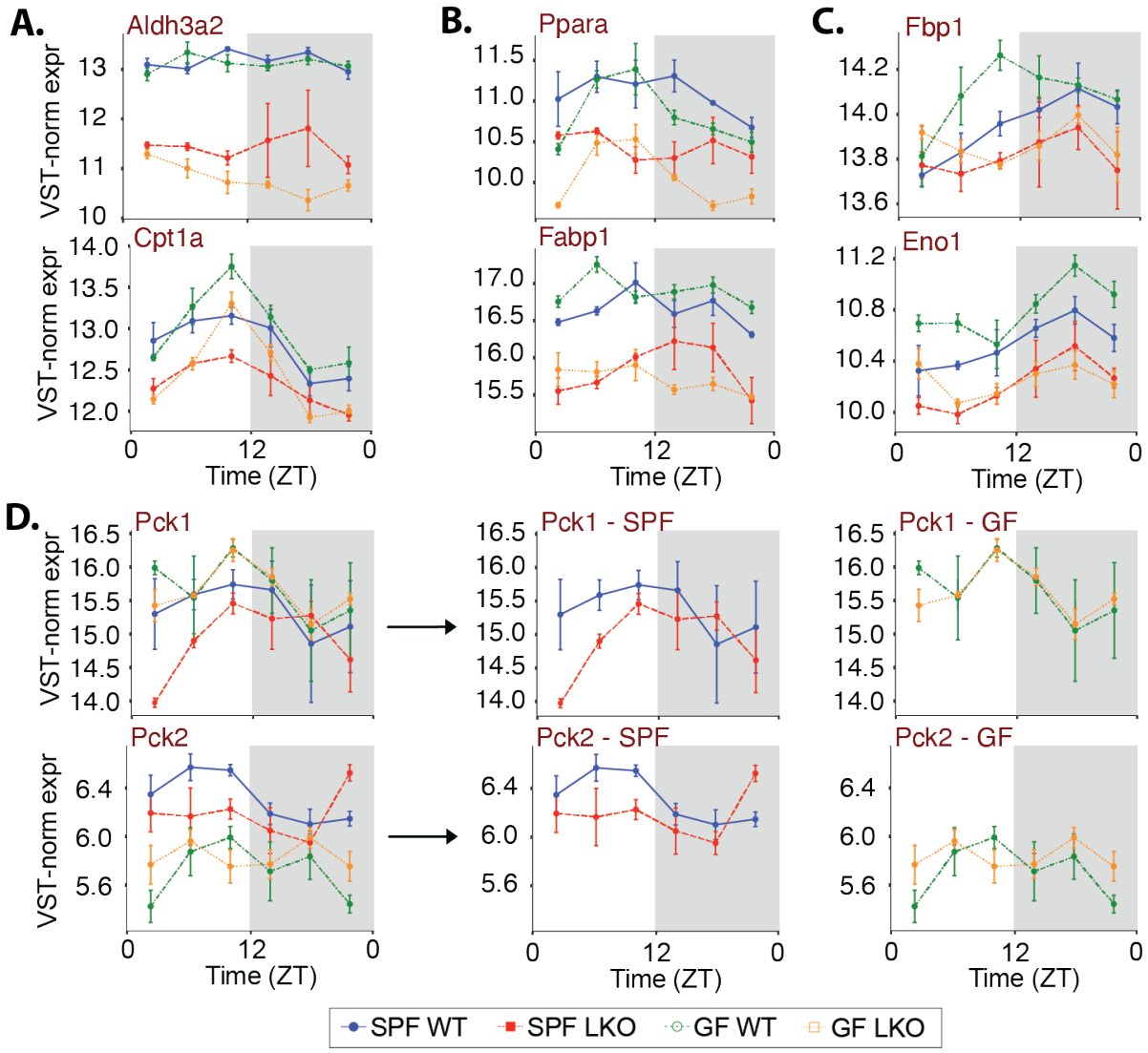

Figure 3.23: **Gut microbes work through the liver clock to impart unique expression patterns of key gluconeogenic genes.** Diurnal transcriptome analysis of liver samples collected every 4 hours over 24-hours from animals maintained in 12:12 LD (ZT2, 6, 10, 14, 18, 22) from SPF and GF, WT and LKO male mice (n = 3/timepoint/group). Variance-stabilizing transformed (VST)-normalized expression of leading-edge genes in fatty acid metabolism (A), PPAR signaling (B), and gluconeogenesis (C,D) differentially expressed between WT and LKO in SPF and GF, with the exception of *Pck1* and *Pck2* (D) which are only differentially expressed in SPF (SPF and GF groups also shown separately). Data represent mean±SEM.

3.4.6 Liver clock and gut microbes drive unique hepatic transcriptome oscillations that influence gluconeogenesis and fatty acid metabolic pathway expression

Given previous studies [181], we identified all significantly oscillating transcripts within each group via eJTK (Figure 3.18A, Approach 2). SPF LKO exhibited more oscillating transcripts than WT (1503 vs 1104), and GF LKO exhibited a similar increase relative to GF WT (3580 vs 2544) (Figure 3.24A). Only 155 transcripts were oscillating in all groups, while many were uniquely oscillating in a single group. This emergence of unique oscillators in the absence of a functional liver clock mirrored the pattern observed in ASV relative abundance in repeat-collected stool (Figure 3.14C,D). These data reveal that loss of key drivers (i.e., the liver clock or gut microbes) results in emergence of unique oscillatory elements both in the hepatic transcriptome and gut microbiota community, which may contribute to a loss in metabolic homeostasis *in vivo*.

We then compared oscillating gene expression patterns. While SPF WT transcripts exhibit clear diurnal patterns, oscillations were significantly dampened in LKO, regardless of microbial status (Figure 3.25). Conversely, the oscillation patterns were well-preserved in GF WT, reinforcing that the liver clock is the main driver of core oscillating transcripts. We next partitioned oscillating transcripts to those that are system-driven, liver-clock-driven, liver clock-independent, microbe-driven, and microbe-independent (Figure 3.24B,C). System-driven transcripts exhibited a conserved oscillation pattern across groups, while the other sets exhibited dampened oscillations. For example, the microbe-independent transcripts demonstrated robust oscillation across GF groups, with clear dampening of oscillation across SPF groups. Interestingly, the only subset of transcripts that exhibited a unique pattern were the liver-clock-driven oscillating transcripts (Figure 3.24B). While both WT groups exhibited robust oscillations in liver clock-driven transcripts, LKO exhibited severe dampening. Between LKO groups, SPF LKO displayed a more preserved organization of

oscillating transcripts, while the highest level of disorganization was observed in GF LKO relative to WT. This suggests that the liver clock and gut microbes impart combinatorial action on the temporal organization of specific liver-clock-driven diurnal hepatic gene expression.

Next, we applied Metascape [270] to statistically determine which pathways were significantly enriched by each group of oscillating transcripts ($q < 0.05$, summarized in Tables A.2, A.3, A.4, and A.5). Examining pathways enriched by SPF WT oscillating liver transcripts relative to other groups, we observed each factor (liver clock and gut microbiota) elicited similar levels, reduced levels, or total absence of enrichment (Figure 3.26). Both SPF and GF WT exhibited similar enrichment across many pathways, supporting our finding that hepatic transcriptome oscillation patterns are primarily driven by the liver clock. However, we observed enrichment of Reactome "Pyruvate Metabolism" only in SPF WT oscillating transcripts. This loss of oscillating pyruvate metabolism transcripts could contribute to the observed reduction in gluconeogenic output detected in SPF LKO and both GF groups (Figure 3.6A). KEGG "2-oxocarboxylic acid metabolism", which includes pyruvate metabolism, also exhibited loss of enrichment in both LKO groups while WT groups exhibited enrichment (Figure 3.26).

In addition to glucose pathways, we also noted differential enrichment of lipid metabolic pathways (Figure 3.26). Reactome "Metabolism of lipids" was differentially enriched in all groups, where SPF WT exhibited the greatest enrichment, SPF LKO was intermediate, and both GF groups exhibited the lowest enrichment. This signifies a deviation from normal (SPF WT) oscillation patterns in transcripts that are key mediators of lipid metabolism. Importantly, several fatty acid pathways, including "Fatty acid metabolism", "Biosynthesis of unsaturated fatty acids", several linoleic acid pathways, "Peroxisome", and "PPAR signaling pathway" lacked any significant enrichment in SPF LKO oscillating transcripts, and reduced or absent enrichment across both GF groups. The recurrence of altered fatty acid metabolic pathway enrichment, alongside altered pathways associated with gluconeogenesis

expression, supports our previous claim of concurrent and synchronized regulation of these two metabolic pathways that impart key impacts on global glucose regulation.

Overall, the liver clock and gut microbes independently impart a unique influence on oscillating transcripts, and absence of both drivers results in further disorganization of oscillating transcripts. Although LKO and GF mice exhibit increased, unique oscillating transcripts, the normal enrichment of key gluconeogenesis and fatty acid metabolic pathways is reduced or lost in LKO and GF, further supporting the impaired efficiency of these metabolic processes *in vivo*.

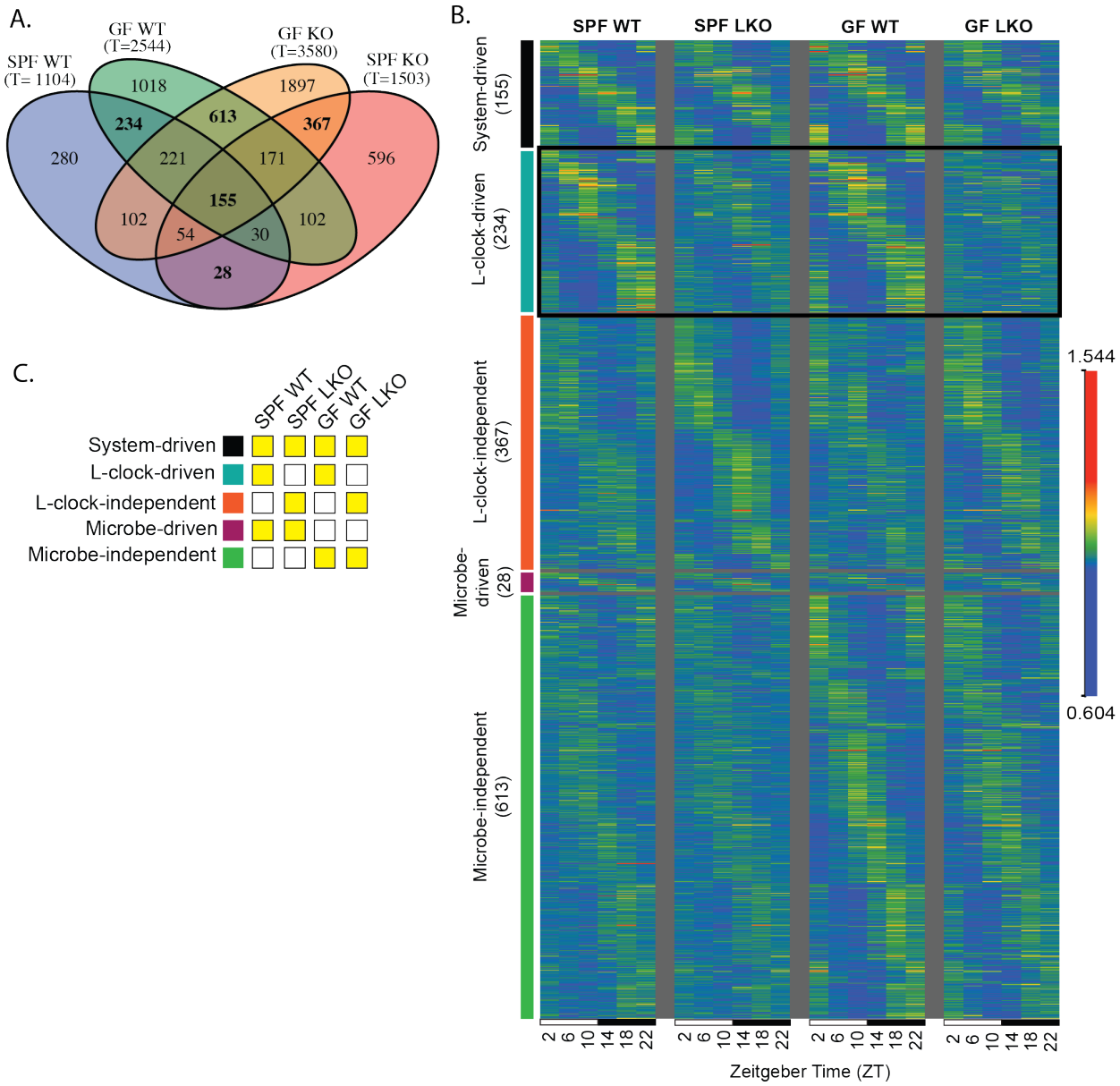

Figure 3.24: **Liver clock and gut microbes drive unique hepatic transcriptome oscillations.** Diurnal transcriptome analysis of liver samples collected every 4 hours over 24-hours from animals maintained in 12:12 LD (ZT2, 6, 10, 14, 18, 22) from SPF and GF, WT and LKO male mice ($n = 3$/timepoint/group). (A) Venn diagram of significantly oscillating transcripts across each group; total number of oscillating transcripts are under each group title; oscillating transcripts identified via eJTK ($GammaBH < 0.05$); bold numbers are visualized in (B). (B,C) Expression of significantly oscillating transcripts that are system-driven, liver-clock-driven or -independent, and microbe-driven or -independent (B); expression normalized by median, transcripts ordered by time of max expression and phase; legend (C) indicates which transcripts are depicted in each by yellow highlight.

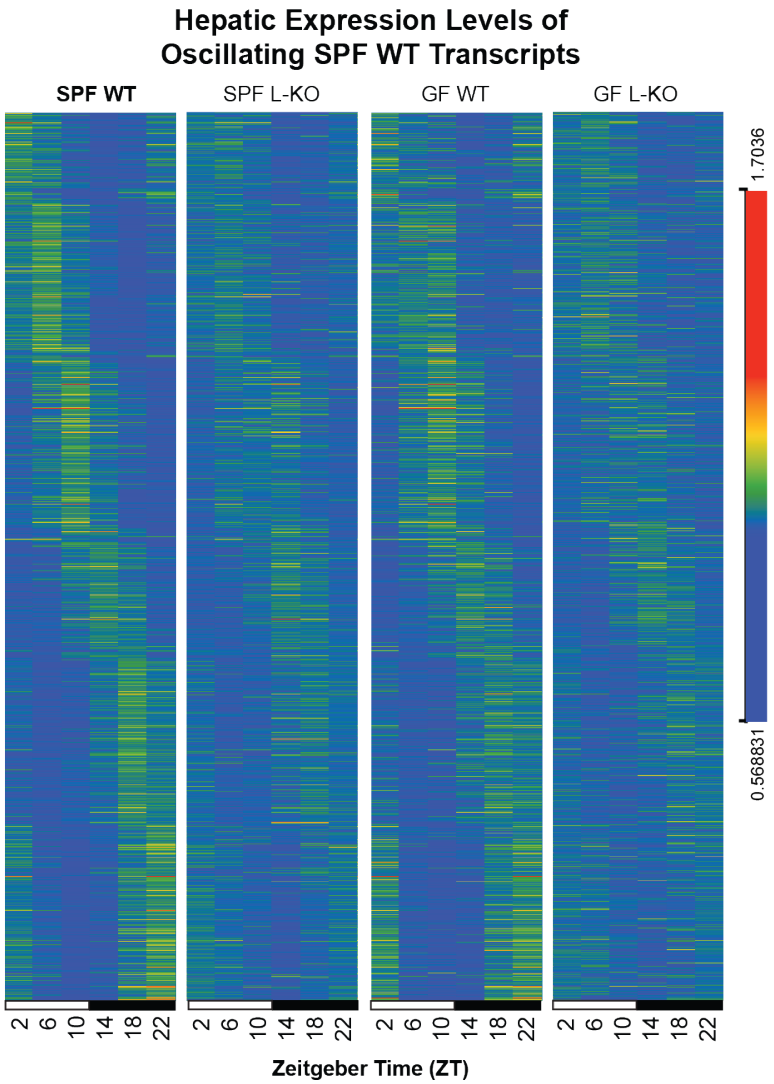

Figure 3.25: **SPF WT transcriptome oscillations are significantly dampened in LKO, regardless of microbes.** Diurnal transcriptome analysis of liver samples collected every 4 hours over 24-hours from animals maintained in 12:12 LD (ZT2, 6, 10, 14, 18, 22) from SPF and GF, WT and LKO male mice ($n = 3$/timepoint/group). Transcript expression profiles of significantly oscillating SPF WT transcripts; expression values normalized by median, transcripts ordered by time of maximum expression and phase.

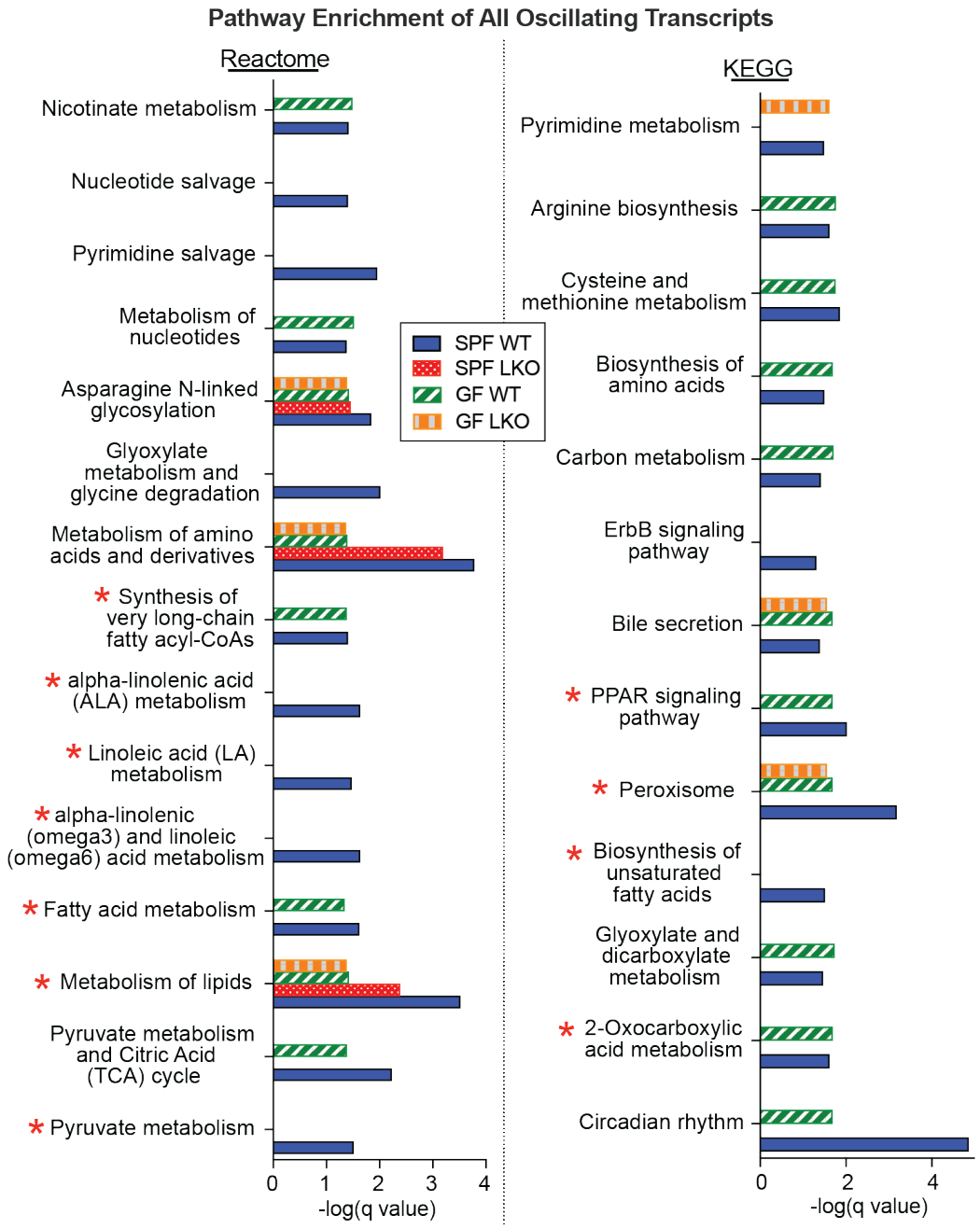

Figure 3.26: **Liver clock and gut microbes uniquely impact functional pathway enrichment of oscillating hepatic transcripts.** Diurnal transcriptome analysis of liver samples collected every 4 hours over 24-hours from animals maintained in 12:12 LD (ZT2, 6, 10, 14, 18, 22) from SPF and GF, WT and LKO male mice ($n = 3$/timepoint/group). Reactome and KEGG pathways significantly enriched by oscillating transcripts within each group; subset of pathways enriched in SPF WT oscillating genes ($q < 0.05$); no bar indicates lack of significance for that group/pathway ($q > 0.05$); pathways marked with red star are addressed intext.

3.4.7 Gut microbes impact liver clock-driven network co-occurrence of transcripts

We then examined whether liver clock or gut microbes imposed an impact on transcript correlations over time by co-occurrence network analysis (Figure 3.18A, Approach 3). We calculated Spearman correlation coefficients via pairwise-comparisons of transcript reads over time to identify significant co-occurrences for network visualization (Figure 3.27 and 3.28; network statistics in Table 3.1). This allowed for the identification of nodes (correlated transcripts, $p < 0.001$) and their corresponding edges (connections between nodes). SPF LKO exhibited a modest increase in total nodes relative to WT (6116 vs. 5603); however, the number of edges increased from 20,922 (WT) to 36,702 (LKO), which is visually recognized by the density of the SPF LKO network compared to WT (Figure 3.27). Conversely, the total number of nodes and edges did not vastly differ between GF WT and LKO (Figure 3.28). Additionally, the overall density of GF networks, regardless of liver clock status, was greatly reduced in comparison to SPF.

Next, KEGG annotations were applied to significantly correlated nodes and edges. While the number of nodes annotated to Carbohydrate (KO09101), Lipid (KO09103), and Amino acid (KO09105) metabolic pathways were not vastly different between groups, SPF LKO exhibited a two-fold increase in edges annotated to these pathways compared to SPF WT , while no difference was observed between GF groups (Table 3.2; Figure 3.29A-C). Despite a modest influence of liver clock or gut microbes on the total number of connected transcripts, loss of functional liver clock, specifically in the presence of microbes results in a significant increase of abnormal connections between transcripts belonging to key metabolic pathways involved in the regulation of gluconeogenesis. This demonstrates the combinatorial action between gut microbes and liver clock in the overall organization of hepatic metabolic gene transcription over time.

These data suggest both the liver clock and gut microbes aid in maintaining temporal co-

expression of critical metabolic functional outputs of hepatic transcripts. Loss of either driver results in the emergence of abnormal connections, specifically those involved in carbohydrate and lipid metabolic pathways.

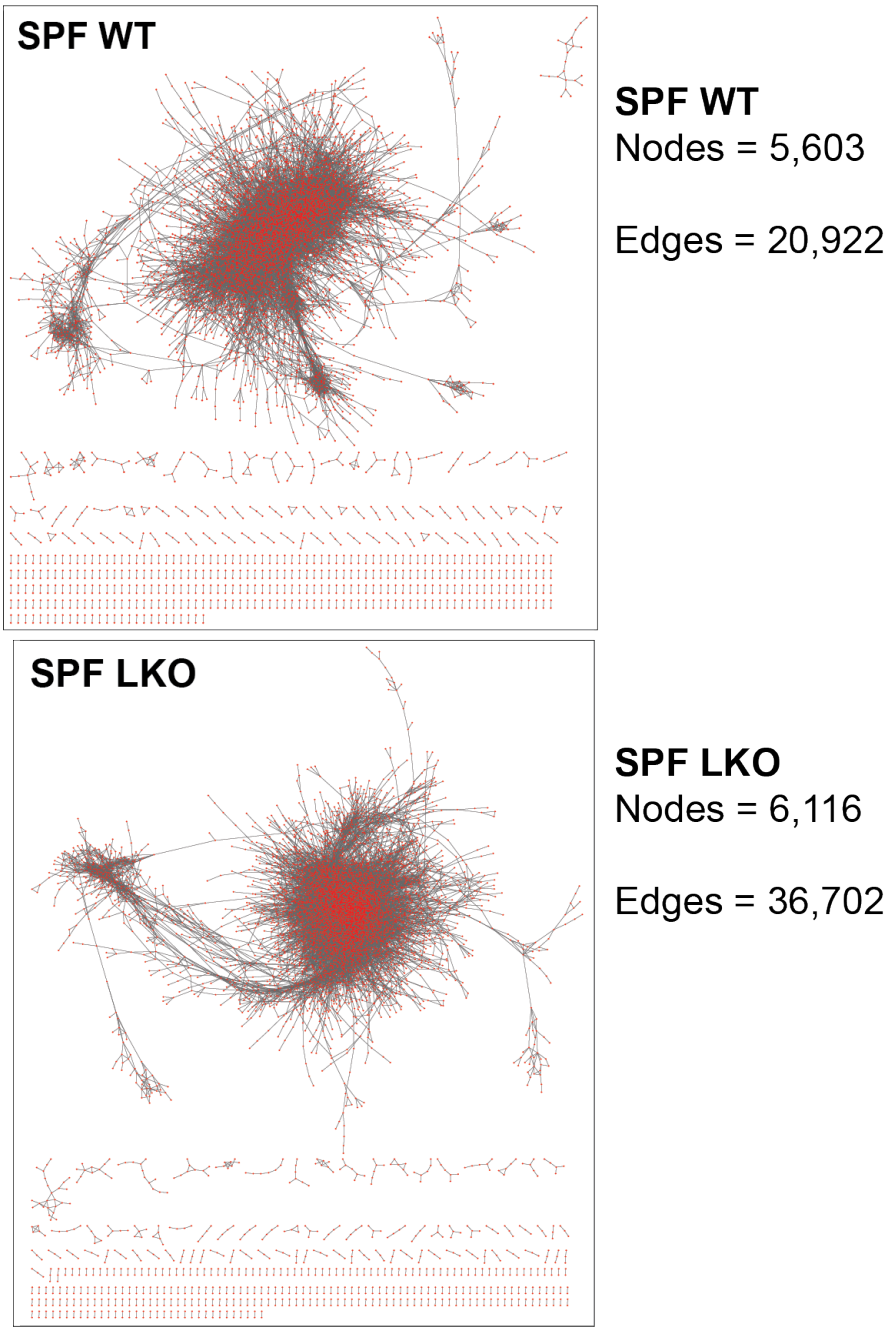

Figure 3.27: **Hepatic transcriptome co-occurrence over time is differentially impacted by the liver clock in the presence of gut microbes.** Network transcriptome analysis of liver samples collected every 4 hours over 24-hours from animals maintained in 12:12 LD (ZT2, 6, 10, 14, 18, 22) from SPF and GF, WT and LKO male mice (n=3/timepoint/group); Network co-occurrence analysis of correlating transcripts over time within each group ($p < 0.001$). Network visualization of SPF groups, and the number of correlating transcripts (nodes) and connections (edges) in each group; red dots represent nodes, grey lines represent edges.

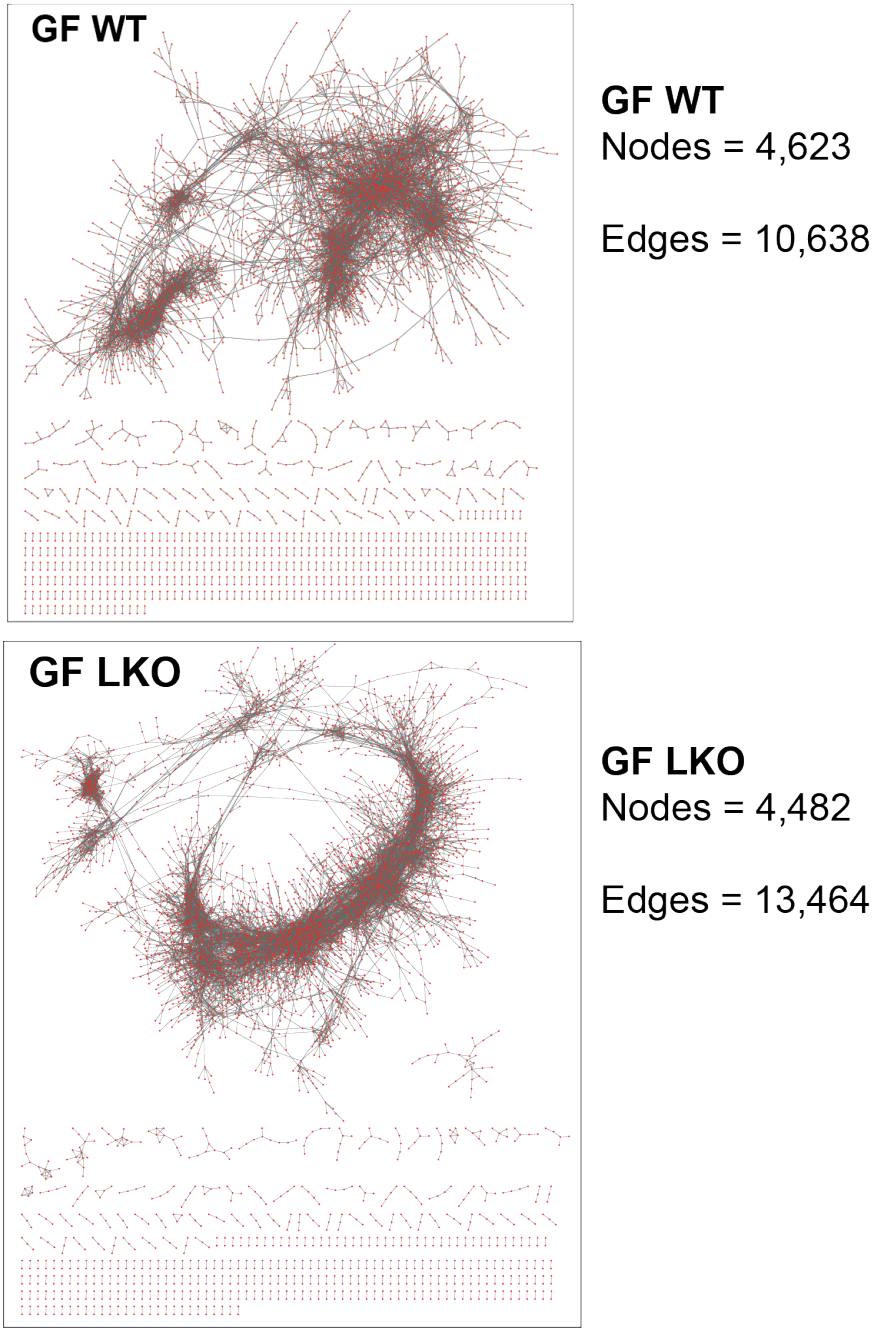

Figure 3.28: **Hepatic transcriptome co-occurrence over time is minimally impacted by the liver clock in the absence of gut microbes.** Network transcriptome analysis of liver samples collected every 4 hours over 24-hours from animals maintained in 12:12 LD (ZT2, 6, 10, 14, 18, 22) from SPF and GF, WT and LKO male mice (n=3/timepoint/group); Network co-occurrence analysis of correlating transcripts over time within each group ($p < 0.001$). Network visualization of GF groups, and the number of correlating transcripts (nodes) and connections (edges) in each group; red dots represent nodes, grey lines represent edges.

Table 3.1: **Network co-occurrence statistics.** Network transcriptome analysis of liver samples collected every 4 hours over 24-hours from animals maintained in 12:12 LD (ZT2, 6, 10, 14, 18, 22) from SPF and GF, WT and LKO male mice (n=3/timepoint/group); Network co-occurrence analysis of correlating transcripts over time within each group ($p < 0.001$).

	SPF WT	SPF LKO	GF WT	GF LKO
Number of nodes	5603	6116	4623	4482
Number of edges	20922	36702	10638	13464
Avg. number of neighbors	8.811	13.836	5.665	7.207
Network diameter	36	33	30	27
Network radius	18	17	17	17
Characteristic path length	7.072	6.587	9.787	9.073
Clustering coefficient	0.225	0.25	0.218	0.248
Network density	0.002	0.003	0.002	0.002
Network heterogeneity	1.3	1.566	1.101	1.179
Network centralization	0.021	0.036	0.013	0.015
Connected components	410	348	462	354

Table 3.2: **Network co-occurrence summarized by KEGG metabolic pathways.** Network transcriptome analysis of liver samples collected every 4 hours over 24-hours from animals maintained in 12:12 LD (ZT2, 6, 10, 14, 18, 22) from SPF and GF, WT and LKO male mice (n=3/timepoint/group); Network co-occurrence analysis of correlating transcripts over time within each group ($p < 0.001$).

	Nodes				Edges			
	SPF WT	SPF LKO	GF WT	GF LKO	SPF WT	SPF LKO	GF WT	GF LKO
Carbohydrate metabolism	127	146	119	113	755	1900	662	700
Lipid metabolism	130	148	142	123	809	1420	731	670
Amino acid metabolism	97	123	103	96	786	1759	508	459

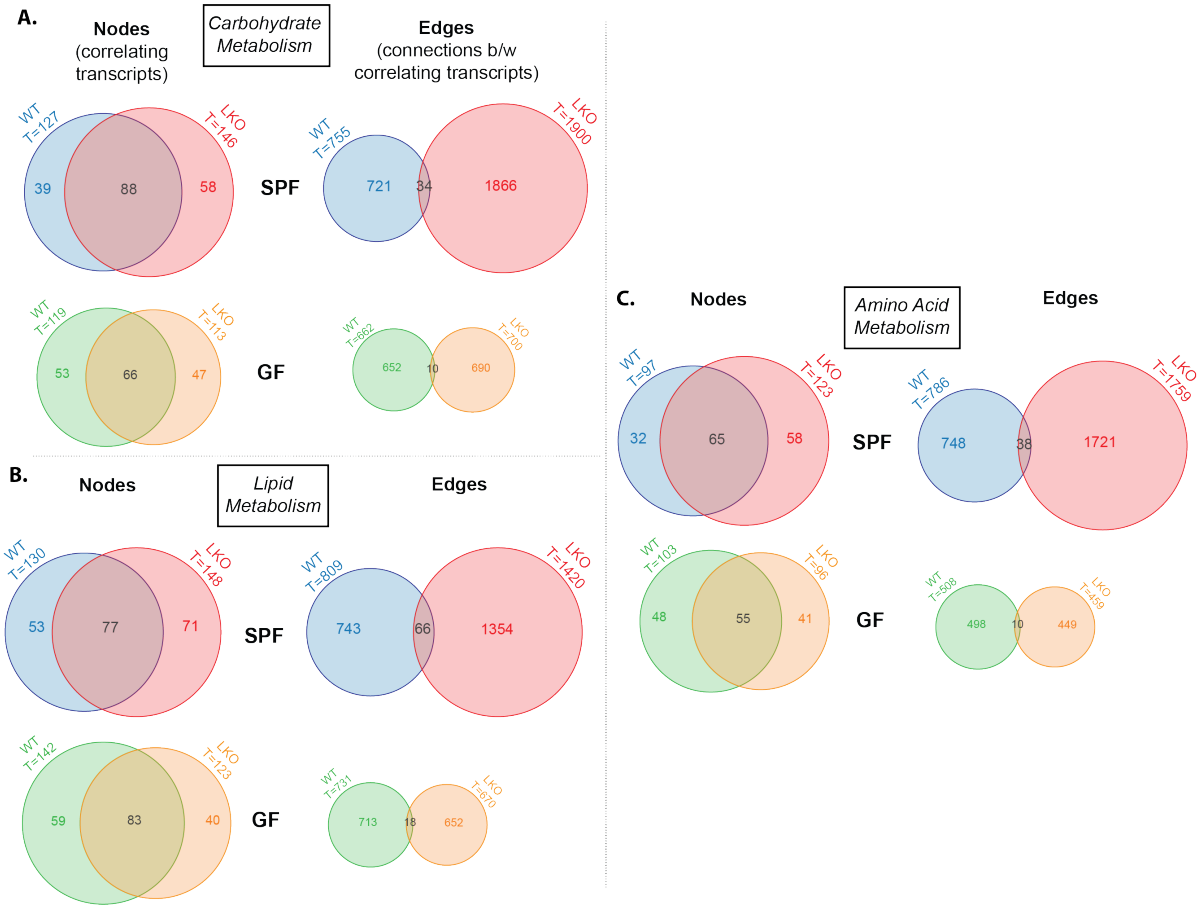

Figure 3.29: **Hepatic metabolic transcriptome co-occurrence over time is differentially impacted by the liver clock and gut microbes.** Network transcriptome analysis of liver samples collected every 4 hours over 24-hours from animals maintained in 12:12 LD (ZT2, 6, 10, 14, 18, 22) from SPF and GF, WT and LKO male mice (n=3/timepoint/group); (A-C) Venn diagrams summarizing correlating transcripts (nodes) and connections (edges) that annotate to carbohydrate (A), lipid (B), and amino acid (C) metabolic pathways by KEGG, and crossover within SPF and GF conditions; venn diagram sizes are proportional within each sub-figure.

3.4.8 Interactions between liver clock and gut microbes result in altered lipid vs carbohydrate fuel utilization

Given that loss of liver clock and gut microbes alters glucose and lipid metabolism, we interrogated how behavior, fuel utilization, and fuel switching were impacted *in vivo* via indirect calorimetry measurements over 4 days with the Promethion High-Definition Multiplexed Respirometry System. First, we detected no differences in basal metabolic rate (BMR) regardless of *Bmal1* or microbial status (Figure 3.30A). While we observed no difference in overall food intake between genotypes (Figure 3.30B), plotting hourly food intake revealed that feeding onset (indicated by arrows) was more robust in SPF LKO mice compared to WT, while no differences were evident in GF mice (Figure 3.30C). The altered feeding bouts in SPF LKO could contribute to the increased oscillating microbes over a 24-hour LD cycle, as observed in the 48-hour stool analysis (Figure 3.14C,D). Interestingly, ambulatory motion over the same period was not different in SPF mice, however GF LKO mice exhibited increased total ambulatory motion relative to their WT counterparts (Figure 3.31D,E). This indicates a liver-clock-microbiota interaction on feeding behavior, while shifts in ambulation due to a disrupted liver clock are exaggerated by a lack of gut microbes.

We next examined energy expenditure (EE) via oxygen consumption (VO_2) and fuel utilization via respiratory exchange ratio (RER; CO_2 produced/O_2 consumed). While no differences were detected between SPF genotypes during the active phase, we observed slight but significantly increased EE in SPF LKO compared to WT during the rest phase (Figure 3.32A,B). These patterns were not evident in GF conditions. We then measured RER and revealed that SPF LKO mice exhibited significantly increased RER during the active period, implying a greater utilization of carbohydrates and reduced utilization of lipids (Figure 3.33A,B). This suggests that a dysfunctional liver clock drives reduced utilization of lipids for fuel when microbes are present, supporting our evidence that gluconeogenesis is also reduced. Conversely, no difference in active RER was detected in GF mice regardless of genotype,

which supports our evidence that LKO mice exhibit reduced gluconeogenesis compared to WT in SPF, but not in GF conditions (Figure 3.6A). Interestingly, we observed decreased RER during the rest period only in GF LKO mice compared to GF WT, but not under SPF conditions (Figure 3.33A,B). This indicates that absence of both a liver clock and gut microbes may in fact enhance oxidation of lipids relative to GF WT mice.

In summary, we reveal microbiota-dependent and -independent effects on liver clock-mediated fuel utilization, and reduced reliance on lipids in SPF LKO that may contribute to reduced gluconeogenesis and alter global metabolic homeostatic outputs (Figure 3.34).

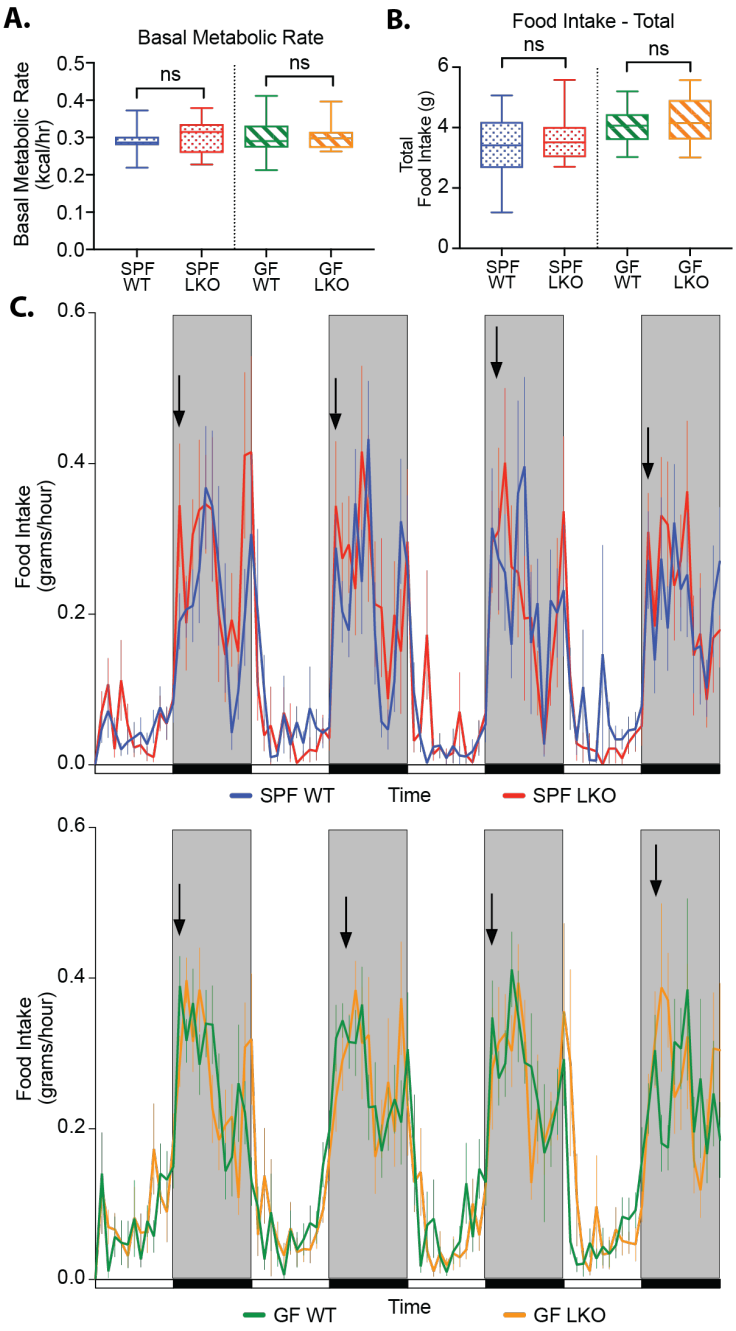

Figure 3.30: **Liver clock and gut microbes differentially alter diurnal patterns of food intake.** Indirect calorimetry assessment of SPF and GF, WT and LKO male mice, measured over 4 consecutive 12:12 LD cycles (n=12-13). (A) Basal metabolic rate (BMR) represented as kcal/hr. (B) Total grams of food intake per LD cycle. (C) Food intake summarized as grams consumed per hour; arrows indicate time of feeding onset during the active period. Data points and bars represent mean±SEM, box plots represent median±min/max. ns=not significant.

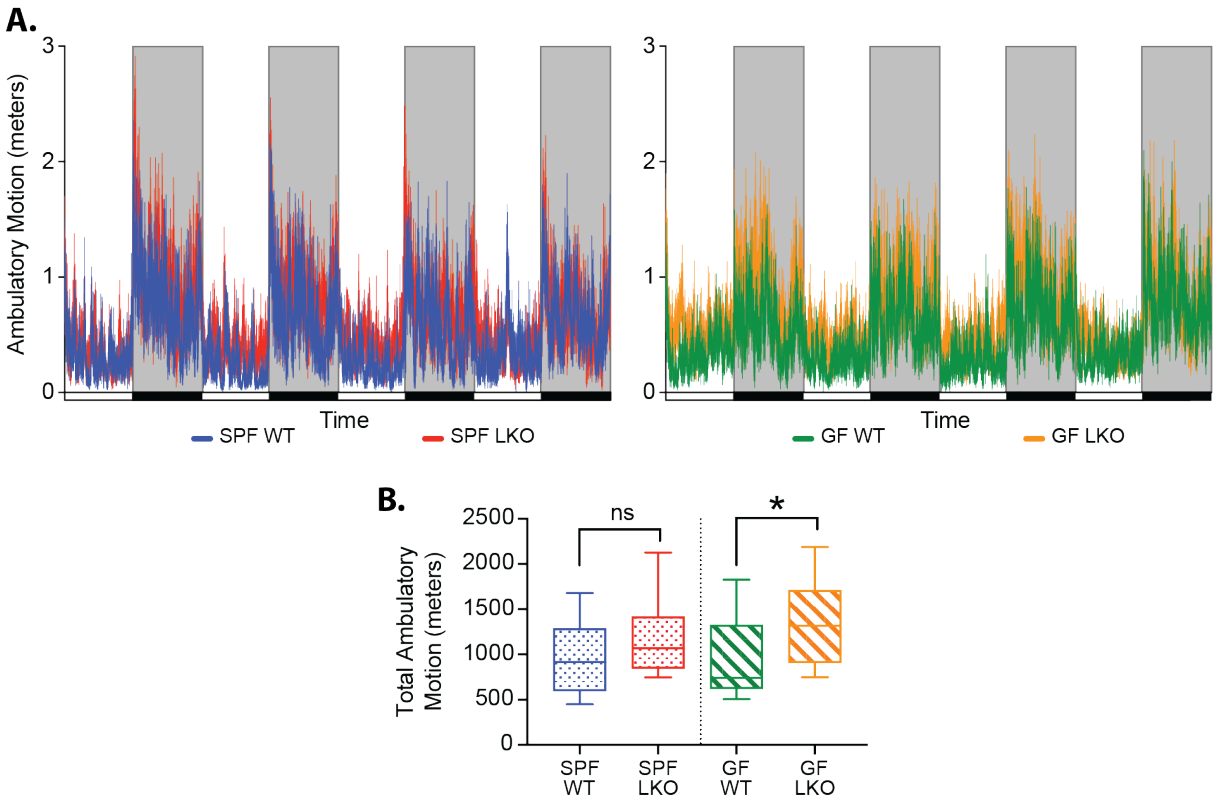

Figure 3.31: **Liver clock and gut microbes differentially alter diurnal patterns of ambulatory activity.** Indirect calorimetry assessment of SPF and GF, WT and LKO male mice, measured over 4 consecutive 12:12 LD cycles (n=12-13). (A) Ambulatory motion measured by meters. (B) Total ambulatory motion measured by meters per LD cycle. Data points and bars represent mean±SEM, box plots represent median±min/max. $*p < 0.05$, ns=not significant.

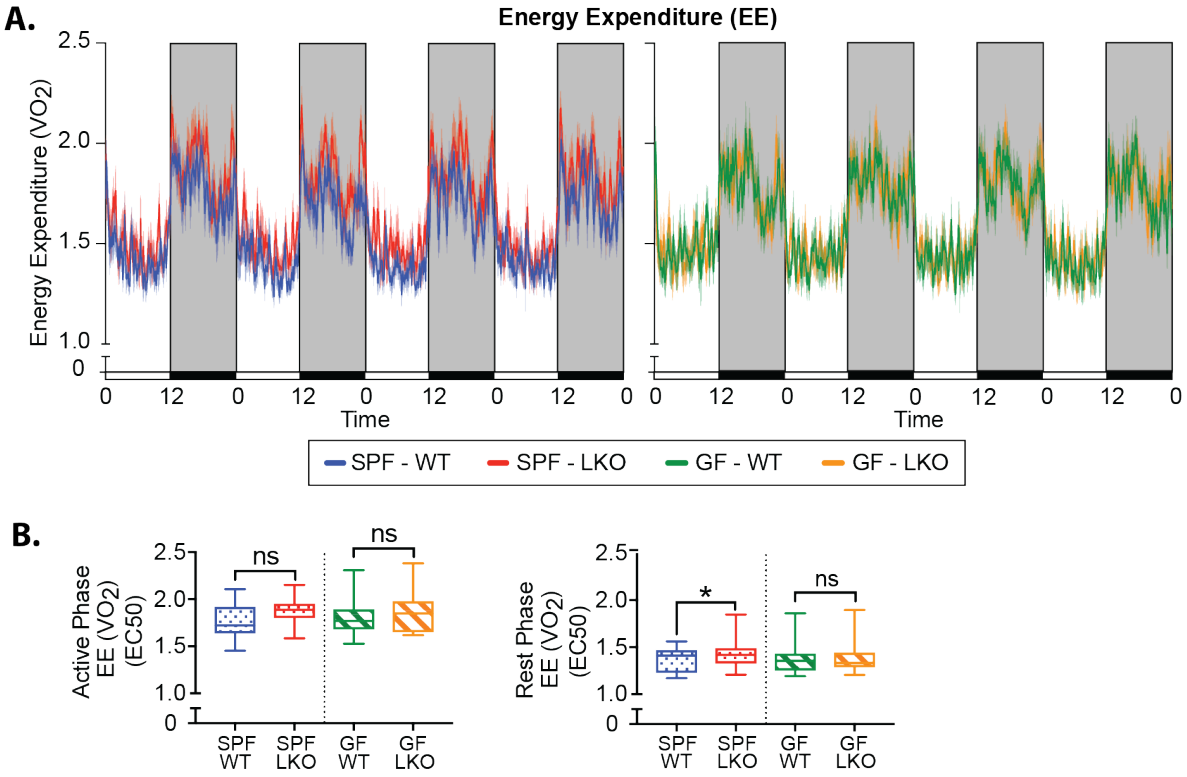

Figure 3.32: **Liver clock and gut microbes differentially alter diurnal patterns of energy expenditure.** Indirect calorimetry assessment of SPF and GF, WT and LKO male mice, measured over 4 consecutive 12:12 LD cycles (n=12-13). (A) Energy expenditure (EE) represented as VO_2. (B) EE divided into active (dark) and rest (light) periods, summarized by EC50 values within each period. Data points represent mean±SEM, box plots represent median±min/max. $*p < 0.05$, ns=not significant.

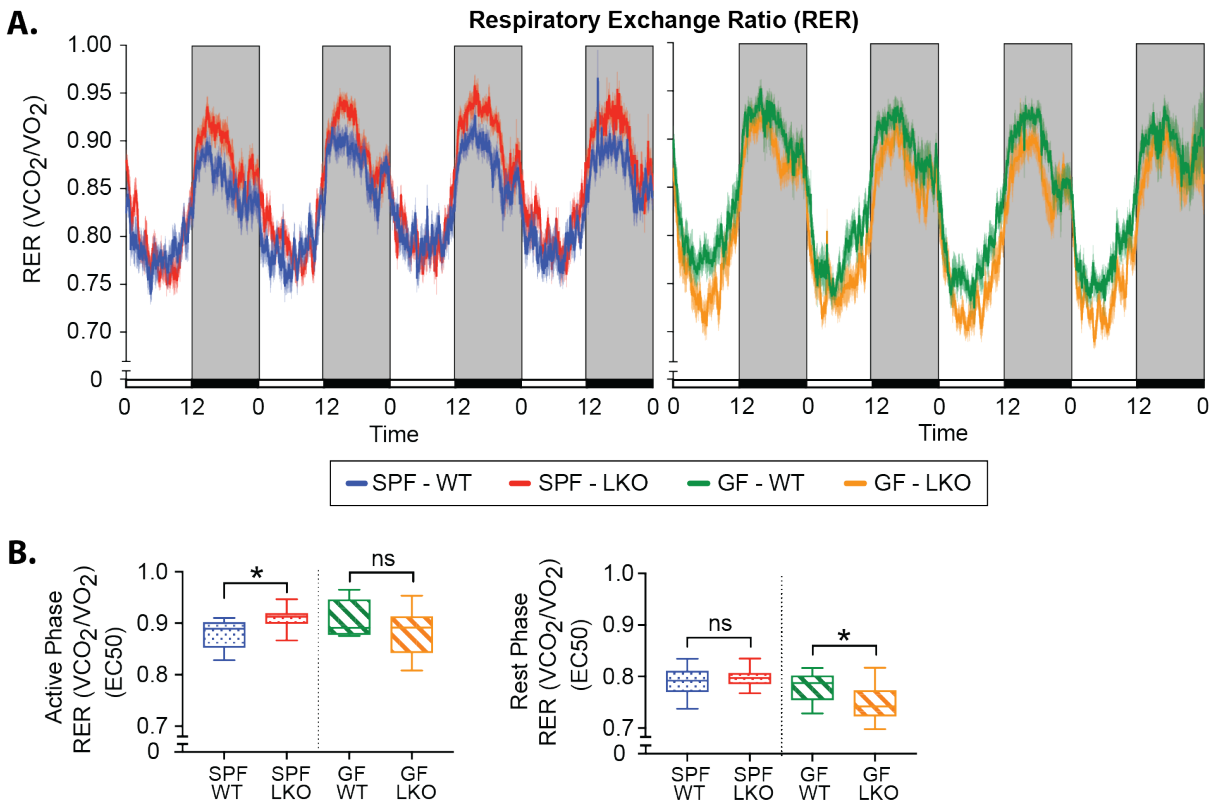

Figure 3.33: **Liver clock and gut microbes differentially alter diurnal patterns of fuel utilization.** Indirect calorimetry assessment of SPF and GF, WT and LKO male mice, measured over 4 consecutive 12:12 LD cycles (n=12-13). (A) Respiratory Exchange Ratio (RER) represented as VCO_2/VO_2. (B) RER during active (dark) and rest (light) phases, summarized by EC50 values. Data points represent mean±SEM, box plots represent median±min/max. $*p < 0.05$, ns=not significant.

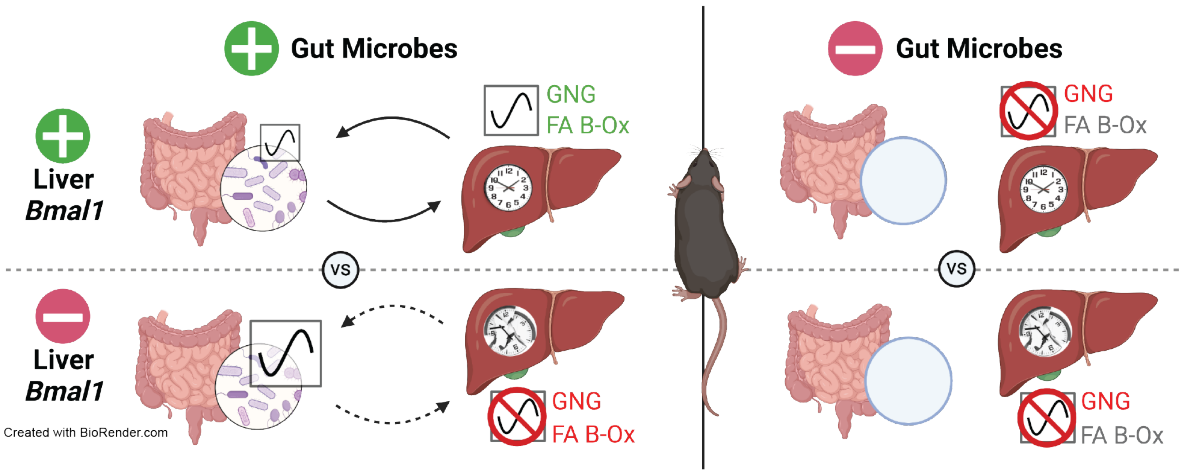

Figure 3.34: **Model Figure: Liver clock and gut microbes partition glucose and lipid metabolism.** Model figure. In SPF conditions, the liver circadian clock drives normal gluconeogenesis and fatty acid β-oxidation, fecal microbial abundance oscillations, and hepatic transcriptome oscillations. Following hepatic Bmal1 deletion, gluconeogenesis and fatty acid β-oxidation are reduced, oscillating microbiota increase, and oscillating hepatic transcripts are not enriched for metabolic pathways. In GF conditions, gluconeogenesis is reduced, and oscillating hepatic transcripts are not enriched for gluconeogenesis and fatty acid β-oxidation metabolic pathways regardless of liver clock functionality. Green indicates upregulation, red indicates downregulation. Solid arrows indicate intact communication, dashed arrows indicate broken communication.

3.5 Discussion

Organismal-level coordination of molecular metabolism governed by the circadian clock is critical for the temporal separation of biochemical processes to maintain energy demands over a 24-hour period. Dysregulation or improper partitioning of these key processes can substantially contribute to metabolic disease development, such as obesity, non-alcoholic fatty liver disease, and type 2 diabetes. The liver is one of the most metabolically active organs, contributing significantly to glucose and lipid homeostasis. Our data demonstrate a bidirectional and cooperative relationship between diurnal patterns of gut microbes and the liver circadian clock that aids in coordination of gluconeogenesis, lipid metabolism, and fuel utilization, as outlined in Figure 3.34. This highly complex, coordinated, and reciprocal dialogue results in refined shifts that drive mammalian global metabolic homeostasis. We reveal that the liver clock serves as the primary driver of diurnal transcriptional networks essential for maintenance of whole-body metabolism, whereas gut microbes are a secondary, yet essential partner that translates environmental cues (e.g. what, when, and how much diet is consumed) to enhance temporal organization of clock-mediated hepatic gene expression. When either system is absent or dysfunctional, disorganization and mistiming of normally coordinated processes occurs and homeostatic mechanisms are lost. These findings provide an initial basis for the interrogations of the mechanistic underpinnings of key host-microbe circadian interactions that direct metabolism in a tissue-specific manner.

A major finding of our study is that contributions of both gut microbes and the hepatic tissue-specific circadian network mediate glucose homeostatic outcomes, which occurs independent of the central clock located within the brain (Figures 3.5A, 3.6A,C). While others have separately implicated gut microbes [157, 159, 289] or the liver circadian clock [130] in the regulation of gluconeogenesis and glucose tolerance, we show that these systems work in conjunction to drive host glucose homeostasis. This appears to be a gluconeogenic-specific effect, supported by our evidence that both insulin sensitivity and hepatic glycogen levels

were largely unaffected by LKO or GF conditions (Figures 3.5D, 3.9A). We find that gut microbes provide essential cues that mediate gluconeogenesis which can only be appropriately coordinated with the liver clock, a primary driver of maintaining metabolic partitioning. This engagement in microbiota replete conditions underpins shifts between glucose and lipid metabolism for fuel utilization. By investigating these animals under GF conditions or following antibiotic-induced depletion of gut microbes in SPF mice (Figure 3.10), we were able to demonstrate that gut microbes contribute to these outcomes, serving in essence as a rheostat to impart signals in real-time that fine-tune and modulate glucose and lipid metabolism. In the presence of gut microbes, gene-targeted deletion of the primary hierarchical driver, hepatic *Bmal1*, results in reduced host catabolic processes, including gluconeogenesis, that are essential to maintain metabolic homeostasis. Together, these data underscore a key role for liver clock-microbiota crosstalk in maintaining circulating glucose levels, particularly during fasting conditions when gluconeogenesis is critical. Whereas each system is greatly impacted by environmental signals that influence metabolic outcomes, understanding their bidirectional dialogue is essential to co-manipulate these systems in a meaningful and effective way.

In addition to differences in glucose homeostasis determined via direct measurements of gluconeogenesis, we also identified that hepatic *Bmal1* and gut microbes coordinate diurnal patterns in lipid metabolism and subsequent fuel utilization via transcriptome analysis and indirect calorimetry, respectively (Figures 3.26, 3.33). These findings, particularly in GF animals, provide additional insights into the role of liver *Bmal1* in these processes, where previous work performed by our group and others in conventionally-raised *Bmal1* WT vs. LKO mice showed the liver clock regulates lipid homeostasis via mechanisms involving AKT activation and m6A RNA methylation [13, 290]. Due to the significant influence that fatty acid β-oxidation imparts on gluconeogenesis [287], it is possible that our observations of liver clock-mediated gluconeogenic outputs under SPF and GF conditions may be a direct

result of reduced hepatic fatty acid β-oxidation flux. Previous studies showed GF mice with a functional liver clock exhibit upregulation of fatty acid β-oxidation, even under high fat diet-fed conditions [154], which could be due, in part, to differential regulation of hepatic PPAR signaling [291] and may provide protection against HF DIO. Our studies in GF WT and LKO mice suggest that gut microbes also interact with the liver clock in the regulation of lipid metabolism, yet the precise microbial component driving these outcomes remains to be determined.

In addition to the metabolic implications of gut microbes on the host, we also demonstrate bidirectionality from the host liver clock to gut microbes. Here, functionality of the liver clock impacts diurnal oscillations of fecal microbiota relative abundances. Loss of a primary hepatic driver, such as *Bmal1*, results in the emergence of downstream secondary microbiota oscillators that could directly feedback onto the host, disrupting proper feedback mechanisms. Previously, Liang *et al.*, [178] showed that global loss of *Bmal1* in mice abolished fecal microbial abundance rhythms compared to WT. In contrast, our work shows that absence of tissue-specific *Bmal1* results in an almost 2-fold increase in oscillating ASVs, particularly within the families Lachnospiraceae and Ruminococcaceae (Figure 3.17). This indicates that the tissue-specific liver clock is a key player in maintaining normal rhythmicity of specific oscillating gut microbiota. Others have shown that these bacteria families positively correlate with and contribute to secondary bile acid metabolism [221, 292], which are known to regulate circadian rhythms and metabolism [217, 227]. Further, previous studies have revealed that PPAR signaling is linked to bile acid synthesis and regulation [293, 294]. In fact, we observed reduced levels of transcripts involved in PPAR signaling in hepatic *Bmal1* deficient mice. Whether the observed gain in oscillating ASVs in LKO SPF mice contributes to altered circulating bile acid pools that impact glucose metabolism remains to be investigated. The concept of gain in oscillation has been previously identified in the context of microbiota relative abundances and associated metabolites in metabolic disease

[141, 199], yet their precise meaning remains unclear. Importantly, not only do we observe a gain in oscillations of gut microbiota, but we also revealed an increase in oscillations of the host liver transcriptome in absence of either a functional liver clock or gut microbes (Figure 3.24A). These gains of rhythmicity confer differential enrichment of key metabolic pathways compared to SPF WT (Figure 3.26). This finding corresponds to previous observations that the emergence of unique oscillations can significantly alter functional transcriptome enrichment that impacts metabolic homeostasis [181, 191, 295].

Together, our physiological and multi-omic data highlight significant communication between the host hepatic circadian clock and gut microbiota, underscoring the importance of proper diurnal coordination of these two systems. We show that gut microbiota play a key role in mammalian global metabolic homeostasis which is mediated through interactions and coordination with primary drivers of hepatic circadian clock networks. Broadly, our physiological characterization provides novel insights into the roles of genetics and gut microbiome on host metabolism, and the metabolic consequences of breaking their interactions. Future studies may reveal the key microbially-derived or -associated factors that mediate this interaction which can be explored in our model system. Understanding how these microbial mediators interact with circadian networks, particularly in human subjects, will be an important step in the field. These findings could have broad translational implications for how these two systems could be targeted to improve metabolic homeostasis in humans.

3.6 Future Directions

This study examined the complex, multi-factorial relationship between circadian genetics and the gut microbiome, providing an in-depth dissection into the resulting effects of disrupting these interactions on host glucose and lipid metabolism. Given these findings, a key future direction is to identify the molecular signals derived from the gut microbiome that impact liver clock-mediated gluconeogenesis and overall metabolic organization over a 24-hour pe-

riod. This can be explored using a combination of metabolomics analyses and metagenomic or metatranscriptomic sequencing of repeat-collected stool and intestinal luminal samples collected over 24 hours, which would inform on altered microbial outputs to the host and provide a broader view of microbial functions impacted by presence of a functional liver clock. We have performed some preliminary measurements of specific groups of microbially-associated metabolites that have been previously shown to impact host metabolism (see Chapter 1 for details). Thus far, we have measured levels of the SCFAs butyric acid, propionic acid, and acetic acid in cecal contents collected from male mice over 24 hours, revealing minimal differences between SPF WT and LKO except for ZT22 at the end of the dark cycle (Figure 3.35). We also measured the abundance of specific microbial genes in repeat-collected stool samples from SPF WT and LKO male and female mice over a 48-hour period. These genes included butyryl-CoA:acetate CoA-transferase (*but*; involved in butyrate production and identified in Roseburia) [254], dissimilatory sulfite reductase (*dsrAB*; involved in hydrogen sulfide production) [139], and taurine:pyruvate aminotransferase (*tpa*; involved in deamination of taurine and identified in *Bilophia wadsworthia*) (Figure 3.36). Only *tpa* revealed significant differences at specific timepoints between groups, suggesting that taurine deconjugation of bile salts may be impacted by a dysfunctional liver clock. Expanding on this, we next examined bile acid profiles of ileal luminal contents from SPF and GF, WT and LKO male mice over 24 hours using LC-MS/MS (Figure 3.37). This revealed a potential phase advance in taurocholic acid abundance, with the peak abundance occurring at ZT22 in SPF WT mice which exhibited a phase-advancement to ZT14 in SPF LKO mice (Figure 3.37A, lower left panel). We also analyzed relative abundance profiles of bile acid species related to both taurocholic acid and taurodeoxycholic acid between SPF WT and LKO; here, we observed similar temporal shifts in the profiles of these bile acids between SPF WT and LKO groups (Figure 3.37B). The question now remains whether these bile acid profiles are responsible for reduced gluconeogenesis in SPF LKO mice. We plan to expose SPF LKO and

GF mice to bile acids, particularly taurocholic acid, at different timepoints over 24 hours, then measure gluconeogenic output by PTT. Gluconeogenic restoration in SPF LKO mice would indicate that timed delivery of specific bile acids can bypass the disrupted liver clock to drive gluconeogenesis. Restoration in GF mice would indicate that specific bile acid delivery is sufficient for normal host gluconeogenesis, and that other microbial signals are not required. If gluconeogenesis is not restored in any case, it is possible that a single metabolite or group of metabolites is not sufficient to convey the phenotypes related to gluconeogenesis and fatty acid β-oxidation outlined in the Results, and instead a combination of metabolites derived from the LKO-associated microbiota. Untargeted metabolomics and metagenomic sequencing analysis may identify additional targets that mediate gluconeogenesis in LKO conditions and implicate specific microbiota community members. This could lead to future studies aimed at genetically deleting certain microbial functions within the community, such as bile acid metabolism genes, or constructing mock microbial communities with or without the implicated microbial community members.

Given the intimate relationship between fatty acid β-oxidation and gluconeogenesis, another important future direction is to further characterize the lipid metabolic phenotype impacted by the liver clock. We observed significantly increased body weight and food intake in male SPF LKO compared to WT, and no difference between GF genotypes (Figure 3.1B,C). However, we did not find significant differences in liver weight or mesenteric and gonadal fat depots to indicate increased lipogenesis and lipid storage in peripheral adipose depots (Figure 3.2A,B). We also found no differences in lipid deposition in the liver across all groups. Additionally, we measured circulating triglyceride and cholesterol levels in male mice, finding significant differences only at certain timepoints (Figure 3.38). Interestingly, we did observe significantly increased cholesterol levels at several timepoints in GF LKO mice compared to WT, suggesting a microbe-independent effect of liver clock disruption on some aspects of circulating lipids. Despite observing transcriptional profiles indicating sig-

nificant changes in lipid metabolic programming (Figure 3.20C), these lack of differences in overt lipid deposition measurements are more than likely observed because we only examined mice fed a low-fat, undefined chow diet. Therefore, we suspect that exposure to HF diet would impact the liver clock-microbiome relationship, perhaps exacerbating the lipid and associated gluconeogenic outputs that we observe under chow-fed conditions in SPF mice. A few studies have previously examined the effects of HF dietary intake in *Bmal1* liver-deficient SPF mice, observing increased body weight gain and disrupted mitochondrial functional outputs [129], as well as increased triglyceride content in circulation and in the liver [296] compared to WT. We plan to fully examine the role of gut microbes on liver clock disruption and host metabolic outcomes in the context of HF diet.

One category of mechanisms that may play a role in liver clock and microbiota mediation of host metabolism are epigenetic and post-transcriptional modifications. Previous work from our lab identified m6A RNA methylation patterns as key to the regulation of circadian clock-mediated liver lipid metabolism [13]. Relating to circadian regulation of gluconeogenesis, HDAC3 depletion in a mouse model resulted in reduced hepatic glucose production, potentially by reducing levels of Acetyl-CoA via sequestration for lipid storage [11], and hepatic *Bmal1* has been demonstrated to regulate gluconeogenesis via HDAC5 [297]. However, the role that gut microbes may play in this regulation remains unknown. Gut microbiota have been shown to modulate host HDAC3 activity via production of specific metabolites [298, 299], so it is indeed possible that HDAC-*Bmal1* activity may alter expression of gluconeogenesis and fatty acid β-oxidation genes in the liver differentially in the presence or absence of gut microbes. Future studies aimed at deciphering the precise mechanisms behind microbiota-host interactions should include the consideration of epigenetic modifications as potential hubs of metabolic regulation.

Along similar mechanistic lines, we still have a limited understanding of how peripheral tissue clocks other than the liver are impacted by gut microbes, and whether the gut-liver

interactions presented in this chapter involve crosstalk with any other tissues. Tissues such as the pancreas, skeletal muscle, and adipose tissue are quite relevant to the regulation of glucose and lipid metabolism, and disruptions to their peripheral circadian clocks result in unique metabolic phenotypes [75]. A few studies have examined this relationship using mice with a conditionally-active liver clock and clock disruption in all other tissues, exploring how crosstalk between the skeletal muscle clock and liver clock contribute to the coordination of food intake patterns and glucose homeostasis [300, 301]. This mouse model may also help to reveal whether liver circadian clock coordination with gut microbes involves other peripheral tissues or clocks.

Another major question that remains is the mechanism by which the liver clock, or lack thereof, drives oscillations in gut microbiota abundance. Studies that have examined the effects of circadian disruption through different, such as global loss of *Bmal1* or HF-diet exposure, reveal a loss of microbial abundance oscillations and organization [141, 178]. Interestingly, we observe a significant increase in oscillating microbial abundance in stool from LKO male mice over 48 hours (Figure 3.14C,D), suggesting that other cues must dominate in the absence of a functional liver clock. Our metabolic cage experiments suggest that SPF LKO mice may exhibit a more robust onset of feeding at the start of the dark cycle compared to WT, potentially influencing oscillations in host functions (i.e., bile acid production) that influence gut microbiota rhythms. (Figure 3.30C). Resetting food intake patterns by a TRF regimen would inform on whether liver-clock-associated microbial oscillations are indeed driven by changes in food intake. It would be informative to measure food anticipatory activity to determine if liver-clock functionality exhibits any influence on endogenous food anticipation in absence of light cues. Aside from timing of food intake, there may also be endogenous factors driving microbial oscillations in the absence of a liver clock. SPF LKO mice exhibit an emergence of unique oscillating hepatic transcripts (Figure 3.25A), suggesting that downstream circadian effectors may emerge and alter host metabolism and

gut microbiota. Future examination of the hepatic pathways enriched by these emerging transcriptome oscillations would shed light on the identity of these secondary circadian effectors. This question could be explored by examination of mice with a conditionally active liver clock and global clock deficiency in all other tissues. This model would aid in identifying whether the liver clock alone can drive microbial oscillations, in the absence of all other clocks and independent of normal locomotor activity and food intake patterns [125]. Finally, HF-diet exposure has also been demonstrated to disrupt the hepatic metabolic transcriptome and functional outputs [302], and thus may also disrupt the impact of the liver clock on gut microbes. In a preliminary study, we fed SPF WT and LKO male mice either RC or HF diet, collected stool every 6 hours over 48 hours, and performed 16S rRNA sequencing. While we confirmed previous findings that a broken liver clock results in emerging Clostridia ASVs, HF diet severely blunted this effect (Figure 3.39). This suggests that HF-diet disrupts the ability of the liver clock to modulate microbial oscillations. Thus, future identification of the hepatic pathways that are altered under HF-diet may help to elucidate the host mediators of microbiota abundance oscillations.

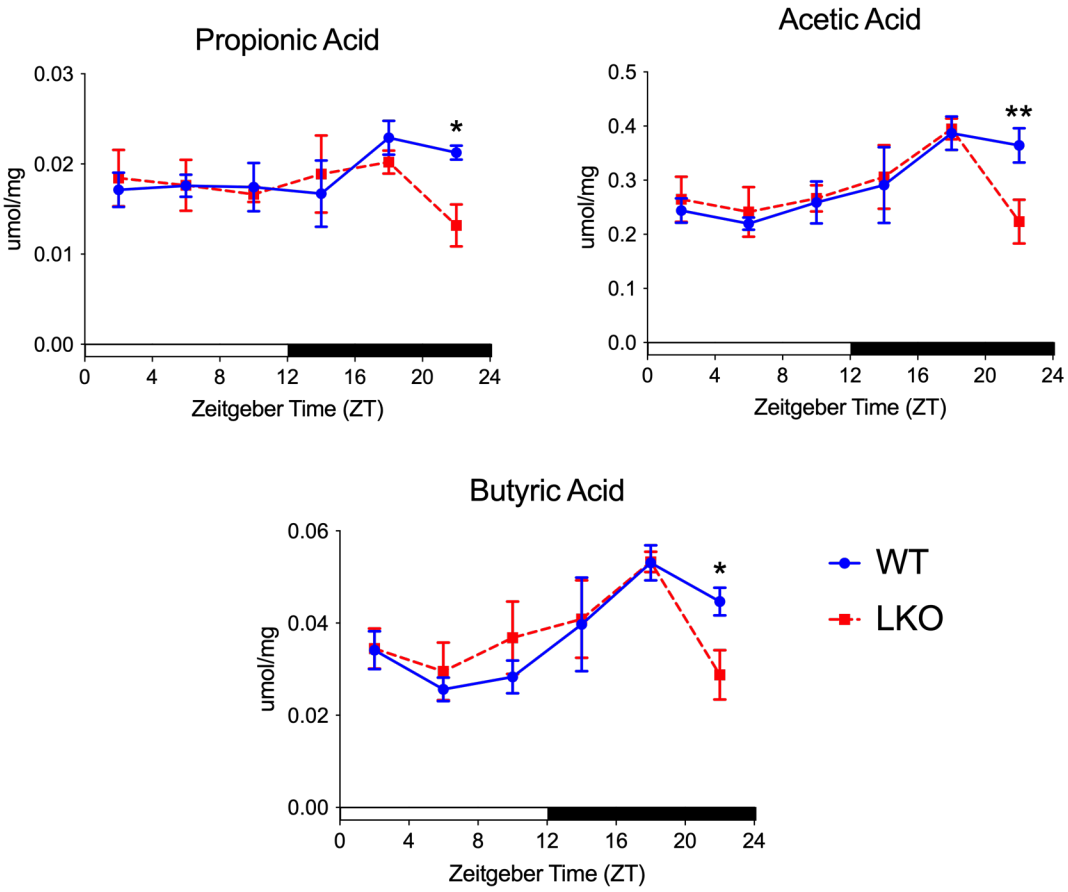

Figure 3.35: **SCFA levels in cecal contents over 24 hours.** SCFA levels in cecal contents collected at ZT 2, 6, 10, 14, 18, and 22 from SPF WT and LKO male mice. Data points represent mean±SEM, $^{**}p < 0.01$, $^{*}p < 0.05$.

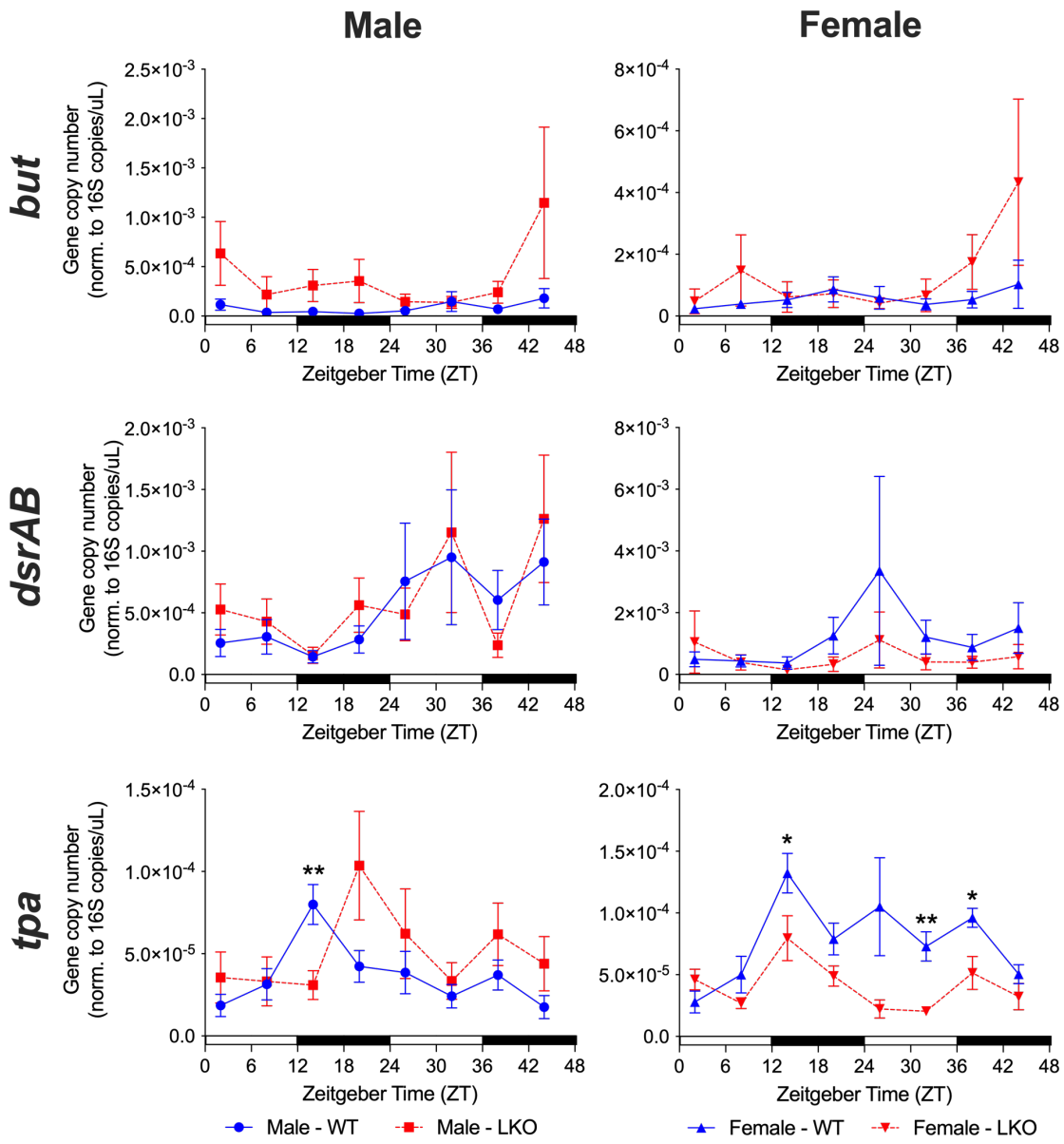

Figure 3.36: **Microbial gene abundance in stool over time.** Microbial gene abundance measured via qPCR in stool collected every 6 hours over 2 12:12 LD cycles from SPF WT and LKO, male and female mice; normalized to 16S gene copies per μL. *but* = butyryl-CoA: acetate CoA-transferase; *dsrAB* = dissimilatory sulfite reductase; *tpa* = taurine:pyruvate aminotransferase (from *Bilophila wadsworthia*. Data points represent mean±SEM, $^{**}p < 0.01$, $^{*}p < 0.05$.

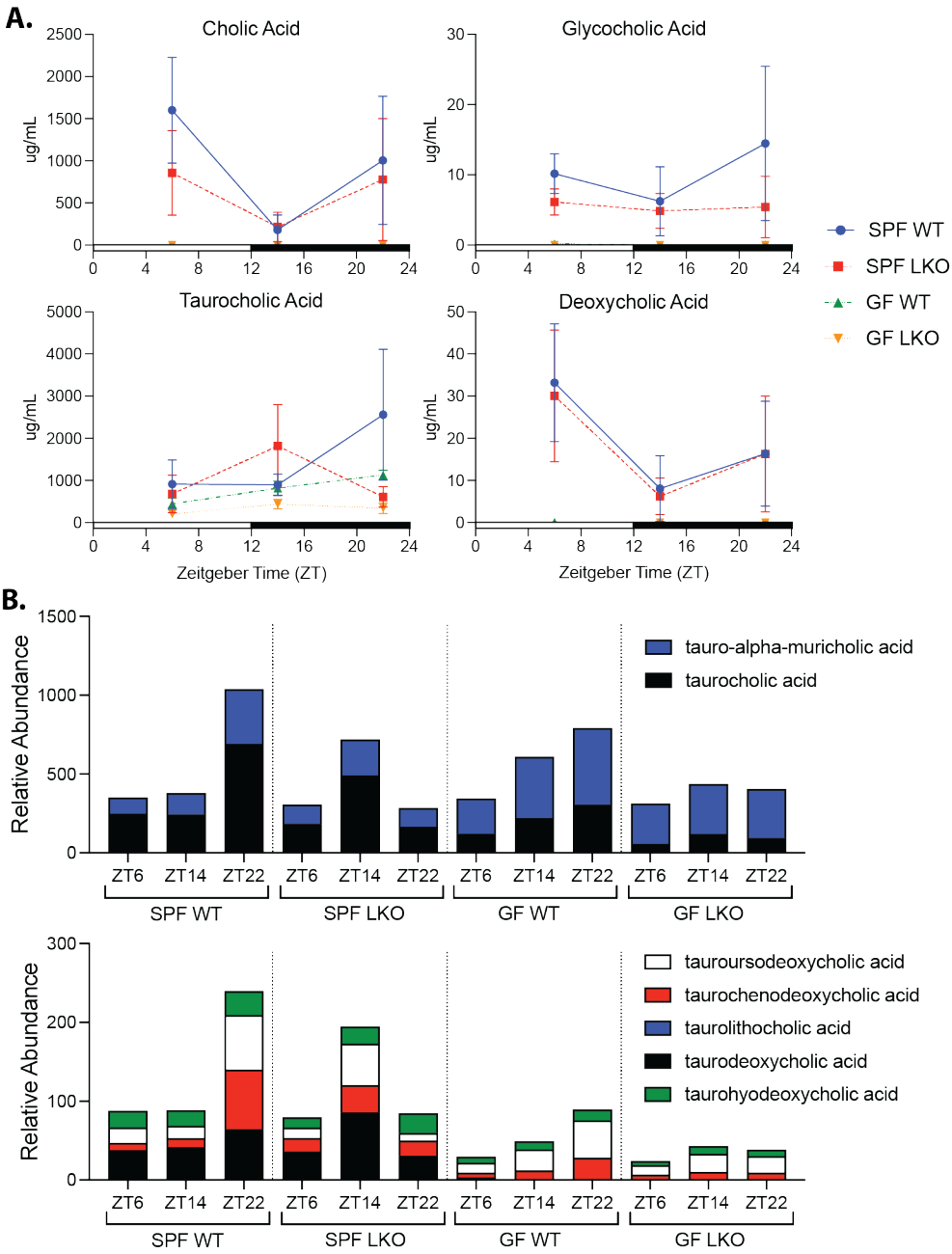

Figure 3.37: **Bile acid metabolomics of ileum luminal contents.** Bile acid metabolomics analysis of ileum luminal contents collected at ZT6, 14, and 22 from SPF and GF, WT and LKO male mice. (A) Absolute abundance of bile acids. (B) Relative abundance of bile acid groups, normalized to either taurocholic acid (top panel) or taurodeoxycholic acid (lower panel). Data points represent mean±SEM, bar graphs represent mean.

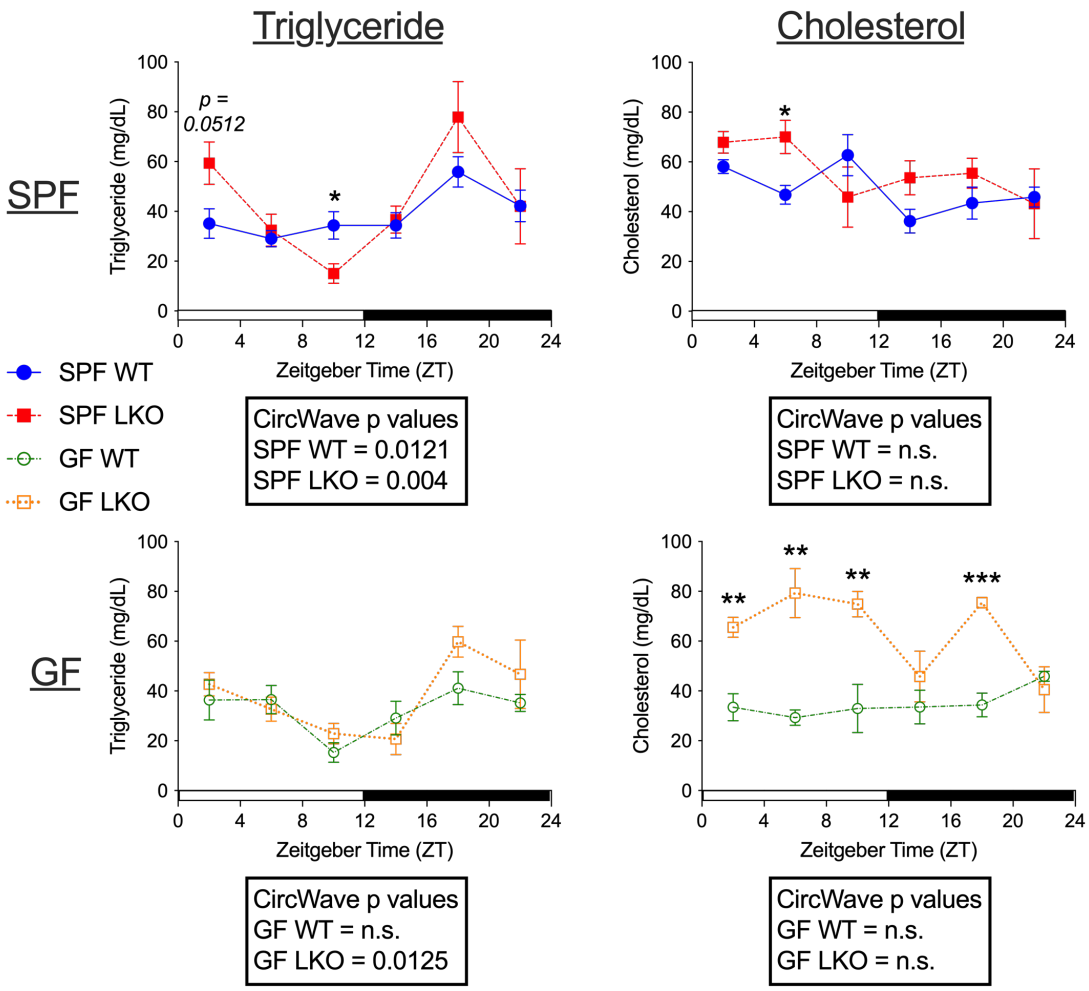

Figure 3.38: **Circulating triglyceride and cholesterol levels over time.** Triglyceride and cholesterol levels measured in plasma collected over 24 hours from SPF and GF, WT and LKO male mice. Data points represent mean±SEM, $^{**}p < 0.01$, $^{*}p < 0.05$.

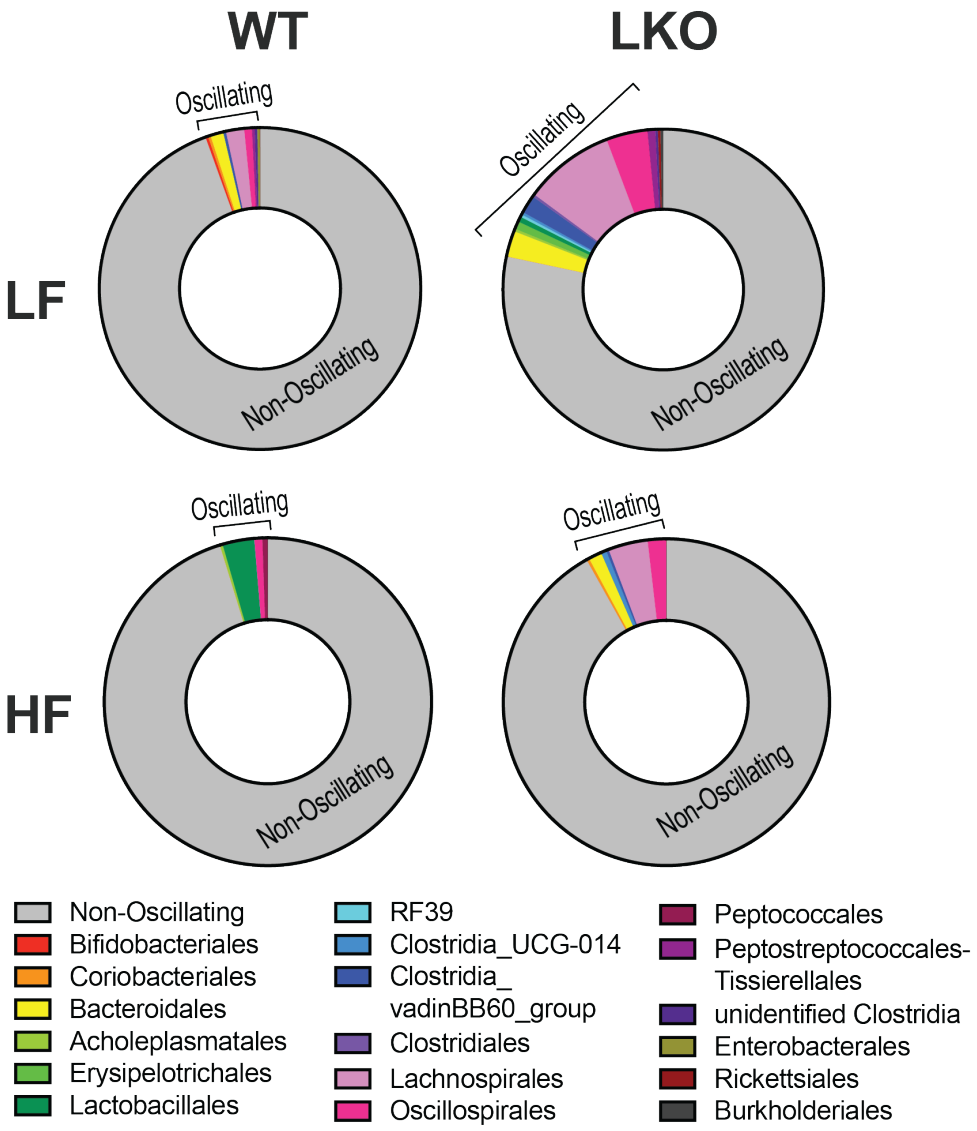

Figure 3.39: **HF diet disrupts liver clock influence on oscillating gut microbiota.** 16S rRNA gene sequencing analysis of stool sampled from WT and LKO male mice given either regular chow (RC) or high-fat (HF) diet. Stool collected every 6 hours over two consecutive 24-hr LD cycles (8 samples per animal) via repeat collections from the same mouse (n=2-3/group). Proportion of non-oscillating (grey area) vs significantly oscillating (colored areas) ASVs identified via eJTK; oscillating ASVs divided by taxonomic class.

CHAPTER 4

HIGH-FAT DIET DISRUPTS REG3G AND GUT MICROBIAL RHYTHMS PROMOTING METABOLIC DYSFUNCTION

4.1 Preface

The contents of this chapter were modified and adapted from "K. Frazier, A. Kambal, E. A. Zale, J. F. Pierre, N. Hubert, S. Miyoshi, J. Miyoshi, D. L. Ringus, D. Harris, K. Yang, K. Carroll, J. B. Hermanson, J. S. Chlystek, K. A. Overmyer, C. M. Cham, M. W. Musch, J. J. Coon, E. B. Chang, V. A. Leone, High-fat diet disrupts REG3γ and gut microbial rhythms promoting metabolic dysfunction. Cell Host & Microbe. 30, 809-823.e6 (2022)" [303]. K. Frazier, E. Zale, J. Pierre, S. Miyoshi, J. Miyoshi, M. Musch, and V. Leone performed mouse experiments. K. Frazier, A. Kambal, E. Zale, and C. Cham performed enteroid experiments. E. Zale, K. Yang, K. Carroll, and V. Leone performed qPCR. K. Frazier, A. Kambal, E. Zale, D. Ringus, D. Harris, and K. Yang performed bacterial cultivations and conditioned media preparation. J. Pierre and J. Hermanson performed immunostaining and downstream quantification. N. Hubert performed 16S sequencing analysis. J. Chlystek, K. Overmyer, and J. Coon performed metabolomics analysis. K. Frazier, E. Chang, and V. Leone wrote the manuscript. K. Frazier, J. Hermanson, E. Chang, and V. Leone edited the manuscript. V. Leone conceived the project.

4.2 Abstract

Gut microbial diurnal oscillations are important diet-dependent drivers of host circadian rhythms and metabolism that ensure optimal energy balance. Yet, the interplay between diet, microbes, and host factors that sustain intestinal oscillations is complex and poorly understood. Here, we report the host C-type lectin AMP *Reg3*γ works with key ileal microbes to orchestrate these interactions in a bidirectional manner and does not correlate with the intestinal core circadian clock. HF diet is the primary driver of microbial oscillators that impair host metabolic homeostasis, resulting in arrhythmic host *Reg3*γ expression that secondarily drives abundance and oscillation of key gut microbes. This illustrates transkingdom coordination of biological rhythms primarily influenced by diet, and reciprocal sensor-effector signals between host and microbial components that ultimately drive metabolism. Restoring the gut microbiota's capacity to sense and transduce dietary signals mediated by specific host factors such as *Reg3*γ could be harnessed to improve metabolic dysfunction.

4.3 Introduction

As described in Chapter 1, gut microbes are intricately intertwined with the host circadian clock, where disruption via environmental manipulations [180], high-fat (HF) diet [141, 179], or via genetic mutation [178, 181], results in loss of gut microbiome oscillations. Diurnal microbiome oscillations in cecum, colon, and stool are driven, in part, by time of feeding and nutrient delivery to the gut over 24 hours. However, we previously revealed that despite a unique community membership, gut microbes from mice fed via continuous parenteral nutrition still exhibited diurnal oscillations relative to enterally-fed counterparts [141]. This suggests additional gut signals, whether host-derived, microbially-derived, or both, can play a role in gut microbial rhythmicity.

While host factors drive microbial rhythms, microbes provide feedback that influence

host diurnal patterns both locally and peripherally. In mice, gut microbes drive rhythmicity and amplitude of circadian clock and innate immune factors in IECs that influence host lipid metabolism [186]. Antibiotic depletion of gut microbes or their complete absence, i.e. germ-free (GF), significantly impairs circadian dynamics of IEC TLR expression and downstream genes that drive intestinal AMP synthesis, a group of host-derived molecules targeting specific microorganisms that aid in maintaining gut homeostasis [235].

One particular AMP associated with host-microbe diurnal patterns is Regenerating islet-derived protein 3 gamma (*Reg3*γ). REG3γ is a MyD88-dependent C-type lectin made by IECs throughout the GI tract, and highly expressed in the distal small intestine [237, 304, 305]. Microbial signals such as LPS and flagellin activate host TLR-MyD88 signaling cascades to drive expression of the cytokine IL-22 in innate lymphoid cells, which induces expression and secretion of AMPS [306]. REG3γ targets Gram-positive bacteria by binding and oligomerizing to the peptidoglycan layer on the bacterial membrane, then forming a permeabilizing pore [307, 308]. REG3γ aids in separating IECs from mucosa-associated microbes by inhibiting colonization, while DIO ablates *Reg3*γ expression [309, 310]. Antibiotic depletion of gut microbes significantly impairs diurnal *Reg3*γ expression in colon and ileum [190]. *Reg3*γ-deficient mice exhibit loss of host-microbial separation [311, 312] and disrupted diurnal rhythms of mucosa-associated microbial abundance within the colon [181]. How diurnal *Reg3*γ expression aids in maintaining normal gut microbial oscillations and the implications for host metabolic health remain unexplored.

Here, we investigated whether signals derived from specific gut bacteria are required to drive host diurnal expression patterns of *Reg3*γ, and if these endogenous cues can "reset" bacterial oscillations. We aimed to identify whether microbial signals were lost in HF diet-induced gut dysbiosis, further exacerbating host metabolic disruption. Using both *in vivo* and *in vitro* approaches, we show distal small intestine *Reg3*γ diurnal expression is not under circadian clock control, but is regulated locally by specific, diet-dependent oscillating

bacteria. We reveal small molecules derived from bacteria promoted by regular chow (RC), but not HF, induce *Reg3γ* expression in vitro, and these bacteria exhibit unique resistance to REG3γ's antimicrobial action. Finally, we reveal *Reg3γ* deficiency coupled with HF permits a gain in oscillation in relative abundances of specific gut microbes normally susceptible to REG3γ. Together, our data demonstrate a reciprocating, synchronized relationship between rhythmic, diet-selected small intestine gut microbes and REG3γ, where desynchronization of these local interactions can result in metabolic disruption and perhaps DIO.

4.4 Results

4.4.1 Diurnal expression of small intestine Reg3g *does not correlate with the core circadian clock gene network and requires diet-induced gut microbiota*

We first examined impacts of diet and microbe status on core circadian clock genes within distal ileum mucosal scrapings obtained from GF and SPF mice fed RC or HF every 4 hours over 24 hours. We observed some significant, yet modest core circadian clock gene expression changes within specific Zeitgeber times (ZT), i.e., *Bmal1*, *Clock*, *Cry1*, over a 12:12 LD cycle (Figure 4.1). Despite changes within ZT, neither diet nor gut microbe status impacted diurnal rhythmicity and amplitude of core circadian clock genes in mucosal scrapings (Table B.1).

We next examined diurnal transcript levels of several highly expressed AMPs in mucosal scrapings of RC or HF-fed SPF and GF mice. RC-fed SPF mice exhibited significantly increased transcript levels within specific ZTs relative to all other groups, particularly in REG3 family members, including *Reg3γ* and *Reg3β* (Figure 4.2). Additional AMPs, including β-1,4-glycosidase *Lysozyme1 (Lyz1)*, ribonuclease *Angiogenin4 (Ang4)*, and α-defensin *Cryptidin4 (Crypt4)* did not exhibit significant differences between groups. *Reg3γ* exhibited

diurnal rhythmicity in both SPF and GF RC-fed mice, while *Reg3β* only exhibited diurnal rhythmicity in GF RC-fed mice, despite significantly reduced overall expression and amplitude in GF animals (Table B.1). Peak *Reg3γ* and *Reg3β* expression in SPF RC-fed mice corresponded to ZT10, 2 hours prior to lights off and presumably prior to onset of feeding. *Mucin-2 (Muc2)* expression, which has been previously associated with *Reg3γ* [240], was also significantly elevated in RC-fed SPF mice at ZT10 (Figure 4.2). Only RC-fed GF mice exhibited diurnal *Muc2* expression, although overall levels were not changed relative to SPF RC-fed mice.

We confirmed *Reg3γ* diurnal patterns were also evident at the translational level. Similar REG3γ diurnal patterns were observed in SPF RC-fed, but not in SPF HF-fed counterparts via immunostaining (Figure 4.3A,B), while no differences in either level of expression or oscillations were evident via immunostaining for LYZ1 (Figure 4.3A,C) between diets. Further analysis of mucosal scrapings from SPF RC and HF-fed mice via Western blot revealed both diet and ZT-dependent REG3γ oscillations (Figure 4.3C). Since *Reg3γ* is expressed by both absorptive enterocytes and Paneth cells [304, 305, 307], we next determined if diurnal and diet-dependent *Reg3γ* expression was lost in all compartments following HF feeding. We performed mucosal villus to crypt cell fractionation using timed EDTA exposure of the gut epithelium, followed by qPCR for *Reg3γ* at ZT2 and 10, the nadir and peak of expression. Pooled fractions 1-8 contained absorptive enterocytes and fraction 9 contained crypts (including Paneth cells). We first confirmed cell fraction composition via marker genes *sucrase-isomaltase* (villus epithelial marker) and *Lyz1* (Paneth cell marker) (Figure 4.4A). Only fractions 1-8 from RC-fed mice exhibited ZT-dependent *Reg3γ* expression, while crypt expression was not different between ZT2 and 10 in RC or HF-fed mice (Figure 4.4B). Together, these data show the core circadian clock gene network is stable regardless of microbe status or diet; however, diurnal rhythms of host *Reg3γ* expression within the villus epithelium are driven by presence of gut microbes, including microbes selected by diet.

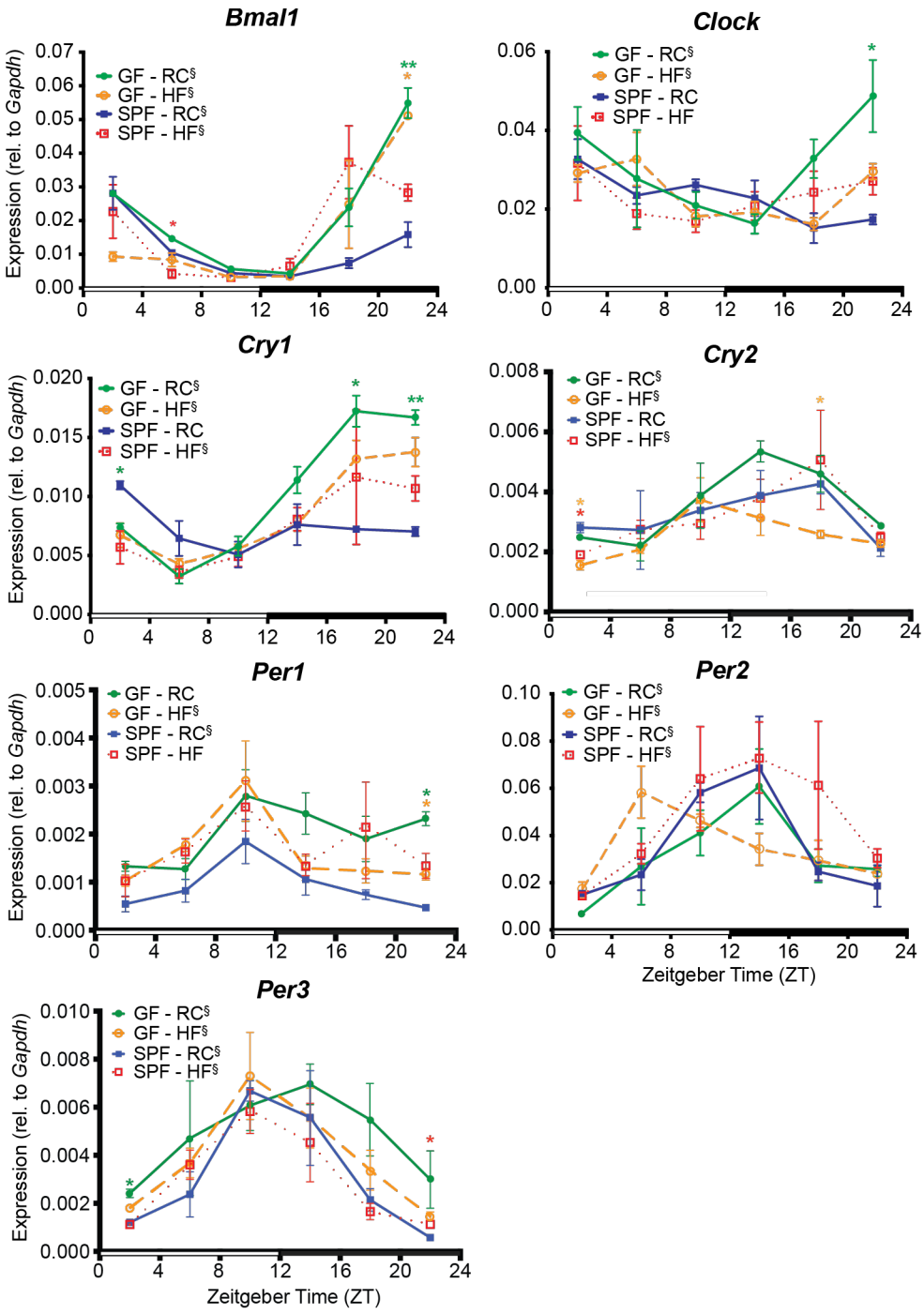

Figure 4.1: **Diet and gut microbes elicit modest changes in core circadian clock gene expression.** Circadian clock gene expression in mucosal scrapings collected every 4 hours from RC or HF-fed GF and SPF mice (n=2-3 mice/treatment/timepoint) over a 12:12 LD cycle (indicated by open and closed bars). Data represent mean±SEM. ξ indicates significant ($p < 0.05$) co-sinor expression patterns detected via CircWave. $*p < 0.05$, $**p < 0.01$; star color indicates group exhibiting significance relative to SPF-RC.

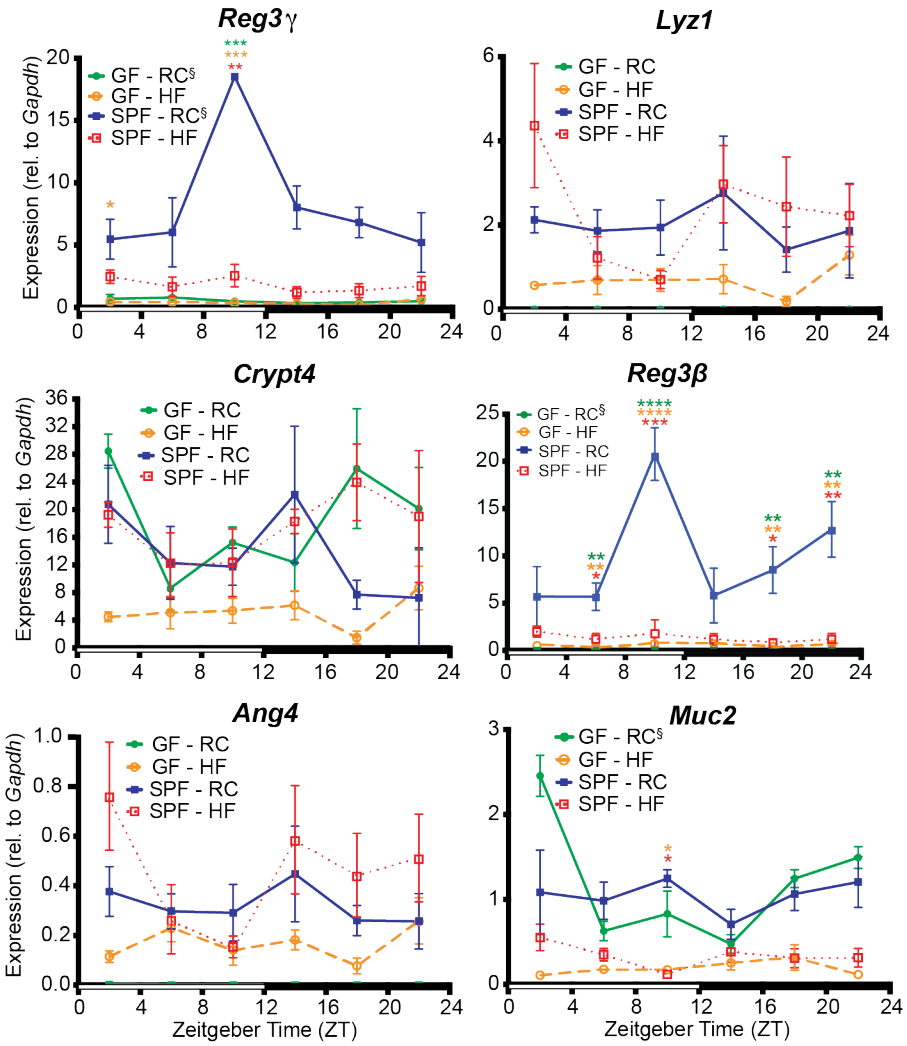

Figure 4.2: **Diurnal patterns of small intestine *Reg3γ* expression requires presence of diet-induced gut microbes.** Antimicrobial peptide (AMP) and *Mucin2 (Muc2)* gene expression in mucosal scrapings collected every 4 hours from RC or HF-fed GF and SPF mice (n=2-3 mice/treatment/timepoint) over a 12:12 LD cycle (indicated by open and closed bars). Data represent mean±SEM. ξ indicates significant ($p < 0.05$) co-sinor expression patterns detected via CircWave. $*p < 0.05$, $**p < 0.01$; star color indicates group exhibiting significance relative to SPF-RC.

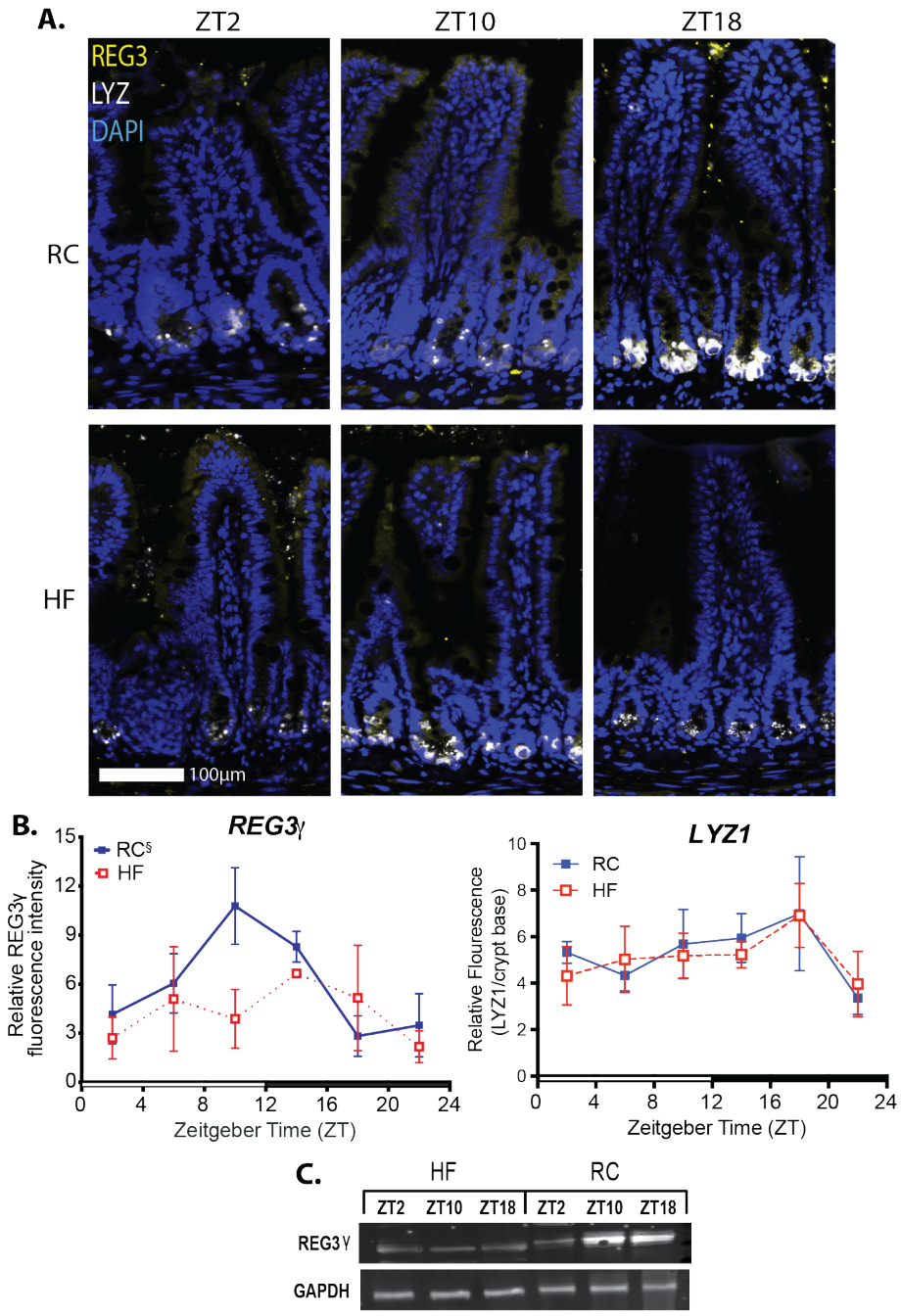

Figure 4.3: **Diet-dependent diurnal *Reg3*γ is also evident at the protein level.** (A) Representative immunostaining images for REG3γ (yellow) and LYZ1 (white) in distal ileum sections from RC and HF-fed SPF mice at ZT 2, 10, and 18. (B) Corresponding REG3γ and LYZ1 fluorescence intensity quantification at ZT 2, 6, 10, 14, 18, and 22. (C) REG3γ protein levels by Western blot in mucosal scrapings from RC and HF-fed SPF mice at ZT 2, 10, and 18. Data represent mean±SEM. ξ indicates significant ($p < 0.05$) co-sinor expression patterns detected via CircWave.

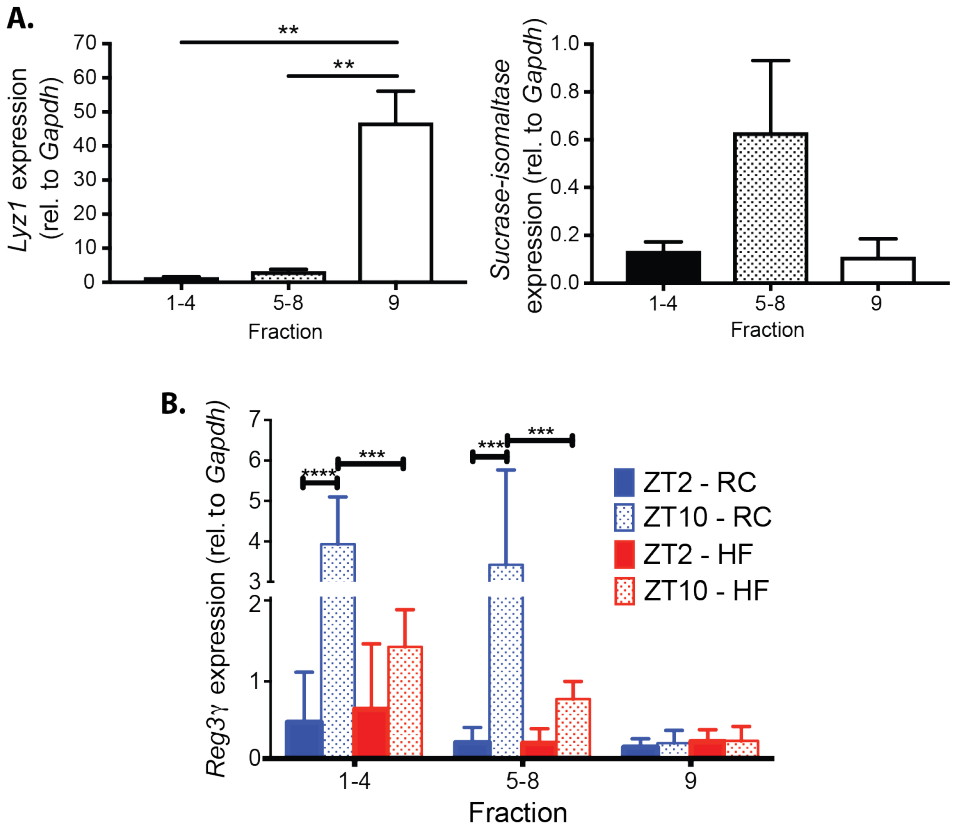

Figure 4.4: **Mucosal cell fractionation reveals enterocyte-specificity of diurnal *Reg3γ*.** (A) *Lyz1* and *Sucrase-Isomaltase* expression relative to *Gapdh* in distal ileum epithelial fractions from SPF RC or HF-fed mice. (B) *Reg3γ* expression in distal ileum epithelial fractions from RC or HF-fed SPF mice at ZT2 and 10. Fractions 1-4,5-8=absorptive enterocytes, fraction 9=crypts harboring stem cells and Paneth cells. Data represent mean±SEM. $****p < 0.0001$, $***p < 0.001$, $**p < 0.01$.

4.4.2 HF diet alters ileal microbiota community membership and dampens microbial diurnal oscillations

We examined microbial community membership within distal ileal luminal contents collected every 4 hours from RC or HF-fed SPF mice via 16S rRNA gene amplicon sequencing and QIIME. HF significantly increased relative abundance of Operational Taxonomic Units (OTUs) belonging to the phyla Firmicutes and decreased Bacteroidetes, while no differences were detected in less abundant phyla (Figure 4.5). Beta-diversity analysis using Bray-Curtis and Canberra distances (Figure 4.6A) revealed significant differences between RC and HF microbial communities (Table B.2).

Absolute 16S rRNA gene copy number, determined via qPCR averaged across ZT in ileal luminal contents, was not different between RC and HF (Figure 4.6B). Significant differences were only observed between RC and HF-fed mice at ZT6, while diurnal rhythmicity was not detected in RC or HF-fed mice (Figure 4.6C). However, while 16S rRNA gene copy number exhibited a similar amplitude in RC and HF-fed mice, HF elicited a phase-shift relative to RC. Distinct OTU differences were observed between RC and HF-fed mice (Figure 4.7), where HF significantly increased Clostridiales and decreased Bacteroidales relative to RC (Table B.3).

To determine whether RC or HF impacted diurnal oscillations, we applied eJTK to luminal content relative abundance data as previously described ([141]). Similar to cecum and feces, approximately 15% of ileal taxa oscillated under RC and was dramatically reduced by HF (Figure 4.8A). 81 unique oscillating OTUs were observed in luminal contents of RC-fed mice, while 14 unique OTUs were present in HF-fed mice; only two oscillating OTUs overlapped in RC and HF (Figure 4.8B; Table B.4). Oscillating RC OTUs annotated to genus were absent, decreased in overall abundance, or lost oscillation under HF (Figure 4.8C). Despite decreased percentage of oscillating OTUs in HF, several gained oscillations (Figure 4.8D). Two OTUs exhibiting oscillations under both RC and HF were annotated

to genera *Ruminococcus* and *Oscillospira*, exhibiting diet-dependent effects on their overall abundances (Figure 4.8E, Table B.4). Together, these data reveal HF dramatically alters distal ileum microbial membership, selecting for a unique set of oscillating taxa relative to RC, despite an overall decrease of oscillating OTUs.

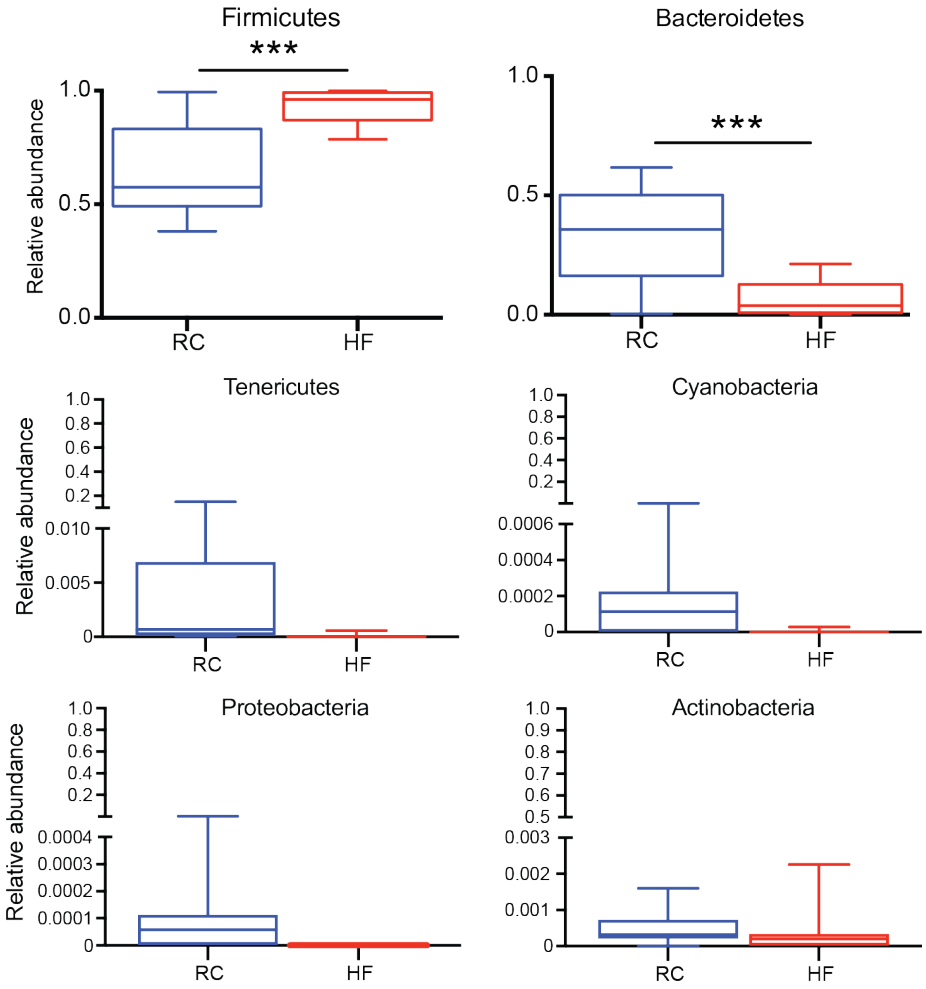

Figure 4.5: **Diet drives abundance of dominant phyla in distal small intestine luminal gut microbe community membership.** 16S rRNA gene amplicon sequencing of distal ileum luminal contents from RC or HF-fed SPF mice collected at ZT 2, 6, 10, 14, 18, and 22 (n=2-3 mice/treatment/ZT). Relative abundances of dominant (Firmicutes and Bacteroidetes) and non-dominant phyla averaged across timepoints within diet condition. Box plots represent median±min/max; $***p < 0.001$.

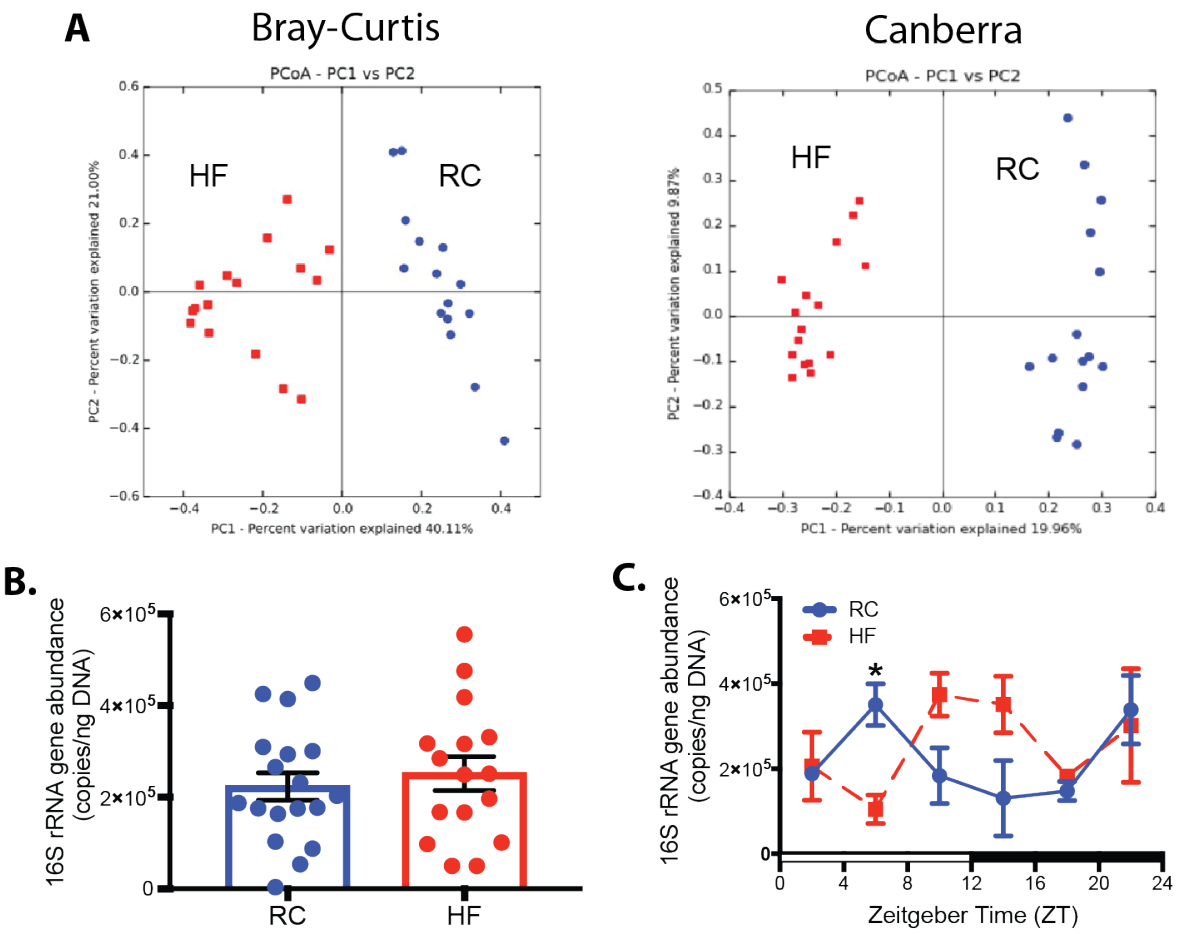

Figure 4.6: **Diet drives overall profile differences in distal small intestine luminal gut microbe community membership.** 16S rRNA gene amplicon sequencing of distal ileum luminal contents from RC or HF-fed SPF mice collected at ZT 2, 6, 10, 14, 18, and 22 (n=2-3 mice/treatment/ZT). (A) Bray-Curtis and Canberra Principle Coordinate Analysis (PCoA) of 16S rRNA sequences. (B) Absolute 16S rRNA gene copy number, timepoints pooled. (C) Absolute 16S rRNA gene copy number determined via qPCR over time. Data represents mean±SEM, $*p < 0.05$.

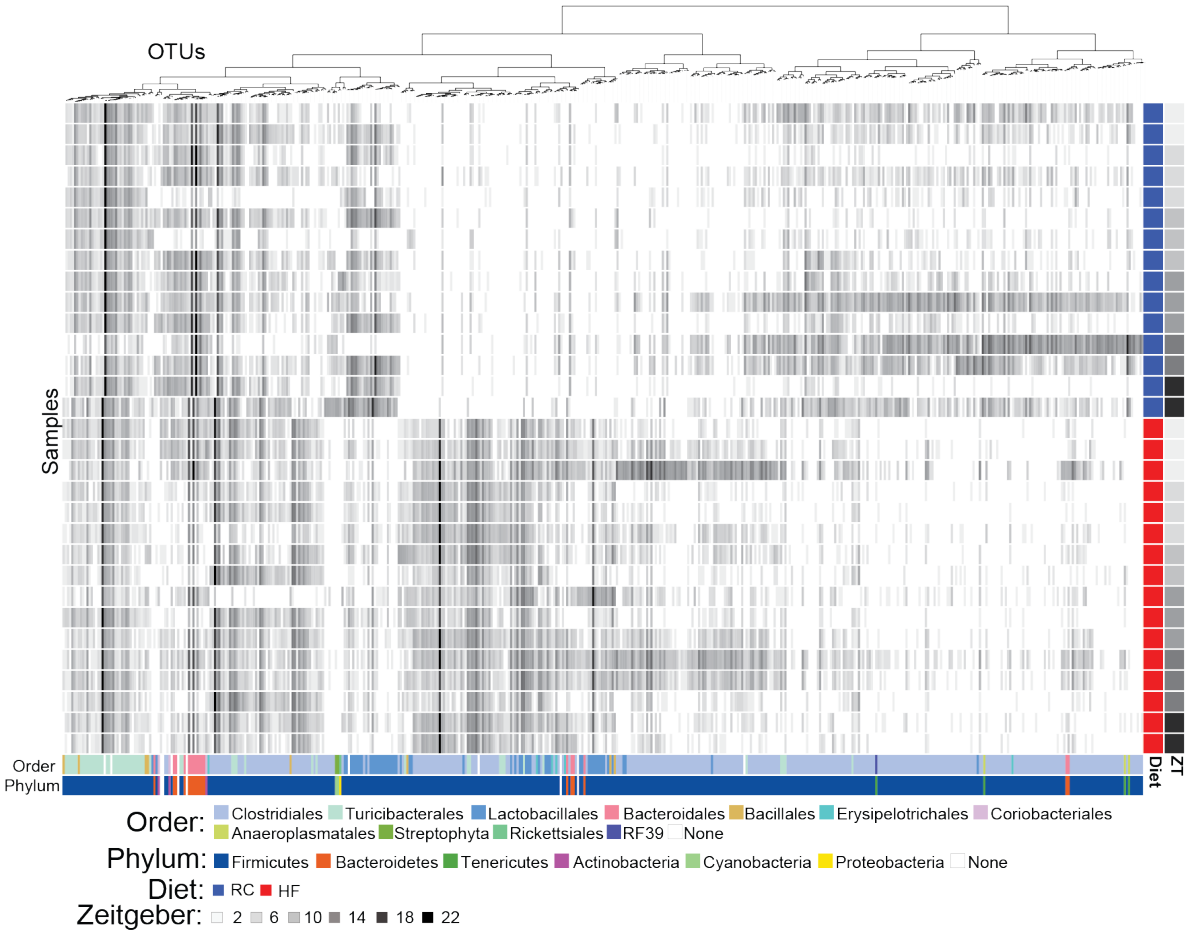

Figure 4.7: **Diet shapes overall distal small intestine luminal gut microbe community membership.** 16S rRNA gene amplicon sequencing of distal ileum luminal contents from RC or HF-fed SPF mice collected at ZT 2, 6, 10, 14, 18, and 22 (n=2-3 mice/treatment/ZT). anvi'o heatmap of 16S rRNA relative abundances. Columns = OTUs, rows = samples. Colored bars at the bottom represent taxonomy; blue and red bars to the right represent diet; gray bars represent ZT.

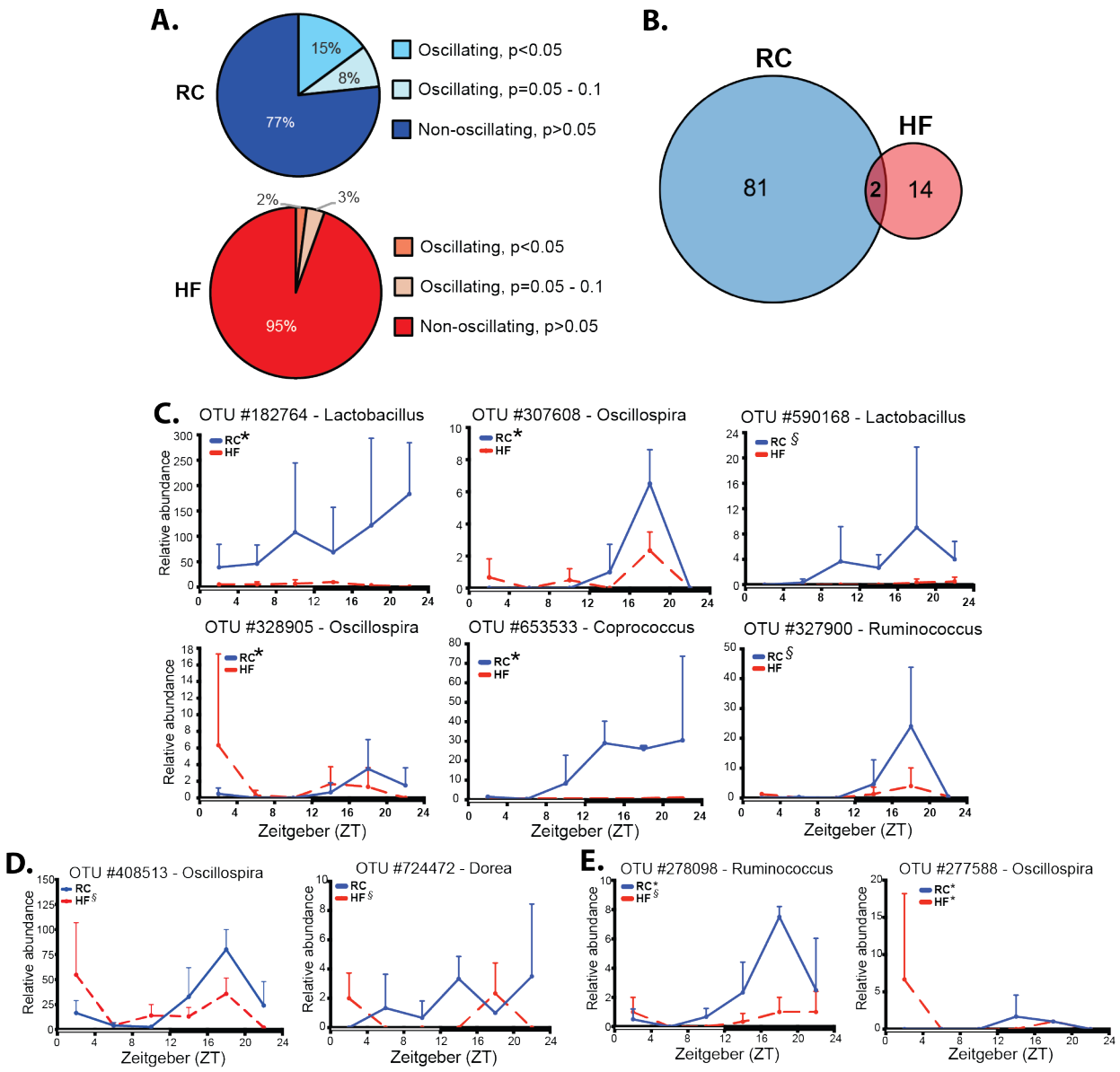

Figure 4.8: **HF diet drives overall loss of oscillating gut microbe community members in distal small intestine lumen.** 16S rRNA gene amplicon sequencing of distal ileum luminal contents from RC or HF-fed SPF mice collected at ZT 2, 6, 10, 14, 18, and 22 (n=2-3 mice/treatment/ZT). (A) Percentage of oscillating and non-oscillating OTUs determined via eJTK. (B) Numbers of unique and shared oscillating OTUs. (C-E) Relative abundances of OTUs annotated to genus that significantly oscillate only in RC-fed mice (C), only in HF-fed mice (D), and in both conditions (E). Data points represent mean±SEM, * indicates $p < 0.05$, ξ indicates p=0.05 – 0.1 significant oscillation detected via eJTK.

4.4.3 Specific taxa promoted by RC or HF correlate with distal small intestine diurnal Reg3g *expression*

Based on Pearson correlation analysis results, only 3 OTUs in luminal contents from RC and HF-fed mice significantly correlated with *Reg3γ* expression. A *Lactobacillus* OTU positively correlated with *Reg3γ* expression, while Clostridiaceae and Peptostreptococcaceae OTUs negatively correlated (Figure 4.9A). The identified Lactobacillus OTU oscillated only in RC, with dramatically reduced overall abundance in HF-fed counterparts across all ZTs (Figure 4.9B, left panel). Surprisingly, while OTUs that negatively correlated with *Reg3γ* did not oscillate in either RC- or HF-fed mice, their relative abundances were significantly increased across all ZTs in HF relative to RC (Figure 4.9B, middle and right panels). These associations were also apparent at a higher taxonomic classification level, where relative abundances of the families Lactobacillaceae, Peptostreptococcaceae, and Clostridiaceae exhibited nearly identical positive and negative correlations with *Reg3γ* expression (Figure 4.9C). Lactobacillaceae was increased during the mid to late dark cycle only in RC, while Peptostreptococcaceae and Clostridiaceae were significantly increased at several ZTs in HF-fed counterparts (Figure 4.9D). These data reveal diet drives unique distal small intestine microbiota membership and serves as the primary driver of microbial oscillations. Lactobacillaceae are enriched by RC and exhibit oscillations, while specific *Lactobacillus* OTUs positively correlate with host diurnal *Reg3γ* expression. Conversely, HF feeding diminishes microbial oscillations and promotes overall expansion of the families Clostridiaceae and Peptostreptococcaceae, both of which negatively correlate with *Reg3γ* expression.

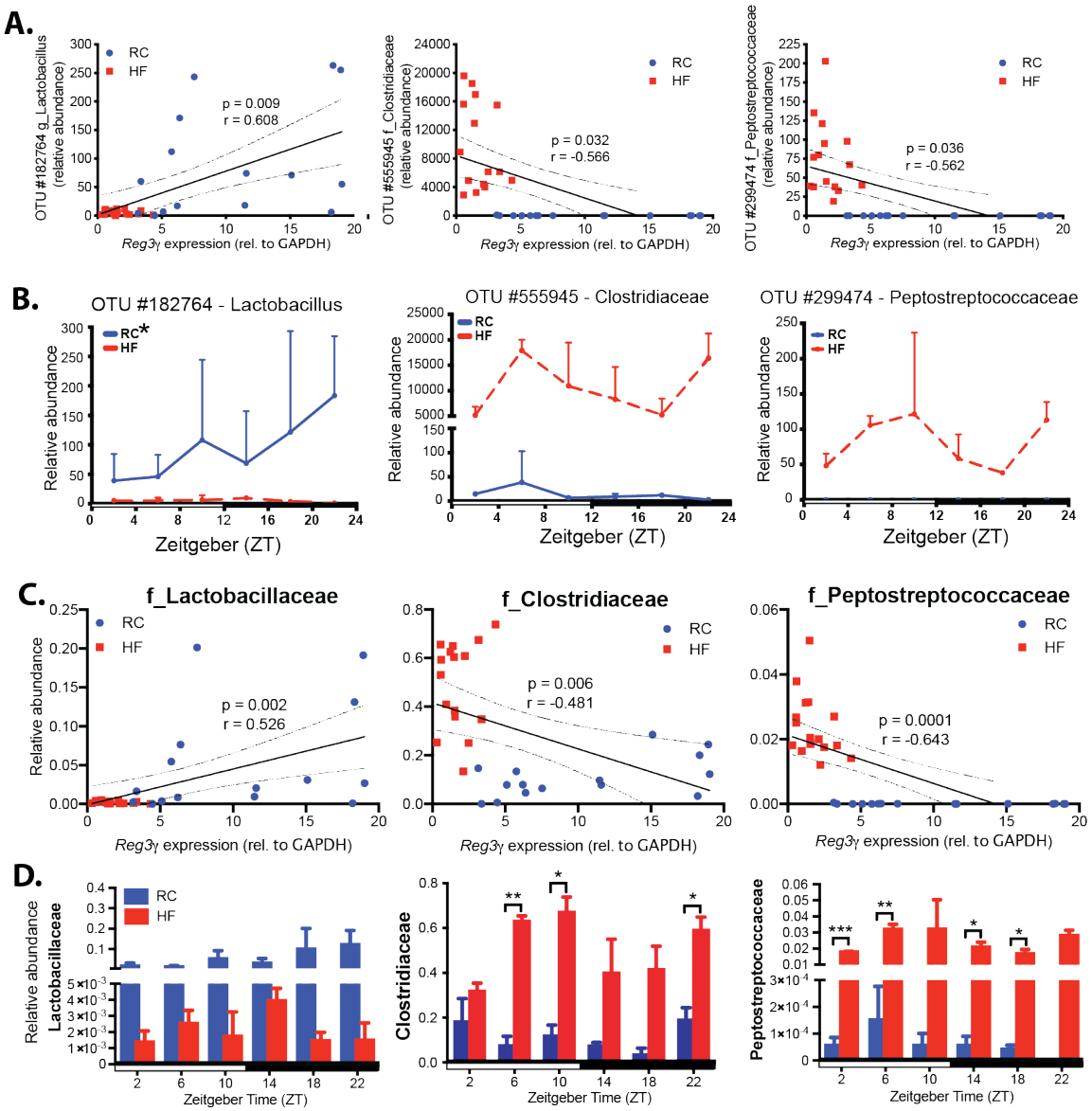

Figure 4.9: **Diet-induced abundance of microbial community members and families significantly correlates with *Reg3γ* expression.** 16S rRNA gene amplicon sequencing of distal ileum luminal contents from RC or HF-fed SPF mice collected at ZT 2, 6, 10, 14, 18, and 22 (n=2-3 mice/treatment/ZT). (A) *Reg3γ* expression vs. relative abundances of OTUs exhibiting significant Pearson correlations (Bonferroni $p < 0.05$). Linear regression lines with 95% confidence bands shown. (B) Relative abundance of OTUs exhibiting significant negative correlation with *Reg3γ* mucosal expression. (C) *Reg3γ* expression vs. relative abundances of OTUs at the family level that exhibit significant Pearson correlations. Linear regression lines with 95% confidence bands shown. (D) Relative abundance of indicated bacterial family that include OTUs that positively or negatively correlate with *Reg3γ* expression. Data points represent mean±SEM, box plots represent median±min/max. $*p < 0.05$, $**p < 0.01$, $***p < 0.001$.

4.4.4 Complex gut microbiota or individual bacteria strains induced by diet directly influence Reg3g *expression* in vitro

We examined the direct impact of diet-induced microbial communities on *Reg3γ* mRNA in vitro using 3-dimensional intestinal enteroids derived from distal ileum of WT mice. Lysate derived from ileal luminal contents of RC-fed SPF mice harvested at ZT10 (peak of host *Reg3γ* expression, Figure 4.2) significantly induced *Reg3γ* expression in enteroids compared to HF lysate after 24hr exposure ($p < 0.05$, Figure 4.10A), indicating diet-induced gut microbiota directly and differentially impact *Reg3γ*.

Next, we determined if type strains belonging to the bacteria families significantly correlated with *Reg3γ in vivo* (Figure 4.9C) could directly influence expression *in vitro*. Conditioned media was prepared from *Lactobacillus rhamnosus* GG (LGG, Lactobacillaceae RC-representative), *Peptostreptococcus anaerobius* (Clostridiaceae HF-representative), and *Peptoanaerobacter stomatis* Sizova (P. stomatis, Peptostreptococcaceae HF-representative). Enteroids exposed to LGG conditioned media for 12 hours exhibited significant induction of *Reg3γ* expression (Figure 4.10B). Neither *P. anaerobius* nor *P. stomatis* conditioned media significantly induced *Reg3γ* expression. These results indicate bacteria correlated with diet composition exhibit a direct and differential capacity to influence *Reg3γ* expression.

We next tested if co-exposure of enteroids to conditioned media from a HF-induced bacteria (such as *P. stomatis*) could override influences of RC-selected bacteria (such as LGG) on *Reg3γ* expression. As expected, we observed LGG alone induced *Reg3γ* expression whereas *P. stomatis* alone resulted in no induction (Figure 4.10C). However, co-exposure of enteroids to *P. stomatis* suppressed *Reg3γ* induction even in the presence of LGG. These data suggest bacteria selected by HF elicits a suppressive influence on *Reg3γ* expression, regardless of exposure to inductive conditioned media.

To test whether *MyD88* signaling is required for LGG or *P. stomatis* to impact *Reg3γ* expression, as previously shown [237, 313], we exposed enteroids from SPF *MyD88*$^{+/-}$ or

MyD88$^{-/-}$ littermate mice to different bacterial conditioned media. LGG significantly induced *Reg3*γ in *MyD88*$^{+/-}$, but not in *MyD88*$^{-/-}$ enteroids, implying LGG requires MYD88, while no induction was observed with *P. stomatis* regardless of MyD88 status (Figure 4.11A). To further delineate whether LGG- or *P. stomatis*-derived small molecules differentially impacted *Reg3*γ expression, we first performed size fractionation of conditioned media. Small molecules less than 3kDa derived from LGG were sufficient to induce *Reg3*γ expression, whereas the suppressive effect of *P. stomatis* was evident in all fractions containing small molecules less than 30kDa (Figure 4.11B). This suggests LGG-derived small molecules induce *Reg3*γ, while *P. stomatis*-derived molecules components suppress *Reg3*γ expression in a *MyD88*-dependent manner.

We next tested whether heat-treatment of the 3kDa LGG conditioned media fraction would impact its ability to induce *Reg3*γ expression. Heat-treatment resulted in decreased capacity to induce *Reg3*γ by 30-40% relative to untreated 3kDa fractionated LGG in enteroids derived from SPF WT mice (Figure 4.11C), indicating a breakdown or inactivation of key small molecules that induce *Reg3*γ expression. Taken together, these studies reveal LGG-derived small molecules are heat-labile and that strain-specific compounds may be necessary to induce *Reg3*γ.

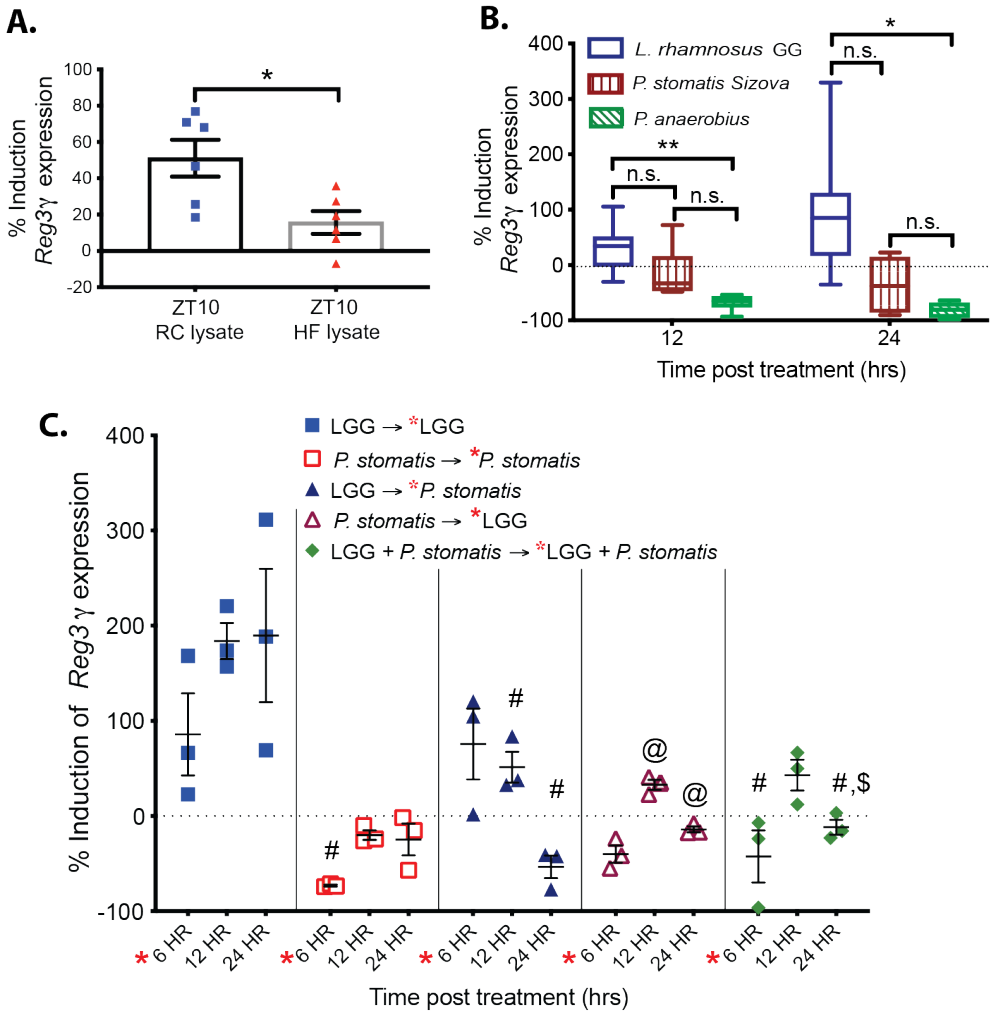

Figure 4.10: **Diet-induced Gram-positive bacterial factors drive host *Reg3γ* expression.** Induction of *Reg3γ* expression in: (A) WT enteroids following 24hr exposure to lysate of ileal luminal contents obtained from RC or HF-fed SPF WT mice at ZT10, relative to PBS vehicle control (n=6 technical replicates/treatment, representative of 3 independent experiments), (B) WT enteroids following 12 or 24hr exposure to conditioned media from cultured bacteria strains, relative to blank media control (n=3-6 technical replicates/treatment, representative of 3 independent experiments), and (C) WT enteroids following 6, 12 or 24hr exposure to conditioned media from cultured bacteria strains, relative to blank media control; red star indicates after 6 hours, enteroids were either collected or exposed to a second treatment (n=3 technical replicates/treatment, representative of 2 independent experiments, symbols indicate significant differences relative to: # = 12hr LGG; @ = 6hr *P. stomatis*; $ = 12hr *P. stomatis* → LGG). Data points represent mean±SEM, box plots represent median±min/max. $*p < 0.05$, $**p < 0.01$, n.s. = not significant.

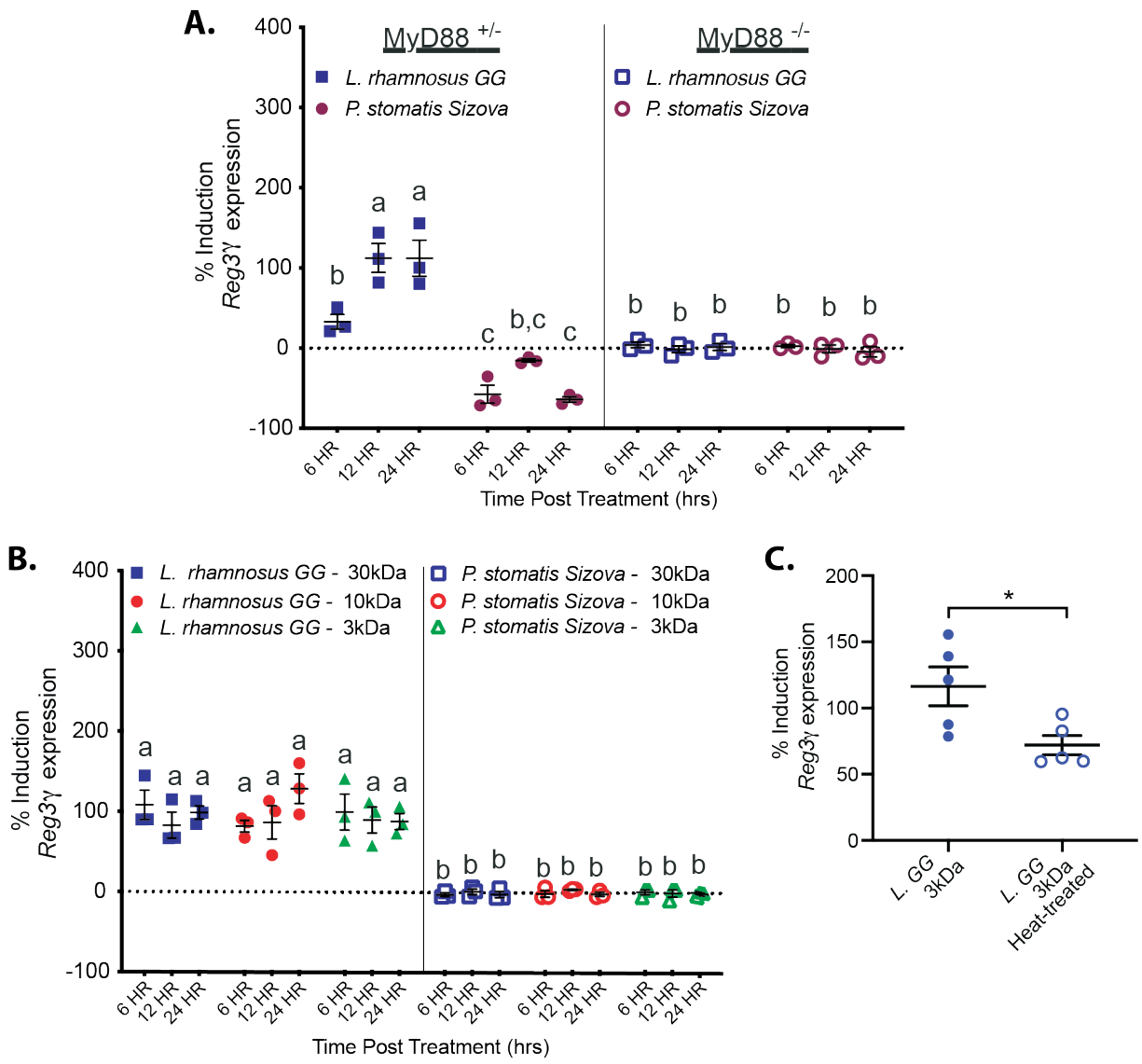

Figure 4.11: **Diet-induced heat-sensitive bacterial small molecules require *MyD88* to drive host *Reg3γ* expression.** Induction of *Reg3γ* expression in: (A) *MyD88*$^{+/-}$ or *MyD88*$^{-/-}$ enteroids 6, 12 or 24hr exposure to conditioned media from cultured bacteria strains, relative to blank media control (n=3 technical replicates/treatment, representative of 2 independent experiments), (B) WT enteroids following exposure to size-fractionated conditioned media from LGG or *P. stomatis* for 6, 12, or 24 hours (n=3 technical replicates/treatment, representative of 2 independent experiments), and (C) WT enteroids following exposure to size-fractionated LGG conditioned media ± heat treatment after 12hr exposure (n=5 technical replicates/treatment, representative of 2 independent experiments). Data points represent mean±SEM, box plots represent median±min/max. $*p < 0.05$; data with the same letter are not significantly different ($p > 0.05$).

4.4.5 Diet-induced Gram-positive bacteria are uniquely resistant to REG3g

Thus far, our observations revealed specific Gram-positive bacteria directly induce or suppress ileal *Reg3*γ expression. To elucidate bidirectionality of this dynamic, we determined if REG3γ exhibited differential bactericidal action against several representative Gram negative and positive bacteria, including *P. stomatis*, LGG, and *Lactobacillus reuteri*, using murine recombinant REG3γ (rREG3γ). We recapitulated previous findings showing Gram-negative bacteria were resistant to rREG3γ, whereas Gram-positive *Enterococcus faecalis* Portland CFUs remaining were reduced by approximately 70% at 10μM [307] (Figure 4.12A). Similarly, *P. stomatis* CFUs remaining dramatically declined at 5 and 10μM rREG3γ. Interestingly, *L. reuteri* behaved similarly to *P. stomatis* in decline, whereas LGG appeared only susceptible at low rREG3γ concentrations and resistant at high concentrations. This suggests that diet-induced bacteria can be uniquely susceptible to REG3γ, further revealing that only certain *Lactobacillus* may be resistant to REG3γ's antimicrobial properties relative to other Gram-positive bacteria.

Given our findings that *Lactobacillus* species exhibit differential susceptibility to REG3γ's antimicrobial actions, we next tested whether LGG and *L. reuteri* conditioned media could equally induce *Reg3*γ expression in enteroids. Similar to 3kDa LGG heat-treated conditioned media, we noted that 3kDa *L. reuteri* exhibited reduced capacity to induce *Reg3*γ expression relative to 3kDa LGG (Figure 4.12B). These data further support the notion that small molecules derived from LGG uniquely induce *Reg3*γ expression and are not universally produced by all *Lactobacillus*.

To further characterize and differentiate unique small molecules produced by LGG and *L. reuteri*, we performed mass spec analyses via LC-MS/MS of 3kDa and heat-treated conditioned medias and observed over 15,000 unique features. Principal coordinate analysis of small molecules revealed that 3kDa *L. reuteri* exhibited unique features relative to both 3kDa LGG untreated and heat-treated, separated primarily by PC1 (Figure 4.13A). 3kDa

LGG untreated and heat-treated profiles were more similar, but still exhibited significant separation by PC2. Differential and fold-change (FC) analysis ($p < 0.05, |log2(FC)| > 1$) revealed 859 unique small molecules that were differentially abundant between 3kDa untreated vs heat-treated LGG, whereas 3kDa LGG vs 3kDa *L. reuteri* revealed 1439 unique different features, with an overlap of 149 between each comparison (Figure 4.13B). Volcano plots revealed reduced fold changes in differential abundance of small molecules between LGG 3kDa untreated vs heat-treated LGG (-7.51 to 6.88), while 3kDa LGG compared to 3kDa *L. reuteri* exhibited greater magnitude of fold change (-10.69 to 9.88) (Figure 4.13C). This indicates greater differences in the small molecule profiles between LGG and *L. reuteri* than those observed following heat-treatment of LGG. The top 25 differentially abundant molecules exhibiting the highest positive and negative fold change relative to LGG 3kDa are shown in Table B.5. While the identity of many metabolites remains unknown, several were identified as branched-chained amino acids (BCAAs) (Table B.5, highlighted blue). Although it remains to be determined which specific small molecules drive induction or suppression of *Reg3*γ expression, these data demonstrate significant differences in the small molecule profile from each bacteria that could differentially modulate *Reg3*γ expression.

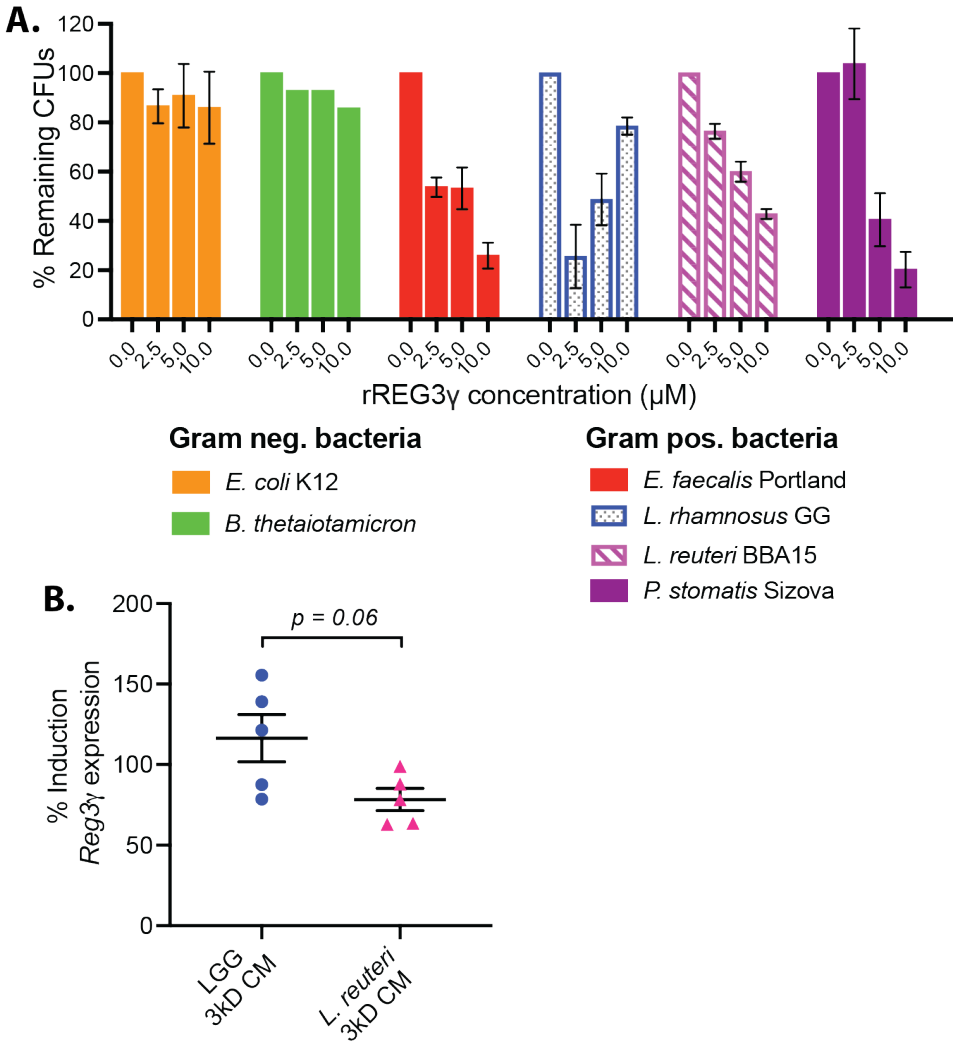

Figure 4.12: **Gram-positive bacteria exhibit unique susceptibility to REG3γ's antimicrobial properties and ability to induce *Reg3γ in vitro*.** (A) Percent remaining CFUs of Gram – and + bacterial strains following 2hr exposure to rREG3γ relative to vehicle control (n=2 replicates/strain, representative of 3 independent experiments). Data represent mean±stdev. (B) Percent induction of *Reg3γ* expression in enteroids derived from RC-fed GF WT mice following 12 or 24hr exposure to size-fractionated (3kDa) conditioned media from cultured strains LGG and *L. reuteri* relative to their respective blank media control (n=5 technical replicates/treatment, representative of 3 independent experiments). Data represents mean±SEM.

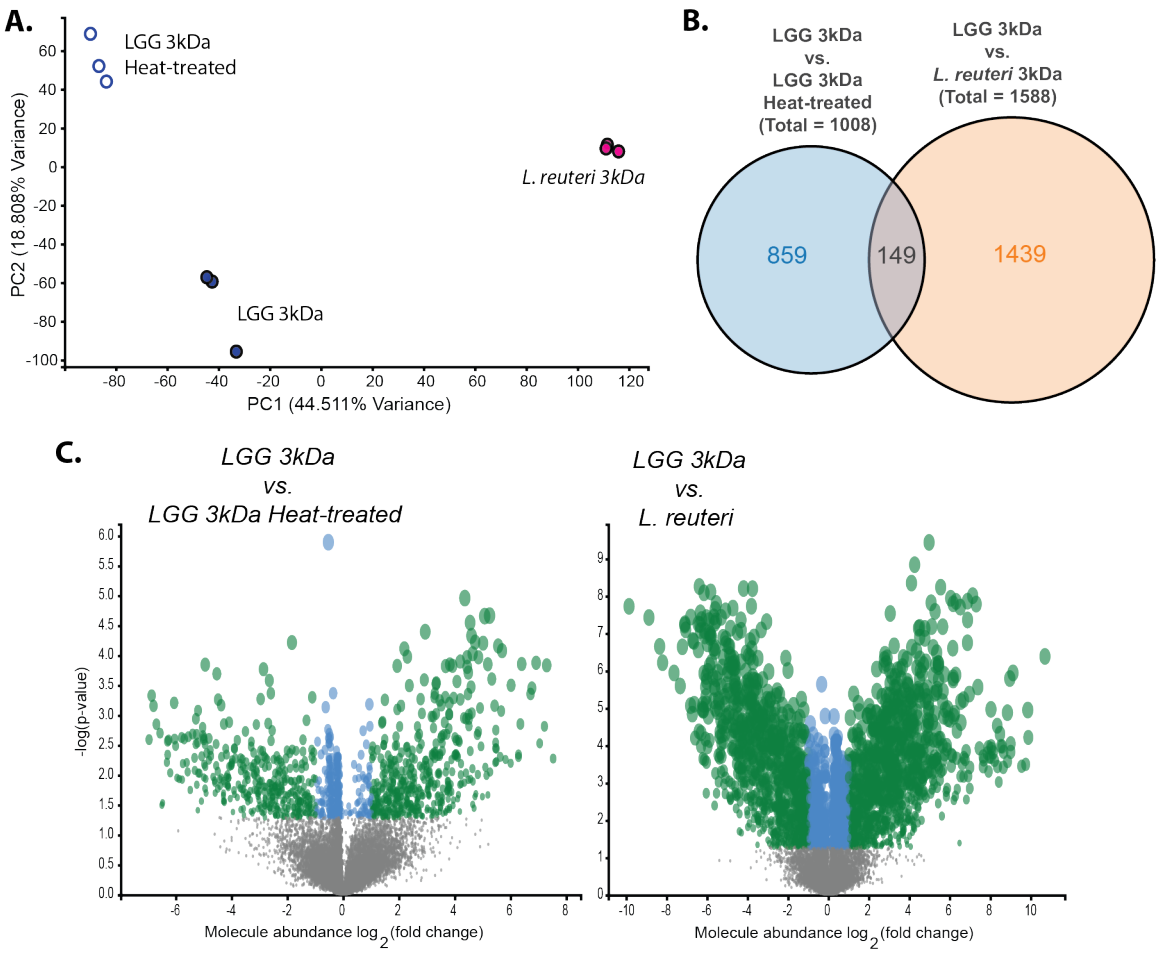

Figure 4.13: ***Lactobacillus* bacteria that differentially induce *Reg3γ* exhibit unique small molecule profiles.** Unbiased LC-MS/MS analysis of 3kDa size fractionated *L. reuteri* BBA15, LGG, and heat-treated LGG conditioned medias (3 technical replicates/strain). (A) Principal component analysis (PCA) based on the relative abundance of MS features (fold-change of peak areas). (B) Summary of differentially abundant ($p < 0.05$ and $|log2(foldchange(FC))| > 1$) MS features between comparisons. (C) Volcano plots comparing log2(FC) and -log(p-value); gray dots indicate $p > 0.05$ and $|log2(FC)| < 1$, blue dots indicate $p < 0.05$ and $|log2(FC)| < 1$, green dots indicate $p < 0.05$ and $|log2(FC)| > 1$.

4.4.6 Diurnal distal ileum Reg3g *expression exhibits* Lactobacillus *strain specificity and is influenced by diet composition*

To translate our *in vitro* findings *in vivo*, we monoassociated RC-fed GF mice with *Lactobacillus* strains exhibiting unique capacity to induce *Reg3γ* expression as well as those with unique resistance to REG3γ's antimicrobial properties, namely LGG and *L. reuteri* (Figure 4.14C). *Reg3γ* expression was significantly increased in ileal mucosal scrapings only from LGG-monoassociated mice harvested at ZT10, the expected peak of expression, which was not observed in GF control or *L. reuteri*-monoassociated mice. Only LGG-monoassociated mice exhibited *Reg3γ* oscillations, while low and constant expression levels were observed in GF and *L. reuteri*-monoassociated counterparts across all 3 ZTs. Interestingly, *L. reuteri* monoassociation resulted in significantly increased weight gain over 4 weeks relative to GF and LGG-monoassociated counterparts, although no significant differences in gonadal fat pad weights were observed (Figure 4.14A,B).

We next determined the interaction between diet composition and LGG monoassociation in the context of *Reg3γ* expression. LGG-monoassociated mice and their GF counterparts were fed either RC or HF. LGG-HF resulted in a modest, yet significant, body weight increase compared to LGG-RC at 3- and 4 weeks post-association (Figure 4.15A). Both GF-HF and LGG-RC mice exhibited significantly increased gonadal fat relative to GF-RC (Figure 4.15B). *Reg3γ* expression was significantly increased in ileal mucosal scrapings only in LGG-RC, but not LGG-HF mice harvested at ZT2 and 10 (nadir and peak expression in RC-fed SPF mice) in which ZT10 tended to be higher; however, *Lyz1* expression was increased only in LGG-RC mice (Figure 4.15C,D). Together, these data reveal an interaction between diet composition and specific bacteria that directly impacts diurnal distal ileum *Reg3γ* that corresponds with changes in host metabolic outcomes.

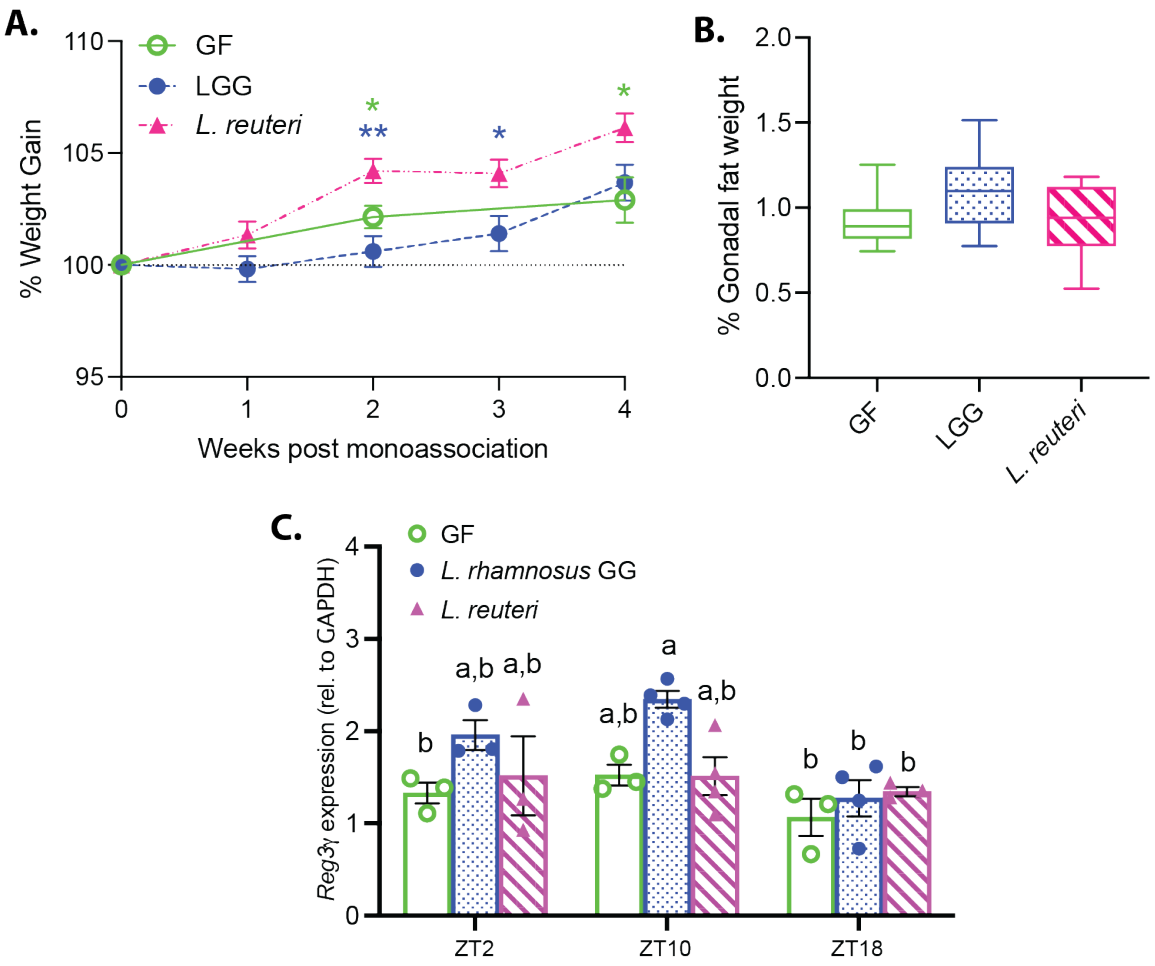

Figure 4.14: ***Lactobacillus* bacteria differentially induce *Reg3γ* *in vivo*.** (A) Percent weight gain relative to baseline in RC-fed GF, LGG-monoassociated, or *L. reuteri*-monoassociated WT mice (n=9-11 mice/treatment). (B) Gonadal fat pad weight expressed as percent of body weight of RC-fed GF, LGG-monoassociated, or *L. reuteri*-monoassociated WT mice (n=9-11 mice/treatment). (C) *Reg3γ* expression in mucosal scrapings of GF, LGG-monoassociated, or *L. reuteri*-monoassociated WT mice fed RC (n=3-4 mice/treatment/ZT). Data points represent mean±SEM, box plots represent median±min/max. $*p < 0.05$, $**p < 0.01$, color relative to GF control. Bars with the same letter are not significantly different ($p > 0.05$).

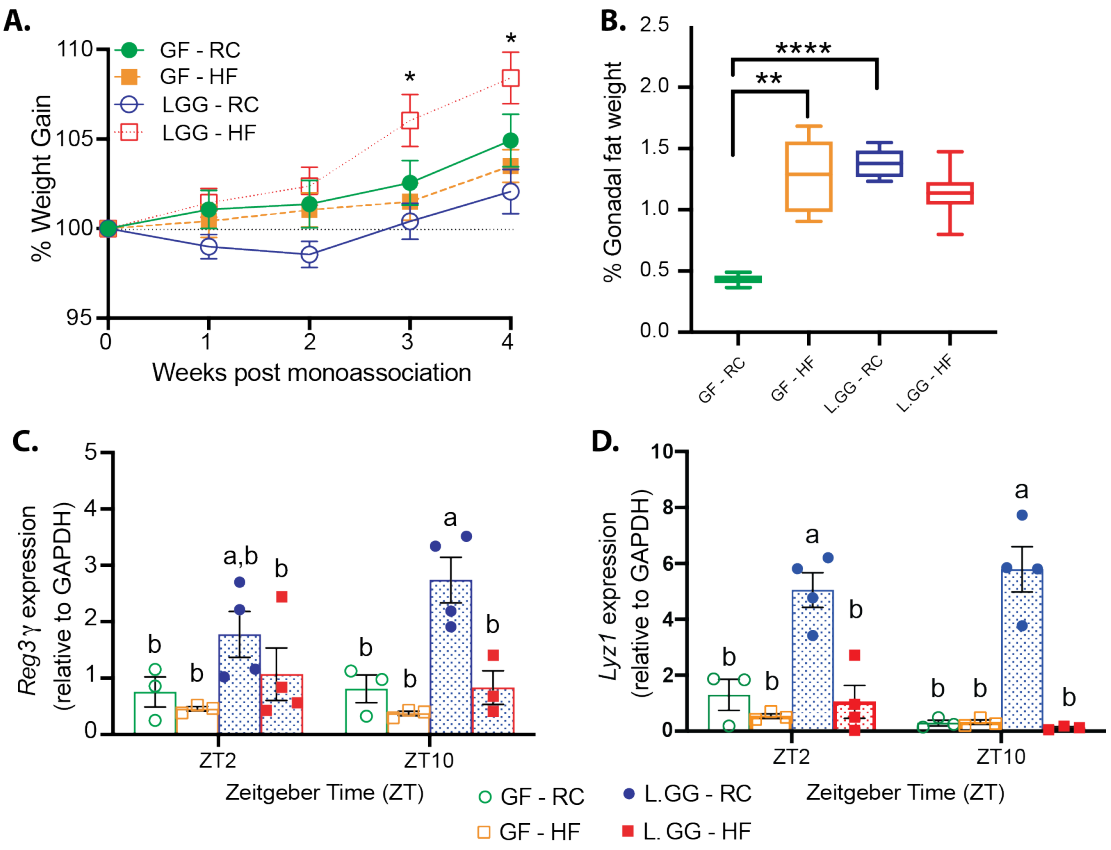

Figure 4.15: ***Lactobacillus* bacteria differentially induce *Reg3γ* *in vivo* in a diet-dependent manner.** (A) Percent weight gain relative to baseline of RC or HF-fed GF or LGG-monoassociated WT mice (n=6-8 mice/treatment). (B) Gonadal fat pad weight expressed as percent of body weight of GF or LGG-monoassociated mice fed RC or HF (n=6-8 mice/treatment). (C,D) *Reg3γ* (C) and *Lyz1* (D) expression in mucosal scrapings of GF or LGG-monoassociated WT mice fed RC or HF (n=3-4 mice/treatment/timepoint, representative of 2 independent experiments). Data points represent mean±SEM, box plots represent median±min/max. $*p < 0.05$, $**p < 0.01$, $****p < 0.0001$, relative to GF-RC control. Bars with the same letter are not significantly different ($p > 0.05$).

4.4.7 REG3g deficiency does not impact small intestinal core circadian clock gene expression and promotes diet-independent glucose intolerance

We next examined how host REG3γ deficiency impacts host-microbe dynamics in RC and HF-fed SPF global *Reg3γ* knockout (*Reg3γ*$^{-/-}$) and heterozygote littermate control (*Reg3γ*$^{+/-}$) mice. Diet or genetic background did not affect overall and diurnal circadian clock expression, further supporting independence between the core circadian clock gene network and *Reg3γ* (Figure 4.16; Table B.1). Significantly elevated and diurnal *Reg3γ* expression were evident in RC *Reg3γ*$^{+/-}$ mice, peaking at ZT10, with no detectable transcript in *Reg3γ*$^{-/-}$ mice (Figure 4.17A). Diet or genotype had no effect on levels, diurnal rhythms, or amplitude of *Crypt4*, *Lyz1*, *Ang4*, and *Tlr* expression (Figures 4.17A,B; Table B.1). RC-fed *Reg3γ*$^{+/-}$ mice exhibited increased overall levels and diurnal patterns of *Muc2* expression, which peaked at ZT10 mirroring *Reg3γ*; however, *Muc2* expression was reduced and arrhythmic in HF-fed *Reg3γ*$^{+/-}$ as well as RC and HF-fed *Reg3γ*$^{-/-}$ mice (Figure 4.17C). These data suggest independence of *Reg3γ* and other AMPs from the core circadian clock, while *Reg3γ* appears to mediate diet effects on *Muc2* expression and rhythmicity, which may impact diurnal rhythms in distal ileum mucosal barrier function.

We also examined the metabolic outcomes of HF diet in the presence and absence of *Reg3γ*. *Reg3γ*$^{-/-}$ mice were equally susceptible to HF DIO relative to *Reg3γ*$^{+/-}$ littermates, where body weight increased approximately 12% relative to RC-fed counterparts over 4 weeks (Figure 4.18A). Liver weights were not different, while HF significantly increased gonadal and mesenteric fat relative to RC regardless of genetic background (Figure 4.18B). Interestingly, RC-fed *Reg3γ*$^{-/-}$ mice exhibited significantly worse glucose tolerance, with slower glucose clearance rates and increased area under the curve (AUC) compared to RC-fed *Reg3γ*$^{+/-}$ controls, while HF decreased blood glucose clearance rate regardless of genetic background relative to RC-fed *Reg3γ*$^{+/-}$ mice (Figure 4.18C). These data suggest

REG3γ does not alter HF DIO outcomes but may play a functional role in how diet impacts glucose tolerance.

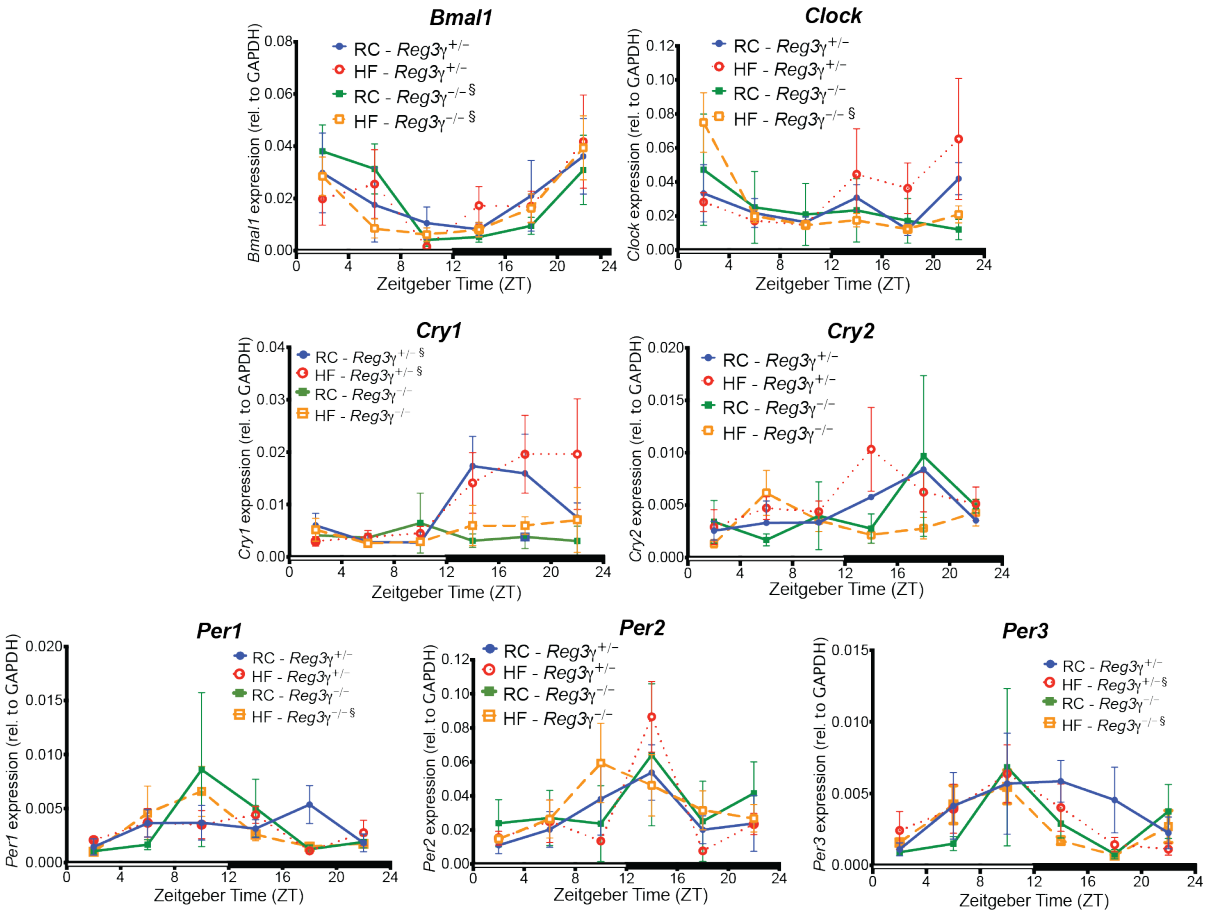

Figure 4.16: ***Reg3γ* deficient mice exhibit no changes in intestinal core circadian clock gene expression.** Diurnal circadian clock gene expression in mucosal scrapings from *Reg3γ*$^{+/-}$ or *Reg3γ*$^{-/-}$ mice fed RC or HF. Data points represent mean±SEM. ξ indicate significant ($p < 0.05$) co-sinor expression patterns detected via CircWave.

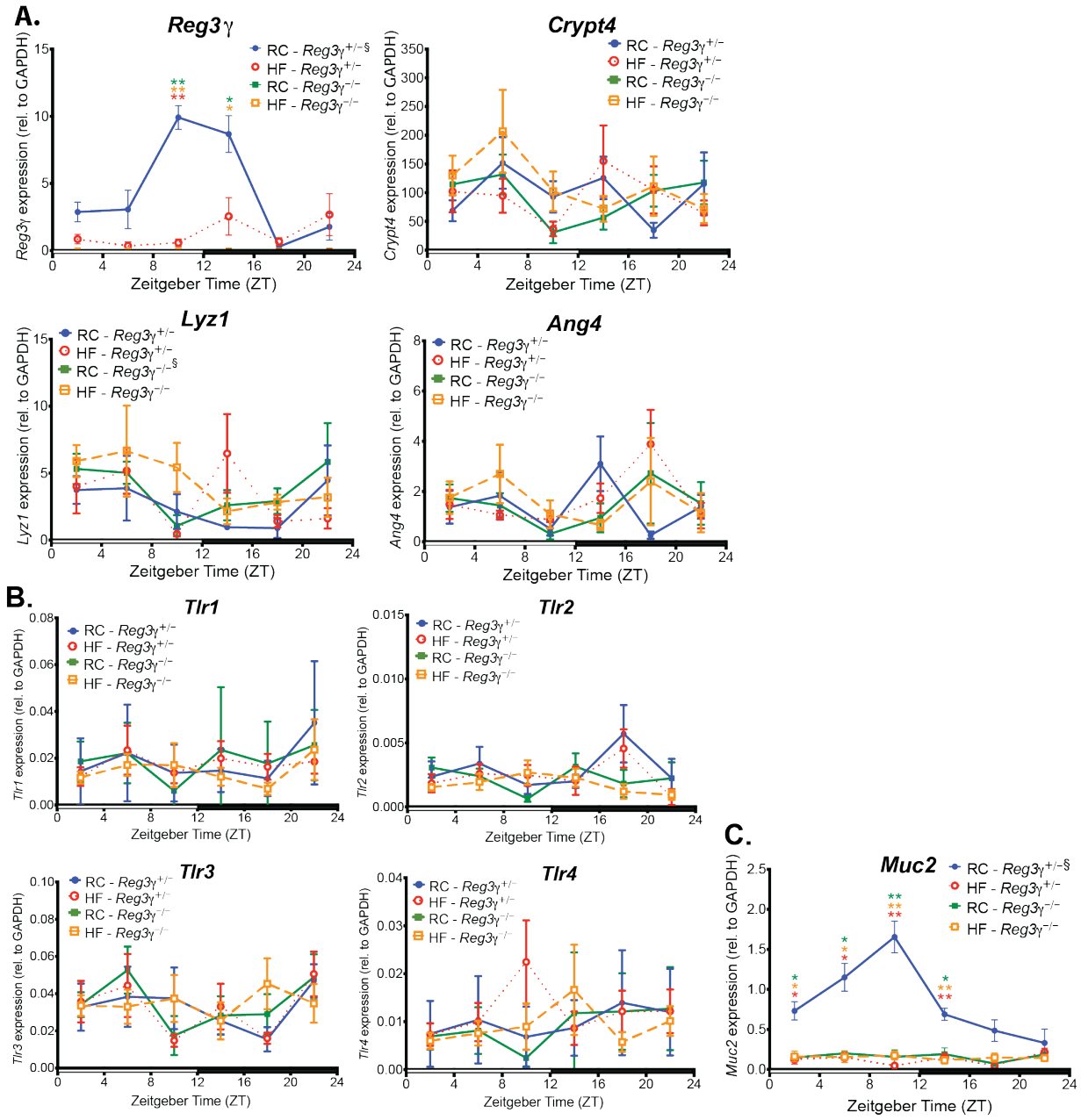

Figure 4.17: ***Reg3γ* deficient mice exhibit no changes in TLR gene expression.** Diurnal AMP (A), *Tlr* (B), and *Muc2* (C) gene expression in mucosal scrapings from *Reg3γ*$^{+/-}$ or *Reg3γ*$^{-/-}$ mice fed RC or HF. Data points represent mean±SEM. $*p < 0.05$, $**p < 0.01$; star color indicates group exhibiting significance relative to *Reg3γ*$^{+/-}$ RC control. ξ indicate significant ($p < 0.05$) co-sinor expression patterns detected via CircWave.

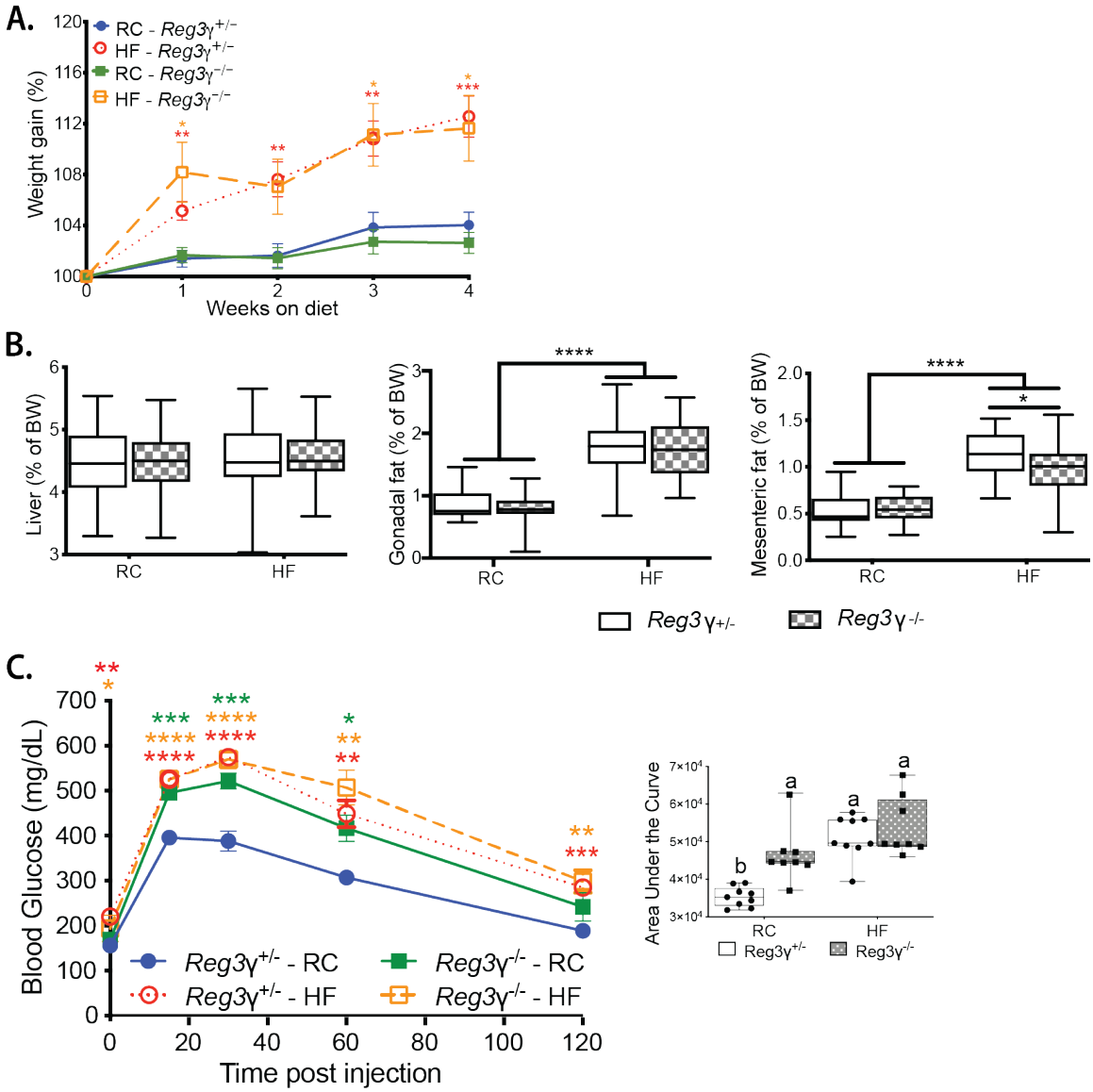

Figure 4.18: ***Reg3γ* deficiency impacts glucose homeostasis in a diet-dependent manner.** (A) Percent weight change from baseline in RC or HF-fed *Reg3γ*$^{+/-}$ or *Reg3γ*$^{-/-}$ mice (n=23-25 mice/treatment). (B) Liver, gonadal fat pad, and mesenteric fat pad weight expressed as percent of body weight of *Reg3γ*$^{+/-}$ or *Reg3γ*$^{-/-}$ mice fed RC or HF (n=24-25 mice/treatment). (C) Glucose tolerance test in *Reg3γ*$^{+/-}$ or *Reg3γ*$^{-/-}$ mice fed RC or HF (n=8-9 mice/condition). Inset graph represents Area Under the Curve (AUC). Bars with the same letter are not significantly different ($p > 0.05$). Data points represent mean±SEM, box plots represent median±min/max. $*p < 0.05$, $**p < 0.01$, $***p < 0.001$, $****p < 0.0001$; star color indicates group exhibiting significance relative to *Reg3γ*$^{+/-}$ RC control.

4.4.8 HF diet overwhelms the modest influence of REG3G on ileal microbiota and shifts specific bacterial families correlated with Reg3g

We determined the influence of diet vs. *Reg3γ* status on luminal contents and mucosal scrapings gut microbial community membership and oscillations via 16S rRNA gene amplicon sequencing in samples from *Reg3γ*$^{+/-}$ and *Reg3γ*$^{-/-}$ mice. Regardless of genotype, HF significantly increased relative abundance of Firmicutes with a corresponding decrease in Bacteroidetes, as well as modest changes in Actinobacteria abundance (Figure 4.19A). No differences were observed in relative abundances of the phyla Proteobacteria, Cyanobacteria, and Tenericutes. This was also evident at higher taxonomic resolution beyond the level of phylum (Figure 4.20; Table B.3). Additionally, 16S rRNA gene copy number in luminal contents was not different between groups, although diurnal rhythmicity was only apparent in RC-fed *Reg3γ*$^{-/-}$ mice (Figure 4.19B; Table B.1).

Beta-diversity analyses using Bray Curtis distances revealed HF shifted community membership regardless of genotype in luminal contents, (Figure 4.21A; Table B.2). However, significant differences in community membership were observed between genotypes, but only when fed RC, indicating a diet-dependent genotype effect (Figure 4.21B, left panel), which was ablated by HF (Figure 4.21B, right panel). We further explored the impact of diet compared to REG3γ on microbial community membership at the family level in luminal contents. HF resulted in decreased relative abundance of Lactobacillaceae and increased Peptostreptococcaceae and Clostridiaceae regardless of genotype (Figure 4.22A). Lactobacillaceae relative abundance was decreased in HF-fed *Reg3γ*$^{-/-}$ at ZT14 relative to RC-fed *Reg3γ*$^{+/-}$ mice, while both Peptostreptococcaceae and Clostridiaceae tended to be lower at nearly all ZTs in RC-fed mice regardless of genotype (Figure 4.22B). Mucosal scrapings exhibited nearly identical patterns (data not shown). These data confirm that diet broadly reshapes distal ileum microbes with a modest and diet-dependent effect of REG3γ.

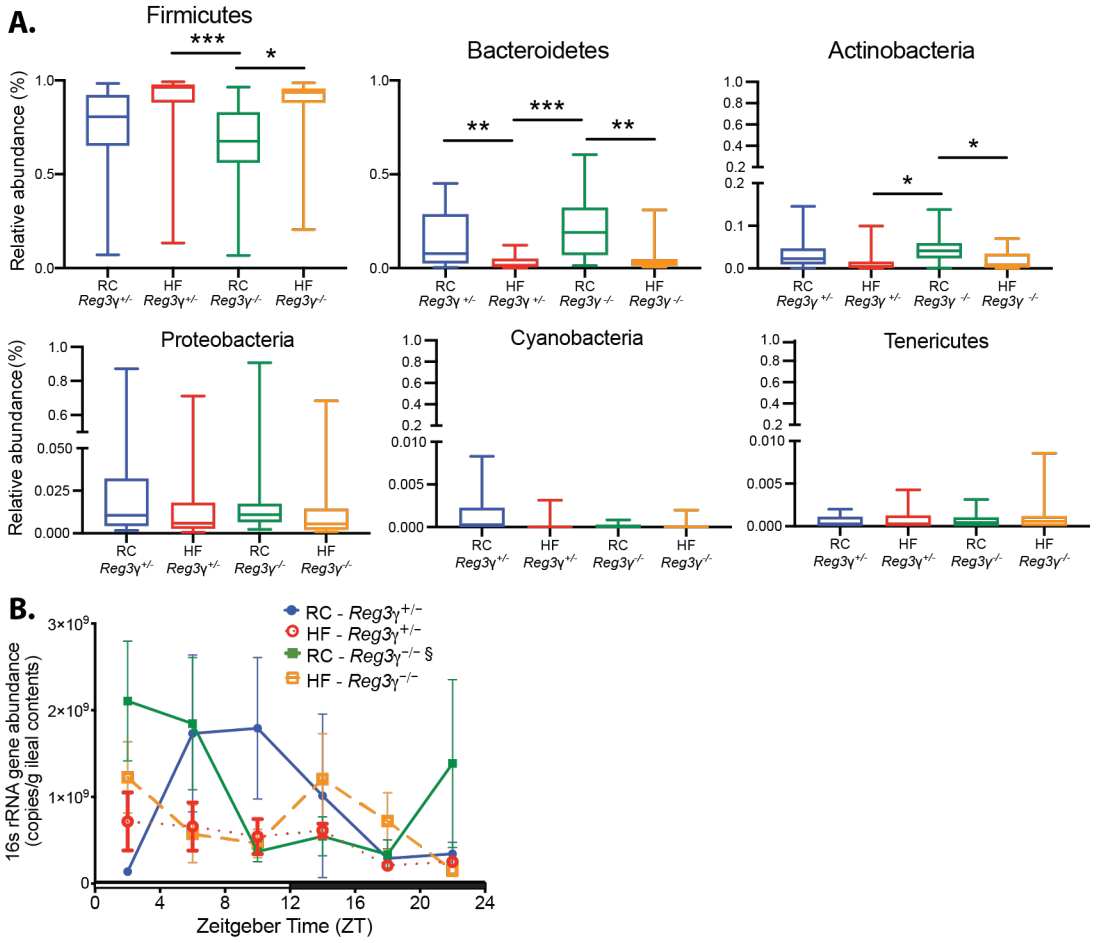

Figure 4.19: **Compared to *Reg3γ*, diet is the primary driver of microbial abundance of major phyla.** 16S rRNA gene amplicon sequencing of distal ileum luminal contents from RC or HF-fed SPF *Reg3γ*$^{+/-}$ or *Reg3γ*$^{-/-}$ mice collected at ZT 2, 6, 10, 14, 18, and 22 (n=2-5 mice/ZT). (A) Relative abundances of dominant bacterial phyla averaged across timepoints. (B) 16S rRNA gene copy number in luminal contents.

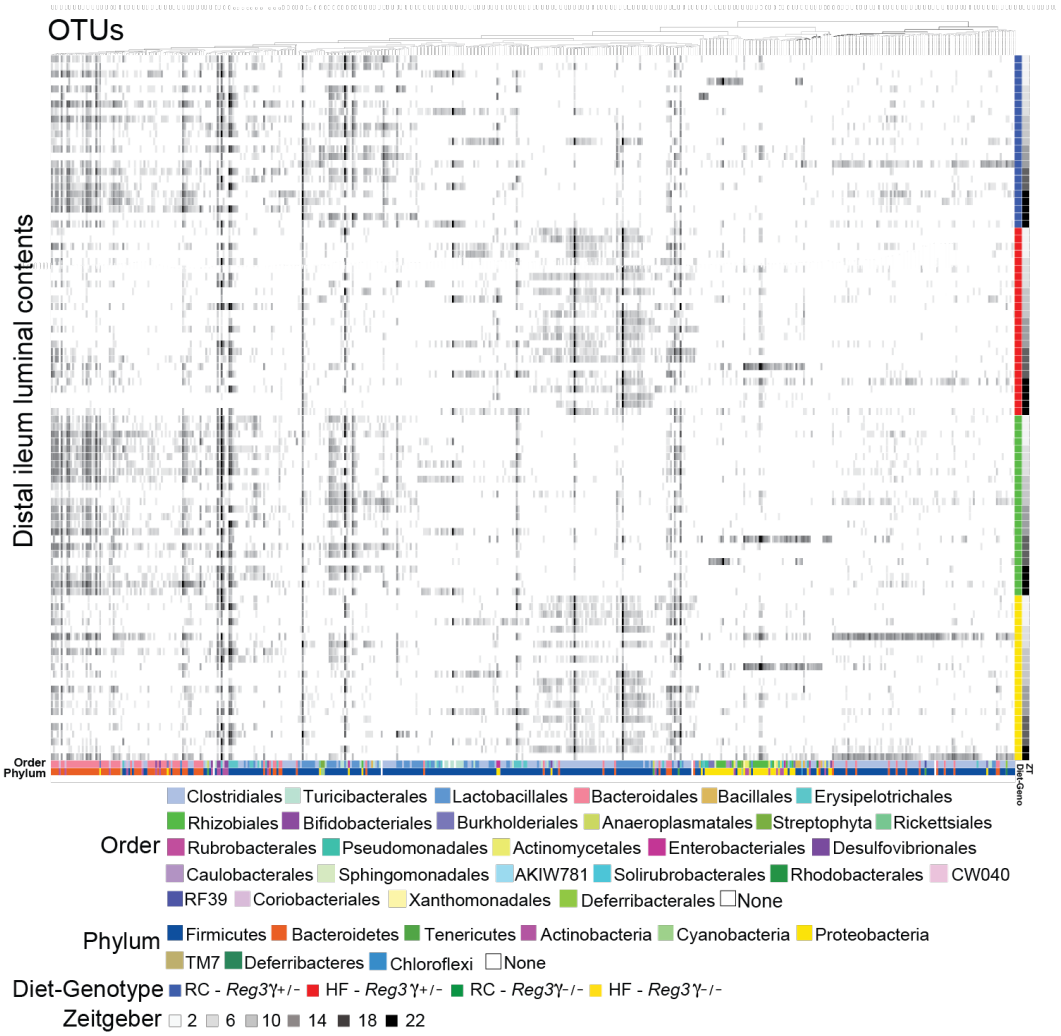

Figure 4.20: ***Reg3γ* modestly impacts distal small intestine gut microbe community membership, secondary to diet.** 16S rRNA gene amplicon sequencing of distal ileum luminal contents from RC or HF-fed SPF *Reg3γ*$^{+/-}$ or *Reg3γ*$^{-/-}$ mice collected at ZT 2, 6, 10, 14, 18, and 22 (n=2-5 mice/ZT). anvi'o heatmap of 16S rRNA relative abundances in luminal contents. Columns represent OTUs, rows represent samples. Colored bars at bottom represent taxonomic assignment. Colored bars at right represent diet, gray bars represent ZT.

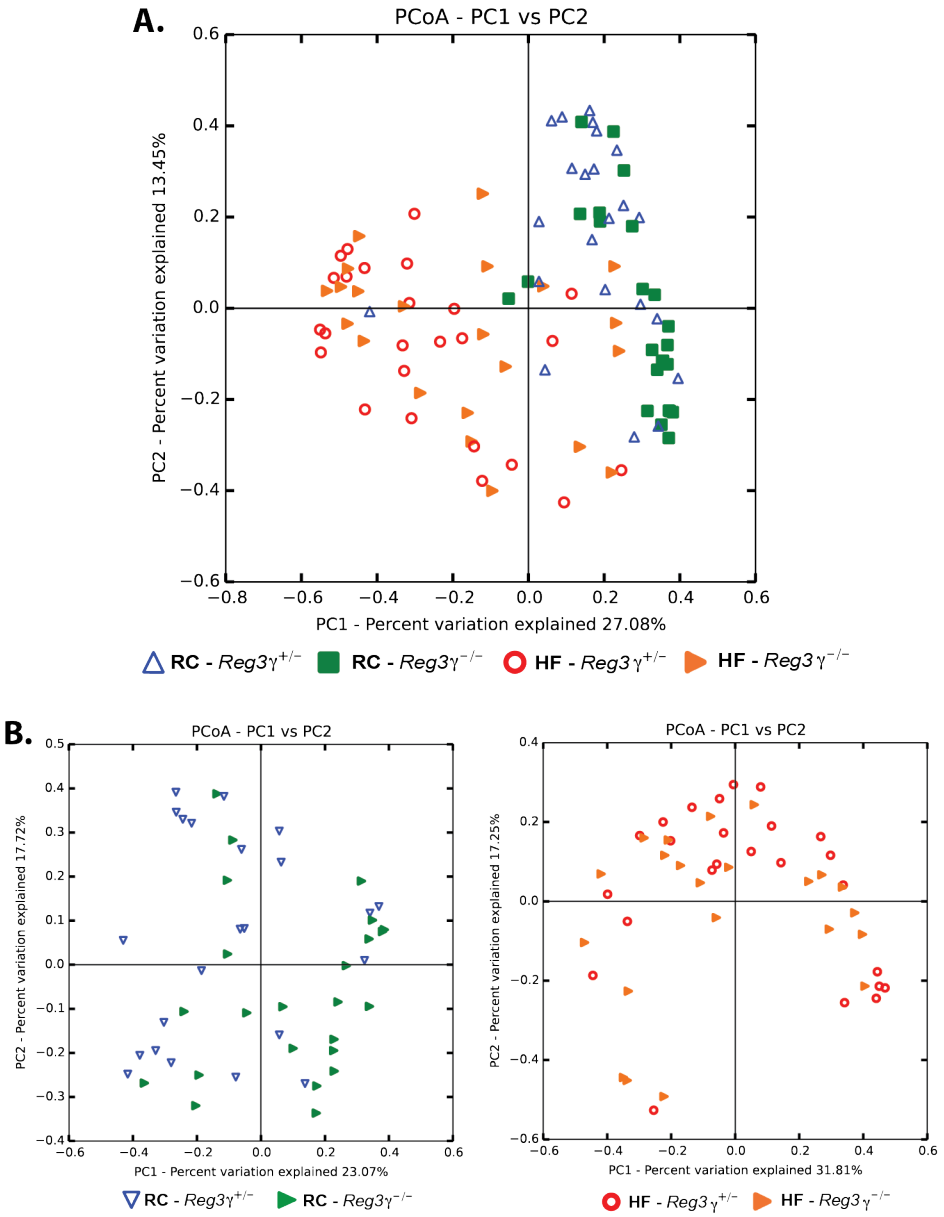

Figure 4.21: ***Reg3γ* modestly impacts distal small intestine gut microbe community membership profiles, only on RC diet.** 16S rRNA gene amplicon sequencing of distal ileum luminal contents from RC or HF-fed SPF *Reg3γ*$^{+/-}$ or *Reg3γ*$^{-/-}$ mice collected at ZT 2, 6, 10, 14, 18, and 22 (n=2-5 mice/ZT). Bray-Curtis PCoA of 16S rRNA sequences comparing all groups (A), and separated by diet (B).

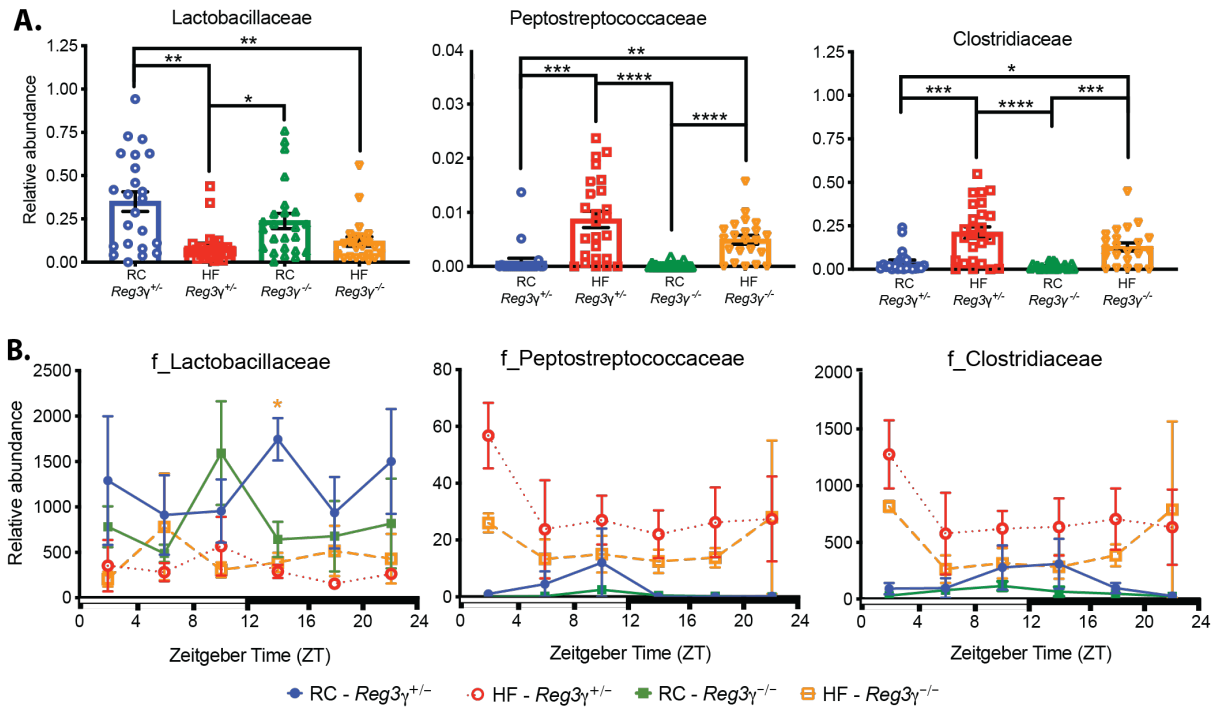

Figure 4.22: ***Reg3γ* exhibits minimal impact on ileal microbial community membership at the family level compared to diet.** 16S rRNA gene amplicon sequencing of distal ileum luminal contents from RC or HF-fed SPF *Reg3γ*$^{+/-}$ or *Reg3γ*$^{-/-}$ mice collected at ZT 2, 6, 10, 14, 18, and 22 (n=2-5 mice/ZT). (A) Average relative abundance of indicated bacterial family in luminal contents. (B) Relative abundances of bacteria families over 24 hours.

4.4.9 Reg3g *deficiency coupled with HF promotes gain of oscillation in Clostridiales and bacteria that are susceptible to REG3g's bactericidal action*

We next examined diurnal dynamics of the gut microbiota based on diet and host genotype. Examination of 16S rRNA amplicon sequences from luminal contents via eJTK revealed diet-dependent differences in oscillations of specific taxa between genotypes (Figure 4.20, Table B.4). Here, we observed RC-fed *Reg3γ*$^{+/-}$ mice displayed significantly more oscillating OTUs than HF-fed counterparts, while both *Reg3γ*$^{-/-}$ diet groups exhibited nearly identical numbers (Figure 4.23A, upper panel, Table B.4). Interestingly, mucosal scrapings exhibited opposite patterns, where *Reg3γ*$^{-/-}$ mice exhibited more oscillating OTUs regardless of diet (Figure 4.23A, lower panel).

Further examination revealed RC-fed *Reg3γ*$^{+/-}$ mice exhibited the highest diversity of oscillating taxa at the level of order in luminal contents relative to all other groups (Figure 4.23B, left panel; Table 4.1). In *Reg3γ*$^{+/-}$ mice, HF resulted in fewer oscillating Lactobacillales and Clostridiales as compared to RC-fed control counterparts. However, in *Reg3γ*$^{-/-}$ mice, HF decreased oscillating Bacteroidales with concomitant increases in oscillating Clostridiales. We observed that mucosal scrapings exhibited unique OTU oscillatory properties relative to luminal contents (Figure 4.23B, right panel; Table 4.1). Here, regardless of genotype, RC exhibited far less diversity in oscillating OTUs relative to luminal contents. Regardless of diet, *Reg3γ*$^{-/-}$ mice also exhibited the highest number of oscillating Bacteroidales and Clostridiales relative to *Reg3γ*$^{+/-}$ counterparts.

Finally, we examined oscillations of taxa that correlated with and induced *Reg3γ* in our previous *in vivo* and *in vitro* experiments, including Lactobacillaceae, Clostridiaceae, and Peptostreptococcaceae. Here, we observed many oscillating *Lactobacillus* OTUs exhibited increased relative abundance in RC-fed mice, regardless of genotype (Figure 4.24). 60% of these OTUs oscillated only in RC-fed mice, indicating *Lactobacillus* diurnal rhythms are

dependent on RC. Despite an overall lack of species-level annotation, two *Lactobacillus* OTUs were classified as *L. reuteri*. Although the relative abundance of *L. reuteri* was increased in RC, these OTUs only oscillated in HF when diurnal *Reg3γ* expression was impaired. Similarly, nearly all oscillating Clostridiaceae and Peptostreptococcaceae OTUs were only observed when diurnal *Reg3γ* expression patterns were impaired (HF feeding) or completely absent (genetic ablation). This expands our findings in SPF WT mice, where HF was the main driver of shifting relative abundance patterns and overall number of oscillating microbiota (Figure 4.8). This suggests bacteria that are normally susceptible to REG3γ, i.e., *L. reuteri*, Clostridiaceae, and Peptostreptococcaceae, only gain rhythmicity following HF-diet reshaping of distal ileum microbiota coupled with complete loss of a host-derived secondary signal, such as REG3γ.

A. Distal ileum luminal contents

Condition	Oscillating OTUs ($p < 0.05$)	Oscillating OTUs ($p = 0.05 – 0.1$)	Total OTUs
Reg3γ$^{+/-}$ - RC	23	14	358
Reg3γ$^{+/-}$ - HF	14	8	291
Reg3γ$^{-/-}$ - RC	18	26	312
Reg3γ$^{-/-}$ - HF	21	21	349

Distal ileum mucosal scrapings

Condition	Oscillating OTUs ($p < 0.05$)	Oscillating OTUs ($p = 0.05 – 0.1$)	Total OTUs
Reg3γ$^{+/-}$ - RC	12	11	384
Reg3γ$^{+/-}$ - HF	19	18	393
Reg3γ$^{-/-}$ - RC	50	24	380
Reg3γ$^{-/-}$ - HF	34	39	393

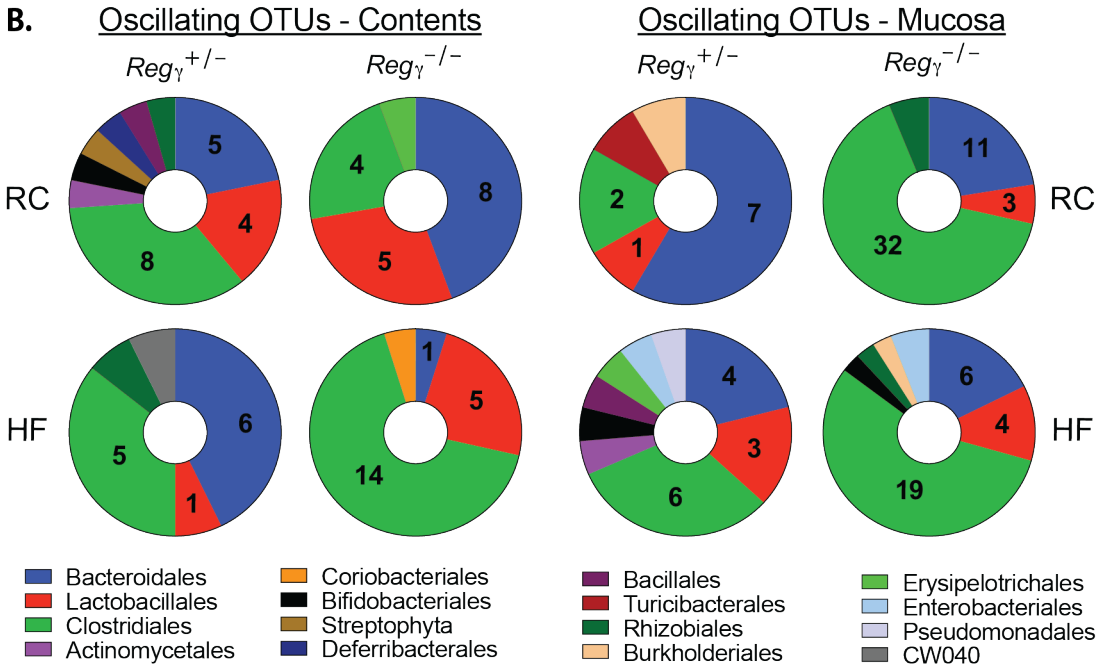

Figure 4.23: **Diet coupled with *Reg3γ* deficiency induces unique microbial community member specific diurnal oscillations.** 16S rRNA gene amplicon sequencing of distal ileum luminal contents and mucosal scrapings from RC or HF-fed SPF *Reg3γ*$^{+/-}$ or *Reg3γ*$^{-/-}$ mice collected at ZT 2, 6, 10, 14, 18, and 22 (n=2-5 mice/ZT). (A) Number of significantly oscillating OTUs detected via eJTK in luminal contents and mucosal scrapings. (B) Proportion of significantly oscillating OTUs detected via eJTK divided by Order level classification in luminal contents (left) and mucosal scrapings (right). Pie charts indicate number of significantly oscillating OTUs.

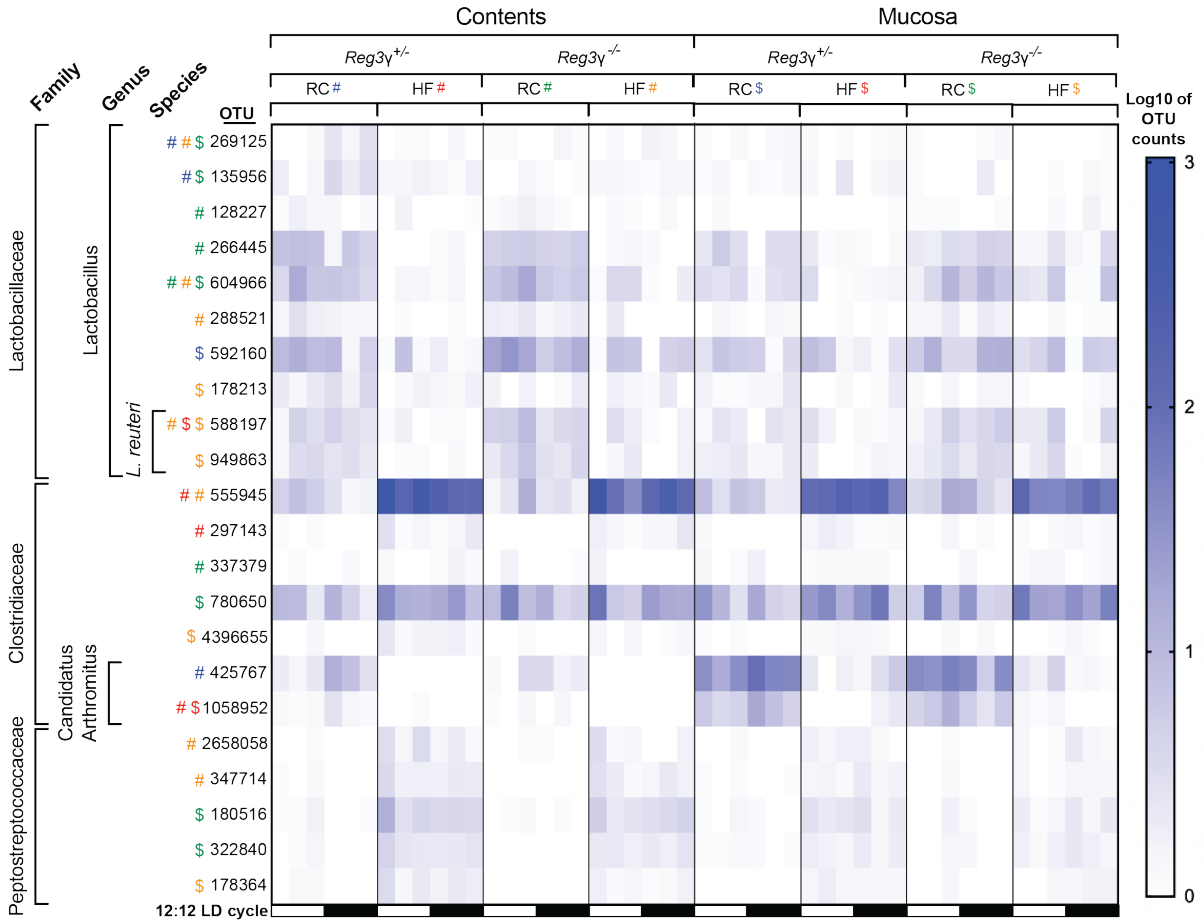

Figure 4.24: **HF diet and loss of *Reg3*γ permits certain microbial community members to gain oscillation.** 16S rRNA gene amplicon sequencing of distal ileum luminal contents and mucosal scrapings from RC or HF-fed SPF *Reg3*$\gamma^{+/-}$ or *Reg3*$\gamma^{-/-}$ mice collected at ZT 2, 6, 10, 14, 18, and 22 (n=2-5 mice/ZT).

Table 4.1: **Total oscillating OTUs by taxonomic group.** 16S rRNA gene amplicon sequencing of distal ileum luminal contents and mucosal scrapings from RC or HF-fed SPF *Reg3γ*$^{+/-}$ or *Reg3γ*$^{-/-}$ mice collected at ZT 2, 6, 10, 14, 18, and 22 (n=2-5 mice/ZT). Numbers of eJTK oscillating OTUs in distal ileum luminal contents and mucosal scrapings at the taxonomic levels of order and family in RC and HF-fed *Reg3γ*$^{+/-}$ and *Reg3γ*$^{-/-}$ mice.

Order	Family	Luminal Contents				Mucosal Scrapings			
		Reg3γ$^{+/-}$		*Reg3γ*$^{-/-}$		*Reg3γ*$^{+/-}$		*Reg3γ*$^{-/-}$	
		RC	HF	RC	HF	RC	HF	RC	HF
Actinomycetales	Micrococcaceae	0	0	0	0	0	1	0	0
	Mycobacteriaceae	1	0	0	0	0	0	0	0
Bifidobacteriales	Bifidobacteriaceae	1	0	0	0	0	1	0	1
Coriobacteriales	Coriobacteriaceae	0	0	0	1	0	0	0	0
Bacteroidales	Bacteroidaceae	0	0	0	0	0	0	1	0
	Porphyromonadaceae	0	0	0	0	0	1	1	0
	Rikenellaceae	1	0	1	1	0	0	1	0
	S24-7	4	6	7	0	7	3	8	6
Deferribacterales	Deferribacteraceae	1	0	0	0	0	0	0	0
Streptophyta	Unassigned Streptophyta	1	0	0	0	0	0	0	0
Bacillales	Staphylococcaceae	1	0	0	0	0	1	0	0
Lactobacillales	Enterococcaceae	0	0	0	0	0	1	0	0
	Lactobacillaceae	2	0	3	4	1	1	3	3
	Streptococcaceae	2	1	2	1	0	1	0	1
Turicibacterales	Turicibacteraceae	0	0	0	0	1	0	0	0
Clostridiales	[Mogibacteriaceae]	0	0	0	0	0	0	1	1
	Clostridiaceae	1	2	1	1	0	1	1	1
	Lachnospiraceae	0	0	0	2	0	3	6	5
	Peptococcaceae	0	0	0	0	0	0	1	0
	Peptostreptococcaceae	0	0	0	2	0	0	2	1
	Ruminococcaceae	2	1	1	3	1	0	6	3
	Unassigned Clostridiales	5	2	2	6	1	2	15	8
Erysipelotrichales	Erysipelotrichaceae	0	0	1	0	0	1	0	0
Enterobacteriales	Enterobacteriaceae	0	0	0	0	0	1	0	2
Pseudomonadales	Pseudomonadaceae	0	0	0	0	0	1	0	0
Rhizobiales	Brucellaceae	1	1	0	0	0	0	3	1
Burkholderiales	Comamonadaceae	0	0	0	0	0	0	0	1
	Oxalobacteraceae	0	0	0	0	1	0	0	0
CW040	F16	0	1	0	0	0	0	1	0

4.5 Discussion

Biological rhythms are essential to all life forms for coordination of internal events with environmental cues to maximize efficiency in metabolic, neural, immune, and other critical functions. Circadian rhythms consist of a feedback loop of transcription factors that induce rhythmic gene expression patterns to orchestrate a hierarchy of downstream events to achieve this efficiency. However, the gut microbiome, which also exhibits rhythms, cannot entrain to photic environmental cues, instead responding to signals such as meal timing, content, and amount. Three major findings of our study underscore the uniqueness of gut microbial rhythms, as well as provide insight into a dynamic interaction between microbes and local host factors in the small intestine. First, we define a temporal push-pull relationship between specific microbial oscillators and the innate immune AMP *Reg3γ*, which exhibits diurnal rhythmicity but is not correlated with the core circadian clock. Second, we demonstrate HF, low-fiber diet results in loss of functional microbial oscillators and an expansion of community members that do not induce *Reg3γ*. Third, the combination of HF and loss of *Reg3γ* allows emergence of specific microbial oscillators. Taken together, the disruption of these primary (diet) and secondary (*Reg3γ*) circadian drivers may contribute to metabolic imbalances.

While an essential role of small intestinal microbes in regulating circadian networks and metabolism has been demonstrated, initial studies only focused on host parameters and outcomes without examining gut microbiota membership, function, and rhythmicity. Our work expands on these previous findings. Further, Brooks *et al.* recently revealed that diurnal oscillations in IEC attachment of SFB drives *Reg3γ* rhythmicity in a global clock-dependent manner that is impacted by time of feeding, preventing infection with known food-borne pathogens [187]. However, diet composition was not explored in these studies. Here, we further demonstrate a dynamic, bidirectional interaction between dietary composition, several diet-induced gut microbes and *Reg3γ* through the lens of metabolic homeostasis and circadian rhythms.

In our model system, we demonstrate that the small intestinal core circadian clock gene network is not correlated with either diet- or microbe-derived cues (Figure 4.1), confirming previous work [186]. These results underscore the uniqueness of the intestine relative to other peripheral tissues; we previously showed rhythmicity of hepatic core circadian clock genes is exquisitely sensitive to diet-induced microbial cues [141]. Importantly, we show distal small intestine diurnal *Reg3γ* regulation is instead correlated with microbial diurnal cues under RC conditions (Figure 4.2). HF-diet induced gut dysbiosis in SPF mice results in arrhythmic *Reg3γ*, underscoring the importance of microbes as key drivers of this phenomenon. Interestingly, we note that *Reg3β*, which targets Gram negative bacteria (Figure 4.2), exhibits a similar oscillatory gene expression pattern, also influenced by both presence of gut microbes and dietary intake. This suggests a possible convergent mechanism, i.e., *MyD88*, regulating diurnal expression of REG family proteins. The reason for the lack of coordination between the intestinal circadian clock and REG proteins is unclear; however, it could indicate autonomy of the gut is required to maintain proper timing of essential digestive functions where overtly perturbing rhythmicity of the circadian clock could ultimately compromise host fitness.

Our results demonstrate that RC promotes specific microbes that are essential to drive host diurnal *Reg3γ* expression. Whereas *Lactobacillus* is known to correlate with *Reg3γ* [240], we reveal their diurnal dynamics are intricately intertwined with this phenomenon (Figures 4.8C, 4.14C, 4.15C). We observe that in the small intestine, approximately 15% of microbes oscillate on RC, many of which are eliminated by HF (Figure 4.8A), corroborating previous findings in the distal GI tract [141, 179, 180]. We reveal DIO is not only associated with decreased small intestinal *Reg3γ* expression [309, 311, 314], but also HF-induced gut dysbiosis suppresses both its overall and rhythmic expression patterns (Figures 4.2, 4.10A). Our work supports the idea that diet overwhelms genetics in shaping microbial small intestine membership, where HF elicits greater influence than *Reg3γ* genetic deletion (Figures 4.7,

4.20), confirming previous studies in the distal GI tract [139, 315]. Interestingly, HF coupled with global REG3γ deficiency permits diet-induced gut microbes to increase proportionally and gain oscillations within the community (Figure 4.24). Together, these data reveal diet is the main driver of gut microbiota membership and oscillations, while host-derived cues, such as *Reg3*γ serve a secondary role in shaping rhythmicity of key small intestine gut microbes.

We provide direct evidence that diet-induced representative small intestinal bacteria associate with and directly induce diurnal *Reg3*γ expression requiring MyD88 using both *in vivo* (global KO animals) and *in vitro* (enteroids derived from KO vs. heterozygote littermate mice) approaches [237, 313]. This is in partial contrast to evidence that only global or dendritic cell-specific, but not epithelial cell-specific, MyD88 deficiency resulted in a loss of *Reg3*γ [187]. While we reveal specific *Lactobacillus* correlate with diurnal *Reg3*γ expression, the precise factor they secrete or produce *in vivo* to drive this phenomenon is not clear. However, via mass spectrometry, we show that the profiles of small molecules secreted by individual *Lactobacillus* are unique with little overlap (Figure 4.13). We identified small molecules derived only from specific *Lactobacillus* that can induce *Reg3*γ *in vitro* (Figures 4.11C, 4.12B), which may involve direct activation of IEC TLRs. Whether *Lactobacillus*-mediated diurnal *Reg3*γ expression also requires IL-22/STAT3-mediated induction is unclear and requires further exploration. Work by Gu *et al.* showed that exosome-like nanoparticles isolated from LGG conditioned media increases IL-22 and *Reg3*γ, perhaps mediated through activation of the Aryl hydrocarbon receptor, which is associated with improvement in barrier function *in vivo* [316].

To our knowledge, negative associations between small intestinal *Reg3*γ expression and specific gut microbes have not been well established. We show Clostridiaceae and Peptostreptococcaceae family members as well as certain *Lactobacillus*, i.e., *L. reuteri*, selected by HF diet are poor inducers and may even suppress *Reg3*γ expression *in vitro* in certain instances (Figures 4.10B,C, 4.11A,B, 4.12B). Whereas we were unable to successfully monoassociate

GF mice with *P. stomatis*, despite several attempts, we were able to monoassociate RC-fed GF mice with *L. reuteri*. We noted that LGG, but not *L. reuteri* monocolonization could induce *Reg3γ* expression, confirming our *in vitro* findings (Figure 4.14C). This is in line with work demonstrating that *Reg3γ* overexpression in murine IECs led to expansion of *Lactobacillus* abundance in general, while certain species such as *L. reuteri* were reduced [240]. Further, our work suggests REG3γ antimicrobial action may be more targeted than originally appreciated [307], where *P. stomatis*, *E. faecalis*, and *L. reuteri* are more susceptible than other Gram positive bacteria (Figure 4.12A). The reason for Lactobacillus species differential sensitivity is unclear, however we posit that diurnal induction of and resistance to REG3γ may aid in niche maintenance within the community while contributing to host intestinal health.

Together, we show the primary cue of diet coupled with REG3γ as a secondary cue, through their actions on gut microbial populations, are essential components for regulating rhythmicity of specific bacteria that do not correlate with archetypal circadian clock gene networks. These microbial rhythms are primarily dependent on dynamic diet-host-microbe interactions. We speculate specific bacteria either flourish or are lost because of altered dietary intake leading to *Reg3γ* induction or suppression at crucial times. Improper timing or loss of diurnal *Reg3γ* could render the host more susceptible to infection, as recently shown [187], or worse pathogenesis of chronic diseases, such as DIO. These interactions are a prime example of transkingdom coordination that is essential for the mammalian host to adapt to changes in daily dietary intake. Further, our findings suggest that HF diet may blunt the metabolic benefits of certain probiotics, such as LGG, whose affects are mediated through interactions with host REG3γ. It may be possible that in order to enhance the effectiveness of probiotic administration, concomitant dietary planning and meal timing should be considered.

4.6 Future Directions

A major question that remains following our studies is which microbially-derived factors are responsible for modulating *Reg3γ* expression and oscillations within the host. By size fractionation and heat-treatment of conditioned media from the RC-induced representative strain LGG, we have identified that these factors are smaller than 3kDa and are heat-sensitive. Preliminary results from our unbiased LC-MS/MS analysis identify several BCAAs that were differentially abundant between conditioned media capable of modulating *Reg3γ* expression (Figure B.5, BCAAs highlighted in blue). Previous studies show that BCAAs significantly interact with the immune system; BCAAs are required for lymphocyte protein synthesis and induce increases in lymphocyte populations, as well as contribute to host infection protection and susceptibility [317]. One study also demonstrated that dietary BCAAs can specifically induce small intestinal expression of the β-defensin AMP expression in piglets [318], thus it is possible that other AMPs such as REG3γ are affected. This could be examined by exposing ileal enteroids or SPF mice on HF diet or GF mice to BCAAs by diet incorporation or intraperitoneal injection, and measuring *Reg3γ* ileal expression, particularly over 24 hours in mice. If BCAA treatment does not induce *Reg3γ*, they are either incapable of induction, or they are not sufficient alone and require the presence of additional small molecules. Further metabolomics analysis of bacterially-derived conditioned media may reveal other potential mediators of host *Reg3γ* expression. Metagenomic sequencing of diet-induced microbiota communities and individual Lactobacillus strains, such as LGG and *L. reuteri*, may also point to certain relevant functional outputs of these bacteria and corroborate metabolomics analysis. Previous work showed bacteria expressing bile salt hydrolase (BSH), such as *Lactobacillus*, are associated with *Reg3γ* expression [233, 319]. Whether BSH mediates production of small molecules that directly induce *Reg3γ* expression is unknown. However, the ability of *Lactobacillus* species to express BSH could influence their diurnal oscillations, which may relate to food intake timing and bile acid delivery or reuptake in the

ileum [179].

In addition to further profiling of broad functional outputs of certain bacteria such as LGG and *L. reuteri*, we plan to expand our analysis to other *Lactobacillus* strains. While we utilized LGG as a RC-representative, *Reg3γ*-inducing strain, we plan to investigate indigenous isolates from our mouse colony that exhibit similar interactions with *Reg3γ*. In addition to our indigenous isolate identified as *L. reuteri*, we also isolated other *Lactobacillus* strains, including a *Lactobacillus murinus*, a *Lactobacillus intestinalis*, and a *Lactobacillus johnsonii*. Exposure of these strains to r*Reg3γ* in the bactericidal assay presented in Figure 4.12A again revealed that *L. reuteri* was susceptible to killing action (Figure 4.25A), whereas *L. murinus*, *L. intestinalis*, and *L. johnsonii* all exhibited resistance to rREG3γ killing action at higher concentrations, similar to LGG. Further, we exposed WT enteroids to conditioned media from *L. murinus* or *L. reuteri*, revealing that *L. murinus* induced *Reg3γ* similar to LGG and confirming that *L. reuteri* does not drive induction (Figure 4.25B). We have yet to test *L. intestinalis* and *L. johnsonii*, however, we hypothesize that these strains will exhibit a similar response and induction pattern to LGG. Further, we plan to monoassociate GF mice with these isolates in comparison to *L. reuteri* and measure induction of distal ileal *Reg3γ* expression over 24 hours in various dietary conditions. Association of different *Reg3γ*-associated Lactobacillus strains may also differentially induce other physiological mechanisms related to DIO, such as the migration of anti-inflammatory macrophages to adipose tissue as previously shown [240]. These studies would validate our examination of LGG as an RC-representative, *Reg3γ*-promoting strain with indigenous strains from our own mouse colony.

The physiological significance of a gain or loss of microbial oscillations in the context of *Reg3γ* induction and DIO remains to be elucidated. Overall, we observed a robust loss in rhythmicity of microbial abundance following exposure to HF diet, however this study and others have also revealed that HF diet and dysregulated metabolism result in a gain of certain microbial oscillators [141, 179, 199]. The underlying drivers that promote a gain

in oscillation, aside from time of feeding or the endogenous circadian clock, as well as their physiological relevance, have yet to be defined. This could be explored via timed exposure of RC or HF-fed mice to *Reg3γ*-inducing bacterial strains or conditioned medias. It is possible that timed exposure of certain bacteria may induce diurnal intestinal *Reg3γ* expression, even in HF diet conditions. Additionally, it remains to be explored whether the diurnal patterns of *Reg3γ* expression are required to induce oscillations in the abundance of RC-associated microbiota. Characterization of oscillating microbiota following constant *Reg3γ* IEC-overexpression in different dietary conditions would shed light on this, as well as whether the oscillations are specifically responsible for conveying changes in host metabolism.

Several studies point to the dual function of REG3γ as both an AMP and metabolic hormonal signal, yet precise mechanisms remain poorly defined, particularly in HF DIO [320]. We show that global *Reg3γ* deficiency worsens glucose sensitivity under RC feeding conditions and is not exacerbated by HF diet (Figure 4.18C). This evidence is unique relative to a previous report [321], yet is corroborated by other evidence that *Reg3γ* overexpression in IECs improves glucose tolerance [240]. While we employed a global knockout, this evidence that the IEC compartment drives glucose tolerance is promising, yet further investigation is required to elucidate the direct influence of diurnal *Reg3γ* signaling on metabolism. Examination of *Reg3γ* transgenic expression at specific times over 24 hours may reveal differences in glucose tolerance, directly linking diurnal *Reg3γ* with tolerance. These differences in metabolic characterization between studies could also be due to microbiome variation between animal vivaria, housing conditions (individual vs. group), or our use of heterozygote mice as controls instead of true WT with full *Reg3γ* expression. We identified modest differences in luminal small intestine microbes between *Reg3γ*$^{+/-}$ and *Reg3γ*$^{-/-}$ mice only when fed RC, while others have not observed this [311]. Yet, *Reg3γ* overexpression in IECs did show differences in microbiota community membership profiles [240]. Transgenic expression of IEC-*Reg3γ* in GF conditions, or mice monoassociated with HF-induced microbiota,

may reveal whether specific microbial communities or microbes in general are required for *Reg3γ*-associated glucose tolerance.

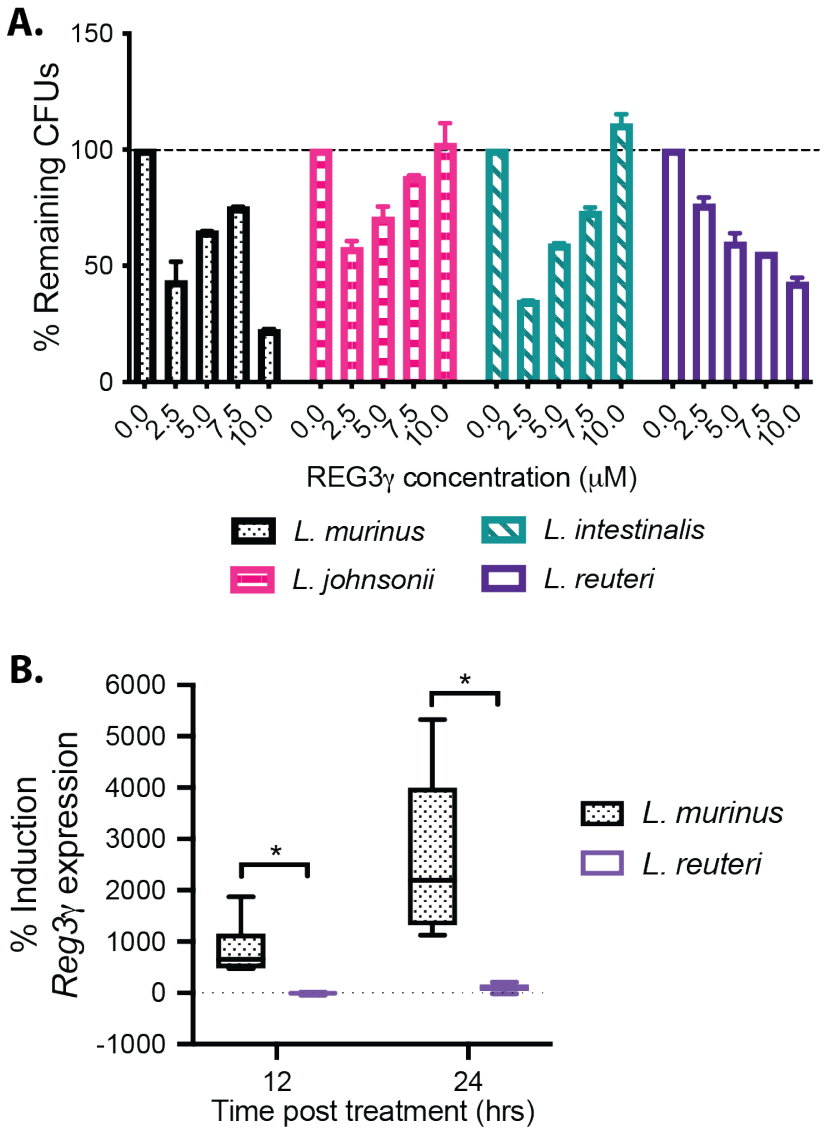

Figure 4.25: **Indigenous *Lactobacillus* isolates differentially respond to and induce *Reg3γ* expression.** (A) Percent remaining CFUs of indigenous Lactobacillus strains following 2hr exposure to rREG3γ relative to vehicle control (n=2 replicates/strain, representative of 3 independent experiments). Data represent mean±stdev. (B) *Reg3γ* expression in enteroids derived from SPF WT mice following 12 or 24hr exposure to CM from *L. murinus* and *L. reuteri* isolates (n=6 technical replicates/treatment; data representative of 1 independent experiment). Box-whisker plots represent mean±min/max. $^*p < 0.05$ via Welch's t test.

CHAPTER 5

CONCLUDING REMARKS

Throughout this dissertation, we examined the hypothesis that reciprocal diurnal interactions between the host and gut microbiota result in differential host metabolic programming and outcomes. In Chapter 3, we explored this hypothesis by characterizing communication between the liver circadian clock and gut microbes, which programs hepatic gluconeogenesis and lipid metabolism. Using a systems-biology, multi-omic approach in an *in vivo* model, we revealed for the first time the contribution of the individual roles of a host peripheral tissue clock component vs. gut microbes. We identified that liver clock status imparts significant control over the populations of oscillating microbes in stool, while overall community structure and abundance remain largely unaffected. We also demonstrated that interactions between the liver clock and gut microbes drive coordination of circadian clock networks to maintain rhythms in glucose and lipid metabolism, occurring independent of the central brain clock. Our focus on the peripheral tissue liver circadian clock is extremely relevant due to the direct signaling and communication between the liver and the gut, as well as its known governance over glucose and lipid homeostasis. Together, we revealed a complex network of unique and combinatorial effects of the liver clock and gut microbes on host metabolism, emphasizing the need to understand how these interactions arise in further detail.

In Chapter 4, we explored the diurnal crosstalk between the innate immune factor *Reg3*γ and specific diet-induced ileal gut microbiota. We show that *Reg3*γ is synchronized with a select subset of microbes to orchestrate bi-directional host-microbe interactions, independent from the core intestinal circadian clock. We defined how mutually-interdependent, specific distal ileum microbial "oscillator" populations are integrated to maintain local host intestinal homeostasis and broader metabolism. This is based on observations that gut microbial community membership and their diurnal patterns, promoted by a low-fat, high fiber RC diet, are required to drive diurnal distal ileum *Reg3*γ expression. Regardless of diet, this dynamic

is either completely abolished in GF conditions, or significantly dampened by Western HF diet-induced gut dysbiosis in SPF counterparts. We further demonstrate that both type and indigenous bacteria strains from particular families induced by RC or HF diet differentially induce or repress *Reg3γ* expression, some with unique susceptibility to *REG3γ*'s bactericidal action. Coupled with host *REG3γ* deficiency, HF diet not only promotes expansion of rare microbial community members but results in a gain of microbial diurnal oscillations that may further contribute to disrupted local and peripheral host metabolism. Together, the interactions we identified are key examples of transkingdom co-evolution where mammalian hosts have selected specific microbes to work in concert with innate immune mechanisms, driving biological rhythms that adapt to variations in dietary intake.

The knowledge gained here provides a framework for the potential identification of mediators and interventions aimed at restoring diurnal host-microbe interactions and alleviating incidence of metabolic diseases. One important concept across both chapters is the shared relevance of *Lactobacillus* oscillating bacterial strains. In Chapter 3, we identified that *Lactobacillus murinus* was one of the few microbial features identified to the species level that gained significant oscillation in stool from LKO mice compared to WT. This pattern supports our finding that loss of hepatic *Bmal1* results in an overall significant increase in oscillating microbial features by approximately two-fold. In Chapter 4, we identified that *Lactobacillus reuteri* was one of the microbial features that only exhibit a gain of oscillation in the condition of HF diet, loss of *Reg3γ* expression, or a combination of both. This pattern also supports our general finding that specific microbial features only gained oscillation in the combined condition of HF diet and loss of *Reg3γ*. The mechanistic importance of this gain of oscillation by specific *Lactobacillus* species remains to be delineated. Interestingly, many *Lactobacillus* strains are well-known and characterized to deconjugate primary glyco- or tauro-conjugated bile acids via the enzyme bile salt hydrolase (BSH). Among many other *Lactobacillus* strains, both *L. murinus* and *L. reuteri* have been identified as carrying a

version of the BSH gene in 93-100% of sequenced strains [319]. Bile acids have been previously shown to regulate circadian rhythms and metabolism [217, 227], as well as *Reg3γ* expression and synthesis [322]. If hepatic *Bmal1* or *Reg3γ* status alters diurnal patterns of bile acid metabolism by certain *Lactobacillus* strains, this could be one mechanism by which host metabolic state is impacted by changes in oscillating bacteria. Further investigation of the direct physiological outcomes of altered *Lactobacillus* strain abundance oscillations is required to determined whether bile acids play a role in either metabolic context.

Another important concept that is shared between chapters is the potential mechanistic importance of oscillatory patterns of gut microbes. Although much remains to be delineated concerning the physiological significance of a gain or loss of microbial oscillations, one possibility is that changes in diurnal patterns of microbial functional outputs, such as metabolite production, could signal to the host at the wrong time of day, thus misaligning host physiological responses. If these microbially-derived outputs and host responses were characterized and identified in human-based studies, specific timing regimens of probiotic delivery could be one clinical method by which to realign the host. In the context of Chapter 3 of this thesis, lipid and glucose metabolic dysfunction due to hepatic circadian clock misalignment and associated gain of microbial oscillations may be corrected by constant delivery of certain Ruminococcaceae, Lachnospiraceae, or *Lactobacillus* bacteria in the form of a probiotic. Similarly, in the context of Chapter 4, the negative metabolic implications of HF diet, particularly in combination with reduction or loss of host *REG3γ*, may be reversed or prevented by timed delivery of specific *Lactobacillus* probiotic strains that promote diurnal *Reg3γ* expression in the small intestine. These possibilities depict a promising clinical application for modulating diurnal patterns of microbes and their functions that impact host metabolic physiology, although much remains to be understood concerning the mechanistic underpinnings of microbial oscillations in humans. We are just beginning to apply our knowledge of oscillating gut microbiota abundance patterns and functional outputs derived from from

mouse studies to human cohorts, such as with a recent study that utilized machine learning to predict metabolic disease incidence by bacterial oscillation patterns from timestamped human stool samples [199]. Further examination of similar large-scale human studies will provide essential insights to the potential application of timed probiotic delivery to treat metabolic diseases and more.

Overall, the findings from these two chapters provide a knowledge base, spanning multiple systems, to interrogate the mechanistic underpinnings of key host-microbe circadian interactions that direct metabolism. We explored the hierarchy of primary versus secondary circadian drivers of both the host and gut microbiota, finding that the genetics of the liver circadian clock is the primary driver of diurnal hepatic transcription while gut microbes serve as a key secondary driver. This is also evident in our examination of *Reg3*γ, where diet serves as the primary driver of small intestinal microbiota while diurnal *Reg3*γ expression serves as an important secondary signal. Future studies will focus on elucidating the mechanisms for these interactions by identifying the key host-microbe mediators and examining how other relevant tissues contribute to these complex networks to drive host metabolic outcomes. The relevant network relationships are incredibly complex and require parsing out at many levels to fully dissect how specific disruptions to these interactions impact physiology and metabolism. These data underscore that gut microbes must be considered in host rhythmic gene networks in metabolism and immunity, both those that are independent from and dependent on the core circadian clock.

REFERENCES

[1] Grundy, S. M. A constellation of complications:The metabolic syndrome. *Clinical Cornerstone* **7**, 36–45 (2005).

[2] Kassi, E., Pervanidou, P., Kaltsas, G. & Chrousos, G. Metabolic syndrome: Definitions and controversies. *BMC Medicine* **9**, 48 (2011).

[3] Saklayen, M. G. The Global Epidemic of the Metabolic Syndrome. *Current Hypertension Reports* **20**, 12 (2018).

[4] Alberti, K. G. M., Zimmet, P. & Shaw, J. The metabolic syndrome—a new worldwide definition. *The Lancet* **366**, 1059–1062 (2005).

[5] Barroso, I. & McCarthy, M. I. The genetic basis of metabolic disease. *Cell* **177**, 146–161 (2019).

[6] Elks, C. *et al.* Variability in the Heritability of Body Mass Index: A Systematic Review and Meta-Regression. *Frontiers in Endocrinology* **3** (2012).

[7] Mahajan, A. *et al.* Fine-mapping type 2 diabetes loci to single-variant resolution using high-density imputation and islet-specific epigenome maps. *Nature Genetics* **50**, 1505–1513 (2018).

[8] Turcot, V. *et al.* Protein-altering variants associated with body mass index implicate pathways that control energy intake and expenditure in obesity. *Nature Genetics* **50**, 26–41 (2018).

[9] Pham, T. X. & Lee, J. Dietary Regulation of Histone Acetylases and Deacetylases for the Prevention of Metabolic Diseases. *Nutrients* **4**, 1868–1886 (2012).

[10] Knutson, S. K. *et al.* Liver-specific deletion of histone deacetylase 3 disrupts metabolic transcriptional networks. *The EMBO journal* **27**, 1017–1028 (2008).

[11] Sun, Z. *et al.* Hepatic Hdac3 promotes gluconeogenesis by repressing lipid synthesis and sequestration. *Nature Medicine* **18**, 934–942 (2012).

[12] Wu, J. *et al.* Emerging role of m6 A RNA methylation in nutritional physiology and metabolism. *Obesity Reviews: An Official Journal of the International Association for the Study of Obesity* **21**, e12942 (2020).

[13] Zhong, X. *et al.* Circadian Clock Regulation of Hepatic Lipid Metabolism by Modulation of m6A mRNA Methylation. *Cell Reports* **25**, 1816–1828.e4 (2018).

[14] Stanhope, K. L. Sugar consumption, metabolic disease and obesity: The state of the controversy. *Critical Reviews in Clinical Laboratory Sciences* **53**, 52–67 (2016).

[15] Wali, J. A. *et al.* Cardio-Metabolic Effects of High-Fat Diets and Their Underlying Mechanisms—A Narrative Review. *Nutrients* **12**, 1505 (2020).

[16] Solon-Biet, S. M. *et al.* The Ratio of Macronutrients, Not Caloric Intake, Dictates Cardiometabolic Health, Aging, and Longevity in Ad Libitum-Fed Mice. *Cell Metabolism* **19**, 418–430 (2014).

[17] Carroll, S. & Dudfield, M. What is the Relationship Between Exercise and Metabolic Abnormalities? *Sports Medicine* **34**, 371–418 (2004).

[18] Evans, J. A. & Davidson, A. J. Health consequences of circadian disruption in humans and animal models. *Progress in molecular biology and translational science* **119**, 283–323 (2013).

[19] Baillie-Hamilton, P. F. Chemical Toxins: A Hypothesis to Explain the Global Obesity Epidemic. *The Journal of Alternative and Complementary Medicine* **8**, 185–192 (2002).

[20] Bose, M., Oliván, B. & Laferrère, B. Stress and obesity: The role of the hypothalamic–pituitary–adrenal axis in metabolic disease. *Current Opinion in Endocrinology, Diabetes and Obesity* **16**, 340–346 (2009).

[21] Kolbe, I. & Oster, H. Chronodisruption, Metabolic Homeostasis, and the Regulation of Inflammation in Adipose Tissues. *The Yale Journal of Biology and Medicine* **92**, 317–325 (2019).

[22] Nijhuis, J. *et al.* Neutrophil activation in morbid obesity, chronic activation of acute inflammation. *Obesity* **17**, 2014–2018 (2009).

[23] Cani, P. D. *et al.* Metabolic endotoxemia initiates obesity and insulin resistance. *Diabetes* **56**, 1761–1772 (2007).

[24] Neal, M. D. *et al.* Enterocyte tlr4 mediates phagocytosis and translocation of bacteria across the intestinal barrier. *The Journal of Immunology* **176**, 3070–3079 (2006).

[25] Shi, H. *et al.* Tlr4 links innate immunity and fatty acid–induced insulin resistance. *The Journal of clinical investigation* **116**, 3015–3025 (2006).

[26] Vijay-Kumar, M. *et al.* Metabolic syndrome and altered gut microbiota in mice lacking toll-like receptor 5. *Science* **328**, 228–231 (2010).

[27] Etienne-Mesmin, L., Vijay-Kumar, M., Gewirtz, A. T. & Chassaing, B. Hepatocyte toll-like receptor 5 promotes bacterial clearance and protects mice against high-fat diet–induced liver disease. *Cellular and molecular gastroenterology and hepatology* **2**, 584–604 (2016).

[28] Feinstein R, Kanety H, Papa M Z, Lunenfeld B & Karasik A. Tumor necrosis factor-alpha suppresses insulin-induced tyrosine phosphorylation of insulin receptor and its substrates. *The Journal of Biological Chemistry* **268**, 26055–26058 (1993).

[29] Gauthier, M.-S. & Ruderman, N. B. Adipose tissue inflammation and insulin resistance: All obese humans are not created equal. *Biochemical Journal* **430**, e1–e4 (2010).

[30] Hotamisligil, G. S., Shargill, N. S. & Spiegelman, B. M. Adipose expression of tumor necrosis factor-α: Direct role in obesity-linked insulin resistance. *Science* **259**, 87–91 (1993).

[31] ClÉment, K. *et al.* Weight loss regulates inflammation-related genes in white adipose tissue of obese subjects. *The FASEB Journal* **18**, 1657–1669 (2004).

[32] Lumeng, C. N., Bodzin, J. L. & Saltiel, A. R. Obesity induces a phenotypic switch in adipose tissue macrophage polarization. *The Journal of Clinical Investigation* **117**, 175–184 (2007).

[33] Russo, L. & Lumeng, C. N. Properties and functions of adipose tissue macrophages in obesity. *Immunology* **155**, 407–417 (2018).

[34] Kratz, M. *et al.* Metabolic dysfunction drives a mechanistically distinct proinflammatory phenotype in adipose tissue macrophages. *Cell metabolism* **20**, 614–625 (2014).

[35] Coats, B. R. *et al.* Metabolically activated adipose tissue macrophages perform detrimental and beneficial functions during diet-induced obesity. *Cell reports* **20**, 3149–3161 (2017).

[36] Wang, X. *et al.* Interleukin-22 alleviates metabolic disorders and restores mucosal immunity in diabetes. *Nature* **514**, 237–241 (2014).

[37] Saltiel, A. R. & Kahn, C. R. Insulin signalling and the regulation of glucose and lipid metabolism. *Nature* **414**, 799–806 (2001).

[38] Wilcox, G. Insulin and Insulin Resistance. *Clinical Biochemist Reviews* **26**, 19–39 (2005).

[39] Ramos-Roman, M. A., Lapidot, S. A., Phair, R. D. & Parks, E. J. Insulin Activation of Plasma Nonesterified Fatty Acid Uptake in Metabolic Syndrome. *Arteriosclerosis, Thrombosis, and Vascular Biology* **32**, 1799–1808 (2012).

[40] Petersen, M. C., Vatner, D. F. & Shulman, G. I. Regulation of hepatic glucose metabolism in health and disease. *Nature reviews. Endocrinology* **13**, 572–587 (2017).

[41] Hundal, R. S. *et al.* Mechanism by which metformin reduces glucose production in type 2 diabetes. *Diabetes* **49**, 2063–2069 (2000).

[42] Romere, C. *et al.* Asprosin, a Fasting-Induced Glucogenic Protein Hormone. *Cell* **165**, 566–579 (2016).

[43] Wakil, S. J. & Abu-Elheiga, L. A. Fatty acid metabolism: Target for metabolic syndrome. *Journal of Lipid Research* **50**, S138–S143 (2009).

[44] Fatehi-Hassanabad, Z. & Chan, C. B. Transcriptional regulation of lipid metabolism by fatty acids: A key determinant of pancreatic β-cell function. *Nutrition & Metabolism* **2**, 1 (2005).

[45] Peeters, A. & Baes, M. Role of PPAR in Hepatic Carbohydrate Metabolism. *PPAR Research* **2010**, e572405 (2010).

[46] Sugden, M. C., Bulmer, K., Gibbons, G. F., Knight, B. L. & Holness, M. J. Peroxisome-proliferator-activated receptor-alpha (PPARalpha) deficiency leads to dysregulation of hepatic lipid and carbohydrate metabolism by fatty acids and insulin. *Biochemical Journal* **364**, 361–368 (2002).

[47] Bernal-Mizrachi, C. *et al.* Dexamethasone induction of hypertension and diabetes is PPAR-α dependent in LDL receptor–null mice. *Nature Medicine* **9**, 1069–1075 (2003).

[48] Atherton, H. J. *et al.* A combined 1H-NMR spectroscopy- and mass spectrometry-based metabolomic study of the PPAR-α null mutant mouse defines profound systemic changes in metabolism linked to the metabolic syndrome. *Physiological Genomics* **27**, 178–186 (2006).

[49] Lv, S. *et al.* Glucagon-induced extracellular cAMP regulates hepatic lipid metabolism. *Journal of Endocrinology* **234**, 73–87 (2017).

[50] Kelley, D. E., Goodpaster, B., Wing, R. R. & Simoneau, J.-A. Skeletal muscle fatty acid metabolism in association with insulin resistance, obesity, and weight loss. *American Journal of Physiology-Endocrinology And Metabolism* **277**, E1130–E1141 (1999).

[51] Goodpaster, B. H. & Sparks, L. M. Metabolic flexibility in health and disease. *Cell metabolism* **25**, 1027–1036 (2017).

[52] Smith, R. L., Soeters, M. R., Wüst, R. C. & Houtkooper, R. H. Metabolic flexibility as an adaptation to energy resources and requirements in health and disease. *Endocrine reviews* **39**, 489–517 (2018).

[53] Nauck, M. A. & Meier, J. J. Incretin hormones: Their role in health and disease. *Diabetes, Obesity and Metabolism* **20**, 5–21 (2018).

[54] El, K. *et al.* Gip mediates the incretin effect and glucose tolerance by dual actions on α cells and β cells. *Science advances* **7**, eabf1948 (2021).

[55] Gasbjerg, L. S. *et al.* Separate and combined glucometabolic effects of endogenous glucose-dependent insulinotropic polypeptide and glucagon-like peptide 1 in healthy individuals. *Diabetes* **68**, 906–917 (2019).

[56] Holst, J. J., Knop, F. K., Vilsbøll, T., Krarup, T. & Madsbad, S. Loss of Incretin Effect Is a Specific, Important, and Early Characteristic of Type 2 Diabetes. *Diabetes Care* **34**, S251–S257 (2011).

[57] Godoy-Matos, A. F. The role of glucagon on type 2 diabetes at a glance. *Diabetology & Metabolic Syndrome* **6**, 91 (2014).

[58] Klok, M. D., Jakobsdottir, S. & Drent, M. L. The role of leptin and ghrelin in the regulation of food intake and body weight in humans: A review. *Obesity Reviews* **8**, 21–34 (2007).

[59] Varda, N. M., Medved, M. & Ojsteršek, L. The associations between some biological markers, obesity, and cardiovascular risk in Slovenian children and adolescents. *BMC Pediatrics* **20**, 81 (2020).

[60] Li, M.-D., Li, C.-M. & Wang, Z. The Role of Circadian Clocks in Metabolic Disease. *The Yale Journal of Biology and Medicine* **85**, 387–401 (2012).

[61] Sancar, G. & Brunner, M. Circadian clocks and energy metabolism. *Cellular and molecular life sciences: CMLS* **71**, 2667–2680 (2014).

[62] Rosbash, M. & Hall, J. C. The molecular biology of circadian rhythms. *Neuron* **3**, 387–398 (1989).

[63] Hut, R. A. & Beersma, D. G. M. Evolution of time-keeping mechanisms: Early emergence and adaptation to photoperiod. *Philosophical Transactions of the Royal Society of London. Series B, Biological Sciences* **366**, 2141–2154 (2011).

[64] Berg, J. M., Tymoczko, J. L. & Stryer, L. Gluconeogenesis and Glycolysis Are Reciprocally Regulated. *Biochemistry. 5th edition* (2002).

[65] Bellet, M. M. *et al.* Circadian clock regulates the host response to Salmonella. *Proceedings of the National Academy of Sciences* **110**, 9897–9902 (2013).

[66] Buhr, E. D. & Takahashi, J. S. Molecular components of the Mammalian circadian clock. *Handbook of Experimental Pharmacology* 3–27 (2013).

[67] Takahashi, J. S. Transcriptional architecture of the mammalian circadian clock. *Nature Reviews Genetics* **18**, 164–179 (2017).

[68] Albrecht, U., Sun, Z. S., Eichele, G. & Lee, C. C. A Differential Response of Two Putative Mammalian Circadian Regulators, mper1and mper2, to Light. *Cell* **91**, 1055–1064 (1997).

[69] Challet, E., Poirel, V.-J., Malan, A. & Pévet, P. Light exposure during daytime modulates expression of Per1 and Per2 clock genes in the suprachiasmatic nuclei of mice. *Journal of Neuroscience Research* **72**, 629–637 (2003).

[70] Armstrong, S. M. Melatonin and circadian control in mammals. *Experientia* **45**, 932–938 (1989).

[71] Pfeffer, M., von Gall, C., Wicht, H. & Korf, H.-W. The role of the melatoninergic system in circadian and seasonal rhythms—insights from different mouse strains. *Frontiers in Physiology* 665 (2022).

[72] Stephan, F. K. The "Other" Circadian System: Food as a Zeitgeber. *Journal of Biological Rhythms* **17**, 284–292 (2002).

[73] Damiola, F. *et al.* Restricted feeding uncouples circadian oscillators in peripheral tissues from the central pacemaker in the suprachiasmatic nucleus. *Genes & Development* **14**, 2950–2961 (2000).

[74] Oishi, K., Miyazaki, K. & Ishida, N. Functional CLOCK is not involved in the entrainment of peripheral clocks to the restricted feeding: Entrainable expression of mPer2 and BMAL1 mRNAs in the heart of Clock mutant mice on Jcl:ICR background. *Biochemical and Biophysical Research Communications* **298**, 198–202 (2002).

[75] Eckel-Mahan, K. & Sassone-Corsi, P. Metabolism and the Circadian Clock Converge. *Physiological Reviews* **93**, 107–135 (2013).

[76] Mayeuf-Louchart, A., Zecchin, M., Staels, B. & Duez, H. Circadian control of metabolism and pathological consequences of clock perturbations. *Biochimie* **143**, 42–50 (2017).

[77] Koike, N. *et al.* Transcriptional Architecture and Chromatin Landscape of the Core Circadian Clock in Mammals. *Science (New York, N.Y.)* **338**, 349–354 (2012).

[78] Rey, G. *et al.* Genome-Wide and Phase-Specific DNA-Binding Rhythms of BMAL1 Control Circadian Output Functions in Mouse Liver. *PLOS Biology* **9**, e1000595 (2011).

[79] Zhang, Y. *et al.* The hepatic circadian clock fine-tunes the lipogenic response to feeding through RORα/γ. *Genes & Development* **31**, 1202–1211 (2017).

[80] Zhang, R., Lahens, N. F., Ballance, H. I., Hughes, M. E. & Hogenesch, J. B. A circadian gene expression atlas in mammals: Implications for biology and medicine. *Proceedings of the National Academy of Sciences of the United States of America* **111**, 16219–16224 (2014).

[81] Masri, S. & Sassone-Corsi, P. Plasticity and specificity of the circadian epigenome. *Nature Neuroscience* **13**, 1324–1329 (2010).

[82] Etchegaray, J.-P., Lee, C., Wade, P. A. & Reppert, S. M. Rhythmic histone acetylation underlies transcription in the mammalian circadian clock. *Nature* **421**, 177–182 (2003).

[83] Doi, M., Hirayama, J. & Sassone-Corsi, P. Circadian Regulator CLOCK Is a Histone Acetyltransferase. *Cell* **125**, 497–508 (2006).

[84] Hirayama, J. *et al.* CLOCK-mediated acetylation of BMAL1 controls circadian function. *Nature* **450**, 1086–1090 (2007).

[85] Feng, D. *et al.* A Circadian Rhythm Orchestrated by Histone Deacetylase 3 Controls Hepatic Lipid Metabolism. *Science* **331**, 1315–1319 (2011).

[86] Zhou, B. *et al.* CLOCK/BMAL1 regulates circadian change of mouse hepatic insulin sensitivity by SIRT1. *Hepatology* **59**, 2196–2206 (2014).

[87] Rudic, R. D. *et al.* BMAL1 and CLOCK, Two Essential Components of the Circadian Clock, Are Involved in Glucose Homeostasis. *PLoS Biology* **2** (2004).

[88] Karlsson, B. H., Knutsson, A. K., Lindahl, B. O. & Alfredsson, L. S. Metabolic disturbances in male workers with rotating three-shift work. Results of the WOLF study. *International Archives of Occupational and Environmental Health* **76**, 424–430 (2003).

[89] Pan, A., Schernhammer, E. S., Sun, Q. & Hu, F. B. Rotating night shift work and risk of type 2 diabetes: Two prospective cohort studies in women. *PLoS medicine* **8**, e1001141 (2011).

[90] Kervezee, L., Cermakian, N. & Boivin, D. B. Individual metabolomic signatures of circadian misalignment during simulated night shifts in humans. *PLOS Biology* **17**, e3000303 (2019).

[91] Bunger, M. K. *et al.* Mop3 is an essential component of the master circadian pacemaker in mammals. *Cell* **103**, 1009–1017 (2000).

[92] Shimba, S. *et al.* Brain and muscle Arnt-like protein-1 (BMAL1), a component of the molecular clock, regulates adipogenesis. *Proceedings of the National Academy of Sciences of the United States of America* **102**, 12071–12076 (2005).

[93] Kondratov, R. V., Kondratova, A. A., Gorbacheva, V. Y., Vykhovanets, O. V. & Antoch, M. P. Early aging and age-related pathologies in mice deficient in BMAL1, the core componentof the circadian clock. *Genes & Development* **20**, 1868–1873 (2006).

[94] Samsa, W. E., Vasanji, A., Midura, R. J. & Kondratov, R. V. Deficiency of circadian clock protein BMAL1 in mice results in a low bone mass phenotype. *Bone* **84**, 194–203 (2016).

[95] Turek, F. W. *et al.* Obesity and metabolic syndrome in circadian Clock mutant mice. *Science (New York, N.Y.)* **308**, 1043–1045 (2005).

[96] Barclay, J. L. *et al.* High-fat diet-induced hyperinsulinemia and tissue-specific insulin resistance in \textlessi\textgreaterCry\textless/i\textgreater -deficient mice. *American Journal of Physiology-Endocrinology and Metabolism* **304**, E1053–E1063 (2013).

[97] Costa, M. J. *et al.* Circadian rhythm gene period 3 is an inhibitor of the adipocyte cell fate. *Journal of Biological Chemistry* **286**, 9063–9070 (2011).

[98] Delezie, J. *et al.* The nuclear receptor REV-ERBα is required for the daily balance of carbohydrate and lipid metabolism. *The FASEB Journal* **26**, 3321–3335 (2012).

[99] Grimaldi, B. *et al.* PER2 controls lipid metabolism by direct regulation of PPARγ. *Cell Metabolism* **12**, 509–520 (2010).

[100] Yang, S. *et al.* The Role of mPer2 Clock Gene in Glucocorticoid and Feeding Rhythms. *Endocrinology* **150**, 2153–2160 (2009).

[101] Carrillo, A. J., Duke, P. G. & Dunn, J. D. Episodic Corticosterone Secretion in the Female Rat. *Hormone Research in Paediatrics* **13**, 40–47 (1980).

[102] Yildiz, B. O., Suchard, M. A., Wong, M.-L., McCann, S. M. & Licinio, J. Alterations in the dynamics of circulating ghrelin, adiponectin, and leptin in human obesity. *Proceedings of the National Academy of Sciences* **101**, 10434–10439 (2004).

[103] Muñoz, J. S. G., Rodríguez, D. J. & Morante, J. J. H. Diurnal rhythms of plasma GLP-1 levels in normal and overweight/obese subjects: Lack of effect of weight loss. *Journal of Physiology and Biochemistry* **71**, 17–28 (2015).

[104] Biancolin, A. D. *et al.* The core clock gene, Bmal1, and its downstream target, the SNARE regulatory protein secretagogin, are necessary for circadian secretion of glucagon-like peptide-1. *Molecular Metabolism* **31**, 124–137 (2020).

[105] Martchenko, A. *et al.* Suppression of circadian secretion of glucagon-like peptide-1 by the saturated fatty acid, palmitate. *Acta Physiologica* **222**, e13007 (2018).

[106] Nader, N., Chrousos, G. P. & Kino, T. Circadian rhythm transcription factor CLOCK regulates the transcriptional activity of the glucocorticoid receptor by acetylating its hinge region lysine cluster: Potential physiological implications. *The FASEB Journal* **23**, 1572–1583 (2009).

[107] Lamia, K. A. *et al.* Cryptochromes mediate rhythmic repression of the glucocorticoid receptor. *Nature* **480**, 552–556 (2011).

[108] Logan, R. W. & Sarkar, D. K. Circadian nature of immune function. *Molecular and Cellular Endocrinology* **349**, 82–90 (2012).

[109] Fu, L. & Lee, C. C. The circadian clock: Pacemaker and tumour suppressor. *Nature Reviews Cancer* **3**, 350–361 (2003).

[110] Silver, A. C., Arjona, A., Walker, W. E. & Fikrig, E. The circadian clock controls toll-like receptor 9-mediated innate and adaptive immunity. *Immunity* **36**, 251–261 (2012).

[111] Besedovsky, H., del Rey, A., Sorkin, E. & Dinarello, C. A. Immunoregulatory Feedback Between Interleukin-1 and Glucocorticoid Hormones. *Science* **233**, 652–654 (1986).

[112] Kwak, Y. *et al.* Interferon-gamma alters electrical activity and clock gene expression in suprachiasmatic nucleus neurons. *Journal of Biological Rhythms* **23**, 150–159 (2008).

[113] Godinho-Silva, C. *et al.* Light-entrained and brain-tuned circadian circuits regulate ILC3s and gut homeostasis. *Nature* **574**, 254–258 (2019).

[114] Sun, Y. *et al.* MOP3, a component of the molecular clock, regulates the development of B cells. *Immunology* **119**, 451–460 (2006).

[115] Logan, R. W., Wynne, O., Levitt, D., Price, D. & Sarkar, D. K. Altered circadian expression of cytokines and cytolytic factors in splenic natural killer cells of per1-/- mutant mice. *Journal of Interferon and Cytokine Research* **33**, 108–114 (2013).

[116] Lange, T., Dimitrov, S. & Born, J. Effects of sleep and circadian rhythm on the human immune system. *Annals of the New York Academy of Sciences* **1193**, 48–59 (2010).

[117] Izumo, M. *et al.* Differential effects of light and feeding on circadian organization of peripheral clocks in a forebrain Bmal1 mutant. *eLife* **3**, e04617 (2014).

[118] Dibner, C., Schibler, U. & Albrecht, U. The Mammalian Circadian Timing System: Organization and Coordination of Central and Peripheral Clocks. *Annual Review of Physiology* **72**, 517–549 (2010).

[119] Gachon, F., Olela, F. F., Schaad, O., Descombes, P. & Schibler, U. The circadian PAR-domain basic leucine zipper transcription factors DBP, TEF, and HLF modulate basal and inducible xenobiotic detoxification. *Cell Metabolism* **4**, 25–36 (2006).

[120] Hoogerwerf, W. A. *et al.* Clock gene expression in the murine gastrointestinal tract: Endogenous rhythmicity and effects of a feeding regimen. *Gastroenterology* **133**, 1250–1260 (2007).

[121] Pardini, L., Kaeffer, B., Trubuil, A., Bourreille, A. & Galmiche, J.-P. Human intestinal circadian clock: Expression of clock genes in colonocytes lining the crypt. *Chronobiology International* **22**, 951–961 (2005).

[122] Stokkan, K. A., Yamazaki, S., Tei, H., Sakaki, Y. & Menaker, M. Entrainment of the circadian clock in the liver by feeding. *Science (New York, N.Y.)* **291**, 490–493 (2001).

[123] Chaix, A., Zarrinpar, A., Miu, P. & Panda, S. Time-restricted feeding is a preventative and therapeutic intervention against diverse nutritional challenges. *Cell metabolism* **20**, 991–1005 (2014).

[124] Vollmers, C. *et al.* Time of feeding and the intrinsic circadian clock drive rhythms in hepatic gene expression. *Proceedings of the National Academy of Sciences of the United States of America* **106**, 21453–21458 (2009).

[125] Koronowski, K. B. *et al.* Defining the Independence of the Liver Circadian Clock. *Cell* **177**, 1448–1462.e14 (2019).

[126] Paschos, G. K. *et al.* Obesity in mice with adipocyte-specific deletion of clock component Arntl. *Nature Medicine* **18**, 1768–1777 (2012).

[127] Balsalobre, A. *et al.* Resetting of Circadian Time in Peripheral Tissues by Glucocorticoid Signaling. *Science* **289**, 2344–2347 (2000).

[128] Meyer-Kovac, J. *et al.* Hepatic gene therapy rescues high-fat diet responses in circadian Clock mutant mice. *Molecular Metabolism* **6**, 512–523 (2017).

[129] Jacobi, D. *et al.* Hepatic Bmal1 Regulates Rhythmic Mitochondrial Dynamics and Promotes Metabolic Fitness. *Cell Metabolism* **22**, 709–720 (2015).

[130] Lamia, K. A., Storch, K.-F. & Weitz, C. J. Physiological significance of a peripheral tissue circadian clock. *Proceedings of the National Academy of Sciences of the United States of America* **105**, 15172–15177 (2008).

[131] McDearmon, E. L. *et al.* Dissecting the Functions of the Mammalian Clock Protein BMAL1 by Tissue-Specific Rescue in Mice. *Science (New York, N.Y.)* **314**, 1304–1308 (2006).

[132] Harfmann, B. D. *et al.* Muscle-specific loss of Bmal1 leads to disrupted tissue glucose metabolism and systemic glucose homeostasis. *Skeletal Muscle* **6**, 12 (2016).

[133] Perelis, M. *et al.* Pancreatic β cell enhancers regulate rhythmic transcription of genes controlling insulin secretion. *Science* **350**, aac4250 (2015).

[134] Adrover, J. M. *et al.* A Neutrophil Timer Coordinates Immune Defense and Vascular Protection. *Immunity* **50**, 390–402.e10 (2019).

[135] Druzd, D. *et al.* Lymphocyte Circadian Clocks Control Lymph Node Trafficking and Adaptive Immune Responses. *Immunity* **46**, 120–132 (2017).

[136] Teng, F. *et al.* A circadian clock is essential for homeostasis of group 3 innate lymphoid cells in the gut. *Science Immunology* **4**, 1215 (2019).

[137] Brestoff, J. R. & Artis, D. Commensal bacteria at the interface of host metabolism and the immune system. *Nature Immunology* **14**, 676–684 (2013).

[138] Holmes, E., Li, J. V., Athanasiou, T., Ashrafian, H. & Nicholson, J. K. Understanding the role of gut microbiome–host metabolic signal disruption in health and disease. *Trends in Microbiology* **19**, 349–359 (2011).

[139] Devkota, S. *et al.* Dietary-fat-induced taurocholic acid promotes pathobiont expansion and colitis in Il10-/- mice. *Nature* **487**, 104–108 (2012).

[140] Huang, E. *et al.* Composition of Dietary Fat Source Shapes Gut Microbiota Architecture and Alters Host Inflammatory Mediators in Mouse Adipose Tissue. *JPEN. Journal of parenteral and enteral nutrition* **37** (2013).

[141] Leone, V. *et al.* Effects of diurnal variation of gut microbes and high fat feeding on host circadian clock function and metabolism. *Cell host & microbe* **17**, 681–689 (2015).

[142] Martinez-Guryn, K. *et al.* Small Intestine Microbiota Regulate Host Digestive and Absorptive Adaptive Responses to Dietary Lipids. *Cell Host & Microbe* **23**, 458–469.e5 (2018).

[143] Bäckhed, F. *et al.* The gut microbiota as an environmental factor that regulates fat storage. *Proceedings of the National Academy of Sciences* **101**, 15718–15723 (2004).

[144] David, L. A. *et al.* Diet rapidly and reproducibly alters the human gut microbiome. *Nature* **505**, 559–563 (2014).

[145] Hildebrandt, M. A. *et al.* High-Fat Diet Determines the Composition of the Murine Gut Microbiome Independently of Obesity. *Gastroenterology* **137**, 1716–1724.e2 (2009).

[146] Wu, G. D. *et al.* Linking Long-Term Dietary Patterns with Gut Microbial Enterotypes. *Science (New York, N.y.)* **334**, 105–108 (2011).

[147] Lindefeldt, M. *et al.* The ketogenic diet influences taxonomic and functional composition of the gut microbiota in children with severe epilepsy. *npj Biofilms and Microbiomes* **5**, 1–13 (2019).

[148] Turnbaugh, P. J., Bäckhed, F., Fulton, L. & Gordon, J. I. Diet-induced obesity is linked to marked but reversible alterations in the mouse distal gut microbiome. *Cell Host & Microbe* **3**, 213–223 (2008).

[149] Ley, R. E. *et al.* Obesity alters gut microbial ecology. *Proceedings of the National Academy of Sciences of the United States of America* **102**, 11070–11075 (2005).

[150] Turnbaugh, P. J. *et al.* A core gut microbiome in obese and lean twins. *Nature* **457**, 480–484 (2009).

[151] Turnbaugh, P. J. *et al.* An obesity-associated gut microbiome with increased capacity for energy harvest. *Nature* **444**, 1027–1031 (2006).

[152] Halatchev, I. G., O'Donnell, D., Hibberd, M. C. & Gordon, J. I. Applying indirect open-circuit calorimetry to study energy expenditure in gnotobiotic mice harboring different human gut microbial communities. *Microbiome* **7**, 158 (2019).

[153] Martin, A. M., Sun, E. W., Rogers, G. B. & Keating, D. J. The Influence of the Gut Microbiome on Host Metabolism Through the Regulation of Gut Hormone Release. *Frontiers in Physiology* **10** (2019).

[154] Bäckhed, F., Manchester, J. K., Semenkovich, C. F. & Gordon, J. I. Mechanisms underlying the resistance to diet-induced obesity in germ-free mice. *Proceedings of the National Academy of Sciences* **104**, 979–984 (2007).

[155] El Aidy, S. *et al.* The gut microbiota elicits a profound metabolic reorientation in the mouse jejunal mucosa during conventionalisation. *Gut* **62**, 1306–1314 (2013).

[156] Larsson, E. *et al.* Analysis of gut microbial regulation of host gene expression along the length of the gut and regulation of gut microbial ecology through MyD88. *Gut* **61**, 1124 (2012).

[157] Wichmann, A. *et al.* Microbial Modulation of Energy Availability in the Colon Regulates Intestinal Transit. *Cell Host & Microbe* **14**, 582–590 (2013).

[158] Yadav, H., Lee, J.-H., Lloyd, J., Walter, P. & Rane, S. G. Beneficial Metabolic Effects of a Probiotic via Butyrate-induced GLP-1 Hormone Secretion *. *Journal of Biological Chemistry* **288**, 25088–25097 (2013).

[159] Krisko, T. I. *et al.* Dissociation of Adaptive Thermogenesis from Glucose Homeostasis in Microbiome-Deficient Mice. *Cell Metabolism* **31**, 592–604.e9 (2020).

[160] De Vadder, F. *et al.* Microbiota-Generated Metabolites Promote Metabolic Benefits via Gut-Brain Neural Circuits. *Cell* **156**, 84–96 (2014).

[161] De Vadder, F. *et al.* Microbiota-Produced Succinate Improves Glucose Homeostasis via Intestinal Gluconeogenesis. *Cell Metabolism* **24**, 151–157 (2016).

[162] Vily-Petit, J. *et al.* Intestinal gluconeogenesis shapes gut microbiota, fecal and urine metabolome in mice with gastric bypass surgery. *Scientific Reports* **12**, 1415 (2022).

[163] Frazier, K. & Chang, E. B. Intersection of the Gut Microbiome and Circadian Rhythms in Metabolism. *Trends in Endocrinology & Metabolism* (2019).

[164] Frazier, K., Frith, M., Harris, D. & Leone, V. A. Mediators of Host–Microbe Circadian Rhythms in Immunity and Metabolism. *Biology* **9**, 417 (2020).

[165] Cohen, S. E. & Golden, S. S. Circadian Rhythms in Cyanobacteria. *Microbiol. Mol. Biol. Rev.* **79**, 373–385 (2015).

[166] Ishiura, M. *et al.* Expression of a Gene Cluster kaiABC as a Circadian Feedback Process in Cyanobacteria. *Science* **281**, 1519–1523 (1998).

[167] Johnson, C. H., Zhao, C., Xu, Y. & Mori, T. Timing the day: What makes bacterial clocks tick? *Nature Reviews Microbiology* **15**, 232–242 (2017).

[168] Kim, Y.-I., Dong, G., Carruthers, C. W., Golden, S. S. & LiWang, A. The day/night switch in KaiC, a central oscillator component of the circadian clock of cyanobacteria. *Proceedings of the National Academy of Sciences* **105**, 12825–12830 (2008).

[169] Ivleva, N. B., Gao, T., LiWang, A. C. & Golden, S. S. Quinone sensing by the circadian input kinase of the cyanobacterial circadian clock. *Proceedings of the National Academy of Sciences* **103**, 17468–17473 (2006).

[170] Wood, T. L. *et al.* The KaiA protein of the cyanobacterial circadian oscillator is modulated by a redox-active cofactor. *Proceedings of the National Academy of Sciences* **107**, 5804–5809 (2010).

[171] Rust, M. J., Golden, S. S. & O'Shea, E. K. Light-Driven Changes in Energy Metabolism Directly Entrain the Cyanobacterial Circadian Oscillator. *Science* **331**, 220–223 (2011).

[172] Eelderink-Chen, Z. *et al.* A circadian clock in a nonphotosynthetic prokaryote. *Science Advances* **7**, eabe2086 (2021).

[173] Paulose, J. K., Cassone, C. V., Graniczkowska, K. B. & Cassone, V. M. Entrainment of the Circadian Clock of the Enteric Bacterium Klebsiella aerogenes by Temperature Cycles. *iScience* **19**, 1202–1213 (2019).

[174] Paulose, J. K., Wright, J. M., Patel, A. G. & Cassone, V. M. Human Gut Bacteria Are Sensitive to Melatonin and Express Endogenous Circadian Rhythmicity. *PLoS ONE* **11**, e0146643 (2016).

[175] McFall-Ngai, M. Divining the Essence of Symbiosis: Insights from the Squid-Vibrio Model. *PLOS Biology* **12**, e1001783 (2014).

[176] Boettcher, K. J., Ruby, E. G. & McFall-Ngai, M. J. Bioluminescence in the symbiotic squid Euprymna scolopes is controlled by a daily biological rhythm. *Journal of Comparative Physiology A* **179**, 65–73 (1996).

[177] Heath-Heckman, E. A. C. *et al.* Bacterial Bioluminescence Regulates Expression of a Host Cryptochrome Gene in the Squid-Vibrio Symbiosis. *mBio* **4**, e00167–13 (2013).

[178] Liang, X., Bushman, F. D. & FitzGerald, G. A. Rhythmicity of the intestinal microbiota is regulated by gender and the host circadian clock. *Proceedings of the National Academy of Sciences* **112**, 10479–10484 (2015).

[179] Zarrinpar, A., Chaix, A., Yooseph, S. & Panda, S. Diet and Feeding Pattern Affect the Diurnal Dynamics of the Gut Microbiome. *Cell metabolism* **20**, 1006–1017 (2014).

[180] Thaiss, C. A. *et al.* Transkingdom Control of Microbiota Diurnal Oscillations Promotes Metabolic Homeostasis. *Cell* **159**, 514–529 (2014).

[181] Thaiss, C. A. *et al.* Microbiota Diurnal Rhythmicity Programs Host Transcriptome Oscillations. *Cell* **167**, 1495–1510.e12 (2016).

[182] Deloris Alexander, A. *et al.* Quantitative PCR assays for mouse enteric flora reveal strain-dependent differences in composition that are influenced by the microenvironment. *Mammalian Genome* **17**, 1093–1104 (2006).

[183] Rausch, P. *et al.* Analysis of factors contributing to variation in the C57BL/6J fecal microbiota across German animal facilities. *International Journal of Medical Microbiology* **306**, 343–355 (2016).

[184] Wu, T. *et al.* Chronic glucocorticoid treatment induced circadian clock disorder leads to lipid metabolism and gut microbiota alterations in rats. *Life Sciences* **192**, 173–182 (2018).

[185] Parkar, S. G., Kalsbeek, A. & Cheeseman, J. F. Potential Role for the Gut Microbiota in Modulating Host Circadian Rhythms and Metabolic Health. *Microorganisms* **7** (2019).

[186] Wang, Y. *et al.* The intestinal microbiota regulates body composition through NFIL3 and the circadian clock. *Science* **357**, 912–916 (2017).

[187] Brooks, J. F. *et al.* The microbiota coordinates diurnal rhythms in innate immunity with the circadian clock. *Cell* **0** (2021).

[188] Weger, B. D. *et al.* The Mouse Microbiome Is Required for Sex-Specific Diurnal Rhythms of Gene Expression and Metabolism. *Cell Metabolism* **29**, 362–382.e8 (2019).

[189] Kuang, Z. *et al.* The intestinal microbiota programs diurnal rhythms in host metabolism through histone deacetylase 3. *Science* **365**, 1428–1434 (2019).

[190] Mukherji, A., Kobiita, A., Ye, T. & Chambon, P. Homeostasis in intestinal epithelium is orchestrated by the circadian clock and microbiota cues transduced by TLRs. *Cell* **153**, 812–827 (2013).

[191] Eckel-Mahan, K. L. *et al.* Reprogramming of the Circadian Clock by Nutritional Challenge. *Cell* **155**, 1464–1478 (2013).

[192] Voigt, R. M. *et al.* Circadian disorganization alters intestinal microbiota. *PloS One* **9**, e97500 (2014).

[193] Murakami, M. *et al.* Gut microbiota directs PPARγ-driven reprogramming of the liver circadian clock by nutritional challenge. *EMBO reports* **17**, 1292–1303 (2016).

[194] Mu, C., Yang, Y., Luo, Z., Guan, L. & Zhu, W. The Colonic Microbiome and Epithelial Transcriptome Are Altered in Rats Fed a High-Protein Diet Compared with a Normal-Protein Diet. *The Journal of Nutrition* **146**, 474–483 (2016).

[195] Oishi, K., Uchida, D. & Itoh, N. Low-carbohydrate, high-protein diet affects rhythmic expression of gluconeogenic regulatory and circadian clock genes in mouse peripheral tissues. *Chronobiology International* **29**, 799–809 (2012).

[196] Tognini, P. *et al.* Distinct Circadian Signatures in Liver and Gut Clocks Revealed by Ketogenic Diet. *Cell Metabolism* **26**, 523–538.e5 (2017).

[197] Hatori, M. *et al.* Time restricted feeding without reducing caloric intake prevents metabolic diseases in mice fed a high fat diet. *Cell metabolism* **15**, 848–860 (2012).

[198] Collado, M. C. *et al.* Timing of food intake impacts daily rhythms of human salivary microbiota: A randomized, crossover study. *FASEB journal: official publication of the Federation of American Societies for Experimental Biology* **32**, 2060–2072 (2018).

[199] Reitmeier, S. *et al.* Arrhythmic Gut Microbiome Signatures Predict Risk of Type 2 Diabetes. *Cell Host & Microbe* **28**, 258–272.e6 (2020).

[200] Gao, Z. *et al.* Butyrate improves insulin sensitivity and increases energy expenditure in mice. *Diabetes* **58**, 1509–1517 (2009).

[201] Kars, M. *et al.* Tauroursodeoxycholic Acid May Improve Liver and Muscle but Not Adipose Tissue Insulin Sensitivity in Obese Men and Women. *Diabetes* **59**, 1899–1905 (2010).

[202] Utzschneider, K. M., Kratz, M., Damman, C. J. & Hullarg, M. Mechanisms Linking the Gut Microbiome and Glucose Metabolism. *The Journal of Clinical Endocrinology & Metabolism* **101**, 1445–1454 (2016).

[203] den Besten, G. *et al.* The role of short-chain fatty acids in the interplay between diet, gut microbiota, and host energy metabolism. *Journal of Lipid Research* **54**, 2325–2340 (2013).

[204] Louis, P. & Flint, H. J. Diversity, metabolism and microbial ecology of butyrate-producing bacteria from the human large intestine. *FEMS microbiology letters* **294**, 1–8 (2009).

[205] Vital, M., Howe, A. C. & Tiedje, J. M. Revealing the Bacterial Butyrate Synthesis Pathways by Analyzing (Meta)genomic Data. *mBio* **5**, e00889–14 (2014).

[206] Krautkramer, K. A. *et al.* Diet-Microbiota Interactions Mediate Global Epigenetic Programming in Multiple Host Tissues. *Molecular Cell* **64**, 982–992 (2016).

[207] Corrêa-Oliveira, R., Fachi, J. L., Vieira, A., Sato, F. T. & Vinolo, M. A. R. Regulation of immune cell function by short-chain fatty acids. *Clinical & Translational Immunology* **5**, e73 (2016).

[208] Chang, P. V., Hao, L., Offermanns, S. & Medzhitov, R. The microbial metabolite butyrate regulates intestinal macrophage function via histone deacetylase inhibition. *Proceedings of the National Academy of Sciences of the United States of America* **111**, 2247–2252 (2014).

[209] Lu, Y. *et al.* Short Chain Fatty Acids Prevent High-fat-diet-induced Obesity in Mice by Regulating G Protein-coupled Receptors and Gut Microbiota. *Scientific Reports* **6**, 37589 (2016).

[210] Tolhurst, G. *et al.* Short-chain fatty acids stimulate glucagon-like peptide-1 secretion via the G-protein-coupled receptor FFAR2. *Diabetes* **61**, 364–371 (2012).

[211] Chambers, E. S., Preston, T., Frost, G. & Morrison, D. J. Role of Gut Microbiota-Generated Short-Chain Fatty Acids in Metabolic and Cardiovascular Health. *Current Nutrition Reports* **7**, 198–206 (2018).

[212] Vinolo, M. A. R. *et al.* Tributyrin attenuates obesity-associated inflammation and insulin resistance in high-fat-fed mice. *American Journal of Physiology. Endocrinology and Metabolism* **303**, E272–282 (2012).

[213] Schwiertz, A. *et al.* Microbiota and SCFA in lean and overweight healthy subjects. *Obesity (Silver Spring, Md.)* **18**, 190–195 (2010).

[214] Segers, A. *et al.* The circadian clock regulates the diurnal levels of microbial short-chain fatty acids and their rhythmic effects on colon contractility in mice. *Acta Physiologica (Oxford, England)* e13193 (2018).

[215] Luzader, D. *et al.* Gut Microbial Metabolites Modulate the Amplitude and Phase of PER2 and BMAL1 Circadian Rhythms in Intestinal Epithelial Cells and Organoids. *Gastroenterology* **154**, S–67 (2018).

[216] Tahara, Y. *et al.* Gut Microbiota-Derived Short Chain Fatty Acids Induce Circadian Clock Entrainment in Mouse Peripheral Tissue. *Scientific Reports* **8** (2018).

[217] de Aguiar Vallim, T. Q., Tarling, E. J. & Edwards, P. A. Pleiotropic Roles of Bile Acids in Metabolism. *Cell Metabolism* **17**, 657–669 (2013).

[218] Hylemon, P. B. *et al.* Bile acids as regulatory molecules. *Journal of Lipid Research* **50**, 1509–1520 (2009).

[219] Pineda Torra, I. *et al.* Bile acids induce the expression of the human peroxisome proliferator-activated receptor alpha gene via activation of the farnesoid X receptor. *Molecular Endocrinology (Baltimore, Md.)* **17**, 259–272 (2003).

[220] Sayin, S. I. *et al.* Gut Microbiota Regulates Bile Acid Metabolism by Reducing the Levels of Tauro-beta-muricholic Acid, a Naturally Occurring FXR Antagonist. *Cell Metabolism* **17**, 225–235 (2013).

[221] Devlin, A. S. & Fischbach, M. A. A biosynthetic pathway for a prominent class of microbiota-derived bile acids. *Nature chemical biology* **11**, 685–690 (2015).

[222] Wahlström, A., Sayin, S. I., Marschall, H.-U. & Bäckhed, F. Intestinal Crosstalk between Bile Acids and Microbiota and Its Impact on Host Metabolism. *Cell Metabolism* **24**, 41–50 (2016).

[223] Hofmann, A. F. & Eckmann, L. How bile acids confer gut mucosal protection against bacteria. *Proceedings of the National Academy of Sciences* **103**, 4333–4334 (2006).

[224] Inagaki, T. *et al.* Regulation of antibacterial defense in the small intestine by the nuclear bile acid receptor. *Proceedings of the National Academy of Sciences* **103**, 3920–3925 (2006).

[225] Ding, L. *et al.* Trimethylamine-N-oxide (TMAO)-induced atherosclerosis is associated with bile acid metabolism. *Lipids in Health and Disease* **17**, 286 (2018).

[226] Pols, T. W. H. TGR5 in inflammation and cardiovascular disease. *Biochemical Society Transactions* **42**, 244–249 (2014).

[227] Govindarajan, K. *et al.* Unconjugated Bile Acids Influence Expression of Circadian Genes: A Potential Mechanism for Microbe-Host Crosstalk. *PloS One* **11**, e0167319 (2016).

[228] Duez, H. *et al.* Regulation of Bile Acid Synthesis by the Nuclear Receptor Rev-erbα. *Gastroenterology* **135**, 689–698.e5 (2008).

[229] Lavery, D. J. & Schibler, U. Circadian transcription of the cholesterol 7 alpha hydroxylase gene may involve the liver-enriched bZIP protein DBP. *Genes & Development* **7**, 1871–1884 (1993).

[230] Zhang, Y.-K. J., Guo, G. L. & Klaassen, C. D. Diurnal Variations of Mouse Plasma and Hepatic Bile Acid Concentrations as well as Expression of Biosynthetic Enzymes and Transporters. *PLOS ONE* **6**, e16683 (2011).

[231] Ferrell, J. M. & Chiang, J. Y. Short-Term Circadian Disruption Impairs Bile Acid and Lipid Homeostasis in Mice. *Cellular and Molecular Gastroenterology and Hepatology* **1**, 664–677 (2015).

[232] Ma, K. *et al.* Circadian Dysregulation Disrupts Bile Acid Homeostasis. *PLOS ONE* **4**, e6843 (2009).

[233] Joyce, S. A. *et al.* Regulation of host weight gain and lipid metabolism by bacterial bile acid modification in the gut. *Proceedings of the National Academy of Sciences* **111**, 7421–7426 (2014).

[234] Yao, L. *et al.* A selective gut bacterial bile salt hydrolase alters host metabolism. *eLife* **7**, e37182 (2018).

[235] Mukherjee, S. & Hooper, L. V. Antimicrobial defense of the intestine. *Immunity* **42**, 28–39 (2015).

[236] Hooper, L. V. & Macpherson, A. J. Immune adaptations that maintain homeostasis with the intestinal microbiota. *Nature Reviews Immunology* **10**, 159–169 (2010).

[237] Vaishnava, S., Behrendt, C. L., Ismail, A. S., Eckmann, L. & Hooper, L. V. Paneth cells directly sense gut commensals and maintain homeostasis at the intestinal host-microbial interface. *Proceedings of the National Academy of Sciences* **105**, 20858–20863 (2008).

[238] Salzman, N. H. *et al.* Enteric defensins are essential regulators of intestinal microbial ecology. *Nature Immunology* **11**, 76–82 (2010).

[239] Guo, X. *et al.* High Fat Diet Alters Gut Microbiota and the Expression of Paneth Cell-Antimicrobial Peptides Preceding Changes of Circulating Inflammatory Cytokines. *Mediators of Inflammation* **2017**, e9474896 (2017).

[240] Huang, Y. *et al.* Gut REG3γ-Associated Lactobacillus Induces Anti-inflammatory Macrophages to Maintain Adipose Tissue Homeostasis. *Frontiers in Immunology* **8** (2017).

[241] Paschos, G. K. & FitzGerald, G. A. Circadian Clocks and Metabolism: Implications for Microbiome and Aging. *Trends in Genetics* **33**, 760–769 (2017).

[242] Bishehsari, F. *et al.* Light/Dark Shifting Promotes Alcohol-Induced Colon Carcinogenesis: Possible Role of Intestinal Inflammatory Milieu and Microbiota. *International Journal of Molecular Sciences* **17** (2016).

[243] Gombert, M., Carrasco-Luna, J., Pin-Arboledas, G. & Codoñer-Franch, P. The connection of circadian rhythm to inflammatory bowel disease. *Translational Research* **206**, 107–118 (2019).

[244] Rai, R., Saraswat, V. A. & Dhiman, R. K. Gut Microbiota: Its Role in Hepatic Encephalopathy. *Journal of Clinical and Experimental Hepatology* **5**, S29–S36 (2015).

[245] Bruyneel, M. & Sersté, T. Sleep disturbances in patients with liver cirrhosis: Prevalence, impact, and management challenges. *Nature and Science of Sleep* **10**, 369–375 (2018).

[246] Org, E. *et al.* Sex differences and hormonal effects on gut microbiota composition in mice. *Gut Microbes* **7**, 313–322 (2016).

[247] Iwahana, E., Karatsoreos, I., Shibata, S. & Silver, R. Gonadectomy reveals sex differences in circadian rhythms and suprachiasmatic nucleus androgen receptors in mice. *Hormones and Behavior* **53**, 422–430 (2008).

[248] Palmisano, B. T., Stafford, J. M. & Pendergast, J. S. High-Fat Feeding Does Not Disrupt Daily Rhythms in Female Mice because of Protection by Ovarian Hormones. *Frontiers in Endocrinology* **8** (2017).

[249] Bur, I. M. *et al.* The Circadian Clock Components CRY1 and CRY2 Are Necessary to Sustain Sex Dimorphism in Mouse Liver Metabolism. *Journal of Biological Chemistry* **284**, 9066–9073 (2009).

[250] Weiser, M. M. Intestinal epithelial cell surface membrane glycoprotein synthesis. I. An indicator of cellular differentiation. *The Journal of Biological Chemistry* **248**, 2536–2541 (1973).

[251] Ferraris, R. P., Villenas, S. A. & Diamond, J. Regulation of brush-border enzyme activities and enterocyte migration rates in mouse small intestine. *The American Journal of Physiology* **262**, G1047–1059 (1992).

[252] Sato, T. *et al.* Long-term expansion of epithelial organoids from human colon, adenoma, adenocarcinoma, and Barrett's epithelium. *Gastroenterology* **141**, 1762–1772 (2011).

[253] Schindelin, J., Rueden, C. T., Hiner, M. C. & Eliceiri, K. W. The ImageJ ecosystem: An open platform for biomedical image analysis. *Molecular Reproduction and Development* **82**, 518–529 (2015).

[254] Louis, P., Young, P., Holtrop, G. & Flint, H. J. Diversity of human colonic butyrate-producing bacteria revealed by analysis of the butyryl-CoA:acetate CoA-transferase gene. *Environmental Microbiology* **12**, 304–314 (2010).

[255] Hall, M. & Beiko, R. G. 16S rRNA Gene Analysis with QIIME2. *Methods in Molecular Biology (Clifton, N.J.)* **1849**, 113–129 (2018).

[256] Callahan, B. J. *et al.* DADA2: High-resolution sample inference from Illumina amplicon data. *Nature Methods* **13**, 581–583 (2016).

[257] Bokulich, N. A. *et al.* Optimizing taxonomic classification of marker-gene amplicon sequences with QIIME 2's q2-feature-classifier plugin. *Microbiome* **6**, 90 (2018).

[258] Yarza, P. *et al.* Uniting the classification of cultured and uncultured bacteria and archaea using 16S rRNA gene sequences. *Nature Reviews Microbiology* **12**, 635–645 (2014).

[259] Caporaso, J. G. *et al.* QIIME allows analysis of high-throughput community sequencing data. *Nature Methods* **7**, 335–336 (2010).

[260] Hutchison, A. L. *et al.* Improved Statistical Methods Enable Greater Sensitivity in Rhythm Detection for Genome-Wide Data. *PLOS Computational Biology* **11**, e1004094 (2015).

[261] Eren, A. M. *et al.* Anvi'o: An advanced analysis and visualization platform for 'omics data. *PeerJ* **3**, e1319 (2015).

[262] Vital, M. *et al.* A gene-targeted approach to investigate the intestinal butyrate-producing bacterialcommunity. *Microbiome* **1**, 8 (2013).

[263] Jandu, N. *et al.* Conditioned Medium from Enterohemorrhagic Escherichia coli-Infected T84 Cells Inhibits Signal Transducer and Activator of Transcription 1 Activation by Gamma Interferon. *Infection and Immunity* **74**, 1809–1818 (2006).

[264] Cash, H. L., Whitham, C. V. & Hooper, L. V. Refolding, purification, and characterization of human and murine RegIII proteins expressed in Escherichia coli. *Protein Expression and Purification* **48**, 151–159 (2006).

[265] He, Y. *et al.* Multi-Omic Single-Shot Technology for Integrated Proteome and Lipidome Analysis. *Analytical Chemistry* **93**, 4217–4222 (2021).

[266] Dobin, A. *et al.* STAR: Ultrafast universal RNA-seq aligner. *Bioinformatics* **29**, 15–21 (2013).

[267] Love, M. I., Huber, W. & Anders, S. Moderated estimation of fold change and dispersion for RNA-seq data with DESeq2. *Genome Biology* **15**, 550 (2014).

[268] Sergushichev, A. A. An algorithm for fast preranked gene set enrichment analysis using cumulative statistic calculation (2016).

[269] Demsar, J. *et al.* Orange: Data Mining Toolbox in Python. *Journal of Machine Learning Research* 2349–2353 (2013).

[270] Zhou, Y. *et al.* Metascape provides a biologist-oriented resource for the analysis of systems-level datasets. *Nature Communications* **10**, 1523 (2019).

[271] Cline, M. S. *et al.* Integration of biological networks and gene expression data using Cytoscape. *Nature Protocols* **2**, 2366–2382 (2007).

[272] Weir, J. B. d. V. New methods for calculating metabolic rate with special reference to protein metabolism. *The Journal of Physiology* **109**, 1–9 (1949).

[273] Speakman, J. R. Measuring Energy Metabolism in the Mouse – Theoretical, Practical, and Analytical Considerations. *Frontiers in Physiology* **4** (2013).

[274] Riachi, M., Himms-Hagen, J. & Harper, M.-E. Percent relative cumulative frequency analysis in indirect calorimetry: Application to studies of transgenic mice. *Canadian Journal of Physiology and Pharmacology* (2011).

[275] Renom, G., Bulois, P., Hafraoui, S., Colombel, J. F. & Degand, P. M. Simple gas chromatography analysis of faecal butyrate: Application to patients at risk of pouchitis. *Clinical Chemistry and Laboratory Medicine* **39**, 15–19 (2001).

[276] Rousseeuw, P. J. & Croux, C. Alternatives to the Median Absolute Deviation. *Journal of the American Statistical Association* **88**, 1273–1283 (1993).

[277] Brademan, D. R. *et al.* Argonaut: A Web Platform for Collaborative Multi-omic Data Visualization and Exploration. *Patterns (New York, N.Y.)* **1**, 100122 (2020).

[278] Frazier, K. *et al.* Gut Microbes and the Liver Circadian Clock Partition Glucose and Lipid Metabolism (2022).

[279] Eggink, H. M. *et al.* Complex interaction between circadian rhythm and diet on bile acid homeostasis in male rats. *Chronobiology International* **34**, 1339–1353 (2017).

[280] Sharabi, K., Tavares, C. D. J., Rines, A. K. & Puigserver, P. Molecular Pathophysiology of Hepatic Glucose Production. *Molecular aspects of medicine* **46**, 21–33 (2015).

[281] Kraus-Friedmann, N. Hormonal regulation of hepatic gluconeogenesis. *Physiological Reviews* **64**, 170–259 (1984).

[282] Zhang, E. E. *et al.* Cryptochrome mediates circadian regulation of cAMP signaling and hepatic gluconeogenesis. *Nature Medicine* **16**, 1152–1156 (2010).

[283] Kornmann, B., Schaad, O., Bujard, H., Takahashi, J. S. & Schibler, U. System-Driven and Oscillator-Dependent Circadian Transcription in Mice with a Conditionally Active Liver Clock. *PLOS Biology* **5**, e34 (2007).

[284] Postic, C. *et al.* Dual roles for glucokinase in glucose homeostasis as determined by liver and pancreatic beta cell-specific gene knock-outs using Cre recombinase. *The Journal of Biological Chemistry* **274**, 305–315 (1999).

[285] Storch, K.-F. *et al.* Intrinsic circadian clock of the mammalian retina: Importance for retinal processing of visual information. *Cell* **130**, 730–741 (2007).

[286] Casanova, E. *et al.* A CamKIIα iCre BAC allows brain-specific gene inactivation. *genesis* **31**, 37–42 (2001).

[287] Jones, J. G. Hepatic glucose and lipid metabolism. *Diabetologia* **59**, 1098–1103 (2016).

[288] Randle, P. J. Regulatory interactions between lipids and carbohydrates: The glucose fatty acid cycle after 35 years. *Diabetes/Metabolism Reviews* **14**, 263–283 (1998).

[289] Zarrinpar, A. *et al.* Antibiotic-induced microbiome depletion alters metabolic homeostasis by affecting gut signaling and colonic metabolism. *Nature Communications* **9**, 2872 (2018).

[290] Zhang, D. *et al.* Liver Clock Protein BMAL1 Promotes de Novo Lipogenesis through Insulin-mTORC2-AKT Signaling. *The Journal of Biological Chemistry* **289**, 25925 (2014).

[291] Montagner, A. *et al.* Hepatic circadian clock oscillators and nuclear receptors integrate microbiome-derived signals. *Scientific Reports* **6**, 20127 (2016).

[292] Theriot, C. M., Bowman, A. A. & Young, V. B. Antibiotic-Induced Alterations of the Gut Microbiota Alter Secondary Bile Acid Production and Allow for Clostridium difficile Spore Germination and Outgrowth in the Large Intestine. *mSphere* **1** (2016).

[293] Burri, L., Thoresen, G. H. & Berge, R. K. The Role of PPAR Activation in Liver and Muscle. *PPAR Research* **2010**, e542359 (2010).

[294] Li, T. & Chiang, J. Y. L. Regulation of Bile Acid and Cholesterol Metabolism by PPARs. *PPAR Research* **2009**, 501739 (2009).

[295] Solanas, G. *et al.* Aged Stem Cells Reprogram Their Daily Rhythmic Functions to Adapt to Stress. *Cell* **170**, 678–692.e20 (2017).

[296] Chaix, A., Lin, T., Le, H. D., Chang, M. W. & Panda, S. Time-Restricted Feeding Prevents Obesity and Metabolic Syndrome in Mice Lacking a Circadian Clock. *Cell Metabolism* (2018).

[297] Li, J. *et al.* BMAL1 functions as a cAMP-responsive coactivator of HDAC5 to regulate hepatic gluconeogenesis. *Protein & Cell* **9**, 976–980 (2018).

[298] Yuille, S., Reichardt, N., Panda, S., Dunbar, H. & Mulder, I. E. Human gut bacteria as potent class i histone deacetylase inhibitors in vitro through production of butyric acid and valeric acid. *PloS one* **13**, e0201073 (2018).

[299] Wu, S.-e. *et al.* Microbiota-derived metabolite promotes hdac3 activity in the gut. *Nature* **586**, 108–112 (2020).

[300] Greco, C. M. *et al.* Integration of feeding behavior by the liver circadian clock reveals network dependency of metabolic rhythms. *Science advances* **7**, eabi7828 (2021).

[301] Smith, J. G. *et al.* Interrogating metabolic interactions between skeletal muscle and liver circadian clocks in vivo. *bioRxiv* (2022).

[302] Kirpich, I. A. *et al.* Integrated hepatic transcriptome and proteome analysis of mice with high-fat diet-induced nonalcoholic fatty liver disease. *The Journal of nutritional biochemistry* **22**, 38–45 (2011).

[303] Frazier, K. *et al.* High-fat diet disrupts REG3γ and gut microbial rhythms promoting metabolic dysfunction. *Cell Host & Microbe* **30**, 809–823.e6 (2022).

[304] Narushima, Y. *et al.* Structure, chromosomal localization and expression of mouse genes encoding type III Reg, RegIII alpha, RegIII beta, RegIII gamma. *Gene* **185**, 159–168 (1997).

[305] Nata, K. *et al.* Molecular cloning, expression and chromosomal localization of a novel human REG family gene, REG III. *Gene* **340**, 161–170 (2004).

[306] Hooper, L. V., Littman, D. R. & Macpherson, A. J. Interactions between the microbiota and the immune system. *Science (New York, N.Y.)* **336**, 1268–1273 (2012).

[307] Cash, H. L., Whitham, C. V., Behrendt, C. L. & Hooper, L. V. Symbiotic bacteria direct expression of an intestinal bactericidal lectin. *Science (New York, N.Y.)* **313**, 1126–1130 (2006).

[308] Mukherjee, S. *et al.* Antibacterial membrane attack by a pore-forming intestinal C-type lectin. *Nature* **505**, 103–107 (2014).

[309] Everard, A. *et al.* Microbiome of prebiotic-treated mice reveals novel targets involved in host response during obesity. *The ISME journal* **8**, 2116–2130 (2014).

[310] Loonen, L. M. *et al.* REG3γ-deficient mice have altered mucus distribution and increased mucosal inflammatory responses to the microbiota and enteric pathogens in the ileum. *Mucosal Immunology* **7**, 939–947 (2014).

[311] Vaishnava, S. *et al.* The antibacterial lectin RegIIIγ promotes the spatial segregation of microbiota and host in the intestine. *Science (New York, N.Y.)* **334**, 255–258 (2011).

[312] Wang, L. *et al.* Intestinal REG3 Lectins Protect against Alcoholic Steatohepatitis by Reducing Mucosa-Associated Microbiota and Preventing Bacterial Translocation. *Cell Host & Microbe* **19**, 227–239 (2016).

[313] Natividad, J. M. M. *et al.* Differential Induction of Antimicrobial REGIII by the Intestinal Microbiota and Bifidobacterium breve NCC2950. *Applied and Environmental Microbiology* **79**, 7745–7754 (2013).

[314] Everard, A. *et al.* Cross-talk between Akkermansia muciniphila and intestinal epithelium controls diet-induced obesity. *Proceedings of the National Academy of Sciences* **110**, 9066–9071 (2013).

[315] Carmody, R. N. *et al.* Diet dominates host genotype in shaping the murine gut microbiota. *Cell Host & Microbe* **17**, 72–84 (2015).

[316] Gu, Z. *et al.* Exosome-Like Nanoparticles From Lactobacillus rhamnosusGG Protect Against Alcohol-Associated Liver Disease Through Intestinal Aryl Hydrocarbon Receptor in Mice. *Hepatology Communications* **5**, 846–864 (2021).

[317] Calder, P. C. Branched-chain amino acids and immunity. *The Journal of nutrition* **136**, 288S–293S (2006).

[318] Ren, M. *et al.* Different lipopolysaccharide branched-chain amino acids modulate porcine intestinal endogenous β-defensin expression through the sirt1/erk/90rsk pathway. *Journal of agricultural and food chemistry* **64**, 3371–3379 (2016).

[319] O'Flaherty, S., Briner Crawley, A., Theriot, C. M. & Barrangou, R. The Lactobacillus Bile Salt Hydrolase Repertoire Reveals Niche-Specific Adaptation. *mSphere* **3** (2018).

[320] Shin, J. H. & Seeley, R. J. Reg3 Proteins as Gut Hormones? *Endocrinology* **160**, 1506–1514 (2019).

[321] Bluemel, S. *et al.* The Role of Intestinal C-type Regenerating Islet Derived-3 Lectins for Nonalcoholic Steatohepatitis. *Hepatology Communications* **2**, 393–406 (2018).

[322] Tremblay, S. *et al.* Bile acid administration elicits an intestinal antimicrobial program and reduces the bacterial burden in two mouse models of enteric infection. *Infection and immunity* **85**, e00942–16 (2017).

APPENDIX A
SUPPLEMENTAL DATA FOR CHAPTER 3

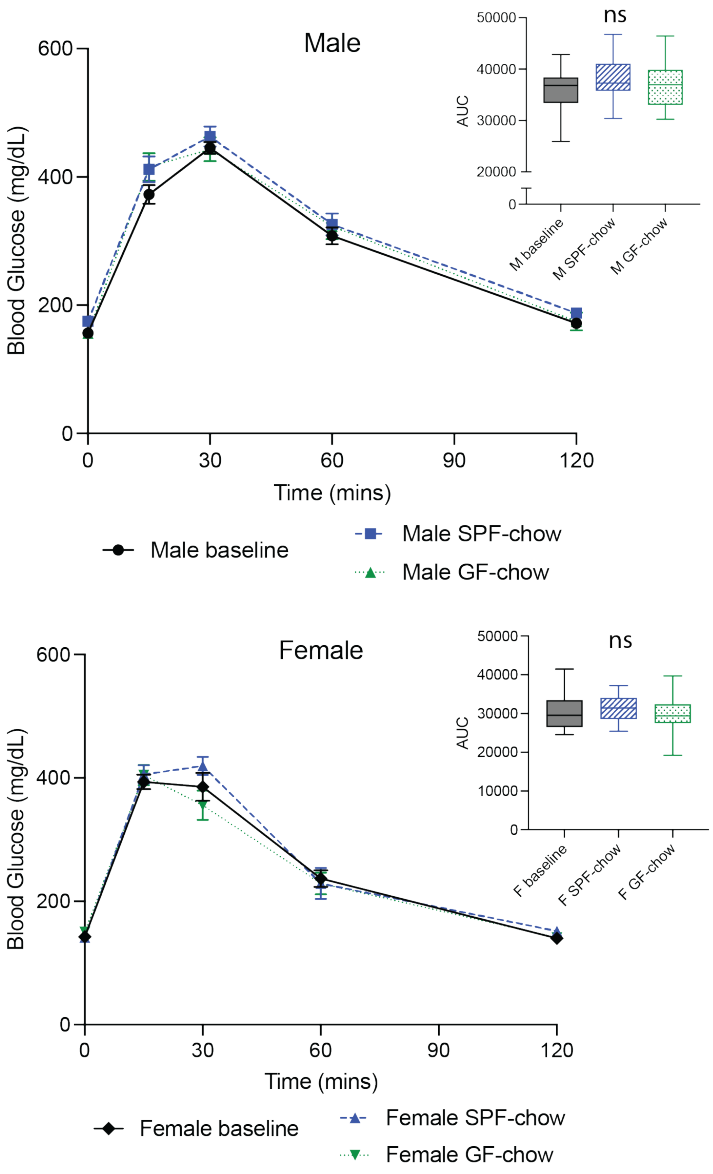

Figure A.1: **Different regular chow rodent diets do not impact glucose tolerance in SPF male or female mice.** GTT results for male (upper panel) and female (lower panel) mice at baseline and after 1 month on SPF-RC (Envigo 2018S) or GF-RC (LabDiet 5K67) diet (n=10/diet group). Data points represent mean±SEM, box plots represent median±min/max. Associated graphs represent area under the curve (AUC). ns = not significant.

Table A.1: **Macronutrient breakdown of SPF and GF RC diets.** SPF regular chow (RC) diet is Envigo 2018S; GF RC diet is LabDiet 5K67.

Study Diets	SPF Regular Chow[1]	GF Regular Chow[2]
Metabolizable energy (kcal/g)	3.1	3.14
Fat (%)	18	16.28
Saturated fatty acids	0.9	1.17
Monounsaturated fatty acids	1.3	1.38
Polyunsaturated fatty acids	3.4	3.25
Protein (%)	24	22.11
Carbohydrate (%)	58	61.65
Crude fiber (%)	3.5	4.0

[1]SPF Regular chow (RC), 2018S Harlan Teklad Global 18% Protein Rodent Diet. Ingredients: Ground wheat, ground corn, wheat middlings, dehulled soybean meal, corn gluten meal, soybean oil, calcium carbonate, dicalcium phosphate, brewers dried yeast, iodized salt, L-lysine, DL-methionine, choline chloride, kaolin, magnesium oxide, vitamin E acetate, menadione sodium bisulfite complex (source of vitamin K activity), manganous oxide, ferrous sulfate, zinc oxide, niacin, calcium pantothenate, copper sulfate, pyridoxine hydrochloride, riboflavin, thiamin mononitrate, vitamin A acetate, calcium iodate, vitamin B12 supplement, folic acid, biotin, vitamin D3 supplement, cobalt carbonate.

[2]GF Regular chow (RC), LabDiet JL Rat and Mouse/Auto 6F 5K67. Ingredients: Ground wheat, ground corn, ground oats, wheat middlings, fish meal, dehulled soybean meal, soybean oil, dehydrated alfalfa meal, corn gluten meal, dicalcium phosphate, brewers dried yeast, calcium carbonate, menadione sodium bisulfite complex (source of vitamin K), salt, DL-methionine, choline chloride, magnesium oxide, thiamin mononitrate, pyridoxine hydrochloride, cholecalciferol (vitamin D3), vitamin A acetate, manganous oxide, calcium pantothenate, ferrous sulfate, calcium iodate, DL-alpha tocopheryl acetate (vitamin E), folic acid, vitamin B12 supplement, riboflavin-5-phosphate, zinc oxide, ferrous carbonate, nicotinic acid, copper sulfate, zinc sulfate, cobalt carbonate, biotin.

Table A.2: **Oscillating transcript enrichment of Circadian and Carbohydrate Metabolism pathways.** CORUM, GO, KEGG, Reactome, and Wiki pathway enrichment of oscillating hepatic transcripts related to circadian rhythms and carbohydrate metabolism within SPF and GF, WT and LKO male mice ($q - value < 0.05$ indicated by X, analysis via Metascape).

			SPF		GF	
			WT	L-KO	WT	L-KO
Circadian		CORUM_CLOCK-BMAL1-CRY1_COMPLEX	X		X	
		CORUM_CLOCK-BMAL1-CRY2_COMPLEX	X		X	
		GO_CIRCADIAN_REGULATION_OF_GENE_EXPRESSION	X	X	X	X
		GO_CIRCADIAN_RHYTHM	X		X	
		GO_REGULATION_OF_CIRCADIAN_RHYTHM	X		X	
		GO_RHYTHMIC_PROCESS	X		X	
		KEGG_CIRCADIAN_RHYTHM	X		X	
Carbohydrate Metabolism	Insulin	GO_CELLULAR_RESPONSE_TO_INSULIN_STIMULUS		X	X	X
		GO_INSULIN_RECEPTOR_SIGNALING_PATHWAY		X		X
		GO_INSULIN_SECRETION			X	
		GO_NEGATIVE_REGULATION_OF_CELLULAR_RESPONSE_TO_INSULIN_STIMULUS				X
		GO_NEGATIVE_REGULATION_OF_INSULIN_RECEPTOR_SIGNALING_PATHWAY				X
		GO_REGULATION_OF_CELLULAR_RESPONSE_TO_INSULIN_STIMULUS				X
		GO_REGULATION_OF_INSULIN_RECEPTOR_SIGNALING_PATHWAY		X		X
		GO_REGULATION_OF_INSULIN_SECRETION			X	
		GO_RESPONSE_TO_INSULIN		X	X	X
	Glucose/Glycogen/Pyruvate	GO_CELLULAR_GLUCOSE_HOMEOSTASIS			X	X
		GO_CELLULAR_RESPONSE_TO_GLUCOSE_STIMULUS			X	
		GO_GLUCOSE_HOMEOSTASIS		X	X	X
		GO_GLUCOSE_IMPORT			X	
		GO_GLUCOSE_METABOLIC_PROCESS	X		X	X
		GO_GLYCOGEN_BIOSYNTHETIC_PROCESS	X			X
		GO_GLYCOGEN_METABOLIC_PROCESS	X		X	X
		GO_REGULATION_OF_GLUCOSE_METABOLIC_PROCESS	X		X	X
		GO_RESPONSE_TO_GLUCOSE			X	X
		KEGG_2-OXOCARBOXYLIC_ACID_METABOLISM	X		X	
		REACTOME_PYRUVATE_METABOLISM	X			
		REACTOME_PYRUVATE_METABOLISM_AND_CITRIC_ACID_(TCA)_CYCLE	X		X	
	5-carbon Sugars	GO_DEOXYRIBOSE_PHOSPHATE_CATABOLIC_PROCESS			X	
		GO_DEOXYRIBOSE_PHOSPHATE_METABOLIC_PROCESS			X	
		GO_RIBOSE_PHOSPHATE_BIOSYNTHETIC_PROCESS			X	X
		GO_RIBOSE_PHOSPHATE_METABOLIC_PROCESS		X	X	X
	(Miscellaneous)	CORUM_CYTOCHROME_BC1-COMPLEX,_MITOCHONDRIAL		X		
		GO_CARBOHYDRATE_DERIVATIVE_BIOSYNTHETIC_PROCESS	X		X	X
		GO_CARBOHYDRATE_DERIVATIVE_CATABOLIC_PROCESS			X	
		GO_CARBOHYDRATE_HOMEOSTASIS		X	X	X
		GO_CARBOHYDRATE_METABOLIC_PROCESS	X		X	X
		GO_CARBOHYDRATE_TRANSPORT	X		X	X
		GO_CELLULAR_CARBOHYDRATE_METABOLIC_PROCESS	X		X	X
		GO_CELLULAR_GLUCAN_METABOLIC_PROCESS	X		X	X
		GO_CELLULAR_POLYSACCHARIDE_METABOLIC_PROCESS			X	
		GO_CELLULAR_RESPIRATION			X	
		GO_CELLULAR_RESPONSE_TO_CARBOHYDRATE_STIMULUS			X	X
		GO_CELLULAR_RESPONSE_TO_HEXOSE_STIMULUS			X	X
		GO_CELLULAR_RESPONSE_TO_MONOSACCHARIDE_STIMULUS			X	X
		GO_CELLULAR_RESPONSE_TO_OXIDATIVE_STRESS			X	X
		GO_GANGLIOSIDE_METABOLIC_PROCESS	X			
		GO_GLUCAN_BIOSYNTHETIC_PROCESS	X			X
		GO_GLUCAN_METABOLIC_PROCESS	X		X	X
		GO_GLYCOSYL_COMPOUND_BIOSYNTHETIC_PROCESS			X	X
		GO_GLYCOSYL_COMPOUND_CATABOLIC_PROCESS			X	
		GO_GLYCOSYL_COMPOUND_METABOLIC_PROCESS	X		X	X
		GO_MONOCARBOXYLIC_ACID_BIOSYNTHETIC_PROCESS	X		X	X
		GO_MONOSACCHARIDE_BIOSYNTHETIC_PROCESS			X	
		GO_MONOSACCHARIDE_METABOLIC_PROCESS	X	X	X	X
		GO_MONOSACCHARIDE_TRANSMEMBRANE_TRANSPORT				X
		GO_REGULATION_OF_CARBOHYDRATE_METABOLIC_PROCESS			X	
		GO_REGULATION_OF_CELLULAR_CARBOHYDRATE_METABOLIC_PROCESS			X	
		GO_RESPONSE_TO_CARBOHYDRATE			X	X
		GO_RESPONSE_TO_MONOSACCHARIDE			X	X
		GO_TRICARBOXYLIC_ACID_CYCLE			X	
		GO_TRICARBOXYLIC_ACID_METABOLIC_PROCESS			X	
		KEGG_CARBON_METABOLISM	X		X	
		KEGG_GLYOXYLATE_AND_DICARBOXYLATE_METABOLISM	X		X	
		KEGG_OXIDATIVE_PHOSPHORYLATION		X		
		REACTOME_METABOLISM_OF_CARBOHYDRATES			X	
		WIKI_ELECTRON_TRANSPORT_CHAIN		X		
		WIKI_GLUTATHIONE_AND_ONE_CARBON_METABOLISM	X		X	
		WIKI_ONE_CARBON_METABOLISM	X		X	
		WIKI_ONE_CARBON_METABOLISM_AND_RELATED_PATHWAYS	X		X	

Table A.3: **Oscillating transcript enrichment of Lipid Metabolism pathways.** CORUM, GO, KEGG, Reactome, and Wiki pathway enrichment of oscillating hepatic transcripts related to lipid metabolism within SPF and GF, WT and LKO male mice ($q - value < 0.05$ indicated by X, analysis via Metascape).

			SPF		GF	
			WT	L-KO	WT	L-KO
Lipid Metabolism	Fatty Acids	GO_CELLULAR_KETONE_METABOLIC_PROCESS	X		X	X
		GO_FATTY_ACID_BETA-OXIDATION	X		X	X
		GO_FATTY_ACID_BIOSYNTHETIC_PROCESS	X		X	
		GO_FATTY_ACID_CATABOLIC_PROCESS	X		X	X
		GO_FATTY_ACID_METABOLIC_PROCESS	X		X	X
		GO_FATTY_ACID_OXIDATION	X		X	X
		GO_LONG-CHAIN_FATTY_ACID_METABOLIC_PROCESS			X	
		GO_METHYL-BRANCHED_FATTY_ACID_METABOLIC_PROCESS			X	
		GO_NEGATIVE_REGULATION_OF_FATTY_ACID_METABOLIC_PROCESS	X			X
		GO_REGULATION_OF_CELLULAR_KETONE_METABOLIC_PROCESS	X		X	X
		GO_REGULATION_OF_FATTY_ACID_BETA-OXIDATION			X	X
		GO_REGULATION_OF_FATTY_ACID_METABOLIC_PROCESS	X		X	X
		GO_REGULATION_OF_FATTY_ACID_OXIDATION	X		X	X
		GO_VERY_LONG-CHAIN_FATTY_ACID_METABOLIC_PROCESS			X	
		KEGG_BIOSYNTHESIS_OF_UNSATURATED_FATTY_ACIDS	X			
		KEGG_FATTY_ACID_DEGRADATION			X	
		REACTOME_FATTY_ACID_METABOLISM	X		X	
		REACTOME_ALPHA-LINOLEIC_ACID_(ALA)_METABOLISM	X			
		REACTOME_ALPHA-LINOLEIC_(OMEGA3)_AND_LINOLEIC_(OMEGA6)_ACID_METABOLISM	X			
		REACTOME_LINOLEIC_ACID_(LA)_METABOLISM	X			
		WIKI_FATTY_ACID_BIOSYNTHESIS			X	
	Cholesterol	GO_CHOLESTEROL_BIOSYNTHETIC_PROCESS			X	
		GO_CHOLESTEROL_HOMEOSTASIS	X		X	X
		GO_CHOLESTEROL_METABOLIC_PROCESS			X	
		GO_POSITIVE_REGULATION_OF_CHOLESTEROL_METABOLIC_PROCESS	X		X	
		GO_REGULATION_OF_CHOLESTEROL_METABOLIC_PROCESS			X	
		REACTOME_CHOLESTEROL_BIOSYNTHESIS		X	X	
		REACTOME_CHOLESTEROL_BIOSYNTHESIS_VIA_DESMOSTEROL			X	
		REACTOME_CHOLESTEROL_BIOSYNTHESIS_VIA_LATHOSTEROL			X	
		WIKI_CHOLESTEROL_BIOSYNTHESIS		X	X	
	Bile Acids	GO_BILE_ACID_BIOSYNTHETIC_PROCESS			X	
		GO_BILE_ACID_METABOLIC_PROCESS	X		X	X
		KEGG_BILE_SECRETION	X		X	X
		KEGG_PRIMARY_BILE_ACID_BIOSYNTHESIS			X	
		REACTOME_BILE_ACID_AND_BILE_SALT_METABOLISM			X	
		REACTOME_SYNTHESIS_OF_BILE_ACIDS_AND_BILE_SALTS			X	
		REACTOME_SYNTHESIS_OF_BILE_ACIDS_AND_BILE_SALTS_VIA_24-HYDROXYCHOLESTEROL			X	
		REACTOME_SYNTHESIS_OF_BILE_ACIDS_AND_BILE_SALTS_VIA_7ALPHA-HYDROXYCHOLESTEROL			X	
	Peroxisome	GO_ESTABLISHMENT_OF_PROTEIN_LOCALIZATION_TO_PEROXISOME				X
		GO_PEROXISOMAL_TRANSPORT				X
		GO_PEROXISOME_ORGANIZATION			X	
		GO_PROTEIN_LOCALIZATION_TO_PEROXISOME				X
		GO_PROTEIN_TARGETING_TO_PEROXISOME				X
		KEGG_PEROXISOME	X	X	X	X
		KEGG_PPAR_SIGNALING_PATHWAY	X		X	X
		REACTOME_PEROXISOMAL_LIPID_METABOLISM			X	X
		REACTOME_PEROXISOMAL_PROTEIN_IMPORT			X	X
		WIKI_PPAR_SIGNALING_PATHWAY	X		X	

Table A.3, continued

Lipid Metabolism	(Miscellaneous)	GO_GLYCEROLIPID_METABOLIC_PROCESS		X	X	X
		GO_ACYLGLYCEROL_BIOSYNTHETIC_PROCESS			X	X
		GO_ACYLGLYCEROL_METABOLIC_PROCESS			X	X
		GO_CANALICULAR_BILE_ACID_TRANSPORT				X
		GO_CELLULAR_LIPID_CATABOLIC_PROCESS	X		X	X
		GO_CELLULAR_RESPONSE_TO_STEROID_HORMONE_STIMULUS				X
		GO_CELLULAR_RESPONSE_TO_STEROL			X	X
		GO_DITERPENOID_METABOLIC_PROCESS			X	
		GO_FATTY-ACYL-COA_METABOLIC_PROCESS			X	X
		GO_GLYCEROLIPID_BIOSYNTHETIC_PROCESS		X	X	X
		GO_GLYCEROPHOSPHOLIPID_BIOSYNTHETIC_PROCESS				X
		GO_GLYCEROPHOSPHOLIPID_METABOLIC_PROCESS				X
		GO_GLYCOSPHINGOLIPID_METABOLIC_PROCESS	X			
		GO_ISOPRENOID_METABOLIC_PROCESS			X	
		GO_LIPID_BIOSYNTHETIC_PROCESS	X	X	X	X
		GO_LIPID_CATABOLIC_PROCESS	X		X	X
		GO_LIPID_DROPLET_ORGANIZATION	X		X	
		GO_LIPID_HOMEOSTASIS			X	X
		GO_LIPID_LOCALIZATION	X		X	X
		GO_LIPID_MODIFICATION	X		X	X
		GO_LIPID_OXIDATION	X		X	X
		GO_LIPID_PHOSPHORYLATION				X
		GO_LIPID_STORAGE	X		X	
		GO_LIPID_TRANSPORT	X		X	X
		GO_LIPOPROTEIN_METABOLIC_PROCESS				X
		GO_LONG-CHAIN_FATTY-ACYL-COA_METABOLIC_PROCESS			X	X
		GO_MEMBRANE_LIPID_METABOLIC_PROCESS			X	
		GO_NEGATIVE_REGULATION_OF_GLUCOCORTICOID_RECEPTOR_SIGNALING_PATHWAY	X		X	
		GO_NEGATIVE_REGULATION_OF_LIPID_LOCALIZATION	X		X	
		GO_NEUTRAL_LIPID_BIOSYNTHETIC_PROCESS			X	X
		GO_NEUTRAL_LIPID_CATABOLIC_PROCESS			X	
		GO_NEUTRAL_LIPID_METABOLIC_PROCESS			X	X
		GO_PHOSPHATIDIC_ACID_METABOLIC_PROCESS				X
		GO_PHOSPHATIDYLCHOLINE_BIOSYNTHETIC_PROCESS			X	
		GO_PHOSPHOLIPID_BIOSYNTHETIC_PROCESS		X	X	X
		GO_PHOSPHOLIPID_METABOLIC_PROCESS		X	X	X
		GO_POSITIVE_REGULATION_OF_LIPID_BIOSYNTHETIC_PROCESS	X	X	X	X
		GO_POSITIVE_REGULATION_OF_LIPID_METABOLIC_PROCESS	X		X	X
		GO_POSITIVE_REGULATION_OF_STEROID_METABOLIC_PROCESS	X			
		GO_POSITIVE_REGULATION_OF_TRIGLYCERIDE_BIOSYNTHETIC_PROCESS			X	X
		GO_POSITIVE_REGULATION_OF_TRIGLYCERIDE_METABOLIC_PROCESS			X	X
		GO_REGULATION_OF_LIPID_BIOSYNTHETIC_PROCESS	X	X	X	X
		GO_REGULATION_OF_LIPID_CATABOLIC_PROCESS			X	X
		GO_REGULATION_OF_LIPID_LOCALIZATION	X		X	
		GO_REGULATION_OF_LIPID_METABOLIC_PROCESS	X	X	X	X
		GO_REGULATION_OF_LIPID_TRANSPORT			X	
		GO_REGULATION_OF_PHOSPHOLIPID_METABOLIC_PROCESS				X
		GO_REGULATION_OF_STEROID_METABOLIC_PROCESS		X	X	
		GO_REGULATION_OF_TRIGLYCERIDE_BIOSYNTHETIC_PROCESS			X	X
		GO_REGULATION_OF_TRIGLYCERIDE_METABOLIC_PROCESS			X	X
		GO_RESPONSE_TO_STEROID_HORMONE				X
		GO_RESPONSE_TO_STEROL			X	
		GO_SPHINGOLIPID_CATABOLIC_PROCESS	X			
		GO_SPHINGOLIPID_METABOLIC_PROCESS	X		X	
		GO_STEROID_BIOSYNTHETIC_PROCESS		X	X	
		GO_STEROID_METABOLIC_PROCESS	X	X	X	X
		GO_STEROL_BIOSYNTHETIC_PROCESS			X	
		GO_STEROL_HOMEOSTASIS	X		X	X
		GO_STEROL_METABOLIC_PROCESS			X	
		GO_TERPENOID_METABOLIC_PROCESS			X	
		GO_TRIGLYCERIDE_BIOSYNTHETIC_PROCESS			X	X
		GO_TRIGLYCERIDE_METABOLIC_PROCESS			X	X
		KEGG_GLYCEROLIPID_METABOLISM			X	X
		KEGG_GLYCEROPHOSPHOLIPID_METABOLISM			X	X
		KEGG_PHOSPHATIDYLINOSITOL_SIGNALING_SYSTEM				X
		KEGG_STEROID_BIOSYNTHESIS			X	
		KEGG_TERPENOID_BACKBONE_BIOSYNTHESIS			X	
		KEGG_TRIACYLGLYCEROL_BIOSYNTHESIS			X	X
		REACTOME_FATTY_ACYL-COA_BIOSYNTHESIS			X	
		REACTOME_GLYCEROPHOSPHOLIPID_BIOSYNTHESIS			X	X
		REACTOME_METABOLISM_OF_LIPIDS	X	X	X	X
		REACTOME_METABOLISM_OF_STEROIDS			X	
		REACTOME_PHOSPHOLIPID_METABOLISM			X	X
		REACTOME_SYNTHESIS_OF_VERY_LONG-CHAIN_FATTY_ACYL-COAS	X		X	

Table A.4: **Oscillating transcript enrichment of Protein Metabolism pathways.** CORUM, GO, KEGG, Reactome, and Wiki pathway enrichment of oscillating hepatic transcripts related to protein metabolism within SPF and GF, WT and LKO male mice ($q - value < 0.05$ indicated by X, analysis via Metascape).

			SPF		GF	
			WT	L-KO	WT	L-KO
Protein Metabolism	Proteins	GO_CELLULAR_PROTEIN_CATABOLIC_PROCESS	X	X	X	X
		GO_GLYCOPROTEIN_BIOSYNTHETIC_PROCESS				X
		GO_GLYCOPROTEIN_METABOLIC_PROCESS				X
		GO_LIPOPROTEIN_METABOLIC_PROCESS				X
		GO_MODIFICATION-DEPENDENT_PROTEIN_CATABOLIC_PROCESS		X	X	X
		GO_POSITIVE_REGULATION_OF_CELLULAR_PROTEIN_CATABOLIC_PROCESS				X
		GO_POSITIVE_REGULATION_OF_PROTEIN_CATABOLIC_PROCESS				X
		GO_PROTEASOMAL_PROTEIN_CATABOLIC_PROCESS		X	X	X
		GO_PROTEASOME-MEDIATED_UBIQUITIN-DEPENDENT_PROTEIN_CATABOLIC_PROCESS		X	X	X
		GO_PROTEOLYSIS_INVOLVED_IN_CELLULAR_PROTEIN_CATABOLIC_PROCESS	X	X	X	X
		GO_REGULATION_OF_CELLULAR_PROTEIN_CATABOLIC_PROCESS				X
		GO_REGULATION_OF_LIPOPROTEIN_PARTICLE_CLEARANCE			X	
		GO_REGULATION_OF_PROTEASOMAL_PROTEIN_CATABOLIC_PROCESS				X
		GO_REGULATION_OF_PROTEASOMAL_UBIQUITIN-DEPENDENT_PROTEIN_CATABOLIC_PROCESS				X
		GO_REGULATION_OF_PROTEIN_CATABOLIC_PROCESS			X	X
		GO_REGULATION_OF_PROTEOLYSIS_INVOLVED_IN_CELLULAR_PROTEIN_CATABOLIC_PROCESS				X
		GO_SCF-DEPENDENT_PROTEASOMAL_UBIQUITIN-DEPENDENT_PROTEIN_CATABOLIC_PROCESS				X
		GO_UBIQUITIN-DEPENDENT_PROTEIN_CATABOLIC_PROCESS			X	X
	Peptides AA	GO_ALPHA-AMINO_ACID_BIOSYNTHETIC_PROCESS			X	
		GO_ALPHA-AMINO_ACID_CATABOLIC_PROCESS	X		X	
		GO_ALPHA-AMINO_ACID_METABOLIC_PROCESS	X	X	X	X
		GO_AMINO_ACID_ACTIVATION				X
		GO_AROMATIC_AMINO_ACID_FAMILY_CATABOLIC_PROCESS	X		X	
		GO_ASPARTATE_FAMILY_AMINO_ACID_BIOSYNTHETIC_PROCESS			X	
		GO_ASPARTATE_FAMILY_AMINO_ACID_CATABOLIC_PROCESS			X	
		GO_ASPARTATE_FAMILY_AMINO_ACID_METABOLIC_PROCESS	X		X	
		GO_CELLULAR_AMINO_ACID_BIOSYNTHETIC_PROCESS			X	
		GO_CELLULAR_AMINO_ACID_CATABOLIC_PROCESS	X		X	
		GO_CELLULAR_AMINO_ACID_METABOLIC_PROCESS	X	X	X	X
		GO_CELLULAR_MODIFIED_AMINO_ACID_METABOLIC_PROCESS	X		X	
		GO_CELLULAR_RESPONSE_TO_AMINO_ACID_STARVATION				X
		GO_CELLULAR_RESPONSE_TO_PEPTIDE		X	X	X
		GO_CELLULAR_RESPONSE_TO_PEPTIDE_HORMONE_STIMULUS		X	X	X
		GO_CYSTEINE_CATABOLIC_PROCESS			X	
		GO_CYSTEINE_METABOLIC_PROCESS			X	
		GO_GLUTAMINE_FAMILY_AMINO_ACID_METABOLIC_PROCESS	X			
		GO_GLUTAMINE_METABOLIC_PROCESS				X
		GO_GLYCINE_METABOLIC_PROCESS			X	
		GO_L-CYSTEINE_CATABOLIC_PROCESS			X	
		GO_L-CYSTEINE_METABOLIC_PROCESS			X	
		GO_METHIONINE_BIOSYNTHETIC_PROCESS	X			
		GO_METHIONINE_METABOLIC_PROCESS	X		X	
		GO_NEGATIVE_REGULATION_OF_PROTEIN_SERINE/THREONINE_KINASE_ACTIVITY				X
		GO_ORNITHINE_METABOLIC_PROCESS		X		
		GO_PEPTIDE_BIOSYNTHETIC_PROCESS		X	X	X
		GO_PEPTIDE_HORMONE_SECRETION			X	
		GO_PEPTIDE_SECRETION			X	
		GO_PEPTIDYL-ASPARAGINE_MODIFICATION				X
		GO_PROTEIN_N-LINKED_GLYCOSYLATION_VIA_ASPARAGINE				X
		GO_REGULATION_OF_CYCLIN-DEPENDENT_PROTEIN_SERINE/THREONINE_KINASE_ACTIVITY			X	
		GO_REGULATION_OF_PEPTIDE_HORMONE_SECRETION			X	
		GO_REGULATION_OF_PEPTIDE_TRANSPORT		X	X	X
		GO_RESPONSE_TO_AMINO_ACID_STARVATION			X	X
		GO_RESPONSE_TO_PEPTIDE		X	X	X
		GO_RESPONSE_TO_PEPTIDE_HORMONE		X	X	X
		GO_S-ADENOSYLHOMOCYSTEINE_METABOLIC_PROCESS			X	
		GO_S-ADENOSYLMETHIONINE_METABOLIC_PROCESS			X	
		GO_SERINE_FAMILY_AMINO_ACID_CATABOLIC_PROCESS			X	
		GO_SERINE_FAMILY_AMINO_ACID_METABOLIC_PROCESS	X		X	
		GO_SULFUR_AMINO_ACID_BIOSYNTHETIC_PROCESS	X			
		GO_SULFUR_AMINO_ACID_CATABOLIC_PROCESS			X	
		GO_SULFUR_AMINO_ACID_METABOLIC_PROCESS	X		X	
		GO_TAURINE_METABOLIC_PROCESS			X	
		GO_TRANSMEMBRANE_RECEPTOR_PROTEIN_TYROSINE_KINASE_SIGNALING_PATHWAY				X
		KEGG_ARGININE_BIOSYNTHESIS	X		X	
		KEGG_BIOSYNTHESIS_OF_AMINO_ACIDS	X		X	
		KEGG_CYSTEINE_AND_METHIONINE_METABOLISM	X		X	
		KEGG_GLYCINE,_SERINE_AND_THREONINE_METABOLISM			X	
		KEGG_LYSINE_DEGRADATION			X	
		KEGG_LYSINE_DEGRADATION,_LYSINE_=>_SACCHAROPINE_=>_ACETOACETYL-COA			X	
		KEGG_METHIONINE_DEGRADATION			X	
		KEGG_TRYPTOPHAN_METABOLISM			X	
		REACTOME_ASPARAGINE_N-LINKED_GLYCOSYLATION	X	X	X	X
		REACTOME_GLYOXYLATE_METABOLISM_AND_GLYCINE_DEGRADATION	X			
		REACTOME_METABOLISM_OF_AMINO_ACIDS_AND_DERIVATIVES	X	X	X	X
		REACTOME_OXYGEN-DEPENDENT_PROLINE_HYDROXYLATION_OF_HYPOXIA-INDUCIBLE_FACTOR_ALPHA			X	
		REACTOME_SULFUR_AMINO_ACID_METABOLISM			X	X
		WIKI_TRYPTOPHAN_METABOLISM			X	

Table A.5: **Oscillating transcript enrichment of Nucleotide Metabolism pathways.** CORUM, GO, KEGG, Reactome, and Wiki pathway enrichment of oscillating hepatic transcripts related to nucleotide metabolism within SPF and GF, WT and LKO male mice ($q - value < 0.05$ indicated by X, analysis via Metascape).

		SPF		GF	
		WT	L-KO	WT	L-KO
Nucleotide Metabolism	GO_2'-DEOXYRIBONUCLEOTIDE_METABOLIC_PROCESS			X	
	GO_DEOXYRIBONUCLEOSIDE_MONOPHOSPHATE_METABOLIC_PROCESS	X			
	GO_DEOXYRIBONUCLEOTIDE_METABOLIC_PROCESS			X	
	GO_DNA_BIOSYNTHETIC_PROCESS		X		
	GO_MRNA_CATABOLIC_PROCESS				X
	GO_MRNA_METABOLIC_PROCESS				X
	GO_NCRNA_METABOLIC_PROCESS			X	X
	GO_NICOTINAMIDE_NUCLEOTIDE_BIOSYNTHETIC_PROCESS				X
	GO_NICOTINAMIDE_NUCLEOTIDE_METABOLIC_PROCESS			X	X
	GO_NUCLEAR-TRANSCRIBED_MRNA_CATABOLIC_PROCESS				X
	GO_NUCLEOBASE-CONTAINING_COMPOUND_CATABOLIC_PROCESS			X	X
	GO_NUCLEOBASE-CONTAINING_SMALL_MOLECULE_BIOSYNTHETIC_PROCESS			X	X
	GO_NUCLEOBASE-CONTAINING_SMALL_MOLECULE_METABOLIC_PROCESS	X	X	X	X
	GO_NUCLEOSIDE_BIOSYNTHETIC_PROCESS			X	
	GO_NUCLEOSIDE_BISPHOSPHATE_BIOSYNTHETIC_PROCESS			X	X
	GO_NUCLEOSIDE_BISPHOSPHATE_METABOLIC_PROCESS	X	X	X	X
	GO_NUCLEOSIDE_METABOLIC_PROCESS	X		X	X
	GO_NUCLEOSIDE_MONOPHOSPHATE_METABOLIC_PROCESS		X	X	
	GO_NUCLEOSIDE_PHOSPHATE_BIOSYNTHETIC_PROCESS	X		X	X
	GO_NUCLEOSIDE_PHOSPHATE_METABOLIC_PROCESS	X	X	X	X
	GO_NUCLEOSIDE_TRIPHOSPHATE_METABOLIC_PROCESS		X	X	
	GO_NUCLEOTIDE_BIOSYNTHETIC_PROCESS	X		X	X
	GO_NUCLEOTIDE_METABOLIC_PROCESS	X	X	X	X
	GO_POSITIVE_REGULATION_OF_MRNA_METABOLIC_PROCESS				X
	GO_PTERIDINE-CONTAINING_COMPOUND_METABOLIC_PROCESS			X	
	GO_PURINE_DEOXYRIBONUCLEOSIDE_TRIPHOSPHATE_METABOLIC_PROCESS			X	
	GO_PURINE_DEOXYRIBONUCLEOTIDE_METABOLIC_PROCESS			X	
	GO_PURINE_NUCLEOSIDE_BISPHOSPHATE_BIOSYNTHETIC_PROCESS			X	X
	GO_PURINE_NUCLEOSIDE_BISPHOSPHATE_METABOLIC_PROCESS	X	X	X	X
	GO_PURINE_NUCLEOSIDE_CATABOLIC_PROCESS			X	
	GO_PURINE_NUCLEOSIDE_METABOLIC_PROCESS			X	X
	GO_PURINE_NUCLEOSIDE_MONOPHOSPHATE_METABOLIC_PROCESS		X	X	
	GO_PURINE_NUCLEOSIDE_TRIPHOSPHATE_METABOLIC_PROCESS		X	X	
	GO_PURINE_NUCLEOTIDE_BIOSYNTHETIC_PROCESS			X	X
	GO_PURINE_NUCLEOTIDE_METABOLIC_PROCESS		X	X	X
	GO_PURINE_RIBONUCLEOSIDE_CATABOLIC_PROCESS			X	
	GO_PURINE_RIBONUCLEOSIDE_METABOLIC_PROCESS	X		X	X
	GO_PURINE_RIBONUCLEOSIDE_MONOPHOSPHATE_METABOLIC_PROCESS		X	X	
	GO_PURINE_RIBONUCLEOSIDE_TRIPHOSPHATE_METABOLIC_PROCESS		X	X	
	GO_PURINE_RIBONUCLEOTIDE_BIOSYNTHETIC_PROCESS			X	X
	GO_PURINE_RIBONUCLEOTIDE_METABOLIC_PROCESS		X	X	X
	GO_PURINE-CONTAINING_COMPOUND_BIOSYNTHETIC_PROCESS			X	
	GO_PURINE-CONTAINING_COMPOUND_CATABOLIC_PROCESS			X	
	GO_PURINE-CONTAINING_COMPOUND_METABOLIC_PROCESS	X	X	X	X
	GO_PYRIDINE_NUCLEOTIDE_METABOLIC_PROCESS			X	
	GO_PYRIDINE-CONTAINING_COMPOUND_BIOSYNTHETIC_PROCESS				X
	GO_PYRIDINE-CONTAINING_COMPOUND_METABOLIC_PROCESS	X		X	
	GO_PYRIMIDINE_NUCLEOSIDE_METABOLIC_PROCESS		X		
	GO_PYRIMIDINE-CONTAINING_COMPOUND_BIOSYNTHETIC_PROCESS			X	
	GO_PYRIMIDINE-CONTAINING_COMPOUND_METABOLIC_PROCESS		X		
	GO_REGULATION_OF_DNA_METABOLIC_PROCESS				X
	GO_REGULATION_OF_MRNA_CATABOLIC_PROCESS				X
	GO_REGULATION_OF_MRNA_METABOLIC_PROCESS				X
	GO_RIBONUCLEOSIDE_BIOSYNTHETIC_PROCESS			X	
	GO_RIBONUCLEOSIDE_BISPHOSPHATE_BIOSYNTHETIC_PROCESS			X	X
	GO_RIBONUCLEOSIDE_BISPHOSPHATE_METABOLIC_PROCESS	X	X	X	X
	GO_RIBONUCLEOSIDE_METABOLIC_PROCESS	X		X	X
	GO_RIBONUCLEOSIDE_MONOPHOSPHATE_METABOLIC_PROCESS		X	X	
	GO_RIBONUCLEOSIDE_TRIPHOSPHATE_METABOLIC_PROCESS		X	X	
	GO_RIBONUCLEOTIDE_BIOSYNTHETIC_PROCESS			X	X
	GO_RIBONUCLEOTIDE_METABOLIC_PROCESS		X	X	X
	GO_RNA_CATABOLIC_PROCESS				X
	GO_RNA-DEPENDENT_DNA_BIOSYNTHETIC_PROCESS		X		
	GO_RRNA_METABOLIC_PROCESS			X	X
	GO_TRNA_METABOLIC_PROCESS				X
	KEGG_PURINE_METABOLISM			X	X
	KEGG_PYRIMIDINE_METABOLISM	X			X
	REACTOME_METABOLISM_OF_NUCLEOTIDES	X		X	
	REACTOME_METABOLISM_OF_RNA			X	X
	REACTOME_PURINE_CATABOLISM			X	
	REACTOME_PYRIMIDINE_SALVAGE	X			
	WIKI_PURINE_METABOLISM			X	X

APPENDIX B
SUPPLEMENTAL DATA FOR CHAPTER 4

Table B.1: **Circwave cosinor p-values.**

	Diet			
	RC	HF	RC	HF
	Microbial status			
	SPF		GF	
Gene target	CircWave p-value*			
Bmal1	0.000143	0.000572	6.00E-07	0.000143
Clock	n.s.	n.s.	0.007527	0.007425
Per1	0.008733	n.s.	n.s.	0.02546
Per2	0.001731	0.008238	0.011798	0.014546
Per3	0.00018	0.000197	0.021632	0.000475
Cry1	n.s.	0.02033	0	4.30E-06
Cry2	n.s.	0.048066	0.000561	0.008581
Reg3γ	0.000892	n.s.	0.034354	n.s.
Lyz1	n.s.	n.s.	n.s.	n.s.
Ang4	n.s.	n.s.	n.s.	n.s.
Crypt4	n.s.	n.s.	n.s.	n.s.
Muc2	n.s.	n.s.	0.00331	n.s.
16S rRNA gene copy #	n.s.	-------	n.s.	-------
Reg3β	n.s.	n.s.	0.004168	n.s.
	Diet			
	RC	HF	RC	HF
	Genotype			
	Reg3γ$^{+/-}$		*Reg3γ*$^{-/-}$	
Gene target	CircWave p-value*			
Bmal1	n.s.	n.s.	0.001273	0.001413
Clock	n.s.	n.s.	n.s.	0.000899
Per1	n.s.	n.s.	n.s.	0.031957
Per2	n.s.	n.s.	n.s.	n.s.
Per3	n.s.	0.015857	n.s.	0.003686
Cry1	0.022799	0.021941	n.s.	n.s.
Cry2	n.s.	n.s.	n.s.	n.s.
Reg3γ	1.70E-06	n.s.	n.s.	n.s.
Lyz1	n.s.	n.s.	0.0469	n.s.
Ang4	n.s.	n.s.	n.s.	n.s.
Crypt4	n.s.	n.s.	n.s.	n.s.
Muc2	2.28E-05	n.s.	n.s.	n.s.
16S rRNA gene copy #	n.s.	n.s.	0.0367	n.s.

*Significant co-sinor expression pattern indicated by $p < 0.05$
n.s. = Not significant

Table B.2: **Adonis and ANOSIM R statistics and p-values.** β-diversity analyses between distal ileum luminal contents from RC and HF-fed WT mice, and from distal ileum luminal contents and mucosal scrapings from RC and HF-fed *Reg3γ*$^{+/-}$ and *Reg3γ*$^{-/-}$ mice.

	Canberra: WT RC vs HF				**Bray Curtis: WT RC vs HF**			
Luminal contents	adonis		ANOSIM		adonis		ANOSIM	
	R^2	P value	R	P value	R^2	P value	R	P value
	0.372	0.001	0.862	0.001	0.371	0.001	0.657	0.001

	Bray Curtis: RC *Reg3γ*$^{+/-}$, *Reg3γ*$^{-/-}$ vs HF *Reg3γ*$^{+/-}$, *Reg3γ*$^{-/-}$			
	adonis		ANOSIM	
	R^2	P value	R	P value
	0.2253	0.001	0.3426	0.001

	Bray Curtis: RC, *Reg3γ*$^{+/-}$ vs *Reg3γ*$^{-/-}$				**Bray Curtis: HF, *Reg3γ*$^{+/-}$ vs *Reg3γ*$^{-/-}$**			
Luminal contents	adonis		ANOSIM		adonis		ANOSIM	
	R^2	P value	R	P value	R^2	P value	R	P value
	0.0653	0.003	0.1064	0.0089	0.0234	0.328	0.0086	0.28

	Bray Curtis: *Reg3γ*$^{+/-}$, RC vs HF				**Bray Curtis: *Reg3γ*$^{-/-}$, RC vs HF**			
	adonis	ANOSIM	adonis	ANOSIM				
	R^2	P value	R	P value	R^2	P value	R	P value
	0.2127	0.001	0.532	0.001	0.194	0.001	0.4215	0.001

	Bray Curtis: RC *Reg3γ*$^{+/-}$, *Reg3γ*$^{-/-}$ vs HF *Reg3γ*$^{+/-}$, *Reg3γ*$^{-/-}$			
	adonis		ANOSIM	
	R^2	P value	R	P value
	0.1691	0.001	0.2786	0.001

	Bray Curtis: RC, *Reg3γ*$^{+/-}$ vs *Reg3γ*$^{-/-}$				**Bray Curtis: HF, *Reg3γ*$^{+/-}$ vs *Reg3γ*$^{-/-}$**			
Mucosal scrapings	adonis		ANOSIM		adonis		ANOSIM	
	R^2	P value	R	P value	R^2	P value	R	P value
	0.032	0.136	0.0297	0.148	0.0211	0.4	0.0015	0.38

	Bray Curtis: *Reg3γ*$^{+/-}$, RC vs HF				**Bray Curtis: *Reg3γ*$^{-/-}$, RC vs HF**			
	adonis		ANOSIM		adonis		ANOSIM	
	R^2	P value	R	P value	R^2	P value	R	P value
	0.166	0.001	0.4465	0.001	0.1408	0.001	0.3364	0.001

Table B.3: **OTU relative abundance.** Statistical analysis of OTU relative abundances in distal ileum luminal contents from RC and HF-fed WT mice, and RC and HF-fed *Reg3γ*$^{+/-}$ and *Reg3γ*$^{-/-}$ mice, determined via ANOVA. OTUs exhibiting Bonferroni P-value less than 0.05 are shown.

Taxonomy	OTU ID	Test-stat	FDR P-value	Bonferroni P-value	RC mean relative abundance	HF mean relative abundance
p__Firmicutes; c__Clostridia; o__Clostridiales; f__Clostridiaceae	270200	91.2795535	1.15E-07	1.15E-07	0.06666667	8.5
p__Firmicutes; c__Clostridia; o__Clostridiales	270382	2.14E-08	4.44E-06	1.33E-05	0.13333333	17.125
p__Firmicutes; c__Clostridia; o__Clostridiales; f__Clostridiaceae	272964	42.5045951	4.03E-05	0.00024152	0	11.125
p__Firmicutes; c__Clostridia; o__Clostridiales; f__Clostridiaceae	308802	40.5376344	5.22E-05	0.0003651	0	19.5
p__Firmicutes; c__Clostridia; o__Clostridiales; f__Clostridiaceae	297143	39.8811545	5.25E-05	0.00042022	0	13.5
p__Firmicutes; c__Clostridia; o__Clostridiales; f__Clostridiaceae	555945	38.0056438	6.33E-05	0.0006329	14.6666667	10293.0625
p__Firmicutes; c__Clostridia; o__Clostridiales; f__Peptostreptococcaceae	299474	37.4706922	6.48E-05	0.00071287	0	78.6875
p__Firmicutes; c__Clostridia; o__Clostridiales; f__Peptostreptococcaceae	198209	36.5559682	6.97E-05	0.00087576	0	18.5
p__Firmicutes; c__Clostridia; o__Clostridiales; f__Peptostreptococcaceae	180516	36.403972	6.97E-05	0.00090649	0	6.75
p__Firmicutes; c__Clostridia; o__Clostridiales; f__Clostridiaceae	189407	35.3035256	8.33E-05	0.0011665	0	16.1875
p__Firmicutes; c__Clostridia; o__Clostridiales; f__Peptostreptococcaceae	2658058	34.261319	9.92E-05	0.00148741	0	22.5625
p__Firmicutes; c__Clostridia; o__Clostridiales; f__Peptostreptococcaceae	262060	33.8324487	0.00010182	0.00164586	0.13333333	27.8125
p__Firmicutes; c__Clostridia; o__Clostridiales; f__Clostridiaceae	4396655	33.6200207	0.00010182	0.00173095	0	8.3125
p__Firmicutes; c__Clostridia; o__Clostridiales; f__Clostridiaceae	199268	32.5943636	0.0001165	0.00221353	0	12.9375
p__Firmicutes; c__Clostridia; o__Clostridiales; f__Peptostreptococcaceae	4380137	31.8914956	0.00013132	0.00262637	0	7.5
p__Firmicutes; c__Clostridia; o__Clostridiales; f__Clostridiaceae	191803	30.2844404	0.00017017	0.0039139	0	18
p__Firmicutes; c__Clostridia; o__Clostridiales; f__Clostridiaceae	4238179	29.2910551	0.00018657	0.00503728	6.2	77.8125
p__Firmicutes; c__Clostridia; o__Clostridiales; f__Peptostreptococcaceae	531374	28.4401959	0.00020918	0.00627536	0	5.1875
p__Firmicutes; c__Clostridia; o__Clostridiales; f__Peptostreptococcaceae	514988	27.5382615	0.0002565	0.00795165	0.13333333	19.625
p__Firmicutes; c__Clostridia; o__Clostridiales	316496	26.8123327	0.00030153	0.00964901	0.13333333	22.4375
p__Firmicutes; c__Clostridia; o__Clostridiales; f__Clostridiaceae	331881	26.6387914	0.00030636	0.01010979	0.06666667	8.6875
p__Firmicutes; c__Clostridia; o__Clostridiales; f__Peptostreptococcaceae	322840	25.7399593	0.00036872	0.01290507	0	28.5625
p__Bacteroidetes; c__Bacteroidia; o__Bacteroidales; f__S24-7	211761	25.1705115	0.00041936	0.01509705	14.8	3.1875
p__Firmicutes; c__Clostridia; o__Clostridiales; f__Peptostreptococcaceae	1896700	24.1234347	0.00051895	0.02023918	0	3.875
p__Firmicutes; c__Clostridia; o__Clostridiales	248126	23.2327365	0.00060792	0.0260987	0	11.8125
p__Bacteroidetes; c__Bacteroidia; o__Bacteroidales; f__S24-7	445144	23.0523244	0.00060975	0.02749365	6785.86667	1321.375
p__Bacteroidetes; c__Bacteroidia; o__Bacteroidales; f__S24-7	331720	22.9832477	0.00060975	0.02804873	242.066667	64
p__Firmicutes; c__Clostridia; o__Clostridiales; f__Peptostreptococcaceae	347714	22.7885602	0.0006251	0.02967879	0	9.9375
p__Firmicutes; c__Clostridia; o__Clostridiales; f__Clostridiaceae; g__Clostridium	235424	21.4259046	0.000837	0.04436084	0.4	191.75
p__Firmicutes; c__Clostridia; o__Clostridiales; f__Clostridiaceae	575768	21.3329183	0.0008447	0.04561388	5.06666667	18.625

Table B.3, continued

Taxonomy	OTU ID	Test-stat	FDR P-value	Bonferroni P-value	*Reg3γ*$^{+/-}$ RC mean relative abundance	*Reg3γ*$^{+/-}$ HF mean relative abundance	*Reg3γ*$^{-/-}$ RC mean relative abundance	*Reg3γ*$^{-/-}$ HF mean relative abundance
p__Firmicutes; c__Clostridia; o__Clostridiales; f__Clostridiaceae	555945	20.247	4.39E-07	4.39E-07	47.04	660.68	8.67	385.55
p__Firmicutes; c__Bacilli; o__Lactobacillales; f__Streptococcaceae; g__Lactococcus	716006	16.191	8.23E-06	1.82E-05	50.04	1117.48	14.08	933.09
p__Firmicutes; c__Clostridia; o__Clostridiales; f__Peptostreptococcaceae	198209	15.642	8.23E-06	3.08E-05	0.17	5.84	0.17	3.82
p__Firmicutes; c__Clostridia; o__Clostridiales; f__Peptostreptococcaceae	180516	15.497	8.23E-06	3.54E-05	0.48	6.6	0.17	3.14
p__Firmicutes; c__Clostridia; o__Clostridiales; f__Clostridiaceae	191803	15.342	8.23E-06	4.12E-05	0.13	1.8	0	0.45
p__Firmicutes; c__Bacilli; o__Lactobacillales; f__Streptococcaceae; g__Lactococcus	4468805	14.900	1.06E-05	6.34E-05	0.26	4.92	0	4.73
p__Firmicutes; c__Clostridia; o__Clostridiales	248126	14.315	1.61E-05	0.00011	0.04	2	0	1
p__Firmicutes; c__Bacilli; o__Lactobacillales; f__Streptococcaceae; g__Lactococcus	513080	14.065	1.64E-05	0.00014	0.26	6.96	0.17	5.55
p__Proteobacteria; c__Betaproteobacteria; o__Burkholderiales; f__Alcaligenaceae; g__Sutterella	359809	14.047	1.64E-05	0.00015	12.52	0.68	32.79	3.95
p__Firmicutes; c__Clostridia; o__Clostridiales; f__Clostridiaceae	199268	13.512	2.52E-05	0.00025	0.04	1.56	0.04	0.86
p__Firmicutes; c__Clostridia; o__Clostridiales; f__Peptostreptococcaceae	347714	13.172	3.10E-05	0.00036	0.13	1.68	0	1.09
p__Firmicutes; c__Bacilli; o__Lactobacillales; f__Streptococcaceae; g__Lactococcus	571744	13.068	3.10E-05	0.00040	0.13	2.08	0	2.27
p__Firmicutes; c__Bacilli; o__Lactobacillales; f__Streptococcaceae; g__Lactococcus	1523543	13.050	3.10E-05	0.00040	0	2.48	0	2.41
p__Firmicutes; c__Clostridia; o__Clostridiales; f__Peptostreptococcaceae	514988	12.659	4.02E-05	0.00060	0.09	2.4	0	1.41
p__Bacteroidetes; c__Bacteroidia; o__Bacteroidales; f__S24-7	270984	12.658	4.02E-05	0.00060	14.74	1.28	27.13	4.09
p__Bacteroidetes; c__Bacteroidia; o__Bacteroidales; f__S24-7	416078	12.443	4.71E-05	0.00075	36.30	1	41.17	7.36
p__Bacteroidetes; c__Bacteroidia; o__Bacteroidales; f__S24-7	465480	12.118	6.07E-05	0.00105	0.57	0	2.04	0.09
p__Firmicutes; c__Clostridia; o__Clostridiales; f__Peptostreptococcaceae	178364	12.053	6.07E-05	0.00112	0.17	1.52	0	0.64

Table B.3, continued

p__Firmicutes; c__Bacilli; o__Lactobacillales; f__Streptococcaceae; g__Lactococcus	586387	12.033	6.07E-05	0.00115	0.17	3.08	0	2.55
p__Bacteroidetes; c__Bacteroidia; o__Bacteroidales; f__S24-7	355746	11.715	8.03E-05	0.00161	45.87	2.52	61.96	8.18
p__Firmicutes; c__Clostridia; o__Clostridiales; f__Peptostreptococcaceae	322840	11.517	9.42E-05	0.00198	0.26	2.68	0	1.5
p__Bacteroidetes; c__Bacteroidia; o__Bacteroidales; f__S24-7	315430	11.258	0.0001183	0.00260	18.61	1.04	30.21	6.23
p__Firmicutes; c__Bacilli; o__Lactobacillales; f__Streptococcaceae; g__Lactococcus	345575	11.116	0.0001316	0.00303	0.17	2.44	0	2.86
p__Firmicutes; c__Clostridia; o__Clostridiales; f__Clostridiaceae	272964	10.653	0.0002068	0.00496	0.13	1.16	0	1.05
p__Firmicutes; c__Clostridia; o__Clostridiales; f__Peptostreptococcaceae	2658058	10.583	0.0002143	0.00536	0.04	1.44	0.08	0.73
p__Bacteroidetes; c__Bacteroidia; o__Bacteroidales; f__S24-7	421792	10.427	0.0002438	0.00634	89.91	2.2	106.79	16.41
p__Firmicutes; c__Bacilli; o__Lactobacillales; f__Streptococcaceae; g__Lactococcus	316321	10.330	0.0002606	0.00704	0.13	2.84	0.04	2.32
p__Firmicutes; c__Bacilli; o__Lactobacillales; f__Lactobacillaceae; g__Lactobacillus	604966	10.285	0.0002637	0.00739	10.91	0.56	10.96	2
p__Firmicutes; c__Bacilli; o__Lactobacillales; f__Lactobacillaceae; g__Lactobacillus; s__reuteri	692154	10.208	0.0002678	0.00803	15.13	0.52	18	2
p__Bacteroidetes; c__Bacteroidia; o__Bacteroidales; f__S24-7	453896	10.208	0.0002678	0.00804	32.91	2.96	57.42	9.09
p__Firmicutes; c__Bacilli; o__Lactobacillales; f__Streptococcaceae; g__Lactococcus	288680	9.598	0.0005047	0.015647	0	2.2	0	1.86
p__Firmicutes; c__Clostridia; o__Clostridiales; f__Peptostreptococcaceae	4380137	9.291	0.0006861	0.02196	0	0.8	0	0.23
p__Firmicutes; c__Bacilli; o__Lactobacillales; f__Lactobacillaceae; g__Lactobacillus; s__reuteri	588197	9.229	0.0007129	0.02353	4.04	0.52	5.54	0.86
p__Bacteroidetes; c__Bacteroidia; o__Bacteroidales; f__S24-7	195919	9.164	0.0007435	0.02528	4.39	2.92	19	6.14
p__Firmicutes; c__Bacilli; o__Lactobacillales; f__Lactobacillaceae; g__Lactobacillus	1107027	8.845	0.0010308	0.03608	530.17	134.76	101.54	161.55
p__Firmicutes; c__Clostridia; o__Clostridiales; f__Clostridiaceae	189407	8.606	0.0012965	0.04715	0.22	1.4	0	0.82
p__Bacteroidetes; c__Bacteroidia; o__Bacteroidales; f__S24-7	331720	8.591	0.0012965	0.04797	0.74	0	1.38	0.23

Table B.4: **eJTK OTU rhythmicity.** eJTK oscillation analysis of OTUS identified in luminal contents of RC and HF-fed SPF WT mice, and RC and HF-fed *Reg3γ*$^{+/-}$ and *Reg3γ*$^{-/-}$ mice.

Diet	Taxonomy	OTU_ID	Phase	Mean	Std_Dev	Max	Min	Max_Amp	Tau	P	GammaP	GammaBH
						p < 0.05						
RC	p__Firmicutes; c__Clostridia; o__Clostridiales; f__Clostridiaceae	225316	0	0.867	1.087	3	0	3	0.758	4.13E-05	0.0006	0.081
	p__Firmicutes; c__Clostridia; o__Clostridiales; f__Lachnospiraceae	345709	16	54.067	94.339	339	0	339	0.736	6.52E-05	0.0009	0.081
	p__Firmicutes; c__Bacilli; o__Lactobacillales; f__Lactobacillaceae; g__Lactobacillus	182764	0	90.4	93.203	263	0	263	0.718	9.45E-05	0.0009	0.081
	p__Firmicutes; c__Clostridia; o__Clostridiales	459276	16	6.467	16.796	68	0	68	0.674	0.0002	0.0035	0.081
	p__Firmicutes; c__Clostridia; o__Clostridiales	406247	20	2.067	2.977	10	0	10	0.672	0.0002	0.0036	0.081
	p__Firmicutes; c__Clostridia; o__Clostridiales	1108078	16	3.4	5.401	18	0	18	0.637	0.0005	0.0039	0.081
	p__Firmicutes; c__Clostridia; o__Clostridiales; f__Clostridiaceae	256232	0	0.933	1.526	5	0	5	0.661	0.0003	0.0039	0.081
	p__Firmicutes; c__Clostridia; o__Clostridiales; f__Lachnospiraceae; g__Coprococcus	1105328	12	0.667	1.135	3	0	3	0.629	0.0005	0.0039	0.081
	p__Firmicutes; c__Clostridia; o__Clostridiales	340650	16	0.8	1.833	7	0	7	0.637	0.0005	0.0039	0.081
	p__Firmicutes; c__Clostridia; o__Clostridiales	346719	16	10	19.61	70	0	70	0.637	0.0005	0.0039	0.081
	p__Firmicutes; c__Clostridia; o__Clostridiales; f__Ruminococcaceae	375106	16	0.933	1.769	7	0	7	0.63	0.0005	0.0039	0.081
	p__Firmicutes; c__Clostridia; o__Clostridiales	400599	16	1.333	3.36	13	0	13	0.637	0.0005	0.0039	0.081
	p__Firmicutes; c__Clostridia; o__Clostridiales; f__Lachnospiraceae	355175	16	2.933	4.509	16	0	16	0.654	0.0003	0.0039	0.081
	p__Firmicutes; c__Clostridia; o__Clostridiales; f__Ruminococcaceae	346804	16	0.667	1.491	6	0	6	0.621	0.0006	0.0039	0.081
	p__Firmicutes; c__Clostridia; o__Clostridiales; f__Ruminococcaceae; g__Ruminococcus	278098	20	2	2.658	8	0	8	0.634	0.0005	0.0039	0.081
	p__Firmicutes; c__Clostridia; o__Clostridiales; f__Lachnospiraceae	355771	16	9.4	22.633	81	0	81	0.629	0.0005	0.0039	0.081
	p__Firmicutes; c__Clostridia; o__Clostridiales	307170	16	3.533	7.89	31	0	31	0.654	0.0003	0.0039	0.081
	p__Firmicutes; c__Clostridia; o__Clostridiales	335267	16	0.933	1.948	7	0	7	0.631	0.0005	0.0039	0.081
	p__Firmicutes; c__Clostridia; o__Clostridiales	1571092	16	7.867	16.095	63	0	63	0.611	0.0008	0.0079	0.114
	p__Firmicutes; c__Clostridia; o__Clostridiales	826541	16	2.933	3.415	10	0	10	0.615	0.0007	0.0079	0.114
	p__Firmicutes; c__Bacilli; o__Turicibacterales; f__Turicibacteraceae; g__Turicibacter	347529	4	2.133	1.31	4	0	4	0.605	0.0008	0.0079	0.114
	p__Firmicutes; c__Clostridia; o__Clostridiales; f__Ruminococcaceae; g__Oscillospira	307608	20	1.067	2.323	8	0	8	0.598	0.0009	0.0079	0.114
	p__Tenericutes; c__Mollicutes; o__Anaeroplasmatales; f__Anaeroplasmataceae; g__Anaeroplasma	252684	16	1.467	4.485	18	0	18	0.598	0.0009	0.0079	0.114
	p__Firmicutes; c__Clostridia; o__Clostridiales; f__Lachnospiraceae	344726	0	6.267	9.692	33	0	33	0.579	0.0013	0.0129	0.129
	p__Firmicutes; c__Clostridia; o__Clostridiales	697874	16	1.8	3.468	11	0	11	0.594	0.001	0.0129	0.129
	p__Firmicutes; c__Clostridia; o__Clostridiales; f__Lachnospiraceae; g__Anaerostipes	534926	16	7.4	13.908	56	0	56	0.588	0.0011	0.0129	0.129
	p__Firmicutes; c__Clostridia; o__Clostridiales	229452	16	18.667	49.076	198	0	198	0.579	0.0013	0.0129	0.129
	p__Firmicutes; c__Clostridia; o__Clostridiales	1106614	16	16.667	29.236	98	0	98	0.585	0.0012	0.0129	0.129
	p__Firmicutes; c__Clostridia; o__Clostridiales; f__Lachnospiraceae	305012	16	3.867	7.745	30	0	30	0.595	0.001	0.0129	0.129
	p__Firmicutes; c__Clostridia; o__Clostridiales	408877	16	5.133	11.871	45	0	45	0.579	0.0013	0.0129	0.129
	p__Firmicutes; c__Clostridia; o__Clostridiales	345862	16	8.333	12.451	37	0	37	0.578	0.0013	0.0129	0.129

Table B.4, continued

RC (cont'd)	p__Firmicutes; c__Clostridia; o__Clostridiales	356590	16	15.933	21.947	75	0	75	0.581	0.0013	0.0129	0.129
	k__Bacteria; p__Cyanobacteria; c__Chloroplast; o__Streptophyta	3541	0	7.133	12.516	41	0	41	0.561	0.0018	0.0219	0.2
	p__Firmicutes; c__Clostridia; o__Clostridiales; f__Ruminococcaceae; g__Oscillospira	328905	16	0.867	1.628	6	0	6	0.567	0.0016	0.0219	0.2
	p__Firmicutes; c__Clostridia; o__Clostridiales; f__Ruminococcaceae	331737	16	5.8	11.594	45	0	45	0.555	0.002	0.0292	0.259
	p__Firmicutes; c__Clostridia; o__Clostridiales	1112121	20	16.333	57.426	231	0	231	0.553	0.002	0.0302	0.26
	p__Firmicutes; c__Clostridia; o__Clostridiales; f__Lachnospiraceae	316946	16	1.4	3.46	13	0	13	0.548	0.0022	0.0331	0.26
	p__Firmicutes; c__Clostridia; o__Clostridiales; f__Ruminococcaceae	170926	20	1.067	2.62	10	0	10	0.548	0.0022	0.0331	0.26
	p__Firmicutes; c__Clostridia; o__Clostridiales; f__Ruminococcaceae	434089	0	4.4	8.732	33	0	33	0.541	0.0025	0.0359	0.26
	p__Firmicutes; c__Clostridia; o__Clostridiales; f__Ruminococcaceae; g__Oscillospira	277588	16	0.467	1.258	5	0	5	0.538	0.0026	0.0359	0.26
	p__Firmicutes; c__Clostridia; o__Clostridiales; f__Ruminococcaceae	1110008	16	3.533	7.374	28	0	28	0.541	0.0025	0.036	0.26
	p__Firmicutes; c__Clostridia; o__Clostridiales; f__Ruminococcaceae	318370	16	2	4.131	16	0	16	0.54	0.0025	0.036	0.26
	p__Firmicutes; c__Clostridia; o__Clostridiales	343581	16	12.467	27.131	99	0	99	0.535	0.0027	0.0408	0.269
	p__Firmicutes; c__Clostridia; o__Clostridiales; f__Lachnospiraceae;	354163	20	12.8	20.582	69	0	69	0.534	0.0028	0.0413	0.269
	p__Firmicutes; c__Clostridia; o__Clostridiales; f__Ruminococcaceae; g__Oscillospira	345582	16	1.533	3.775	14	0	14	0.531	0.0029	0.0432	0.269
	p__Firmicutes; c__Clostridia; o__Clostridiales; f__Clostridiaceae	555945	12	14.667	26.81	113	1	113	0.531	0.0029	0.0433	0.269
	p__Firmicutes; c__Clostridia; o__Clostridiales	382220	16	7.333	20.758	83	0	83	0.529	0.003	0.0447	0.269
	p__Firmicutes; c__Clostridia; o__Clostridiales	377946	16	1.667	3.36	11	0	11	0.528	0.003	0.0456	0.269
	p__Firmicutes; c__Clostridia; o__Clostridiales; f__Lachnospiraceae; g__Coprococcus	653533	16	15.267	18.234	61	0	61	0.527	0.0031	0.0464	0.269
	p__Firmicutes; c__Clostridia; o__Clostridiales; f__Ruminococcaceae; g__Oscillospira	167509	16	2.667	9.714	39	0	39	0.519	0.0035	0.0499	0.269
	p__Firmicutes; c__Clostridia; o__Clostridiales	747987	16	1.133	2.276	8	0	8	0.518	0.0035	0.0499	0.269
	p__Firmicutes; c__Clostridia; o__Clostridiales	197290	16	1.2	2.663	10	0	10	0.522	0.0033	0.0499	0.269
	p__Firmicutes; c__Clostridia; o__Clostridiales; f__Ruminococcaceae; g__Oscillospira	327808	16	0.733	1.123	3	0	3	0.517	0.0036	0.0499	0.269
HF	p__Firmicutes; c__Erysipelotrichi; o__Erysipelotrichales; f__Erysipelotrichaceae	167420	0	3.875	7.432	28	0	28	0.684	0.0001	0.0016	0.444
	p__Firmicutes; c__Bacilli; o__Lactobacillales; f__Lactobacillaceae; g__Lactobacillus	306306	12	2.938	3.03	11	0	11	0.582	0.0008	0.0124	0.693
	p__Bacteroidetes; c__Bacteroidia; o__Bacteroidales; f__S24-7	271131	0	1.875	2.058	6	0	6	0.552	0.0014	0.0214	0.693
	p__Firmicutes; c__Clostridia; o__Clostridiales; f__Ruminococcaceae; g__Oscillospira	277588	16	1.438	4.808	20	0	20	0.53	0.0021	0.0312	0.693
	p__Firmicutes; c__Clostridia; o__Clostridiales; f__Lachnospiraceae	352559	0	5.125	12.639	53	0	53	0.508	0.003	0.0453	0.693
	p__Firmicutes; c__Clostridia; o__Clostridiales; f__Lachnospiraceae	345536	4	1	2.208	9	0	9	0.503	0.0033	0.0495	0.693

Table B.4, continued

Diet	Taxonomy	OTU_ID	Phase	Mean	Std_Dev	Max	Min	Max_Amp	Tau	P	GammaP	GammaBH
	p = 0.05 – 0.1											
RC	p__Bacteroidetes; c__Bacteroidia; o__Bacteroidales; f__S24-7	445144	16	6785.867	4072.125	12745	103	12642	0.516	0.0037	0.0549	0.285
	p__Firmicutes; c__Erysipelotrichi; o__Erysipelotrichales; f__Erysipelotrichaceae	167420	16	6.733	6.486	21	0	21	0.516	0.0037	0.0551	0.285
	p__Firmicutes; c__Clostridia; o__Clostridiales	348404	20	4.933	7.602	28	0	28	0.516	0.0037	0.0554	0.285
	p__Firmicutes; c__Clostridia; o__Clostridiales	628218	16	2.2	7.204	29	0	29	0.515	0.0037	0.0561	0.285
	p__Firmicutes; c__Clostridia; o__Clostridiales; f__Ruminococcaceae; g__Oscillospira	276985	16	4.667	10.593	42	0	42	0.51	0.004	0.0594	0.29
	p__Firmicutes; c__Clostridia; o__Clostridiales; f__Ruminococcaceae; g__Oscillospira	1110378	0	7.667	15.023	59	0	59	0.503	0.0045	0.0645	0.29
	p__Firmicutes; c__Clostridia; o__Clostridiales; f__Clostridiaceae	3358082	0	1	1.317	4	0	4	0.498	0.0049	0.0659	0.29
	p__Firmicutes; c__Bacilli; o__Lactobacillales; f__Lactobacillaceae; g__Lactobacillus	549756	20	1.2	1.869	6	0	6	0.498	0.0048	0.0659	0.29
	p__Firmicutes; c__Bacilli; o__Bacillales; f__Staphylococcaceae; g__Staphylococcus; s__soluri	1084865	12	6.467	9.763	33	0	33	0.5	0.0047	0.0659	0.29
	p__Firmicutes; c__Clostridia; o__Clostridiales; f__Lachnospiraceae	262104	16	1.533	3.442	12	0	12	0.499	0.0048	0.0659	0.29
	p__Firmicutes; c__Clostridia; o__Clostridiales	194662	16	3.733	10.408	42	0	42	0.499	0.0048	0.0659	0.29
	p__Firmicutes; c__Clostridia; o__Clostridiales; f__Lachnospiraceae	258202	12	2.467	3.538	11	0	11	0.495	0.005	0.0702	0.302
	p__Firmicutes; c__Clostridia; o__Clostridiales	309054	16	2.067	3.82	14	0	14	0.495	0.005	0.0703	0.302
	p__Firmicutes; c__Bacilli; o__Lactobacillales; f__Lactobacillaceae; g__Lactobacillus	590168	12	3.067	4.864	18	0	18	0.492	0.0053	0.073	0.308
	p__Firmicutes; c__Clostridia; o__Clostridiales	327284	16	4.933	12.678	51	0	51	0.49	0.0054	0.0743	0.309
	p__Firmicutes; c__Clostridia; o__Clostridiales	564961	16	0.867	2.729	11	0	11	0.488	0.0056	0.0764	0.309
	p__Firmicutes; c__Clostridia; o__Clostridiales; f__Ruminococcaceae	343140	16	8.933	16.723	66	0	66	0.488	0.0056	0.0766	0.309
	p__Firmicutes; c__Clostridia; o__Clostridiales; f__Lachnospiraceae	759751	16	11.067	23.245	92	0	92	0.484	0.006	0.0801	0.309
	p__Firmicutes; c__Clostridia; o__Clostridiales; f__Lachnospiraceae	1076587	20	4.933	7.818	31	0	31	0.484	0.006	0.0801	0.309
	p__Firmicutes; c__Clostridia; o__Clostridiales; f__Ruminococcaceae	275218	16	1.933	5.285	21	0	21	0.482	0.0062	0.082	0.309
	p__Proteobacteria; c__Alphaproteobacteria; o__Rickettsiales; f__mitochondria	1892252	16	9.533	24.857	100	0	100	0.481	0.0062	0.0825	0.309
	p__Firmicutes; c__Clostridia; o__Clostridiales	434339	16	2.533	4.064	16	0	16	0.481	0.0062	0.0826	0.309
	p__Firmicutes; c__Clostridia; o__Clostridiales; f__Ruminococcaceae; g__Oscillospira	180235	16	1.2	1.869	6	0	6	0.48	0.0063	0.0834	0.31
	p__Firmicutes; c__Clostridia; o__Clostridiales	339718	20	2.4	6.888	28	0	28	0.476	0.0067	0.0869	0.313
	p__Firmicutes; c__Clostridia; o__Clostridiales	351062	20	7	11.736	44	0	44	0.476	0.0067	0.0869	0.313
	p__Firmicutes; c__Clostridia; o__Clostridiales	336276	16	7.2	12.357	43	0	43	0.475	0.0068	0.0879	0.313
	p__Firmicutes; c__Clostridia; o__Clostridiales	351859	20	6	8.989	26	0	26	0.475	0.0068	0.0879	0.313
	p__Firmicutes; c__Clostridia; o__Clostridiales; f__Clostridiaceae	342504	16	0.467	0.618	2	0	2	0.472	0.007	0.0905	0.315
	p__Firmicutes; c__Clostridia; o__Clostridiales; f__Ruminococcaceae; g__Ruminococcus	327900	20	4.267	9.896	38	0	38	0.472	0.007	0.0905	0.315
	p__Firmicutes; c__Clostridia; o__Clostridiales	272949	16	9.867	28.234	113	0	113	0.469	0.0074	0.0937	0.321
	p__Firmicutes; c__Clostridia; o__Clostridiales	458550	0	11.133	10.831	36	0	36	0.467	0.0077	0.0964	0.326

Table B.4, continued

HF	p__Firmicutes; c__Clostridia; o__Clostridiales; f__Ruminococcaceae; g__Oscillospira	408513	16	22.125	39.141	159	1	158	0.496	0.0037	0.0556	0.693
	p__Firmicutes; c__Clostridia; o__Clostridiales	356590	16	0.375	0.696	2	0	2	0.485	0.0044	0.066	0.693
	p__Firmicutes; c__Clostridia; o__Clostridiales; f__Lachnospiraceae	355175	16	0.125	0.331	1	0	1	0.477	0.005	0.0744	0.693
	p__Firmicutes; c__Clostridia; o__Clostridiales	461487	16	0.188	0.527	2	0	2	0.469	0.0056	0.0847	0.693
	p__Firmicutes; c__Clostridia; o__Clostridiales; f__Lachnospiraceae	355822	16	0.313	0.982	4	0	4	0.469	0.0056	0.0847	0.693
	p__Firmicutes; c__Clostridia; o__Clostridiales	346764	20	0.75	2.437	10	0	10	0.469	0.0056	0.0847	0.693
	p__Firmicutes; c__Clostridia; o__Clostridiales; f__Ruminococcaceae; g__Ruminococcus	278098	20	0.563	0.788	2	0	2	0.468	0.0058	0.0863	0.693
	p__Firmicutes; c__Clostridia; o__Clostridiales	458550	12	0.625	1.364	5	0	5	0.467	0.0058	0.0873	0.693
	p__Firmicutes; c__Clostridia; o__Clostridiales; f__Lachnospiraceae	457614	16	1.375	1.798	7	0	7	0.466	0.0059	0.0889	0.693
	p__Firmicutes; c__Clostridia; o__Clostridiales; f__Lachnospiraceae; g__Dorea	724472	16	0.813	1.424	4	0	4	0.465	0.006	0.09	0.693

Table B.4, continued

Group	Taxonomy	OTU_ID	Phase	Mean	Std_Dev	Max	Min	Max_Amp	Tau	P	GammaP	GammaBH
						p < 0.05						
RC – *Reg3γ*$^{+/-}$	p__Firmicutes; c__Bacilli; o__Lactobacillales; f__Streptococcaceae; g__Lactococcus	716006	12	50.043	221.377	1088	0	1088	0.625	0	0.0002	0.099
	p__Firmicutes; c__Bacilli; o__Lactobacillales; f__Streptococcaceae; g__Streptococcus	1082539	12	0.522	1.137	5	0	5	0.566	0.0001	0.0012	0.212
	p__Cyanobacteria; c__Chloroplast; o__Streptophyta	153978	12	2.696	5.303	21	0	21	0.555	0.0001	0.0016	0.212
	p__Bacteroidetes; c__Bacteroidia; o__Bacteroidales; f__S24-7	331720	20	0.739	1.293	5	0	5	0.541	0.0002	0.0023	0.212
	p__Firmicutes; c__Clostridia; o__Clostridiales; f__Clostridiaceae; g__Candidatus Arthromitus	425767	20	6.609	12.744	59	0	59	0.538	0.0002	0.0024	0.212
	p__Firmicutes; c__Bacilli; o__Lactobacillales; f__Lactobacillaceae; g__Lactobacillus; s	269125	12	0.957	1.429	5	0	5	0.512	0.0003	0.0047	0.344
	p__Bacteroidetes; c__Bacteroidia; o__Bacteroidales; f__Rikenellaceae; g__; s__	264240	20	1.13	2.939	14	0	14	0.48	0.0007	0.01	0.503
	p__Actinobacteria; c__Actinobacteria; o__Bifidobacteriales; f__Bifidobacteriaceae; g__Bifidobacterium	519290	12	0.522	0.827	3	0	3	0.479	0.0007	0.0102	0.503
	p__Bacteroidetes; c__Bacteroidia; o__Bacteroidales; f__S24-7	192906	20	0.348	0.56	2	0	2	0.479	0.0007	0.0103	0.503
	p__Firmicutes; c__Clostridia; o__Clostridiales	351859	16	0.174	0.48	2	0	2	0.472	0.0008	0.0121	0.532
	p__Bacteroidetes; c__Bacteroidia; o__Bacteroidales	801260	20	0.478	1.137	5	0	5	0.444	0.0015	0.0227	0.603
	p__Firmicutes; c__Bacilli; o__Lactobacillales; f__Lactobacillaceae; g__Lactobacillus	135956	12	1.739	2.436	11	0	11	0.44	0.0016	0.0244	0.603
	p__Firmicutes; c__Clostridia; o__Clostridiales	342786	20	0.261	0.845	4	0	4	0.429	0.0021	0.0311	0.603
	p__Firmicutes; c__Clostridia; o__Clostridiales	275139	12	0.957	3.689	18	0	18	0.426	0.0022	0.0334	0.603
	p__Deferribacteres; c__Deferribacteres; o__Deferribacterales; f__Deferribacteraceae; g__Mucispirillum; s__schaedleri	1136443	12	3.957	16.897	83	0	83	0.42	0.0025	0.0372	0.603
	p__Proteobacteria; c__Alphaproteobacteria; o__Rhizobiales; f__Brucellaceae; g__Ochrobactrum	817783	16	0.087	0.282	1	0	1	0.417	0.0027	0.0399	0.603
	p__Actinobacteria; c__Actinobacteria; o__Actinomycetales; f__Mycobacteriaceae; g__Mycobacterium	711803	16	0.087	0.282	1	0	1	0.417	0.0027	0.0399	0.603
	p__Firmicutes; c__Clostridia; o__Clostridiales	831409	12	0.087	0.282	1	0	1	0.417	0.0027	0.0399	0.603
	p__Firmicutes; c__Bacilli; o__Bacillales; f__Staphylococcaceae; g__Staphylococcus; s__sciuri	1084865	12	0.957	1.706	6	0	6	0.413	0.0029	0.0432	0.603
	p__Bacteroidetes; c__Bacteroidia; o__Bacteroidales; f__S24-7	348821	20	0.478	1.137	4	0	4	0.413	0.0029	0.0434	0.603
	p__Firmicutes; c__Clostridia; o__Clostridiales	1108453	12	0.13	0.448	2	0	2	0.412	0.0029	0.0441	0.603
	p__Firmicutes; c__Clostridia; o__Clostridiales; f__Ruminococcaceae	349459	12	0.217	0.832	4	0	4	0.412	0.0029	0.0441	0.603
	p__Firmicutes; c__Clostridia; o__Clostridiales; f__Ruminococcaceae	336691	12	0.261	0.845	4	0	4	0.412	0.003	0.0444	0.603

Table B.4, continued

HF – *Reg3γ*$^{-/-}$	p__Bacteroidetes; c__Bacteroidia; o__Bacteroidales; f__S24-7	338258	16	0.92	1.853	6	0	6	0.512	0.0002	0.0025	0.628
	p__TM7; c__TM7-3; o__CW040; f__F16	401717	20	0.4	1.02	4	0	4	0.497	0.0002	0.0037	0.628
	p__Bacteroidetes; c__Bacteroidia; o__Bacteroidales; f__S24-7	195919	16	2.92	8.849	43	0	43	0.456	0.0007	0.0105	0.628
	p__Proteobacteria; c__Alphaproteobacteria; o__Rhizobiales; f__Brucellaceae; g__Ochrobactrum	256276	20	0.28	0.826	4	0	4	0.452	0.0008	0.0115	0.628
	p__Firmicutes; c__Clostridia; o__Clostridiales; f__Clostridiaceae	555945	12	660.68	533.638	1777	0	1777	0.444	0.0009	0.014	0.628
	p__Bacteroidetes; c__Bacteroidia; o__Bacteroidales; f__S24-7	270984	16	1.28	2.069	8	0	8	0.436	0.0011	0.0168	0.628
	p__Firmicutes; c__Clostridia; o__Clostridiales; f__Clostridiaceae	297143	0	0.92	0.977	3	0	3	0.421	0.0016	0.024	0.628
	p__Bacteroidetes; c__Bacteroidia; o__Bacteroidales; f__S24-7	315430	20	1.04	1.865	7	0	7	0.421	0.0016	0.0241	0.628
	p__Bacteroidetes; c__Bacteroidia; o__Bacteroidales; f__S24-7	389282	4	0.24	0.65	3	0	3	0.406	0.0022	0.0337	0.628
	p__Firmicutes; c__Clostridia; o__Clostridiales	415491	20	0.64	1.694	8	0	8	0.404	0.0023	0.0349	0.628
	p__Firmicutes; c__Clostridia; o__Clostridiales	259870	20	0.2	0.632	3	0	3	0.391	0.0031	0.0461	0.628
	p__Firmicutes; c__Bacilli; o__Lactobacillales; f__Streptococcaceae; g__Streptococcus	661259	20	15.24	14.922	50	0	50	0.39	0.0032	0.0475	0.628
	p__Firmicutes; c__Clostridia; o__Clostridiales; f__Ruminococcaceae; g__Oscillospira	452014	20	0.12	0.325	1	0	1	0.389	0.0032	0.0478	0.628
	p__Bacteroidetes; c__Bacteroidia; o__Bacteroidales; f__S24-7	339017	20	0.52	1.836	9	0	9	0.388	0.0033	0.0489	0.628
RC – *Reg3γ*$^{-/-}$	p__Bacteroidetes; c__Bacteroidia; o__Bacteroidales; f__S24-7	421792	20	106.792	111.521	461	0	461	0.513	0.0002	0.0033	0.526
	p__Bacteroidetes; c__Bacteroidia; o__Bacteroidales; f__Rikenellaceae	264240	12	0.542	1.322	6	0	6	0.511	0.0002	0.0035	0.526
	p__Firmicutes; c__Bacilli; o__Lactobacillales; f__Streptococcaceae; g__Streptococcus	661259	16	4.125	8.964	36	0	36	0.497	0.0003	0.005	0.526
	p__Bacteroidetes; c__Bacteroidia; o__Bacteroidales; f__S24-7	233587	4	0.542	0.957	3	0	3	0.483	0.0005	0.007	0.526
	p__Bacteroidetes; c__Bacteroidia; o__Bacteroidales; f__S24-7	460953	4	1.083	1.288	5	0	5	0.468	0.0007	0.0101	0.526
	p__Bacteroidetes; c__Bacteroidia; o__Bacteroidales; f__S24-7	465480	4	2.042	2.389	9	0	9	0.456	0.0009	0.0135	0.526
	p__Firmicutes; c__Bacilli; o__Lactobacillales; f__Lactobacillaceae; g__Lactobacillus	128227	8	0.417	0.571	2	0	2	0.443	0.0012	0.0183	0.526
	p__Firmicutes; c__Erysipelotrichi; o__Erysipelotrichales; f__Erysipelotrichaceae; g__Allobaculum	4379961	4	1.083	1.754	7	0	7	0.441	0.0013	0.0191	0.526
	p__Bacteroidetes; c__Bacteroidia; o__Bacteroidales; f__S24-7	348821	20	0.75	0.924	3	0	3	0.435	0.0014	0.0215	0.526
	p__Firmicutes; c__Bacilli; o__Lactobacillales; f__Lactobacillaceae; g__Lactobacillus	266445	8	8.292	11.074	51	0	51	0.432	0.0015	0.0231	0.526
	p__Bacteroidetes; c__Bacteroidia; o__Bacteroidales; f__S24-7	463233	0	0.417	1.077	5	0	5	0.428	0.0017	0.0253	0.526
	p__Firmicutes; c__Bacilli; o__Lactobacillales; f__Lactobacillaceae; g__Lactobacillus	604966	8	10.958	8.364	26	0	26	0.425	0.0018	0.0271	0.526
	p__Firmicutes; c__Clostridia; o__Clostridiales	343581	12	0.292	1.02	5	0	5	0.424	0.0018	0.0275	0.526
	p__Firmicutes; c__Clostridia; o__Clostridiales	267694	12	0.292	1.02	5	0	5	0.424	0.0018	0.0275	0.526
	p__Firmicutes; c__Bacilli; o__Lactobacillales; f__Streptococcaceae; g__Streptococcus	1082539	12	0.167	0.471	2	0	2	0.424	0.0018	0.0275	0.526
	p__Bacteroidetes; c__Bacteroidia; o__Bacteroidales; f__S24-7	331043	0	1.333	2.23	9	0	9	0.413	0.0024	0.0353	0.526
	p__Firmicutes; c__Clostridia; o__Clostridiales; f__Ruminococcaceae	1110191	4	0.333	0.624	2	0	2	0.408	0.0026	0.0395	0.526
	p__Firmicutes; c__Clostridia; o__Clostridiales; f__Clostridiaceae	337379	8	0.167	0.373	1	0	1	0.404	0.0028	0.0425	0.526

Table B.4, continued

HF – *Reg3γ*$^{-/-}$	p__Firmicutes; c__Clostridia; o__Clostridiales; f__Peptostreptococcaceae	2658058	0	0.727	1.052	4	0	4	0.651	0	0.0002	0.073
	p__Firmicutes; c__Clostridia; o__Clostridiales	199532	20	5.5	19.085	90	0	90	0.514	0.0004	0.0061	0.576
	p__Firmicutes; c__Clostridia; o__Clostridiales; f__Ruminococcaceae; g__Ruminococcus	265940	20	0.182	0.386	1	0	1	0.501	0.0005	0.0082	0.576
	p__Firmicutes; c__Bacilli; o__Lactobacillales; f__Lactobacillaceae; g__Lactobacillus	269125	16	0.273	0.445	1	0	1	0.485	0.0008	0.0119	0.576
	p__Firmicutes; c__Clostridia; o__Clostridiales; f__Lachnospiraceae; g__[Ruminococcus]; s__gnavus	279026	20	0.409	0.778	3	0	3	0.484	0.0008	0.0121	0.576
	p__Firmicutes; c__Clostridia; o__Clostridiales	248126	0	1	1.087	4	0	4	0.47	0.0011	0.0164	0.576
	p__Actinobacteria; c__Coriobacteriia; o__Coriobacteriales; f__Coriobacteriaceae; g__Adlercreutzia	231510	8	0.227	0.516	2	0	2	0.45	0.0017	0.0252	0.576
	p__Firmicutes; c__Clostridia; o__Clostridiales	1106614	20	1.636	5.49	26	0	26	0.449	0.0017	0.0256	0.576
	p__Bacteroidetes; c__Bacteroidia; o__Bacteroidales; f__Rikenellaceae	194490	20	3.318	9.781	37	0	37	0.449	0.0017	0.0256	0.576
	p__Firmicutes; c__Clostridia; o__Clostridiales	444987	20	0.091	0.287	1	0	1	0.448	0.0017	0.0262	0.576
	p__Firmicutes; c__Bacilli; o__Lactobacillales; f__Lactobacillaceae; g__Lactobacillus	604966	8	2	4.112	17	0	17	0.447	0.0018	0.0269	0.576
	p__Firmicutes; c__Clostridia; o__Clostridiales	307170	20	0.182	0.649	3	0	3	0.443	0.002	0.0294	0.576
	p__Firmicutes; c__Bacilli; o__Lactobacillales; f__Lactobacillaceae; g__Lactobacillus; s__reuteri	588197	8	0.864	1.516	5	0	5	0.441	0.002	0.0305	0.576
	p__Firmicutes; c__Clostridia; o__Clostridiales; f__Peptostreptococcaceae	347714	4	1.091	0.949	3	0	3	0.434	0.0024	0.0355	0.576
	p__Firmicutes; c__Clostridia; o__Clostridiales; f__Lachnospiraceae; g__[Ruminococcus]; s__gnavus	271476	12	0.136	0.343	1	0	1	0.432	0.0025	0.0368	0.576
	p__Firmicutes; c__Clostridia; o__Clostridiales; f__Ruminococcaceae	1110008	20	1.409	4.228	17	0	17	0.43	0.0025	0.0381	0.576
	p__Firmicutes; c__Clostridia; o__Clostridiales	345862	20	0.591	1.749	7	0	7	0.43	0.0025	0.0381	0.576
	p__Firmicutes; c__Clostridia; o__Clostridiales; f__Ruminococcaceae	267612	20	0.545	1.644	7	0	7	0.43	0.0025	0.0381	0.576
	p__Firmicutes; c__Clostridia; o__Clostridiales; f__Clostridiaceae	555945	20	385.545	334.194	1483	0	1483	0.416	0.0034	0.04	0.576
	p__Firmicutes; c__Bacilli; o__Lactobacillales; f__Streptococcaceae; g__Lactococcus	513080	16	5.545	5.533	17	0	17	0.423	0.003	0.04	0.576
	p__Firmicutes; c__Bacilli; o__Lactobacillales; f__Lactobacillaceae; g__Lactobacillus	288521	8	0.227	0.849	4	0	4	0.421	0.0031	0.04	0.576

Table B.4, continued

Group	Taxonomy	OTU_ID	Phase	Mean	Std_Dev	Max	Min	Max_Amp	Tau	P	GammaP	GammaBH
p = 0.05 – 0.1												
RC – *Reg3γ*$^{+/-}$	p__Firmicutes; c__Clostridia; o__Clostridiales; f__Lachnospiraceae	759751	16	0.217	0.412	1	0	1	0.406	0.0033	0.05	0.603
	p__Bacteroidetes; c__Bacteroidia; o__Bacteroidales; f__S24-7	208409	16	0.826	1.049	4	0	4	0.405	0.0034	0.0506	0.603
	p__Firmicutes; c__Clostridia; o__Clostridiales; f__Ruminococcaceae; g__Ruminococcus	268043	12	1.304	3.141	14	0	14	0.403	0.0036	0.0535	0.603
	p__Bacteroidetes; c__Bacteroidia; o__Bacteroidales; f__Rikenellaceae	270391	12	0.826	2.099	10	0	10	0.396	0.0041	0.0614	0.603
	p__Bacteroidetes; c__Bacteroidia; o__Bacteroidales; f__S24-7	338258	0	3.174	3.908	14	0	14	0.393	0.0043	0.0652	0.603
	p__Bacteroidetes; c__Bacteroidia; o__Bacteroidales; f__S24-7	313878	20	0.87	1.541	7	0	7	0.391	0.0045	0.0671	0.603
	p__Firmicutes; c__Clostridia; o__Clostridiales; f__Clostridiaceae; g__Candidatus Arthromitus	376862	16	6.217	11.088	48	0	48	0.391	0.0045	0.0678	0.603
	p__Bacteroidetes; c__Bacteroidia; o__Bacteroidales; f__S24-7	326315	0	0.261	0.529	2	0	2	0.383	0.0052	0.0782	0.603
	p__Firmicutes; c__Bacilli; o__Lactobacillales; f__Lactobacillaceae; g__Lactobacillus; s__reuteri	949863	8	3.348	5.337	19	0	19	0.383	0.0052	0.0783	0.603
	p__Bacteroidetes; c__Bacteroidia; o__Bacteroidales; f__S24-7	423455	20	1.174	2.16	10	0	10	0.382	0.0053	0.0796	0.603
	p__Firmicutes; c__Bacilli; o__Lactobacillales; f__Streptococcaceae; g__Streptococcus	661259	12	16.826	30.595	118	0	118	0.38	0.0056	0.0836	0.603
	p__Firmicutes; c__Clostridia; o__Clostridiales	339718	20	0.087	0.282	1	0	1	0.375	0.0061	0.091	0.603
	p__Firmicutes; c__Clostridia; o__Clostridiales; f__Lachnospiraceae	276531	20	0.174	0.564	2	0	2	0.375	0.0061	0.091	0.603
	p__Firmicutes; c__Clostridia; o__Clostridiales; f__[Mogibacteriaceae	417981	20	0.087	0.282	1	0	1	0.375	0.0061	0.091	0.603
HF – *Reg3γ*$^{+/-}$	p__Bacteroidetes; c__Bacteroidia; o__Bacteroidales; f__Bacteroidaceae; g__Bacteroides; s__acidifaciens	583117	4	0.16	0.612	3	0	3	0.38	0.0039	0.0583	0.628
	p__Firmicutes; c__Clostridia; o__Clostridiales	434339	4	0.28	0.665	2	0	2	0.379	0.004	0.0594	0.628
	p__Firmicutes; c__Erysipelotrichi; o__Erysipelotrichales; f__Erysipelotrichaceae; g__Allobaculum	4426641	16	121.72	218.85	819	0	819	0.359	0.0059	0.0819	0.628
	p__Firmicutes; c__Clostridia; o__Clostridiales	382220	20	0.24	0.991	5	0	5	0.362	0.0056	0.0819	0.628
	p__Firmicutes; c__Clostridia; o__Clostridiales; f__Ruminococcaceae; g__Ruminococcus	268043	16	0.28	0.722	3	0	3	0.362	0.0057	0.0819	0.628
	p__Firmicutes; c__Clostridia; o__Clostridiales; f__Ruminococcaceae	1110008	20	0.4	1.6	8	0	8	0.362	0.0056	0.0819	0.628
	p__Firmicutes; c__Clostridia; o__Clostridiales	346764	20	0.24	0.991	5	0	5	0.362	0.0056	0.0819	0.628
	p__Bacteroidetes; c__Bacteroidia; o__Bacteroidales; f__S24-7	353012	16	0.44	1.098	5	0	5	0.352	0.0068	0.0999	0.628

Table B.4, continued

RC – *Reg3γ*$^{-/-}$	p__Bacteroidetes; c__Bacteroidia; o__Bacteroidales; f__S24-7	313878	0	1.125	1.452	4	0	4	0.395	0.0034	0.0511	0.526
	p__Firmicutes; c__Clostridia; o__Clostridiales; f__Peptococcaceae; g__rc4-4	296726	12	0.083	0.276	1	0	1	0.389	0.0039	0.0578	0.526
	p__Firmicutes; c__Bacilli; o__Bacillales; f__Bacillaceae; g__Anoxybacillus; s__kestanbolensis	1051517	16	0.667	2.211	8	0	8	0.389	0.0039	0.0578	0.526
	p__Bacteroidetes; c__Bacteroidia; o__Bacteroidales; f__S24-7	277120	4	1.542	1.732	5	0	5	0.388	0.0039	0.0589	0.526
	p__Actinobacteria; c__Coriobacteriia; o__Coriobacteriales; f__Coriobacteriaceae; g__Adlercreutzia	231510	8	1	1.323	5	0	5	0.388	0.004	0.0597	0.526
	p__Deferribacteres; c__Deferribacteres; o__Deferribacterales; f__Deferribacteraceae; g__Mucispirillum; s__schaedleri	1136443	12	0.25	1.01	5	0	5	0.385	0.0042	0.0631	0.526
	p__Chloroflexi; c__Chloroflexi; o__AKIW781	1110219	16	3.083	11.888	58	0	58	0.385	0.0042	0.0631	0.526
	p__Firmicutes; c__Bacilli; o__Lactobacillales; f__Streptococcaceae; g__Lactococcus	513080	16	0.167	0.624	3	0	3	0.385	0.0042	0.0631	0.526
	p__Proteobacteria; c__Alphaproteobacteria; o__Rhizobiales; f__Phyllobacteriaceae; g__Phyllobacterium	577289	16	2.208	10.384	52	0	52	0.385	0.0042	0.0631	0.526
	p__Actinobacteria; c__Thermoleophilia; o__Solirubrobacterales	756183	16	0.375	1.438	7	0	7	0.385	0.0042	0.0631	0.526
	p__Bacteroidetes; c__Bacteroidia; o__Bacteroidales; f__Rikenellaceae	270391	0	0.583	1.498	7	0	7	0.382	0.0045	0.067	0.526
	p__Bacteroidetes; c__Bacteroidia; o__Bacteroidales; f__S24-7	343853	8	1.083	1.47	5	0	5	0.377	0.005	0.0745	0.526
	p__Cyanobacteria; c__Chloroplast; o__Streptophyta	153978	16	0.417	0.64	2	0	2	0.371	0.0055	0.0832	0.526
	p__Bacteroidetes; c__Bacteroidia; o__Bacteroidales; f__S24-7	262102	4	0.917	0.997	3	0	3	0.37	0.0057	0.0851	0.526
	p__Bacteroidetes; c__Bacteroidia; o__Bacteroidales; f__S24-7	192906	20	0.583	0.909	3	0	3	0.368	0.0059	0.088	0.526
	p__Firmicutes; c__Bacilli; o__Bacillales; f__Bacillaceae; g__Geobacillus	1565317	16	12.708	45.43	212	0	212	0.365	0.0062	0.0926	0.526
	p__Proteobacteria; c__Alphaproteobacteria; o__Rhizobiales; f__Bradyrhizobiaceae	580625	16	7.625	29.429	144	0	144	0.365	0.0062	0.0926	0.526
	p__Firmicutes; c__Clostridia; o__Clostridiales; f__Lachnospiraceae; g__[Ruminococcus]; s__gnavus	270758	12	0.708	1.369	6	0	6	0.365	0.0062	0.0937	0.526
	p__Bacteroidetes; c__Bacteroidia; o__Bacteroidales; f__S24-7	312440	8	0.75	1.199	4	0	4	0.365	0.0063	0.0942	0.526
	p__Firmicutes; c__Clostridia; o__Clostridiales	863612	0	0.333	0.898	4	0	4	0.364	0.0063	0.0949	0.526
	p__Firmicutes; c__Bacilli; o__Turicibacterales; f__Turicibacteraceae; g__Turicibacter	368490	12	1.333	1.675	5	0	5	0.363	0.0064	0.0959	0.526
	p__Firmicutes; c__Clostridia; o__Clostridiales	453405	0	0.125	0.331	1	0	1	0.358	0.0071	0.0999	0.526
	p__Firmicutes; c__Clostridia; o__Clostridiales	352049	20	0.125	0.331	1	0	1	0.358	0.0071	0.0999	0.526
	p__Bacteroidetes; c__Bacteroidia; o__Bacteroidales; f__Rikenellaceae	264325	8	0.208	0.644	3	0	3	0.36	0.0068	0.0999	0.526
	p__Proteobacteria; c__Alphaproteobacteria; o__Rhizobiales; f__Brucellaceae; g__Ochrobactrum	59527	16	0.292	1.02	5	0	5	0.36	0.0068	0.0999	0.526
	p__Firmicutes; c__Clostridia; o__Clostridiales	835456	0	0.25	0.595	2	0	2	0.359	0.007	0.0999	0.526

Table B.4, continued

HF – *Reg3γ*$^{-/-}$	p__Bacteroidetes; c__Bacteroidia; o__Bacteroidales; f__Rikenellaceae	270391	20	2.5	6.887	26	0	26	0.415	0.0035	0.0506	0.576
	p__Firmicutes; c__Clostridia; o__Clostridiales; f__Lachnospiraceae	701221	20	3.045	9.646	39	0	39	0.412	0.0037	0.0509	0.576
	p__Firmicutes; c__Clostridia; o__Clostridiales	267694	20	2.591	8.294	36	0	36	0.412	0.0037	0.0509	0.576
	p__Firmicutes; c__Clostridia; o__Clostridiales	346764	20	0.636	1.92	8	0	8	0.412	0.0037	0.0509	0.576
	p__Firmicutes; c__Clostridia; o__Clostridiales; f__Lachnospiraceae	170248	20	0.773	2.746	13	0	13	0.412	0.0037	0.0509	0.576
	p__Firmicutes; c__Clostridia; o__Clostridiales; f__Ruminococcaceae; g__Oscillospira	1105687	20	0.636	1.582	6	0	6	0.406	0.0041	0.0509	0.576
	p__Firmicutes; c__Clostridia; o__Clostridiales; f__Ruminococcaceae; g__Oscillospira	1110378	20	0.455	1.076	4	0	4	0.401	0.0045	0.0616	0.576
	p__Firmicutes; c__Bacilli; o__Lactobacillales; f__Enterococcaceae; g__Enterococcus_	1111582	4	0.818	1.946	9	0	9	0.401	0.0045	0.0617	0.576
	p__Bacteroidetes; c__Bacteroidia; o__Bacteroidales; f__S24-7	338258	12	1.409	3.055	12	0	12	0.398	0.0048	0.0629	0.576
	p__Firmicutes; c__Clostridia; o__Clostridiales	827522	8	0.364	1.263	6	0	6	0.397	0.0049	0.0629	0.576
	p__Firmicutes; c__Clostridia; o__Clostridiales; f__Clostridiaceae	337379	4	0.182	0.649	3	0	3	0.399	0.0047	0.0629	0.576
	p__Firmicutes; c__Clostridia; o__Clostridiales; f__Peptostreptococcaceae	299474	0	0.5	1.034	4	0	4	0.399	0.0047	0.0629	0.576
	p__Firmicutes; c__Bacilli; o__Lactobacillales; f__Lactobacillaceae; g__Lactobacillus; s__reuteri	692154	8	2	3.896	13	0	13	0.388	0.0058	0.0679	0.576
	p__Firmicutes; c__Clostridia; o__Clostridiales	265397	20	0.136	0.457	2	0	2	0.387	0.0058	0.0679	0.576
	p__Firmicutes; c__Bacilli; o__Lactobacillales; f__Lactobacillaceae; g__Lactobacillus; s__reuteri	949863	12	0.591	1.154	4	0	4	0.384	0.0062	0.0787	0.576
	p__Firmicutes; c__Clostridia; o__Clostridiales	434339	4	0.864	2.51	12	0	12	0.377	0.007	0.0874	0.576
	p__Firmicutes; c__Bacilli; o__Lactobacillales; f__Streptococcaceae; g__Streptococcus	1083194	8	1.091	4.785	23	0	23	0.376	0.0071	0.088	0.576
	p__Firmicutes; c__Bacilli; o__Lactobacillales; f__Lactobacillaceae; g__Lactobacillus	356529	8	2	3.357	10	0	10	0.376	0.0071	0.0882	0.576
	p__Bacteroidetes; c__Bacteroidia; o__Bacteroidales; f__S24-7	315430	12	6.227	12.373	40	0	40	0.369	0.0081	0.0909	0.576
	p__Proteobacteria; c__Gammaproteobacteria; o__Enterobacteriales; f__Enterobacteriaceae	1111294	4	10.273	40.194	194	0	194	0.37	0.0079	0.0909	0.576
	p__Firmicutes; c__Clostridia; o__Clostridiales	312145	20	0.455	1.196	5	0	5	0.372	0.0077	0.0909	0.576

Table B.5: **Top differentially abundant conditioned media metabolites.** Top 50 conditioned media metabolites significantly different ($p < 0.05$) and with $|log2(foldchange)| > 1$ from LGG 3kDa to either (1) LGG 3kDa heat-treated or (2) *L. reuteri* 3kDa. Metabolites highlighted blue are identified as branched-chained amino acids (BCAAs).

1. LGG 3kDa vs LGG 3kDa heat-treated						
Name	**Formula**	**Molecular Weight**	**RT (min)**	**MS2**	**log2(fold change) from LGG 3kDa**	**p-value**
Positive fold change						
N4-[5-(2-pyridyl)-2-thienyl]morpholine-4-carboxamide	C14 H15 N3 O2 S	198.07904	10.542	DDA for preferred ion	6.880739878	0.035523158
Norharman	C11 H8 N2	168.06848	10.386	DDA for preferred ion	6.812666846	0.012483667
Unknown-7878	C67 H98 N8 O14 P2	1300.66702	34.974	No MS2	6.072517437	0.017749049
Leucyltyrosine-1	C15 H22 N2 O4	294.15735	9.869	DDA for preferred ion	6.057324517	0.024663544
2-methoxyestrone 3-glucosiduronic acid	C25 H32 O9	476.2051	10.068	No MS2	6.020818254	0.032767206
NP-001346-1	C11 H15 N5 O3 S	297.089	7.346	DDA for preferred ion	5.568848975	0.03491075
Unknown-5497	nd*	289.94142	1.123	DDA for preferred ion	5.496724849	0.026017059
MFCD00025555-3	C9 H18 N2 O3	202.13137	3.487	DDA for preferred ion	5.40894976	0.026134185
Leu-Leu-4	C12 H24 N2 O3	244.17819	10.869	DDA for preferred ion	5.331540275	0.045946626
Unknown-9695	C18 H46 N9 O3 P3 S	561.26692	29.691	No MS2	5.295516881	0.001835837
1,2-Benzoquinone	C6 H4 O2	108.02129	4.058	DDA for preferred ion	5.267171391	3.43E-06
Unknown-3839	C13 H26 N10 O5	402.2108	9.08	DDA for preferred ion	5.235166516	0.02564627
Unknown-4228	C50 H78 N10 O8 P2	1008.54732	27.352	DDA for preferred ion	5.216896964	0.001518175
Unknown-639	nd	97.09305	3.892	No MS2	5.050971228	0.022707251
Unknown-7628	C6 H4 N10 O3	264.04799	7.384	DDA for preferred ion	5.038047347	0.019036608
Unknown-10402	nd	326.66846	8.546	No MS2	5.015270972	0.026628589
Unknown-7505	C4 H8 N2 O P2 S2	225.95592	4.075	DDA for preferred ion	5.00896693	0.026547866
Leu-Leu-1	C12 H24 N2 O3	244.17821	11.306	DDA for preferred ion	4.967890106	0.02730868
2-(2-amino-3-methylbutanamido)-3-phenylpropanoic acid-4	C14 H20 N2 O3	264.1469	8.588	DDA for preferred ion	4.959303894	0.005391017
Unknown-9155	C47 H85 N3 O10	851.62374	45.184	No MS2	4.903669148	0.004890269
Unknown-9990	C16 H11 O8 P	362.02032	10.067	No MS2	4.827571849	0.042763623
Unknown-9253	nd	217.09254	7.539	DDA for preferred ion	4.676841688	0.010060489
Unknown-4007	C9 H20 N2	156.16246	1.136	No MS2	4.620840541	0.004582173
Unknown-3557	N/A	460.32526	4.498	No MS2	4.543561499	0.0066924
Unknown-6837	C16 H18 N2 O4	302.12601	9.136	No MS2	4.509281069	0.02215329

Table B.5, continued

1. LGG 3kDa vs LGG 3kDa heat-treated						
Name	**Formula**	**Molecular Weight**	**RT (min)**	**MS2**	**log2(fold change) from LGG 3kDa**	**p-value**
Negative fold change						
Unknown-4795	C8 H20 N5 O4 P	281.12599	20.237	No MS2	-5.254690448	0.018277039
Unknown-7781	C28 H41 N O6	487.29236	47.479	No MS2	-5.314282664	0.011656324
Unknown-7784	C13 H18 N6 O2 S	322.11948	11.038	DDA for preferred ion	-5.413285984	0.007807908
Unknown-5571	C32 H66 N9 O15 P	847.44234	20.911	No MS2	-5.439517788	0.006569197
Unknown-5406	nd	423.72125	20.942	No MS2	-5.448838284	0.001086332
Chivosazole B	C48 H69 N O12	851.48221	27.476	No MS2	-5.451783752	0.005832038
Unknown-8532	nd	626.39872	14.768	No MS2	-5.458875586	0.000614101
Unknown-3130	C31 H61 N6 O17 P	820.38393	17.774	DDA for preferred ion	-5.474553004	0.001609537
Unknown-1800	C17 H32 N2 O8	392.21504	5.71	DDA for preferred ion	-5.475810403	0.04396104
Unknown-7968	C15 H27 N3 O4	313.19943	14.769	No MS2	-5.541401815	0.006361689
Unknown-4577	C21 H32 N2 O8	440.2151	14.229	DDA for preferred ion	-5.650990063	0.000100717
Unknown-2096	C31 H73 N6 O12 P3	814.45016	16.574	No MS2	-5.682071401	0.003816438
Unknown-2333	C45 H79 N8 O18 P	1050.52567	31.088	DDA for preferred ion	-5.80654707	0.005233092
Unknown-1540	C57 H97 N4 O16 P3	1186.6108	26.7	No MS2	-5.990473903	0.006009801
Unknown-9402	C67 H90 N5 O18 P	1283.60166	27.285	No MS2	-6.004945802	0.000629411
Unknown-2428	C18 H34 N2 O8	406.23126	10.484	DDA for preferred ion	-6.269375299	0.007341468
Unknown-815	C39 H70 N5 O7 P3	813.44701	16.604	DDA for preferred ion	-6.270404325	0.002071294
(4E)-5-Hydroxy-4-{(2E,4E,6R)-1-hydroxy-6-[(3R,4R,6R)-6-hydroxy-1,4,8-trimethyl-2,9-dioxabicyclo[3.3.1]non-7-en-3-yl]-4-methyl-2,4-heptadien-1-ylidene}-2,4-dihydro-3H-pyrrol-3-one-1	C22 H29 N O6	403.19843	47.48	DDA for preferred ion	-6.385583469	0.009467347
Unknown-4118	C52 H97 N7 O16 P2 S	1169.6164	25.828	No MS2	-6.702585596	0.006936757
Unknown-3704	C62 H98 N5 O16 P3	1261.62107	27.299	No MS2	-6.751006199	0.006580902
Unknown-2112	C36 H70 N7 O18 P	919.45323	25.584	DDA for preferred ion	-6.902459015	0.002567927
Unknown-2985	C68 H100 N2 O17 P2	1278.64956	27.302	No MS2	-7.031249955	0.002670481
Unknown-1747	C18 H34 N2 O8	406.23143	12.226	DDA for preferred ion	-7.201065821	0.004241965
Unknown-3212	nd	459.72594	25.588	No MS2	-7.283209638	0.013039755
Unknown-1429	C62 H106 N5 O17 P3	1285.67957	31.413	No MS2	-7.513354701	0.016019054

Table B.5, continued

2. LGG 3kDa vs L. reuteri 3kDa						
Name	**Formula**	**Molecular Weight**	**RT (min)**	**MS2**	**log2(fold change) from LGG 3kDa**	**p-value**
Positive fold change						
NP-016455-12	C11 H18 N2 O4	484.25337	14.674	DDA for preferred ion	9.877609466	0.00109205
Biotin l-Sulfoxide-1	C10 H16 N2 O4 S	260.08273	8.807	DDA for preferred ion	8.892202706	0.00050792
Biotin l-Sulfoxide-2	C10 H16 N2 O4 S	260.08275	8.707	DDA for preferred ion	8.362108451	0.0031317
anthramycin	C16 H17 N3 O4	315.12166	17.753	DDA for preferred ion	8.217911372	0.00095819
[Similar to: NP-016455; ?Mass: 132.0784 Da]	C18 H26 N6 O3	374.20501	14.674	DDA for preferred ion	7.652421303	0.00091726
Unknown-3616	C5 H16 N2 O15 P2	406.00226	3.591	No MS2	7.346629284	0.00019058
NP-016455-4	C11 H18 N2 O4	242.12613	13.559	DDA for preferred ion	7.239767135	0.00010837
N-[(2S)-2-Hydroxypropanoyl]-L-tryptophan-1	C14 H16 N2 O4	276.11073	16.647	DDA for preferred ion	7.118533361	0.00108525
Unknown-1941	C21 H32 N4 O10	500.21146	13.744	DDA for preferred ion	7.113860022	0.0006018
NP-016455-1	C11 H18 N2 O4	242.12615	14.662	DDA for preferred ion	7.077578713	2.56E-05
Unknown-1281	C8 H17 N6 O4 P	292.10562	9.713	DDA for preferred ion	6.833828874	0.00816756
Unknown-3274	C17 H29 N3 O5	355.21032	25.175	DDA for preferred ion	6.826313651	0.00137195
Valclavam-1	C14 H23 N3 O6	329.15822	10.73	DDA for preferred ion	6.747928854	0.01052077
2-(2-amino-3-methylbutanamido)-3-phenylpropanoic acid-1	C14 H20 N2 O3	264.14692	9.938	DDA for preferred ion	6.725991269	0.00075795
Unknown-2922	C14 H23 N3 O5	313.16349	12.026	DDA for preferred ion	6.675046892	0.00324238
NP-016455-5	C11 H18 N2 O4	242.1262	14.426	DDA for preferred ion	6.654068147	0.00219815
Tetraacetylethylenediamine-1	C10 H16 N2 O4	228.1105	8.866	DDA for preferred ion	6.612835487	7.93E-07
phe-gln-2	C14 H19 N3 O4	293.13634	16.587	No MS2	6.453262696	0.00019405
Unknown-3648	C10 H6 N10 O5 P2	407.99797	3.607	DDA for preferred ion	6.448911914	0.00019185
N(3)-(4-Methoxyfumaroyl)-2,3-diaminopropionic acid-2	C8 H12 N2 O5	216.0736	3.069	DDA for preferred ion	6.419771368	0.04273614
Unknown-5040	C15 H24 N4 O6	356.16925	13.824	DDA for preferred ion	6.404149803	0.0002635
Guanine	C5 H5 N5 O	151.04918	1.763	No MS2	6.364350539	0.00145747
Unknown-6479	C24 H43 N3 O S3	485.25691	14.664	No MS2	6.350408557	0.00048068
Unknown-5114	C17 H30 N6 O5	398.22709	10.375	DDA for preferred ion	6.339944682	0.00192449
Valylvaline-1	C10 H20 N2 O3	216.14685	3.637	DDA for preferred ion	6.317488919	0.02257494

Table B.5, continued

2. LGG 3kDa vs L. reuteri 3kDa						
Name	**Formula**	**Molecular Weight**	**RT (min)**	**MS2**	**log2(fold change) from LGG 3kDa**	**p-value**
Negative fold change						
Leucyl-leucyl-norleucine-2	C18 H35 N3 O4	357.26193	22.035	DDA for preferred ion	-6.148362246	0.0103971
(3S)-3-{(Z)-[(3S)-3-{(Z)-[(3R)-3-Amino-1-hydroxy-4-methylpentylidene]amino}-1-hydroxybutylidene]amino}-5-methylhexanoic acid-4	C17 H33 N3 O4	343.24637	21.252	DDA for preferred ion	-6.149999775	0.00169572
Unknown-283	C11 H21 N O2 S2	263.10252	1.8	No MS2	-6.177253683	0.0121323
Unknown-2469	nd	112.01446	3.029	No MS2	-6.214204071	0.00250808
Marimastat-6	C15 H29 N3 O5	331.21033	18.308	DDA for preferred ion	-6.277531592	0.00764222
Unknown-4912	C16 H31 N3 O5	345.22596	18.793	DDA for preferred ion	-6.292647646	0.0004256
Adenosine-8	C10 H13 N5 O4	267.09596	2.755	DDA for preferred ion	-6.333147729	0.0360039
Marimastat-8	C15 H29 N3 O5	331.21034	19.38	DDA for preferred ion	-6.498019883	7.99E-05
Unknown-4503	C11 H18 Cl O2 P S	280.04603	1.616	No MS2	-6.523310567	0.02020617
Unknown-357	C2 H7 N7 P2	191.0238	3.838	No MS2	-6.533329744	0.0004276
capuride-2	C9 H18 N2 O2	186.13648	7.595	DDA for other ion	-6.6584297	0.01787683
Unknown-2030	C12 H18 N2 O9	334.10124	1.682	No MS2	-6.854370221	0.00011948
Unknown-2730	C18 H36 N4 O4	372.27316	11.902	DDA for preferred ion	-6.854944734	0.00044837
ILK-2	C18 H36 N4 O4	186.13645	11.884	DDA for preferred ion	-6.862079251	0.00077579
Unknown-1869	C18 H36 N4 O4	372.27284	7.617	DDA for preferred ion	-6.947036953	0.0168312
arg-leu	C12 H25 N5 O3	287.19521	1.595	No MS2	-7.113837899	0.00061584
Unknown-2741	C18 H36 N4 O4	372.2725	12.065	DDA for preferred ion	-7.287463894	0.00064717
Unknown-2010	C18 H36 N4 O4	372.27266	7.418	DDA for preferred ion	-7.370579139	0.01422703
Unknown-1522	C4 H13 N4 O4 P	212.06729	1.307	No MS2	-8.016167128	0.03181052
DL-Arginine-6	C6 H14 N4 O2	174.11139	1.513	DDA for preferred ion	-8.327161182	0.03876264
Unknown-5	nd	210.03641	1.772	DDA for preferred ion	-8.830734234	0.04294733
Citric acid-6	C6 H8 O7	192.02574	1.601	DDA for preferred ion	-8.947382253	0.00040835
Citric acid-7	C6 H8 O7	146.02038	1.599	DDA for other ion	-9.107553917	0.00038776
Citric acid-4	C6 H8 O7	192.0258	1.803	DDA for preferred ion	-9.837951251	0.04316045
Unknown-766	nd	193.0291	1.595	No MS2	-10.68670565	0.0011876